JOURNAL OF ADVANCED DIELECTRICS
Vol. 8, No. 1 (2018) 1850005 (13 pages)

DOI: 10.1142/S2010135X18500054

World Scientific
www.worldscientific.com

Ionic conductivity and relaxation studies in PVDF-HFP:PMMA-based gel polymer blend electrolyte with $LiClO_4$ salt

Khushbu Gohel and D. K. Kanchan*
Department of Physics, Faculty of Science
The M.S. University of Baroda
Vadodara 390002, Gujarat, India
*dkkanchan.ssi@gmail.com

Received 5 January 2018; Revised 8 February 2018; Accepted 12 February 2018; Published 27 February 2018

Poly(vinylidene fluoride-hexafluropropylene) (PVDF-HFP) and poly(methyl methacrylate) (PMMA)-based gel polymer electrolytes (GPEs) comprising propylene carbonate and diethyl carbonate mixed plasticizer with variation of lithium perchlorate ($LiClO_4$) salt concentrations have been prepared using a solvent casting technique. Structural characterization has been carried out using XRD wherein diffraction pattern reveals the amorphous nature of sample up to 7.5 wt.% salt and complexation of polymers and salt have been studied by FTIR analysis. Surface morphology of the samples has been studied using scanning electron microscope. Electrochemical impedance spectroscopy in the temperature range 303–363 K has been carried out for electrical conductivity. The maximum room temperature conductivity of 2.83×10^{-4} S cm^{-1} has been observed for the GPE incorporating 7.5 wt.% $LiClO_4$. The temperature dependence of ionic conductivity obeys the Arrhenius relation. The increase in ionic conductivity with change in temperatures and salt content is observed. Transport number measurement is carried out by Wagner's DC polarization method. Loss tangent (tan δ) and imaginary part of modulus (M'') corresponding to dielectric relaxation and conductivity relaxation respectively show faster relaxation process with increasing salt content up to optimum value of 7.5 wt.% $LiClO_4$. The modulus (M'') shows that the conductivity relaxation is of non-Debye type (broader than Debye peak).

Keywords: Gel polymer electrolyte; ionic conductivity; transport number; Wagner's DC polarization; impedance.

1. Introduction

The development of ionically conducting polymer electrolytes has increased enormous interest due to a wide range of promising applications in various electrochemical devices such as fuel cells, electrochromic devices, super capacitors, solar cells, especially in acquiring a battery that combines compact shape, long life, low cost, environmental safety, and high energy density.[1,2] A lithium ion battery consists of anode and cathode as electrodes and polymer electrolyte as separator, through which ion transport phenomenon occurs. The basic requirements for a polymer electrolyte used in a battery are (1) high ionic conductivity, (2) good mechanical strength, (3) wide electrochemical stability window, (4) appreciable Li^+ transference number, and (5) low electronic conductivity.[3] In addition to these, the polymer also plays a crucial role in the mechanism of ionic conduction. Polymer matrix with polar groups, such as –O–, C=O, =O, –N–, C=N, and C–F with high dielectric constant have the ability to dissolve salts and formation of polymer–salt complexes which dissociate inorganic salt in the polymer matrix. It increases the effective number of mobile ions that take part in the conduction process.[4] These polymer electrolytes have a few points of interest, such as no leakage of electrolytes, ease of preparation of polymer into thin films, high energy density, high compatibility, and no electrolytic degradation as compared to carbonate-based liquid electrolytes. However, solid polymer electrolyte using different polymer hosts such as PEO, PVA, PMMA, PVDF possesses very low ionic conductivity which excludes it from practical applications.[5] As an alternative substitute to replace liquid electrolytes, there has been a great interest in gel polymer electrolytes (GPEs). The GPEs are important electrolyte candidates due to their ionic conductivity of the order of 10^{-4} to 10^{-3} S cm^{-1}.[6] GPEs are acquired by incorporation of a certain amount of liquid plasticizer/solvent into the polymer–salt system which has ability to dissolve the salt and maintain liquid state within the polymer matrix so that the transport of ions occurs in the liquid-rich swollen gelled phase. From a practical application point of view, the GPE should possess the properties of good mechanical strength, ability of absorbing the liquid electrolyte, high ionic conductivity, and electrochemical stability toward both electrodes. Various kinds of polymers such as poly(methyl methacrylate) (PMMA),[7] polyacrylonitrile (PAN),[8] poly(vinyl chloride) (PVC),[9] and poly(vinylidene fluoride) (PVDF),[10] etc. act as host polymers for GPE. All above-said properties of GPE cannot be achieved by using a single polymer as various problems arise, such as poor mechanical strength, compatibility towards lithium

metal anode, and poor interfacial properties.[11] Hence, in the present study, the technique of blending two polymers PVDF-HFP and PMMA is used to improve the properties of the polymer matrix. As a polymer host, PVDF-HFP has received a lot of attention due to its excellent properties such as low degree of crystallinity[12] and high dielectric constant $\varepsilon \approx 8.4$[13] that help in higher dissociation of lithium salt. The PVDF-HFP polymer possesses both amorphous and crystalline phases in which the amorphous HFP part can trap large amounts of liquid electrolytes whereas the crystalline VdF part assists in the improvement of the mechanical stability for the formation of a free-standing film.[14] PMMA-based GPEs offer high ionic conductivity very close to liquid electrolytes 10^{-3} S cm^{-1} at 25°C and even at low temperatures e.g., at −20°C, the conductivity remains quite high.[7] The blending of the polymer increases amorphicity or can hinder the crystalline nature.[15,16]

The plasticizer is a low molecular weight organic solvent which has the ability to dissociate the salt and maintain the liquid state within the polymer matrix.[15] It also helps increase the amorphous phase in the polymer electrolyte. The dissociation increases the number of free mobile ions which contribute toward the conductivity of polymer electrolyte. Moreover, the addition of plasticizers to GPE also softens the polymer backbone which results in high segmental motion that also assists the movement of ions. Hence, a high dielectric permittivity and low viscosity are essential properties of plasticizers to promote the ion-pair dissociation. Single plasticizer cannot fulfil the requirement of the above-mentioned properties. Therefore, in the present study, the mixture of PC ($\varepsilon \approx 64.4$, viscosity at 25°C ≈2.53 mPa S) and DEC ($\varepsilon \approx 2.82$, viscosity at 25°C ≈ 0.748 mPa S) have been taken. Recently, many researchers have reported the various GPEs with various plasticizers to enhance the different properties such as ionic conductivity, structural properties, surface morphology, etc.[17,18]

It is well known that the ionic conductivity of polymer electrolyte depends on the number of charge species and transportation of salt ions occurs through the amorphous region. So, the salt should have low lattice energy and anionic radius so that the ion can diffuse easily through the polymer matrix. Propylene carbonate (PC) and $LiClO_4$ have been used as liquid electrolytes as reported in Ref. 19. The salt $LiClO_4$ possesses smaller dissociation energy with large anion, thereby providing higher concentration of lithium ions in the electrolyte to conduct. Hence, looking into the development in research field of polymer electrolytes, the present study focusses on the ionic conductivity of the polymer gel electrolyte based on $LiClO_4$ salt by changing the polymer structure by blending and using different amounts of salt dissolved in plasticizers.

Hence, in the present study, we have studied the effect of $LiClO_4$ salt concentration on conduction properties, dielectric properties, and relaxation processes of gel polymer blend electrolyte. The electrolyte films have been characterized by X-ray diffraction (XRD), Fourier transform infrared spectroscopy (FTIR), Scanning electron microscopy (SEM), and transport number. The AC conductivity provides considerable information on ion dynamics and conductivity relaxation when results are expressed as a function of frequency. The understanding of conduction mechanism and applicability of Jonschers power law and Arrhenius law in the present polymer blend gel electrolyte with $LiClO_4$ salt have been analyzed.

2. Experimental

2.1. *Materials and sample preparation*

Poly(vinylidene fluoride-co-hexafluoropropylene) (PVDF-co-HFP) with the molecular weight (Mw) of 400,000 from Aldrich and poly(methyl methacrylate) (PMMA) with Mw = 350,000 from Alfa-Aesar and lithium perchlorate ($LiClO_4$, 99.99%) obtained from Aldrich have been used. The organic solvents PC (anhydrous, 99.7%) and diethyl carbonate (DEC, anhydrous, 99.7%) were procured from Sigma Aldrich as plasticizers to prepare GPEs.

The GPE samples of different compositions with variations in salt concentration (listed in Table 1) were prepared by solution casting method. For preparing gel electrolyte films, blend was prepared by dissolving both polymers PVDF-HFP and PMMA (1:1) in acetone. Known amount of $LiClO_4$ salt was dissolved in the plasticizers PC and DEC, which were taken in 1:1 ratio with total amount equal to that of polymers. This electrolyte solution was then mixed into the blend solution for stirring. The solution was stirred until the mixture gets homogeneous in nature. The solution with different amounts of salt was cast onto Teflon Petri dish. The samples were kept above room temperature at about 60°C to form the gel in the films and allowed acetone to evaporate slowly. After the evaporation of acetone, free-standing and flexible thin films of thickness of about 0.12–0.14 mm were peeled off and kept in vacuum desiccators. Then the films were used for different experimental studies.

2.2. *Characterization*

Structural behavior of pure samples and GPE samples is examined by means of XRD analysis. XRD patterns are

Table 1. The various composition of GPE system.

Sample code	Polymers PVDF-HFP+ PMMA (wt.%)	Plasticizers PC+DEC (wt.%)	$LiClO_4$ salt (wt.%)
S1	49	49	2
S2	48	48	4
S3	47.5	47.5	5
S4	46.25	46.25	7.5
S5	45	45	10

recorded using BRUKER D2-Phaser with CuK radiation of wavelength = 1.540 in 2θ range of 5–70° with a step of 0.05°. FTIR study has been carried out on prepared GPE films to investigate the complexation of salt in the blend. FTIR spectroscopic studies are carried out using FTIR 4100 JASCO model in the wave number range of 400–4000 cm^{-1}. The morphological and surface properties of the prepared films are examined by a JEOL JSM-6010LA SEM. The ionic conductivity of the polymer electrolyte films is measured by a high precision Solartron 1260 Impedance analyzer in the frequency range of 1 Hz to 32 MHz at different temperatures between 303 K and 363 K. The impedance measurements are carried out by sandwiching the polymer electrolyte films between two stainless steel electrodes under spring pressure. The ionic conductivity of each sample is calculated using the following equation:

$$\sigma = \frac{t}{R_b A}, \tag{1}$$

where t is the thickness of the films, R_b is the bulk resistance and A is the area of the electrolyte–electrode contact. The transport number of the samples was measured by using Wagner's DC polarization method. The transport numbers were calculated by using the following equation:

$$t_{\text{ion}} = 1 - \frac{i_e}{i_t}, \tag{2}$$

where t_{ion} is the ionic transport number, i_e and i_t are the electronic and total currents, respectively.

3. Results and Discussion

3.1. *XRD analysis*

XRD is a powerful tool to determine the crystallinity and structural changes in a polymer electrolyte system. The XRD patterns of (PVDF-HFP:PMMA)–(PC:DEC)–$LiClO_4$-based GPE at different $LiClO_4$ concentrations are shown in Fig. 1. Diffraction pattern of $LiClO_4$ shows high intense characteristic peaks which revealed the crystalline nature of the salt. Two peaks at 29.7° and 38.3° for the pure PVDF-HFP film have been observed, which confirmed the partial crystallization of PVDF units in the copolymer and overall its semicrystalline nature.[20]

The pattern for pure PMMA shows a broad and less intensive peak at $2\theta \sim 13.8°$ which indicates complete amorphous nature of the PMMA film. From the XRD pattern of GPE samples, it is revealed that the absence of crystalline peaks pertaining to $LiClO_4$ in the polymer complexes confirms the complex formation which seems to occur only in the amorphous phase[21] that confirms the complete dissolution of the salts in the complex matrix, implying that the salt does not have any separate phases in the electrolyte. Figure 1 shows that the prominent peak of PMMA at 13.8° disappeared and the intense peaks $2\theta \approx 29.7°, 38.3°$ of PVDF-HFP decrease

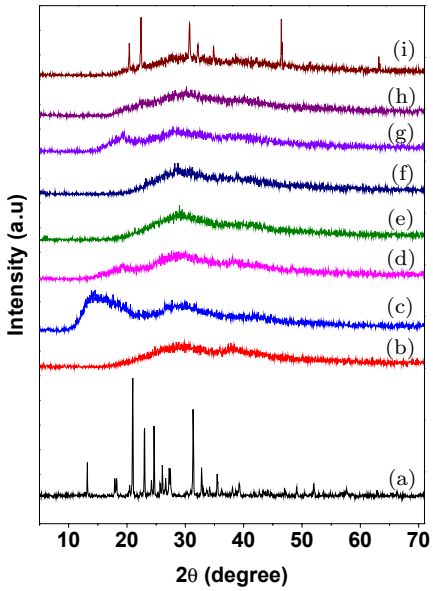

Fig. 1. XRD pattern of (a) $LiClO_4$, (b) pure PVDF-HFP, (c) pure PMMA and (PVDF-HFP:PMMA)–(PC:DEC)–$LiClO_4$ system with $LiClO_4$ content of (d) 0 wt.%, (e) 2 wt.%, (f) 4 wt.%, (g) 5 wt.%, (h) 7.5 wt.%, and (i) 10 wt.%.

together with the broadening and the incorporation of $LiClO_4$ up to 7.5 wt.% which indicates the increase in the amorphicity of the films. The amorphous phase is maintained up to 7.5 wt.% $LiClO_4$ and on further addition, the crystallinity of the complex is found to be increased.

3.2. *FTIR analysis*

FTIR analysis has been used to identify the nature of bonding, functional groups present in a sample and analyze the interactions among atoms or ions in the electrolyte system. These interactions can induce changes in the vibrational modes of the molecules in the polymer electrolyte. This study has been carried out to analyze the molecular interaction and complexation in the polymer complexes. Figure 2 shows the FTIR spectrum of pure PVDF-HFP, pure PMMA and $LiClO_4$. The FTIR spectra of GPE doped with different concentrations of $LiClO_4$ in the wave number range 400–4000 cm^{-1} are presented in Fig. 3.

The characteristic fundamental vibrational modes with wavenumbers exhibited by PVDF-HFP, PMMA, and $LiClO_4$ collected from the FTIR experimental spectra are listed in Table 2. PVDF-HFP contains free electron pairs at the fluorine (F) atoms of CF_2 and CF_3 groups.[22] The peaks at 509 cm^{-1} and 435 cm^{-1} are assigned to the bending and wagging vibrations of $-CF_2$, respectively, and get shifted to 511 cm^{-1} and 441 cm^{-1}, respectively, with the addition of lithium salt. The characteristic peak of PVDF-HFP at 836 cm^{-1} corresponds to the vibration of amorphous phase (vinylidene group) shifted to higher frequency at 838 cm^{-1}.

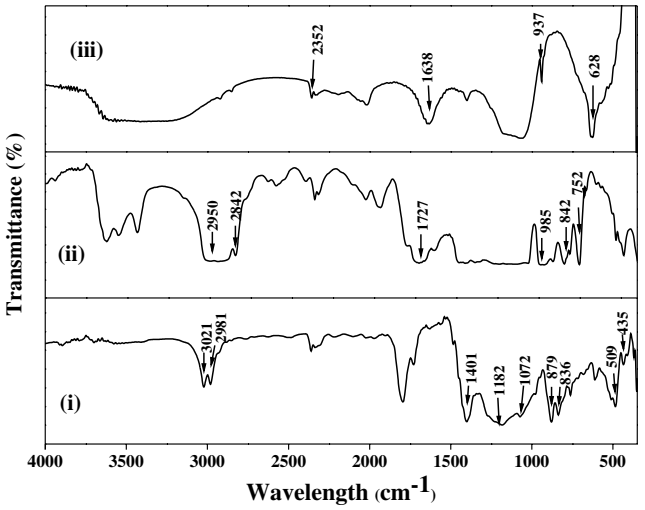

Fig. 2. FTIR spectra of (i) pure PVDF-HFP, (ii) pure PMMA, and (iii) $LiClO_4$.

The characteristics bands of PVDF-HFP at 1401 cm^{-1} attributed to the crystalline phase are broadened, reduced in intensity and shifted to 1405 cm^{-1}, indicating that interaction occurred between polymers and salt and other crystalline peaks at 1182 cm^{-1} and 1072 cm^{-1} of pure PVDF-HFP reduced in intensity and eventually disappearing when blended with PMMA leading to the suppression of semi-crystallinity of PVDF-HFP. It has also been observed that the characteristic peak of pure PVDF-HFP at 1795 cm^{-1} is shifted to 1785 cm^{-1}. The peak at 2842 cm^{-1} position associated with CH_3 asymmetric stretching vibration of PMMA gets shifted from 2844 cm^{-1} to 2848 cm^{-1} and band appearing at 1727 cm^{-1} is allocated to the symmetrical stretching of the carbonyl group C=O in the PMMA backbone that shifts the band toward lower side of the frequency at 1725 cm^{-1} and intensity is reduced significantly with increasing salt concentrations. This indicates the strong interaction of Li ions with the carbonyl group of PMMA. Similar observations were also reported by Shukla *et al.*[23] in their FTIR studies of lithium salt polymer complexes. Apart from this, the peak at 2950 cm^{-1} ascribed to CH_3 asymmetric stretching is shifted to 2954 cm^{-1} in the complexes.

In addition, many of the peaks of the polymer electrolyte system disappeared in the IR spectra. The characteristic peaks of pure $LiClO_4$ are found absent in the polymer electrolyte complexes which confirm good complexation of the salt with host polymers. The disappearance or shifting of frequency from pure polymers shows an interaction of the polymers with salt in GPE samples.

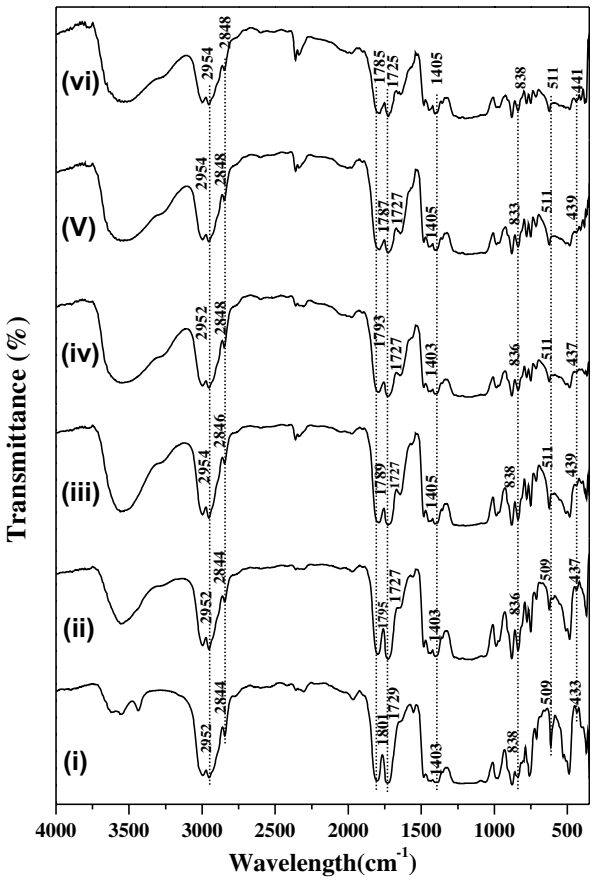

Fig. 3. FTIR spectra of (PVDF-HFP:PMMA)–(PC:DEC)–$LiClO_4$ system with $LiClO_4$ content of (i) 0 wt.%, (ii) 2 wt.%, (iii) 4 wt.%, (iv) 5 wt.%, (v) 7.5 wt.%, and (vi) 10 wt.%.

Table 2. Assignment of important bands of PVDF-HFP, PMMA, and $LiClO_4$.

Materials	Wavenumbers (cm^{-1})	Assignment of bands
PVDF-HFP	3021	Non symmetrical stretching of CH_2 group[17]
	2981	Symmetrical stretching of CH_2 group[17]
	1401,11182,1072	α crystalline phase[17]
	879,836	Vibration of amorphous phase[17]
	509	CF_2 bending[17]
	484,435	CF_2 wagging[17]
PMMA	752	CH_2 rocking with skeleton stretching[24]
	842	C-H rocking vibration[24]
	985	Symmetric stretching C-O bond[24]
	1727	Symmetric stretching of carbonyl group C=O[24]
	2842, 2950	CH_3 asymmetric stretching[24]
$LiClO_4$	628	stretching vibration of ClO_4^-[25]
	937	Symmetrical vibration of ionic pairs between Li+ and ClO_4^-[25]
	1638, 2352	Stretching and bending vibration of OH bonds for absorbing water[25]

3.3. *SEM analysis*

Surface morphology of the GPE films with $LiClO_4$ salt content of 2 wt.%, 4 wt.%, 7.5 wt.%, and 10 wt.% are shown in Fig. 4. The image shows uniformly distributed spherical

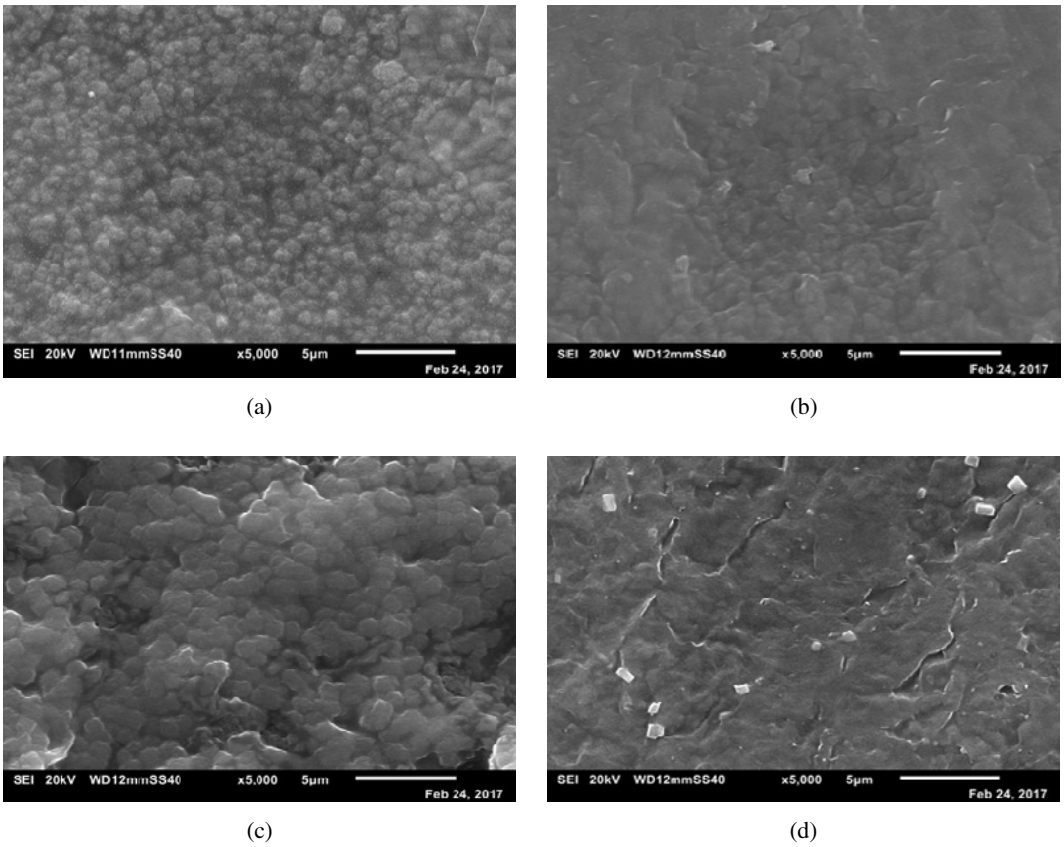

Fig. 4. SEM micrograph of the GPE films containing (a) 2 wt.% $LiClO_4$, (b) 4 wt.% $LiClO_4$, (c) 7.5 wt.% $LiClO_4$, (d) 10 wt.% $LiClO_4$.

structures in the GPE film with 2 wt.% $LiClO_4$. It shows normal porous surface with small pore size. The morphology change to greater pore size when 7.5 wt.% of $LiClO_4$ is doped into the polymer electrolyte. The pores in the polymer complexes help in trapping the large amount of electrolyte solution. Due to this, the swelled nature of the GPE has been observed containing 7.5 wt.% of $LiClO_4$. The observed feature is very similar to those reported by Ramesh *et al.*[26] These microstructures lead to better conducting pathway for Li^+ ions and consequently higher ionic conductivity.

3.4. *Conductivity analysis*

The electrical properties of the GPE films have been studied using the AC technique of complex impedance spectroscopy (CIS) analysis. Typical complex impedance plot of GPE containing 4 wt.% of $LiClO_4$ at 303 K along with their equivalent electrical circuit model fitted with experimental values by using EIS spectrum analyzer software is shown in Fig. 5. The complex plot shows a high frequency depressed semicircle portion which corresponds to the parallel combination of resistor R_b (bulk resistor) and a constant phase element CPE1 and a low frequency spike due to the accumulation of charges (double-layer formation) at the electrolyte–electrode (blocking electrode) interface represented by constant phase element CPE2.[27] Similarly, complex impedance plot for other GPEs at 303 K for different concentrations of $LiClO_4$ (Fig. 5(inset)) is fitted with equivalent circuit and fitted parameters are listed in Table 3.

It is obvious from Fig. 5(inset) that the intercept of the plots on the real axis (Z') decreases as the concentration of lithium salt is varied from 2 wt.% to 7.5 wt.% and reverse

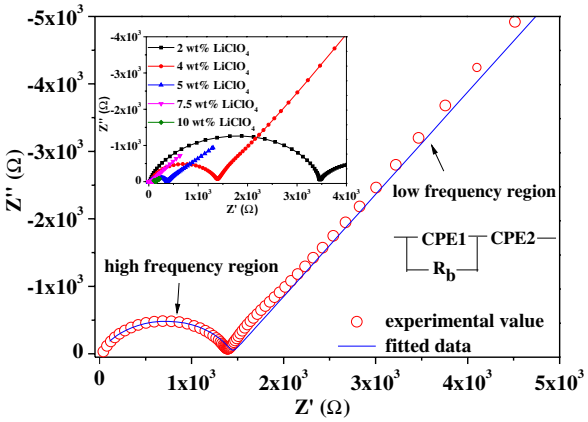

Fig. 5. Impedance plot of GPE containing 4 wt.% of $LiClO_4$ at 303 K along with equivalent circuit model (inset impedance plot of GPE with different concentrations of $LiClO_4$ at 303 K).

Table 3. The parameter of circuit element for GPE system with different concentrations of $LiClO_4$ at 303 K.

Sample code	Bulk resistance (R_b) (Ω)	CPE1 (F)	CPE2 (F)
S1	3451.1	2.346E-09	2.218E-04
S2	1441	4.381E-09	3.413E-05
S3	324.09	2.051E-09	2.900E-04
S4	72.4	2.052E-09	3.691E-04
S5	138	2.977E-08	5.000E-04

trend is seen for the 10 wt.% of $LiClO_4$ salt. From the obtained value of bulk resistance R_b, the ionic conductivity of GPE is calculated using Eq. (1) and given in Table 4. From Table 4, it is clear that the conductivity of (PVDF-HFP: PMMA)–(PC:DEC)–$LiClO_4$ system increases upon the addition of lithium salt up to 7.5 wt.%. The change in the value of the DC conductivity (σ_{DC}) can be explained by the theoretical aspects which is given by

$$\sigma_{DC} = \sum n_i \mu_i q_i, \tag{3}$$

where n_i denotes the charge carrier density, μ_i is the ion mobility and q_i is the charge of the i ion. From this equation, the increase in the DC conductivity has been attributed to the increase in the number of mobile charge carriers n_i and increase in ion mobility μ_i due to increased amorphous nature of the polymer electrolyte which reduces the potential barrier, thereby facilitating ion transport faster.[28] XRD result of the present system which shows the increase in amorphous nature is also in good agreement with variation of conductivity. Ramesh *et al.*[29] have also reported the increase of amorphicity in PVDF-HFP-based polymer electrolyte with the increasing amount of LiTf salt. As the concentration of salt is increased above 7.5 wt.%, the conductivity is found to decrease due to the formation of ion aggregates. The formation of ion cluster is responsible for the decreased number of charge carrier and hence conductivity.

In the present system, the highest value of DC conductivity of the order of 2.83×10^{-4} S cm^{-1} at 303 K is obtained for the electrolyte film containing 7.5 wt.% $LiClO_4$.

3.5. *Temperature-dependent conductivity*

The temperature dependence of ionic conductivity may provide valuable information for ionic conduction behavior. According to Ratner *et al.*,[30] for polymer electrolyte, the temperature-dependent ionic conductivity generally follows two ion transport models: Arrhenius behavior and Vogel Tammann Fulcher (VTF) behavior. In Arrhenius behavior, the plot of σ versus $1000/T$ is typically linear which is indicative of conduction mechanism via hopping mechanism decoupled from segmental motion of polymer chain. In VTF behavior, it shows nonlinear behavior which indicates that the conduction mechanism involves ion hopping coupled with the polymer segmental motion.

Figure 6 shows that the variation of DC conductivity ($\log\sigma_{DC}$) versus reciprocal temperature ($1000/T$) of GPE system with different concentrations of $LiClO_4$ salt.

From the plot, it has been observed that ionic conductivity increases as the temperature increases from 303 K to 363 K for all GPE samples. When the temperature increases, the polymer chains get an easy pathway for the motion of segments, which offer channels for the migration of ions resulting in increased ionic conductivity. According to Mathew *et al.*,[31] in PVAc/PVDF/$LiClO_4$/X, where X=DMC, DEC, PC, GBL system, with the rise in temperature, the polymer expands and produces free volume so that mobile carriers or polymer chain segments can move through the free volume. In order to give a better understanding of the ionic conduction mechanism of the GPE films, the linear behavior of ($\log\sigma_{DC}$) versus reciprocal temperature ($1000/T$) data have been fitted to the Arrhenius relation expressed as

$$\sigma = \sigma_0 \exp\left(\frac{E_a}{K_B T}\right), \tag{4}$$

where σ_0 is the pre-exponential factor, E_a is the activation energy, K_B is the Boltzmann constant and T is the temperature in Kelvin. The activation energy is calculated from the slope of the plot and listed in Table 4. The activation energy for sample containing 10 wt.% $LiClO_4$ is calculated from the slope of fitting line in the temperature region from 303 K to 328 K.

As can be seen from Fig. 7, the sample with maximum ionic conductivity exhibits minimum activation energy. For

Table 4. Conductivity (σ_{DC}), activation energy (E_a), hopping frequency (ω_p) and carrier concentration term (K), Relaxation time ($\tau_{\tan\delta}$), stretching parameter (β) and transport number (t_{ion}) of different GPEs system.

Sample code	Conductivity (σ_{DC}) (S cm^{-1}) at 303 K	Activation energy (E_a) (eV)	Hopping frequency ω_p (Hz)	K (Ω^{-1} cm^{-1} Hz^{-1} K)	Relaxation time $\tau_{\tan\delta}$ (s)	Stretching parameter (β)	Transport number (t_{ion})
S1	5.94×10^{-6}	0.47	1.27 E+07	1.18 E-10	1.24994E-4	0.69	0.97
S2	1.65×10^{-5}	0.39	3.19 E+07	1.57 E-10	9.92865E-6	0.71	0.96
S3	5.73×10^{-5}	0.32	4.01 E+07	4.33 E-10	4.97611E-6	0.61	0.99
S4	2.83×10^{-4}	0.31	6.35 E+07	1.35 E-09	1.98103E-6	0.67	0.99
S5	1.70×10^{-4}	0.53	1.26 E+07	4.10 E-09	9.4626E-6	–	0.97

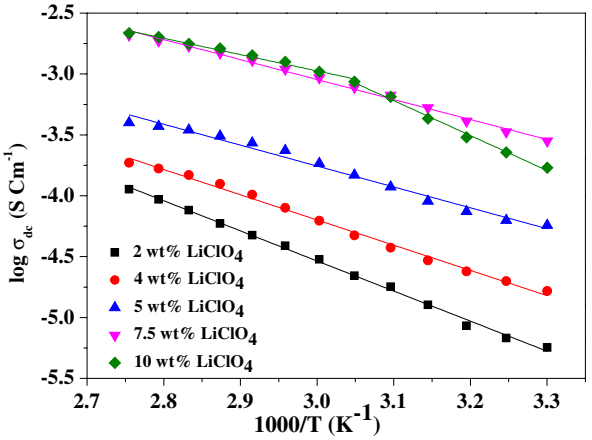

Fig. 6. Temperature dependence of ionic conductivity of GPE with different concentrations of $LiClO_4$.

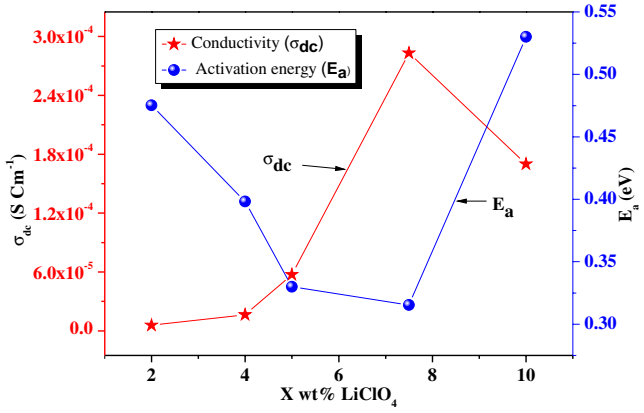

Fig. 7. Conductivity and activation energy versus concentration of $LiClO_4$.

high conducting sample, low activation energy (E_a) is required to acivate the lithium ion for the physical transportation through polymer matrix which is caused by the completely amorphous nature.[32] According to Li *et al.*[33] ions or cluster of ions migrate in the pores of polymer, amorphous domains swelled by electrolyte and along molecular chain of polymer. The migration of lithium ion along the molecular chains of polymer is not appreciable. Hence, it can be stated that increase in conductivity may be due to filled pores with electrolyte and swelled amorphous domain. Thereafter, ion clusters are formed, which mitigate the process of conduction in the polymer electrolyte.

3.6. *Frequency dependent ionic conductivity*

Figure 8 shows the variation of conductivity as a function of frequency at different temperatures for 4 wt.% $LiClO_4$ salt in the GPE system. It is observed from the figure that the frequency-dependent conductivity involves general features which consist of three different regions, (i) a low frequency

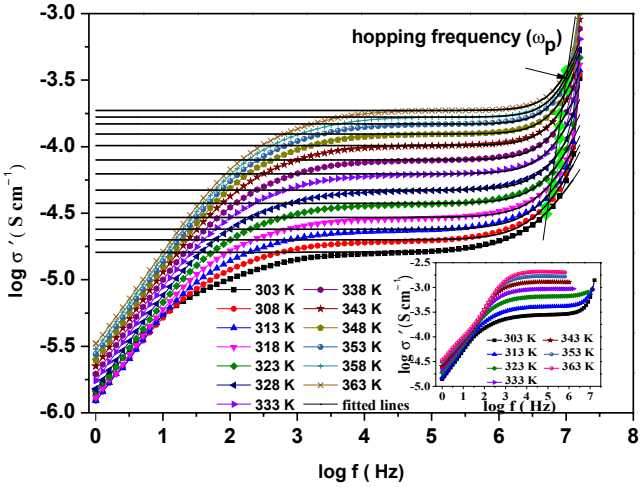

Fig. 8. Variation of conductivity as a function of frequency of GPE with 4 wt.% $LiClO_4$ at different temperatures and the inset shows the variation of conductivity as a function of frequency of GPE with 7.5 wt.% $LiClO_4$ at different temperatures.

dispersive region, (ii) an intermediate frequency plateau region, and (iii) a high frequency dispersion region.[34,35] At lower frequency region, electrode polarization starts with a simultaneous sharp decrease in $\sigma'(\omega)$. This feature may be due to the accumulation of more charges at the electrode–electrolyte interface at low frequency. A low frequency region is followed by an intermediate frequency plateau region in which $\sigma'(\omega)$ remains frequency independent upto a certain frequency. This can be ascribed to the macroscopic DC conductivity of the materials. At intermediate frequency, ions travel much faster and jump from one site to another available site. Successful hop of ion to a neighboring vacant site contributes to the DC conductivity when the frequency is lower than the hopping frequency (ω_p). When the frequency exceeds to hopping frequency (ω_p), the conductivity continues to increase with the increase in frequency. The crossover from the frequency-independent conductivity to the conductivity dispersion indicates that the conductivity relaxation phenomena is occurring. This behavior of the ionic conductivity is according to Jonschers power law: $\sigma(\omega) = \sigma_{DC} + A\omega^n$, where σ_{DC} is the frequency independent DC conductivity, A is the pre-exponential constant, ω is the angular frequency, and n is the power law exponent. Using the above equation, the fitting parameters σ_{DC}, A, and n are obtained. AC conductivity studies also provide information about conductivity relaxation. The ionic conductivity is also ascribed by the factors like concentration of mobile charge carriers and hopping frequency of charge carriers[35] which are estimated by the following equations:

$$\omega_p = \left(\frac{\sigma_{DC}}{A}\right)^{\frac{1}{n}}, \tag{5}$$

$$K = \frac{\sigma_{DC} T}{\omega_p}. \tag{6}$$

From Fig. 8, it is clear that the hopping frequency (shown with solid line) increases with the rise in temperature. This is because increase in temperature results in the expansion of polymer which facilitates the local empty spaces and expands the free volume. These promote the segments and Li ion to move. Consequently, hopping movement of ions is favored and the ions can hop with higher frequency and shorter relaxation time. The AC conductivity plot of higher conducting sample (inset of Fig. 8) does not show high frequency dispersion region as the temperature is increased since the hopping frequency of charge carrier increases or relaxation time is too short to be observed in our system. The shifting of frequency dispersion region of AC conductivity spectrum towards the higher frequency side with rise in temperature is reported by Gondaliya *et al.*[36] in plasticized PEO–$AgCF_3SO_3$–SiO_2 polymer electrolyte system.

The calculated values of hopping frequency (ω_p) and mobile carrier concentration factor (K) for GPE samples containing different salt concentrations at 303 K are tabulated in Table 4. It is observed that as concentration of $LiClO_4$ increases, the transition from frequency-independent plateau region to the AC conductivity dispersion region shift towards the higher frequency side.[37] The increase in the hopping frequency leads to a conclusion that the higher the conductivity of the sample, the shorter is its relaxation time.[38] The carrier concentration term K is following the same trend as conductivity data with increasing salt concentration except GPE containing 10 wt.% $LiClO_4$ where hopping frequency decreases.

To attain better insight on the ion dynamics within polymer electrolyte, the study of scaling behavior of the conductivity spectra is analyzed. The scaling (time temperature superposition principle/thermorheological simplicity) is a tool to examine whether conduction mechanism involving ion dynamics is temperature-dependent or not. Various scaling laws have been proposed for scaling the AC conductivity data.[39–43]

In the present study, Ghosh[42] scaling technique is followed in which the AC conductivity is scaled by the DC conductivity σ_{DC} and the frequency by the crossover frequency f_p which is obtained by fitting conductivity data with power law $\sigma(\omega) = \sigma_{DC} + A\omega^n$.

$$\frac{\sigma'}{\sigma_{DC}} = F\left(\frac{f}{f_p}\right). \tag{7}$$

Scaling of the GPE sample containing 4 wt.% $LiClO_4$ at different temperatures is shown in Fig. 9, from which we note that the scaled spectra at different temperatures for a composition almost merge on a common master curve except a deviation at lower frequencies which might be due to the electrode polarization effect. Thus, we conclude that the relaxation dynamics of charge carriers in the electrolyte follow a common mechanism throughout the entire temperature range which indicates the temperature-independent nature of ion conduction mechanism.[44]

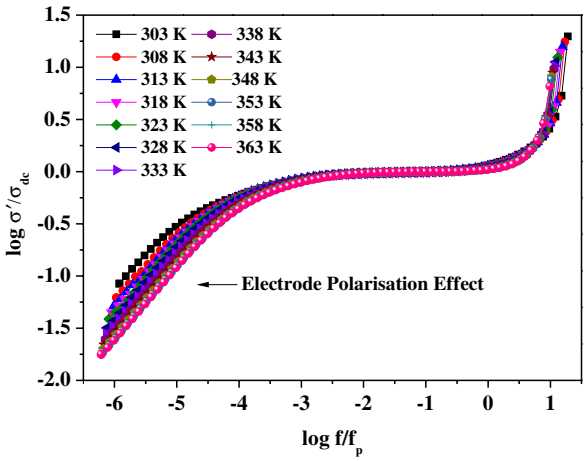

Fig. 9. Scaled conductivity spectra of GPE containing 4 wt.% $LiClO_4$, respectively.

3.7. *Dielectric study*

Dielectric study helps understand the polarization effect at the electrode–electrolyte interface and the conductivity behavior. The frequency-dependent complex dielectric permittivity is given by $\varepsilon^* = \varepsilon' + j\varepsilon''$, where ε' and ε'' are the real and imaginary parts of the dielectric permittivity, known as dielectric constant and dielectric loss, respectively. The significance of these polymer dielectric constant and dielectric loss is to explore the ion conduction and relaxation mechanism. The dielectric constant is a measure of the materials polarization which is associated with the storage of electric charge and also represents the amount of dipole alignment in a given volume.[45] The equation for the dielectric constant (ε') is

$$\varepsilon' = \frac{Z''}{\omega C_0(Z'^2 + Z''^2)}, \tag{8}$$

where Z' and Z'' are the real and imaginary parts of the impedance, ω is angular frequency, and C_0 is the vacuum capacitance.

The dielectric constant (ε') and dielectric loss (ε'') as a function of frequency for GPE with 5 wt.% of $LiClO_4$ at different temperatures are shown in Fig. 10.

At lower frequency region, there is a sharp increase in dielectric constant (ε') which indicates the existence of space charge polarization due to the building up of charge at the interface because of slow periodic reversal effect of the applied field.[46] Hence, the large value of ε' is obtained at lower frequencies. While at high frequency, because of fast periodic reversal effect of the electric field, diffusion of ions is not feasible and incapability of dipoles to orient themselves in the direction of the applied alternating field. Hence, the decrease in the value of ε' has been observed with increasing frequency. It is also revealed from Fig. 10 that the dielectric constant increases with increasing temperatures form 303 K

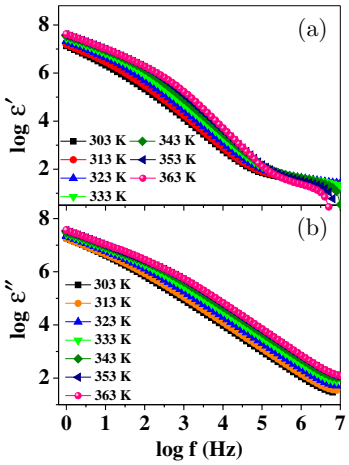

Fig. 10. (a) ε' (dielectric constant) versus log f (b) ε'' (dielectric loss) versus log f for GPE containing 5 wt.% $LiClO_4$ at different temperatures.

to 363 K which is due to the decrease in viscosity of GPE and increasing amorphous nature that facilitates the dipole orientation due to greater freedom of movement of dipole molecular chain of the polymer electrolyte. The dielectric loss (ε'') becomes very large at lower frequencies due to free charge motion within the materials and it decreases with the increase in frequency. However, relaxation effect is masked due to the presence of high conductivity of the material.

Salt concentration dependence of the dielectric constant at 100 Hz, 1 KHz, and 10 KHz is plotted in Fig. 11. It is clear from the figure that the trend observed for dielectric constant is the same as the trend followed by DC conductivity versus salt concentration of $LiClO_4$ salt as studied in the previous section. The highest conducting sample has the highest value of ε'.

At room temperature, the incorporation of $LiClO_4$ up to 7.5 wt.% within the matrix increased the dielectric permittivity $\varepsilon' \approx$ 4.37E+03 to 1.35 E+06 at 100 Hz due to the increased number density of charge carriers as a result of the salt dissociation in the polymer matrix.[47] At 10 wt.% of salt content, Coulomb interaction between Li^+ cations and ClO_4^- anions increases, leading to the re-association of ions to form ion pairs or ion clusters which reduce the mobile charge carrier density and hence their contribution toward electrode polarization thus reduces the value of ε'.[47]

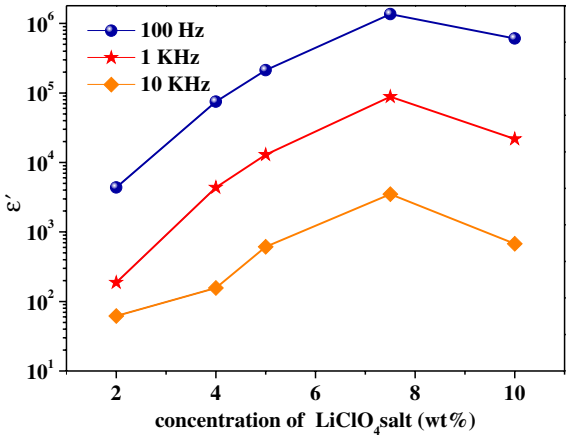

Fig. 11. Variation of dielectric constant with salt concentration variations at 100 Hz, 1 KHz, and 10 KHz.

3.7.1. *Correlation between Z″, tan delta (tan δ) and AC conductivity (σ′)*

Figure 12 shows the Z'' and tan δ versus log f for the GPE sample with 5 wt.% $LiClO_4$ at 308 K. Both Z'' and tan δ show the characteristic peak at different frequencies indicating the occurrence of different relaxation phenomena. The frequency corresponding to Z''_{max} peak of conductivity relaxation can be correlated with the frequency corresponding to a change in ion transport from AC (high frequency dispersion region) to DC (plateau region) in AC conductivity plot (Fig. 12(b)), whereas the peak of tan δ corresponds to the dielectric relaxation where the electrode polarization starts. Furthermore, more information on the relaxation phenomena of system with the variation of salt concentrations is obtained from the plot of loss tangent (tan δ) as a function of frequency.

The value of tan δ is calculated using the following equation:

$$\tan\delta = \frac{\varepsilon''}{\varepsilon'} = \frac{Z'}{Z''}. \tag{9}$$

Figure 13 shows tan δ versus log f curves for GPE for different concentrations of salt at 303 K. This loss tangent plot consists of well-defined peak at characteristic frequency.

The relation between relaxation time ($\tau_{\tan\delta}$) and frequency corresponding to peak (f_p) is

$$\tau_{\tan\delta} = \frac{1}{2\pi f_p}. \tag{10}$$

The loss peak is observed to shift toward higher frequency with increasing salt concentration until 7.5 wt.% $LiClO_4$, thus

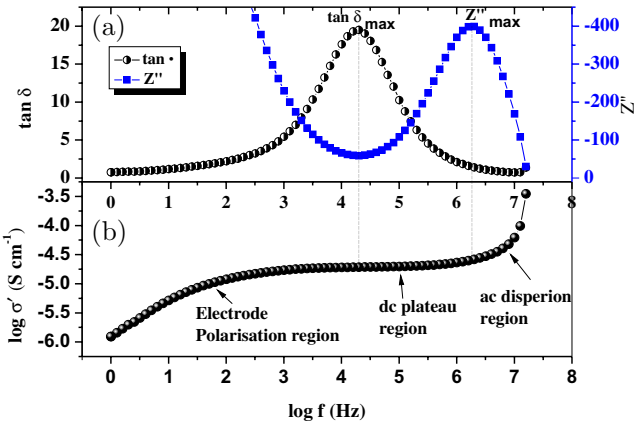

Fig. 12. (a) Z'' and tan δ versus log f (b) log σ' versus log f for the GPE containing 4 wt.% of $LiClO_4$ at 308 K.

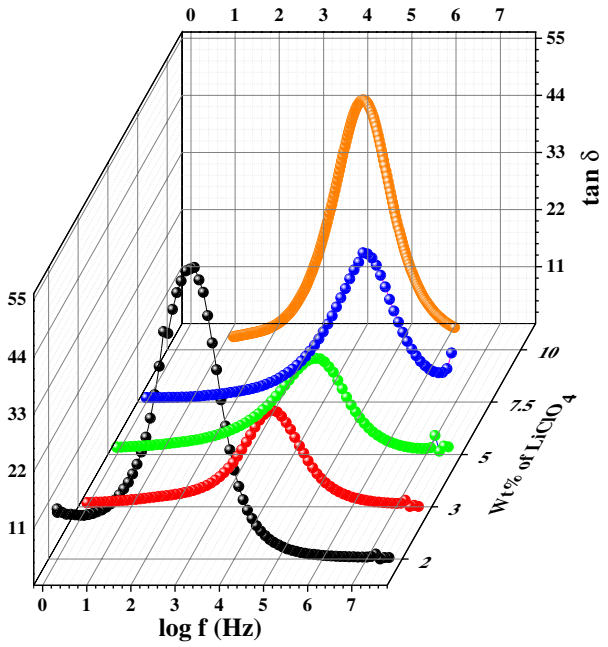

Fig. 13. Variation of loss tangent versus $\log f$ for GPE with different concentrations of $LiClO_4$ at 303 K.

reducing relaxation time. The obtained value of relaxation times are listed in Table 4. The change in the relaxation time is inverse of the DC conductivity variation. The reduction in relaxation time indicates that polymer chain can easily orient through increased amorphous region and/or empty room by incorporating more amounts of salt.

3.8. *Modulus study*

Modulus formalism has been used for further analysis of impedance data which suppresses the electrode–electrolyte polarization effect at lower frequency and highlights the bulk effect at higher frequency. This can be used to study conductivity relaxation behavior. The electric modulus M^* is defined as $M^* = M' + jM''$ or $M^* = j\omega C_0 Z^*$, where M' and M'' are the real and imaginary parts of modulus, respectively.[48]

Figure 14 shows the M'' as a function of $\log f$ for different salt concentrations at 303 K. It shows the characteristic peak at particular frequency (f_{max}) where the value of M'' is maximum. According to Sharma *et al.*,[48] the frequency region where $f < f_{max}$ corresponds to long-range mobility and higher frequency ($f > f_{max}$) part is attributed to ions spatially confined in narrow potential well and the frequency range where peak occurs indicates the transition between long- and short-range mobility.

It is also observed that the position of the peak maximum is shifted to higher frequencies and the height of the peak at high frequency changes with salt concentration. This behavior suggests that the charge carrier hopping has taken place due to the addition of lithium salt due to the increase in

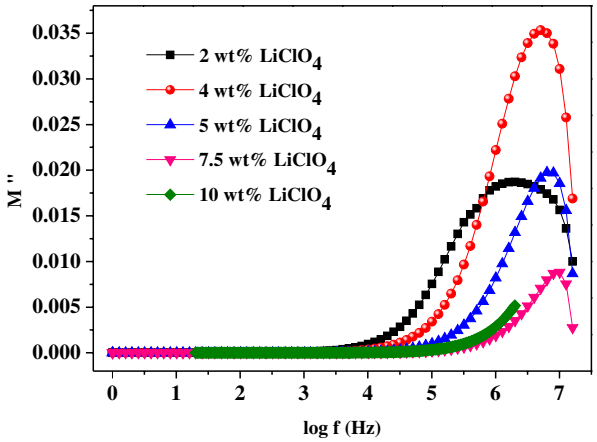

Fig. 14. Variations in imaginary part of modulus (M'') versus $\log f$ for GPE with different concentrations of $LiClO_4$ at 303 K.

the amorphous nature of GPE which indicates the occurrence of a relaxation phenomenon. Similar feature has also been reported by Karmakar *et al.*[49] in PEO–$LiClO_4$ electrolyte system.

In addition to these, the asymmetric and broad nature (broader than ideal Debye peak) of the peaks in M'' curve can be interpreted as being the consequence of the distribution of relaxation time and nonexponential behavior of the conductivity relaxation.[50] The complex electric modulus in the form of a Fourier transform is given by the following relation:

$$M_\infty \left[1 - \int_0^\infty \exp(-i\omega t) \frac{d\phi(t)}{dt}\right]. \tag{11}$$

$M_\infty = \frac{1}{\varepsilon_\infty}$, where ε_∞ is the limiting high frequency real part of permittivity and the function $\phi(t)$ is the relaxation function or Kohlrauch–Williams–Watts (KWW) function represented by[49]

$$\phi(t) = \exp\left(\frac{-t}{\tau}\right)^\beta \tag{12}$$

where β is the nonexponential parameter, $0 < \beta < 1$ is an exponent indicating departure from the debye relaxation ($\beta = 1$), and τ is the relaxation time. The parameter β for the samples are calculated using the formula $\beta = 1.14/\text{FWHM}$ and are listed in Table 4. From Table 4, it is noted that the values of β are less than one, which suggests a greater departure from the ideal Debye response.

The spectroscopic plot, i.e., graphs of Z'' and M'' versus $\log f$ offers a convenient way of presenting the data as suggested by Grant *et al.*[51] They reported the normalized modulus and impedance spectra for ideal solid electrolyte (single RC element) were completely superposable, which can be interpreted as ideal Debye Curve. The plot of Z'' and M'' versus $\log f$ for the sample containing 4 wt.% of $LiClO_4$ at 308 K is shown in Fig. 15. The maxima of Z'' and M'' do not coincide at the same frequency. The peak of Z'' is at lower frequency side, whereas peak of M'' is at higher frequency

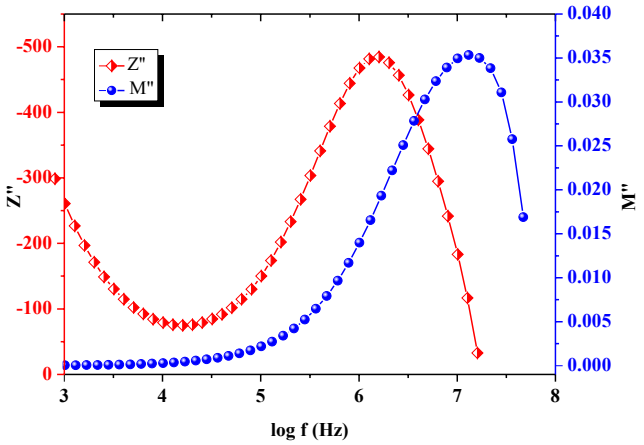

Fig. 15. Spectroscopic plot (Z″ and M″ versus log f) for the GPE containing 4 wt.% of $LiClO_4$ at 308 K.

side having broadened nature indicating wide distribution of relaxation times, i.e., (PVDF-HFP:PMMA)–(PC:DEC)–$LiClO_4$-based GPE films confirm non-Debye nature.

3.9. *Transport number measurements*

For polymer electrolytes to be used in rechargeable battery applications, the main charge carriers should be ions or ionic conductivity should be mainly due to ions only. That is, the fractional contribution of ionic conductivity to the total conductivity should be as close to unity as possible and the fractional contribution of the electronic conductivity should be negligibly small (close to zero). Therefore, it is necessary to determine the fraction of the conductivity due to ions and electrons. The ionic transport numbers (t_{ion}) for the (PVDF-HFP:PMMA)–(PC:DEC)–$LiClO_4$ GPEs were determined by means of the DC polarization technique.[52] In this technique, the polarization current was monitored as a function of time upon the application of a fixed DC voltage across the (stainless steel SS)/GPE/SS cell. The measured current versus time data is plotted for GPE and is shown in Fig. 16.

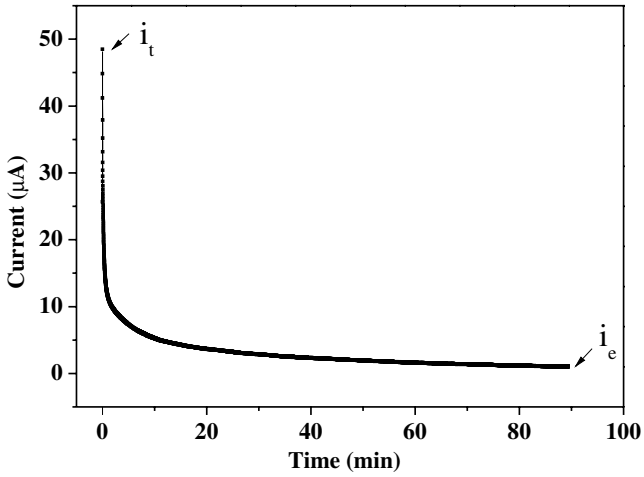

Fig. 16. Polarization current as a function of time for GPE with 4 wt.% $LiClO_4$.

The ionic transport numbers are calculated from the polarization current versus time plot by using Eq. (2). The calculated transport numbers are listed in Table 4. For all the blended polymer gel electrolyte system, the values of the ionic transport number are measured in the range of 0.96–0.99. This suggests that the charge transport in these polymer electrolytes is mainly due to ions and only a negligible contribution comes from electrons.[53]

4. Conclusions

- In the present study, gel polymer blend membranes composed of (PVDF-HFP:PMMA)–(PC:DEC):$LiClO_4$ with different amounts of $LiClO_4$ salt were prepared by a solution casting technique.
- A substantial enhancement in conductivity was observed with the addition of $LiClO_4$. We obtained the maximum ionic conductivity of 2.83×10^{-4} S cm^{-1} for the sample with 7.5 wt.% $LiClO_4$. The increase in the ionic conductivity up to salt concentration of 7.5 wt.% $LiClO_4$ is due to increase in the amorphicity in the gel polymer blend. XRD result, FTIR spectra, and SEM micrographs strongly support our results. At 10 wt.% of $LiClO_4$, the ionic conductivity decreases due to the increase in crystalline nature of GPE.
- The ionic conductivity is temperature-dependent and follows the Arrhenius relation for all systems confirming that ion transport mechanism through hopping mechanism decoupled from polymer chain segmental motion. The lowest activation energy of 0.31 eV and highest conductivity for the sample containing 7.5 wt.% of $LiClO_4$ are due to ease of hopping of ions through amorphous and swelled regions (regions filled with electrolyte) of GPE. This sample possesses lowest relaxation time and shows the presence of micropores which provides pathway for diffusion of ions.
- The increase in the dielectric constant with increasing temperatures as well as salt content reveal the availability of ions due to the dissociation of ion pair and increased amorphicity. The different peak positions of Z″ and M″ spectra confirm the distributed relaxation time and non-Debye nature of the gel electrolyte system. The lower value of $\beta(<1)$ indicates greater departure from ideal Debye-type behavior.
- The high conductivity and ionic transport number (near unity) suggest that these electrolytes are suitable for use in electrochemical devices, especially in lithium ion battery.

References

[1]A. M. Stephan, Review on gel polymer electrolytes for lithium batteries, *Eur. Polym. J.* **42**, 21 (2006).

[2]B. Scrosati, Recent advances in lithium ion battery materials, *Electrochimica Acta* **45**, 2461 (2000).
[3]J. Fang, J. Qiao, D. P. Wilkinson and J. Zhang (eds.), *Electrochemical Polymer Electrolyte Membranes* (CRC Press, 2015).
[4]L. Long, S. Wang, M. Xiao and Y. Meng, Polymer electrolyte for lithium polymers batteries, *J. Mater. Chemis. A* **4**, 10038 (2016).
[5]L. N. Sim and S. M. nad, A. K. Arof, Ftir studies of PEMA/PVDF- HFP blend polymer electrolyte system incorporated with $LiCF_3SO_3$ salt, *Vibr. Spectroscopy* **58**, 57 (2012).
[6]F. Groce, F. Gerace, G. Dautzemberg, S. Passerini, G. Appetecchi and B. Scrosati, Synthesis and characterization of highly conducting gel electrolytes, *Electrochimica Acta* **39**, 2187 (1994).
[7]G. Appetecchi, F. Croce and B. Scrosati, Kinetics and stability of the lithium electrode in poly(methylmethacrylate)-based gel electrolytes, *Electrochimica Acta* **40**, 991 (1995).
[8]N. Krishna Jyothi, K. Vijaya Kumar, G. Sunita Sundari and P. Narayana Murthy, Ionic conductivity and battery characteristic studies of a new PAN-based Na+ ion conducting gel polymer electrolyte system, *Ind. J. Phys.* **90**, 289 (Mar 2016).
[9]A. Subramania, N. T. K. Sundaram, A. R. Priya, R. Gangadharan and T. Vasudevan, Preparation of a microporous gel polymer electrolyte with a novel preferential polymer dissolution process for Li-ion batteries, *J. Appl. Polym. Sci.* **98**, 1891 (2005).
[10]M. Zhang, M. Li, Z. Chang, Y. Wang, J. Gao, Y. Zhu, Y. Wu and W. Huang, A sandwich PVDF/HEC/PVDF gel polymer electrolyte for lithium ion battery, *Electrochimica Acta* **245**, 752 (2017).
[11]H. Choe, J. Giaccai, M. Alamgir and K. Abraham, Preparation and characterization of poly(vinyl sulfone)- and poly(vinylidene fluoride)-based electrolytes, *Electrochimica Acta* **40**, 2289 (1995), International symposium on polymer electrolytes.
[12]R. Miao, B. Liu, Z. Zhu, Y. Liu, J. Li, X. Wang and Q. L. and, PVDF-HFP- based porous polymer electrolyte membranes for lithium-ion batteries, *J. Power Sources* **184**, 420 (2008).
[13]A. Stephan and K. Nahm, Review on composite polymer electrolytes for lithium batteries, *Polymer* **47**, 5952 (2006).
[14]A. M. Stephan, S. Kumar, N. Renganathan and M. Kulandainathan, Characterization of poly (vinylidene fluoridehexafluoropropylene)(PVDFHFP) electrolytes complexed with different lithium salts., *Eur. Polym. J.* **41**, 15 (2005).
[15]L.N. Sim, S. Majid and A. Arof, Characteristics of PEMA/PVDF-HFP blend polymeric gel films incorporated with lithium triflate salt in electrochromic device, *Solid State Ionics* **209**, 15 (2012).
[16]P. Prabakaran and R. Manimuthu, Enhancement of the electrochemical properties with the effect of alkali metal systems on PEO/PVDF-HFP complex polymer electrolytes, *Ionics* **22**, 827 (2016).
[17]K. Isa, Z. Osman, A. Arof, L. Othman, N. Zainol, S. M. Samin, W. Chong and N. Kamarulzaman, Lithium ion conduction and ion-polymer interaction in PVDF-HFP based gel polymer electrolytes, *Solid State Ionics* **268**, 288 (2014).
[18]X. Flora, M. Ulaganathan and S. Rajendran, Role of different plasticizers in li-ion conducting Poly(Acrylonitrile)-Poly(Methyl Methacrylate) hybrid polymer electrolyte, *Int. J. Polymer. Mater. Polymer. Biomater.* **62**, 737 (2013).
[19]S. A. Hashmi, A. Kumar and S. K. Tripathi, Experimental studies on poly methyl methacrylate based gel polymer electrolytes for application in electrical double layer capacitors, *J. Phys. D: Appl. Phys.* **40**, 6527 (2007).
[20]A. Stephan, K. Nahm, M. Kulandainathan, G. Ravi and J. Wilson, Poly(vinylidene fluoride-hexafluoropropylene)(PVDF-HFP) based composite electrolytes for lithium batteries, *Eur. Polym. J.* **42**, 1728 (2006).
[21]M. Ulaganathan, R. Nithya, S. Rajendran and S. Raghu, Li-ion conduction on nanofiller incorporated PVDF-co-HFP based composite polymer blend electrolytes for flexible battery applications, *Solid State Ionics* **218**, 7 (2012).
[22]P. Prabakaran and R. P. Manimuthu, Enhancement of the electrochemical properties with the effect of alkali metal systems on PEO/PVDF-HFP complex polymer electrolytes, *Ionics* **22**, 827 (Jun 2016).
[23]N. Shukla and A. K. Thakur, Role of salt concentration on conductivity optimization and structural phase separation in a solid polymer electrolyte based on PMMA-$LiClO_4$, *Ionics* **15**, 357 (2009).
[24]P. Sharma, D. K. Kanchan and N. Gondaliya, Effect of ethylene carbonate concentration on structural and electrical properties of PEO-PMMA polymer blends, *Ionics* **19**, 777 (2013).
[25]Z. Li, G. Su, D. Gao, X. Wang and X. Li, Effect of Al_2O_3 nanoparticles on the electrochemical characteristics of P(VDF-HFP)-based polymer electrolyte, *Electrochimica Acta* **49**, 4633 (2004).
[26]S. Ramesh and S. Lu, A simple P(VdF-HFP) LiTf system yielding highly ionic conducting and thermally stable solid polymer electrolytes, *J. Molecular Liquids* **177**, 73 (2013).
[27]A. K. Arof, S. Amirudin, S. Z. Yusof and I. M. Noor, A method based on impedance spectroscopy to determine transport properties of polymer electrolytes, *Phys. Chem. Chem. Phys.* **16**, 1856 (2014).
[28]S. Rajedran, V. Bamaand and M. Prabhu, Effect of lithium salt concentration in PVAc/PMMA-based gel polymer electrolytes, *Ionics* **16**, 27 (2010).
[29]S. Ramesh and S. Lu, Effect of lithium salt concentration on crystallinity of poly(vinylidene fluoride-co-hexafluoropropylene)-based solid polymer electrolytes, *J. Molecular Struct.* **994**, 403 (2011).
[30]M. A. Ratner, P. Johansson and D. F. Shriver, Polymer electrolytes: Ionic transport mechanisms and relaxation coupling, *MRS Bullet.* **25**, 3137 (2000).
[31]C. Mathew, K. Kesavan and S. Rajendran, Analysis of plasticizer influence in Poly(vinyl acetate)/Poly(vinylidene fluoride) polymer blend electrolyte, *Ionics* **20**, 439 (2014).
[32]M. Hema, S. Selvasekaranpandian, H. Nithya, A. Sakunthala and D. Arunkumar, Structural and ionic conductivity studies on proton conducting polymer electrolyte based on polyvinyl alcohol, *Ionics* **15**, 487 (2009).
[33]Z. Li, G. Su and X. W. D. Gao, Micro-porous P(VDF-HFP)-based polymer electrolyte filled with Al_2O_3nanoparticles, *Solid State Ionics* **176**, 1903 (2005).
[34]Z. Osman, M. Ghazali, L. Othman and K. Isa, Ac ionic conductivity and dc polarization method of lithium ion transport in PMMA-$LiBF_4$ gel polymer electrolytes, *Result Phys.* **2**, 1 (2012).
[35]N. Shukla, A. K. Thakur and A. S. D. T. Marks, Ion conduction mechanism in solid polymer electrolyte: An applicability of almond-west formalism, *Int. J. Electrochem. Sci.* **9**, 7644 (2014).
[36]N. Gondaliya, D. K. Kanchan, P. Sharma and M. S. Jayswal, Dielectric and electric properties of plasticized PEO-$AgCF_3SO_3$-SiO_2 nanocomposite polymer electrolyte system, *Polym. Composit.* **33**, 2195 (2012).

[37]C. S. Ramya, T. Savitha, S. Selvasekarapandian and G. Hirankumar, Transport mechanism of Cu-ion conducting PVA based solid-polymer electrolyte, *Ionics* **11**, 436 (2005).
[38]R. H. Y. Subban and A. K. Arof, Impedance spectroscopic studies on a binary salt poly (vinyl chloride) based electrolyte, *Ionics* **9**, 375 (2003).
[39]D. L. Sidebottom, Universal approach for scaling the ac conductivity in ionic glasses, *Phys. Rev. Lett.* **82**, 3653 (May 1999).
[40]B. Roling, A. Happe, K. Funke and M. D. Ingram, Carrier concentrations and relaxation spectroscopy: New information from scaling properties of conductivity spectra in ionically conducting glasses, *Phys. Rev. Lett.* **78**, 2160 (Mar 1997).
[41]K. Funke, B. Roling and M. Lange, Dynamics of mobile ions in crystals, glasses and melts, *Solid State Ionics* **105**, 195 (1998).
[42]A. Ghosh and A. Pan, Scaling of the conductivity spectra in ionic glasses: Dependence on the structure, *Phys. Rev. Lett.* **84**, 2188 (Mar 2000).
[43]C. León, P. Lunkenheimer and K. L. Ngai, Test of universal scaling of ac conductivity in ionic conductors, *Phys. Rev. B* **64**, 184304 (Oct 2001).
[44]T. Dam, A. N. Tripathy, M. Paluch, S. S. Jena and D. K. Pradhan, Investigations of relaxation dynamics and observation of nearly constant loss phenomena in PEO_{20}-$LiCF_3SO_3$-ZrO_2 based polymer nano-composite electrolyte, *Electrochimica Acta* **202**, 147 (2016).
[45]Y. M. Yusof, H. A. Illias and M. F. Z. Kadir, Incorporation of nh_4br in PVA-chitosan blend-based polymer electrolyte and its effect on the conductivity and other electrical properties, *Ionics* **20**, 1235 (Sep 2014).
[46]M. Kumar, T. Tiwari and N. Srivastava, Electrical transport behaviour of bio-polymer electrolyte system: Potato starch+ ammonium iodide, *Carbohydrate Polymers* **88**, 54 (2012).
[47]H. J. Woo, S. R. Majid and A. K. Arof, Dielectric properties and morphology of polymer electrolyte based on poly(ε-caprolactone) and ammonium thiocyanate, *Mater. Chemis. Phys.* **134**, 755 (2012).
[48]P. Sharma, D. K. Kanchan, N. Gondaliya, M. Pant and M. S. Jayswal, Conductivity relaxation in Ag+ ion conducting PEO–PMMA–PEG polymer blends, *Ionics* **19**, 301 (Feb 2013).
[49]A. Karmakar and A. Ghosh, Dielectric permittivity and electric modulus of polyethylene oxide (PEO)-$LiClO_4$ composite electrolytes, *Curr. Appl. Phys.* **12**, 539 (2012).
[50]R. Muchakayala, S. Bhavani, K. Kondamareddy and V. Rao, Investigations on electrical properties of PVP:KIO_4 polymer electrolyte films, **19**, 8593 (05 2013).
[51]R. J. Grant, M. D. INGRAM and A. West, An investigation of β-alumina electrolytes by electric modulus spectroscopy, **22**, 729 (07 1977).
[52]D. Kumar and S. A. Hashmi, Ion transport and ionfiller-polymer interaction in poly(methyl methacrylate)-based, sodium ion conducting, gel polymer electrolytes dispersed with silica nanoparticles, *J. Power Sources* **195**, 5101 (2010).
[53]D. Kumar and S. A. Hashmi, Ionic liquid based sodium ion conducting gel polymer electrolytes, *Solid State Ionics* **181**, 416 (2010).

Journal of Materials Science: Materials in Electronics
https://doi.org/10.1007/s10854-019-01585-6

Effect of PC:DEC plasticizers on structural and electrical properties of PVDF–HFP:PMMA based gel polymer electrolyte system

Khushbu Gohel[1] · **D. K. Kanchan**[1]

Received: 18 March 2019 / Accepted: 24 May 2019

Abstract
A gel polymer electrolyte based on poly(vinylidene fluoride–hexafluoropropylene) (PVDF–HFP) and poly(methyl methacrylate) (PMMA) as host polymers, lithium perchlorate ($LiClO_4$) as salt has been prepared with different concentrations of mixture of propylene carbonate (PC) and diethyl carbonate (DEC) (1:1) as plasticizers by using solution casting technique. Changes in structural properties have been studied by X-ray diffraction. Surface morphology has been analyzed using atomic force microscope studies. Electrical conductivity has been carried out by electrochemical impedance spectroscopy in the temperature range 303 K to 343 K. Addition of plasticizers to polymer blend electrolyte has been found to result in an enhancement of the ionic conductivity. A maximum electrical conductivity of 1.03×10^{-3} S cm^{-1} at 303 K has been achieved for the polymer blend gel electrolyte containing 60 wt% of PC:DEC plasticizers. The temperature dependence of the ionic conductivity exhibits Vogel–Tammann–Fulcher type behavior indicating a strong coupling between the ionic conductivity and the polymer chain segmental motions. AC conductivity has been analyzed using Jonscher's power law. A relaxation phenomenon is studied with modulus formalism.

1 Introduction

With increasing demand of energy storage and energy conversion devices in day to day life, polymer electrolytes (PEs) have been found to have increasing interest due to advantageous properties such as leakage proof electrolyte, high ionic conductivity, light in weight, good mechanical strength, high energy density, high specific energy, wide electrochemical stability, easy to prepare, etc. [1]. However, solid PE films have some drawbacks such as relatively low ionic conductivity and electrochemical stability which restricts their use in battery fabrication. Looking into such limitations, Feuillade and Perche in 1975 had introduced gel PE (GPE) also known as plasticized PE [2]. GPE films possess the improved ionic conductivity and significantly enhanced interfacial properties [3]. The ionic conductivity strongly affected by various factors such as

- simultaneous anions and cations motion,
- ion pair formation,
- amorphous nature of film,
- less viscous medium for the motion of ions and
- high dielectric constant.

GPE incorporates both diffusive property of liquids and the cohesive property of solids [4]. GPE based on poly(acrylonitrile) (PAN), poly(vinyl chloride) (PVC), poly(vinylidene fluoride) (PVDF), poly(methyl methacrylate) (PMMA), PVDF–hexafluoropropylene (HFP) has been extensively studied in recent year [5, 6]. The GPE is made-up by blending a large amount of plasticizers into the host polymer such as PAN, PVDF, PMMA, PEO and lithium salt. Polymer forms wide network and establish structural support through which the ion conduction takes place. The ionic conductivity is primary factor of PE to be used as electrolyte in lithium ion batteries. The mobility of ions in the PE determines the conductivity σ and the performance of the PE. A plasticizer, such as ethylene carbonate (EC), propylene carbonate (PC), dimethyl carbonate (DMC), etc. improves the electrical conductivity of PE by enhancing polymer chains flexibility and also improve the stability of electrode/electrolyte interface [7]. Many reports are there with EC and PC plasticizers but the PC + DEC mixture has better properties with such as high

✉ D. K. Kanchan
dkkanchan.ssi@gmail.com

Khushbu Gohel
khushbugohel31@gmail.com

[1] Department of Physics, Faculty of Science, The M.S. University of Baroda, Vadodara, Gujarat 390002, India

Published online: 30 May 2019

dielectric constant and high donor number [3] which increases amorphous content of PE when mixed, reduces ion pairing in PE and lowers the glass transition temperature (T_g) [8]. PC has high dielectric constant ($\varepsilon \approx 64.6$) but has high viscosity ($\eta \approx 2.53$ mPa s), whereas DEC has low dielectric constant ($\varepsilon \approx 2.82$) and low viscosity ($\eta \approx 0.748$ mPa s). Hence, mixture of PC:DEC (1:1) plasticizers having high dielectric constant and lower viscosity is used to achieve high ionic conductivity. In GPE, ionic conduction takes place mainly in the liquid plasticizers, although there are some weak interactions between the polymer matrix and lithium ion. According to Baskaran et al. [9], the addition of plasticizer to the PE decreases the glass transition temperature of the polymer as well as softens the polymer backbone, which result in high segmental motion and thus increases the ionic conductivity. Hence, high dielectric constant (ε), low viscosity (η) are desired properties of organic solvent/plasticizer to form GPE. Mathew et al. [10] reported the influence of plasticizer in PVA/PVDF polymer blend electrolyte and reported that PVDF based polymers are expected to be promising host polymers on account of their high anodic stability due to strong electron withdrawing function group (–C–F) and high dielectric constant ($\varepsilon \approx 8.4$). These properties can promote ionization of salt, thus provide more charge carriers [1]. Generally presence of plasticizers deteriorates the mechanical strength of PE hence, blending of polymers has been considered to enhance mechanical stability in the present study [10]. For this, PMMA is used as a blender with PVDF–HFP polymer due its advantageous properties such as good compatible nature with other polymers, high chemical resistance, surface resistance, electrical properties, etc. [11]. PMMA is not only lightweight and transparent polymer having lesser reactivity toward lithium-metal-based anode but is predominantly insulating with only electronic transport behaviour. It can be modified into an ionically conducting system because it comprises of two probable solvating hetero-atom/polar functional groups (i.e., C=O, O–CH) with electron donating ability, which are important sites for cation coordination playing crucial role in controlling conductivity level and determining the nature of interaction of the ions with the polymer matrix [12]. Lastly, salt is the main component of the PE that provides conducting species to GPE. $LiClO_4$ salt is chosen because of its smaller ionic radius, smaller dissociation energy and the high solubility in most of the organic solvents [10]. In the current work we report the effect of PC:DEC plasticizers in PVDF–HFP:PMMA–$LiClO_4$ system on structural and electrical properties.

2 Materials and methods

2.1 Materials

Poly(vinylidene fluoride-*co*-hexafluoropropylene) (PVDF–HFP) (Mw = 400,000 g mol^{-1}) from Sigma Aldrich and PMMA (Mw = 350,000 g mol^{-1}) was purchased from Alfa Aesar as host polymers. Lithium perchlorate ($LiClO_4$, 99.99%) as salt and organic solvents PC (anhydrous, 99.7%) and diethyl carbonate (DEC, anhydrous, 99.7%) as plasticizers were purchased from Sigma Aldrich to prepare GPE.

2.2 Methods

The samples were prepared by solvent casting technique with the composition shown in Table 1. Appropriate amount of PVDF–HFP and PMMA in equal ratio (1:1) were dissolved in acetone. Weighed amount of $LiClO_4$ salt was then dissolved in different amount of plasticizers PC:DEC which are also taken in equal ratio (1:1). This electrolyte solution was then mixed into the blend solution of polymers. The total mixture was stirred for 8 to 10 h using magnetic stirrer to get homogeneous solution. This solution, which gradually gets viscous due to evaporation of acetone after stirring few hours, was cast onto Teflon Petri dish and kept it above room temperature at about 60 °C to form the gel in the form of film and allowed acetone to evaporate slowly. After the evaporation of acetone, free standing homogeneous and flexible film of thickness of about 0.22 mm were peeled off and kept in vacuum desiccators. The films were used for the different experimental studies. The prepared GPE samples with different weight percentages of plasticizers PC:DEC were subjected to X-ray diffraction analysis, using an X-ray diffractometer (Bruker D2-Phaser) with Cu Kα radiation of wavelength $\lambda = 1.540$ Å in 2θ range of 5°–70° with a step of 0.05°. AFM has been carried out to investigate the surface topology by using easy scan 2 AFM version 2.0 Nanosurf. The ionic conductivity of the various GPE films was measured by impedance spectroscopy in the frequency range 20 Hz to 2 MHz between 303 and 343 K by using a E4980

Table 1 The compositions of GPE system with different concentrations of PC:DEC

Sample code	PVDF–HFP (wt%)	PMMA (wt%)	$LiClO_4$ (wt%)	PC:DEC (wt%)
S1	36.0	36.0	8	20
S2	31.5	31.5	7	30
S3	27.0	27.0	6	40
S4	22.5	22.5	5	50
S5	18.0	18.0	4	60

Agilent LCR meter. The impedance studies were carried out by sandwiching the PE films between two stainless steel electrodes under spring pressure.

3 Results and discussion

3.1 XRD analysis

XRD pattern of PVDF–HFP, PMMA, $LiClO_4$ and PVDF–HFP:PMMA–(PC:DEC)–$LiClO_4$ GPE membranes with different concentrations of PC:DEC plasticizers from 20 to 60 wt% are shown in Fig. 1.

Diffraction pattern of $LiClO_4$ shows high intense characteristics peak which revealed the crystalline nature of the salt. Two broad halos at 29.7° and 38.3° for the pure PVDF–HFP film have been observed which confirmed the amorphous structure of PVDF units in the copolymer [13]. The X-ray pattern for pure PMMA shows a broad halo at $2\theta \approx 13.8°$ which indicates complete amorphous nature of PMMA film. XRD pattern of different composition membranes do not show any characteristics peak of $LiClO_4$ salt indicating the complete dissolution of lithium salt in the polymer matrix [14]. XRD diffraction pattern of GPE samples show no X-ray peaks except a broad peak at about 29°. The increase in the height of peak along with broadening at ~ 29° as the amount of PC:DEC plasticizers increased from 20 to 60 wt% indicates the increasing amorphous nature of the GPE films. This is because when low molecular weight plasticizers PC:DEC are added into the complex system, it promotes the separation of inter and intra chains due to trapping of plasticizer into polymer matrix [14]. Similar features have also been reported by Song et al. in their system 85PVDF–HFP:15$LiBF_4$ + X wt% (EC + PC) systems in which EC:PC has been taken instead of PC:DEC and amount of plasticizer was very high up to 200 wt% [3]. According to Song et al., small-molecule of plasticizer, when added in to the polymer, interrupt the crystalline nature of polymer. Based on the XRD patterns, the degrees of crystallinity of GPE films continues to decrease with the addition of plasticizer amount in the films.

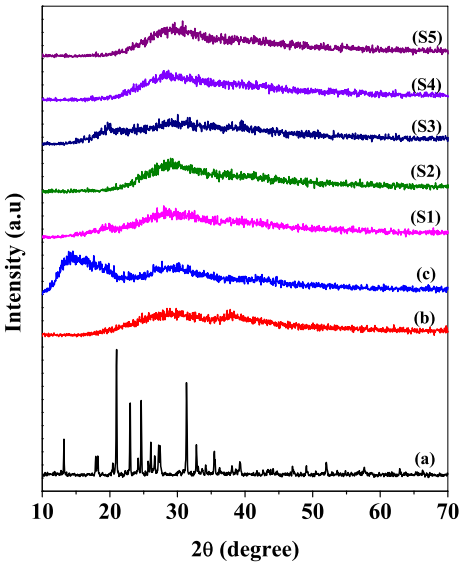

Fig. 1 XRD pattern of (*a*) $LiClO_4$, (*b*) pure PVDF–HFP, (*c*) pure PMMA and PVDF–HFP:PMMA–PC:DEC–$LiClO_4$ salt with PC + DEC content of (*S1*) 20 wt%, (*S2*) 30 wt%, (*S3*) 40 wt%, (*S4*) 50 wt% and (*S5*) 60 wt% respectively

3.2 AFM analysis

In the present study, AFM is used to study the morphological properties of prepared GPE films. Two and three dimensional topographical images of the GPE system containing 30 wt% and 60 wt% PC:DEC are shown in Fig. 2. Two dimensional image of GPE containing 30 wt% PC:DEC shows the presence of pores where as smooth surface has been observed for GPE system containing 60 wt% PC:DEC within the scan are of 63.4 × 63.4 µm. This smooth surface is mainly due to entrapped electrolytes within the pores causes modification in the surface topology which are responsible for easy ionic movement. Another conclusion can be drawn from the figure that the size of pores has been reduced with addition of higher amount of plasticizers indicates plasticizer rich phase of GPE having 60 wt% PC:DEC through which ion conduction takes place. In three dimensional view of topography image, well defined mountain valleys have been observed. The root mean square (rms) roughness values are found to be 552.2 nm and 83.70 nm for the GPE system having 30 wt% and 60 wt% PC:DEC plasticizers respectively. Similar effect has also been reported by Subbu et al. [15] for PEO/PVdC-*co*-AN/$LiClO_4$/EC based system.

3.3 Conductivity study

Ionic conductivity is key factor for PE to be used in device application. The impedance plot of PVDF–HFP:PMMA–PC:DEC–$LiClO_4$ system with different concentrations of PC:DEC content at 303 K is shown in Fig. 3. The plot consists of high frequency semicircle due to bulk effect of GPEs only in the samples with low amount of PC:DEC but a low frequency inclined spike which is due to interface between electrode–electrolyte in all the samples. As plasticizer concentration is increased from 20 to 60 wt%, the disappearance of high frequency circle for the given system indicates the GPE system are mainly high ionic conductor [16].

The intercept of low frequency spike with real axis (Z′) of impedance plot shows the bulk resistance (R_b) of GPEs. From the Fig. 3, it has been observed that the values of R_b

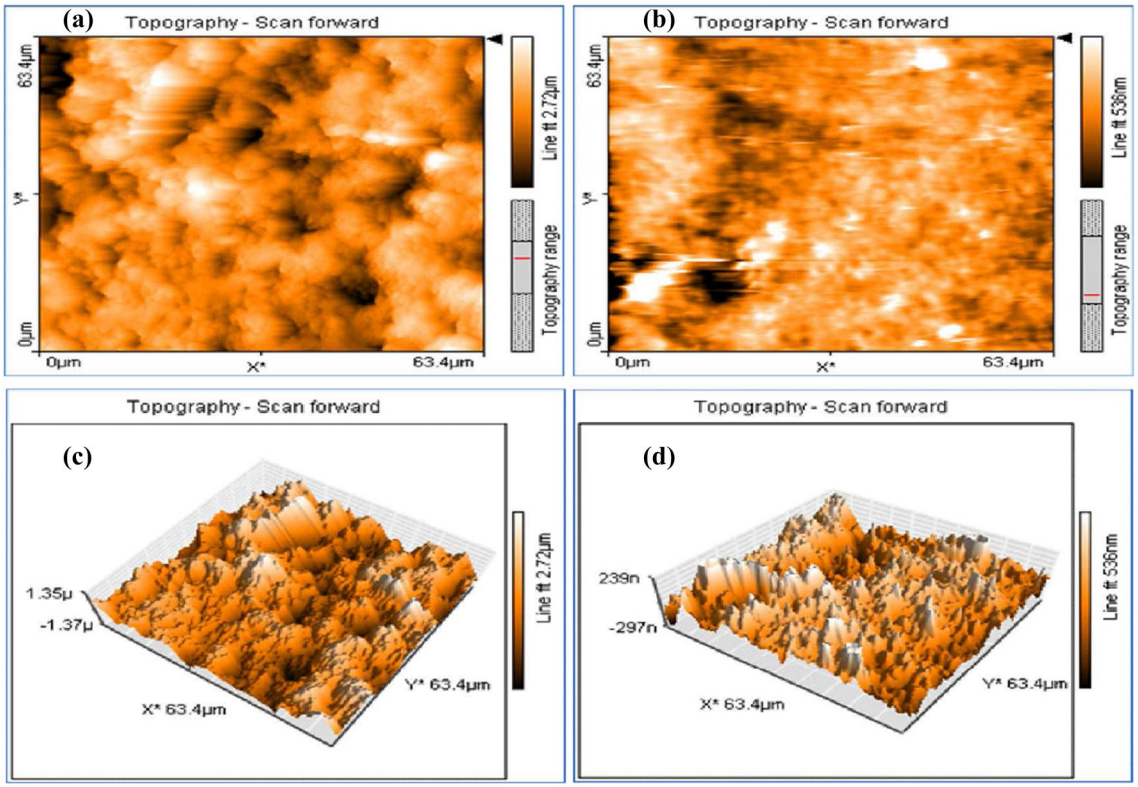

Fig. 2 AFM micrograph of PVDF–HFP:PMMA–PC:DEC–$LiClO_4$ gel polymer electrolyte films: two dimensional view of GPE containing **a** 30 wt% PC:DEC, **b** 60 wt% PC:DEC and three dimensional view of GPE containing **c** 30 wt% PC:DEC and **d** 60 wt% PC:DEC

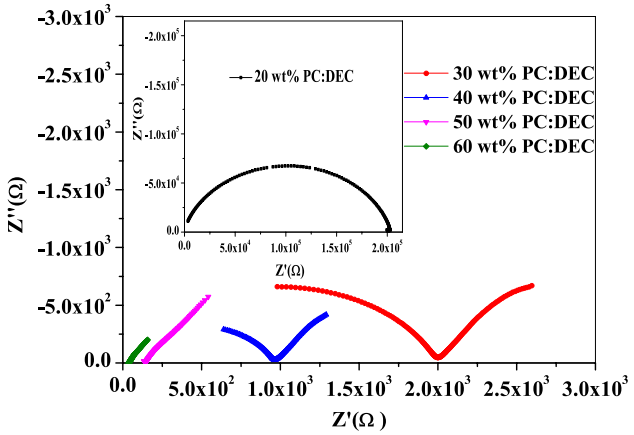

Fig. 3 Impedance plot of PVDF–HFP:PMMA–PC:DEC–$LiClO_4$ system at different concentration of PC:DEC plasticizers at 303 K

decreases as concentration of PC:DEC is increased from 20 to 60 wt%. From the obtained value of R_b, the ionic conductivity σ of the GPE has been calculated using the following equation

$$\sigma = \frac{t}{R_b A}, \tag{1}$$

Table 2 Values of bulk resistance (R_b) and DC conductivity (σ_{dc}) of different GPE system

Sample code	Bulk resistance, R_b (Ω)	DC conductivity, σ_{dc} (S cm^{-1})
S1	286,187.87	1.92E−07
S2	2003.64	1.57E−05
S3	965.6	3.26E−05
S4	144.02	2.62E−04
S5	38.27	1.03E−03

where t is the thickness of the films, A is the contact area of the electrolyte–electrode surface and R_b is the bulk resistance of polymer films. The variation of ionic conductivity with different PC:DEC content are shown in Table 2. It can be seen that the value of the conductivity increases from 1.92E−07 to 1.03E−03 S cm^{-1} with the increasing the amount of PC:DEC plasticizers from 20 to 60 wt%. The value of the DC conductivity (σ_{dc}) can be described by

$$\sigma_{dc} = \sum n_i \mu_i q_i, \tag{2}$$

where n_i denotes the charge carrier density, μ_i is the ion mobility and q_i is the charge of the ith ion. From this

equation, the enhancement in conductivity can be attributed to change in both mobility and carrier concentration. According to Sharma et al. [17], addition of high dielectric constant plasticizer in polymer complexes reduces the interion coulomb interaction and more number of ion contributes toward the conductivity. The purpose of adding PC:DEC plasticizers is to increase the free volume of PEs, resulting in increasing ionic conductivity because the free volume within the polymer increases, rotation of polymer chain occurs more freely and ion transport in PEs becomes more easily. In our system, addition of high dielectric constant and low viscous PC:DEC plasticizer in the polymer matrix results in a dissociation of the salt which increases carrier concentration n_i while carrier mobility μ_i of charge carriers is associated with physical structure of PE. It is believed that in crystalline phase, polymer segments are rigid which resist the mobility of charge carriers and in amorphous nature the polymer segments are flexible which support the easy movement of free charge carriers through polymer matrix. The mobility of charge carrier is affected by the amorphicity of PE. Nevertheless, the XRD result of the present system shows that the amorphicity of GPE increases with increasing the PC:DEC content from 20 to 60 wt% which is in consonance with variation of conductivity. Ulaganathan et al. reported the Li ion conduction in PVAc based hybrid PE system PVAc/PVDF–HFP/$LiClO_4$/X, where X is different plasticizers. He reported the system with maximum conductivity 3.982×10^{-4} S cm^{-1} at 303 K for X = EC. The plasticizer would dissolve enough charge carriers and provides more mobile medium for the ions so as to enhance the conductivity behavior of the sample [18].

3.4 Temperature dependent conductivity

The temperature dependence of ionic conductivity may provide valuable information for ionic conduction behavior. Figure 4 shows complex impedance plot of the system PVDF–HFP:PMMA–PC:DEC–$LiClO_4$ with PC:DEC content of 60 wt% at different temperatures. The intercept of spike with real axis clearly shows a decrease in bulk resistance (R_b) with the increase in temperature and the ionic conductivity of all GPEs system in the temperature range from 303 to 343 K is calculated using Eq. 1.

The variation of log σ_{dc} with the inverse temperature for PVDF–HFP:PMMA–PC:DEC–$LiClO_4$ GPE system at different concentrations of PC:DEC is plotted in Fig. 5. According to Ratner et al., [19] for PE, the temperature-dependent ionic conductivity generally follows Arrhenius behavior and Vogel–Tammann–Fulcher (VTF) behavior which reveal the ion conduction behavior in PE system. In Arrhenius behavior, the plot of log σ versus 1000/T is typically linear which is indicative of conduction mechanism via hopping mechanism decoupled from segmental motion of polymer chain. In VTF

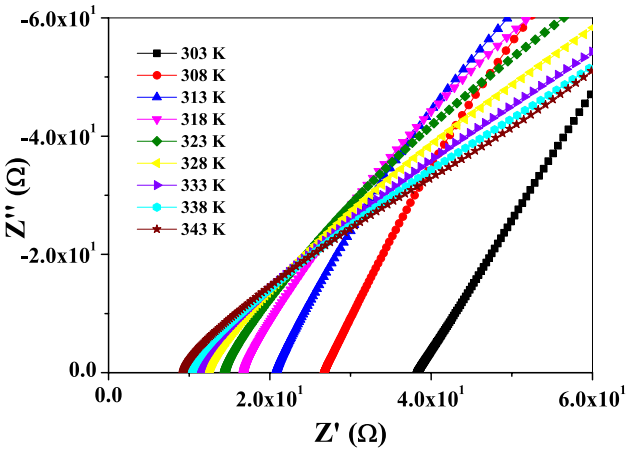

Fig. 4 Impedance plot of PVDF–HFP:PMMA–PC:DEC–$LiClO_4$ GPE containing 60 wt% PC:DEC plasticizers at different temperatures

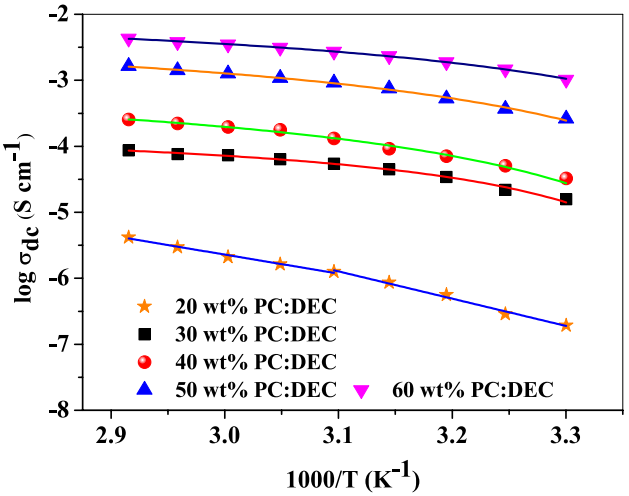

Fig. 5 Temperature dependence of ionic conductivity of PVDF–HFP:PMMA–PC:DEC–$LiClO_4$ GPE with different concentrations of PC:DEC

behavior, it shows nonlinear behavior which indicates that the conduction mechanism involves ion hopping coupled with the polymer segmental motion [20]. The VTF equation is mostly applied for amorphous ionic conductivity, while the Arrhenius equations is applied for ionic conductivity in crystalline system [21]. Figure 5 shows the linear plot of σ_{dc} versus 1000/T for the GPE system containing 20 wt% PC:DEC indicates that temperature dependent conductivity follow Arrhenius relation which is given by

$$\sigma = \sigma_0 exp\left(\frac{-E_a}{K_B T}\right), \tag{3}$$

where σ_0 is the pre-exponential factor, E_a is the activation energy, K_B is the Boltzmann constant and T is the

temperature in Kelvin. This behavior indicates that the ion transport is free from segmental motion. For more than 20 wt% concentration of PC:DEC, temperature dependent ionic conductivity plots show nonlinear behavior (curvature) which seems to obey the VTF relation. In this model, a strong inter relation between the conductivity and segmental motion in polymers is anticipated. The non-linear Arrhenius plot of temperature dependent DC conductivity data is accurately described by the VTF equation as follows:

$$\sigma = \sigma_0 exp\left(\frac{-B}{T - T_0}\right), \tag{4}$$

where σ_0 is the pre-exponential factor, B is the pseudo-activation energy associated with the polymer segmental motion and T_0 ($T_0 = T_g - 50$ K) is the temperature corresponding zero configurational entropy. The VTF behavior has also been observed by Borgohain et al. [22] in PVAc:PVDF:$LiClO_4$ PEs system and it was proposed that the non-linearity behavior of DC ionic conductivity is attributed to the ion transport assisted by the polymer segmental motion. In the present system, Fig. 5 shows the curvature behaviour of the Arrhenius plots which can be attributed to the presence of strong inter-relation between the ionic motion and polymer segmental relaxation means the motion of Li^+ is coupled with polymer segmental motion. It means that the polymer segmental relaxation and ionic motion are strongly coupled in the present GPE system. The parameters in VTF model are evaluated by nonlinear least square VTF fitting and are listed in Table 3.

3.5 AC conductivity

The frequency dependence of the AC conductivity for PVDF–HFP:PMMA–PC:DEC–$LiClO_4$ system with different concentrations of PC:DEC at 303 K is shown in Fig. 6.

The frequency dependent AC conductivity indicates that there are three distinct regions, (i) low frequency dispersion region, (ii) mid frequency independent plateau region, and (iii) high frequency dispersion region. Low frequency dispersion region is due to the accumulation of charge (space charge polarization) at electrode–electrolyte interface due to

Table 3 The Arrhenius and VTF parameters from temperature dependent conductivity

Sample code	Behavior	σ_0	B	T_0
S1	Arrhenius	4.69E−6	–	–
S2	VTF	2.21E−4	57.426	282.13
S3	VTF	1.26E−3	109.365	274.38
S4	VTF	7.38E−3	110.108	270.65
S5	VTF	1.45E−2	92.512	267.79

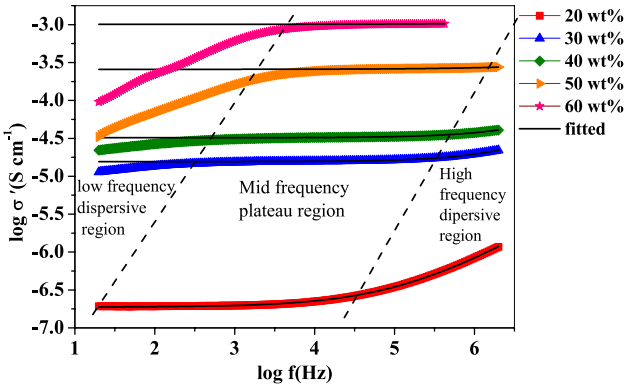

Fig. 6 Frequency dependence of real part (σ') of AC conductivity of PVDF–HFP:PMMA–PC:DEC–$LiClO_4$ GPE with different concentrations of PC:DEC at 303 K

blocking electrode. A mid frequency plateau region is attributed to hopping of the mobile ion due to long range diffusion of ions and known as DC conductivity. High frequency dispersion region is due to short range ion transport attributed to the bulk relaxation of mobile ion hopping which is due to the coulomb interaction of the charge carrier [23]. A crossover from DC ionic to the dispersive conductivity occurs at a particular frequency called crossover frequency. This behavior of AC conductivity follows Jonscher's power law, which is given by

$$\sigma_{ac} = \sigma_{dc} + A\omega^n, \tag{5}$$

where σ_{ac} and σ_{dc} are known as AC and DC conductivity of PEs respectively. While A and n are known as frequency independent pre exponential constant and power law exponent, $0 < n < 1$. The values of n is zero for an ideal Debye dielectric dipolar type material and 1 for an ideal ionic type material [23]. The experimental data is fitted (black solid line as shown in Fig. 6) with Eq. 5. The value of σ_{dc}, A and n obtained by fitting are tabulated in Table 4. From the Fig. 6, it is observed that the high frequency dispersion region is shifted towards higher frequency side as amount of PC:DEC plasticizers is increased which indicates that the system relax much faster. This might be due to increase in plasticizer rich phase with increase in PC:DEC content. For high conducting sample i.e. 60 wt% of PC:DEC, frequency falls outside the experimental frequency range. It is assumed that at a particular frequency i.e. the hopping frequency (ω_p), ac conductivity becomes double of DC conductivity $\sigma_{ac} = 2\sigma_{dc}$ when $\omega = \omega_p$. Hopping frequencies are estimated by following equation and tabulated in Table 4

$$\omega_p = \left(\frac{\sigma_{dc}}{A}\right)^{\frac{1}{n}}. \tag{6}$$

The addition of PC:DEC plasticizer result in increase in DC conductivity and reduction in relaxation time (shown

Table 4 Fitting parameters from Jonscher's power law σ_{dc}, A, n and calculated ω_p, τ of different GPE system

Sample code	DC conductivity (from Jonscher's fitting), σ_{dc} (S cm^{-1})	A	Frequency exponent n	Hopping frequency, ω_p (Hz)	Relaxation time, τ (s)
S1	1.88E−07	1.39E−10	0.61185	1.32E+05	7.60E−06
S2	1.56E−05	1.99E−10	0.7165	6.79E+06	1.47E−07
S3	3.22E−05	4.69E−10	0.67597	1.43E+07	6.97E−08
S4	2.57E−04	1.63E−08	0.48394	4.71E+08	2.13E−09
S5	1.01E−03	4.51E−08	0.46332	2.45E+09	4.08E−10

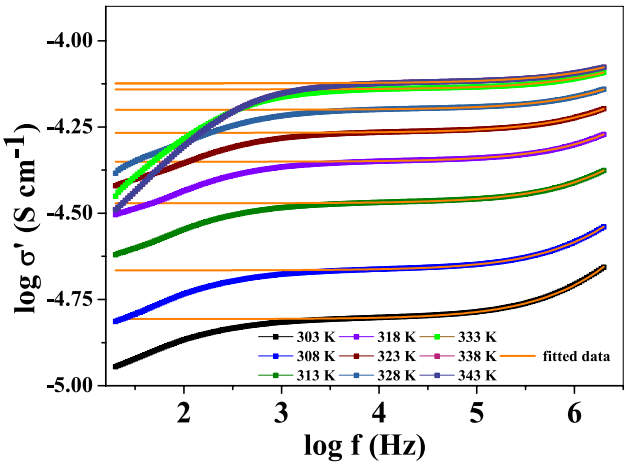

Fig. 7 Variation of log σ' as a function of frequency for PVDF–HFP:PMMA–PC:DEC–$LiClO_4$ GPE containing 30 wt% PC:DEC at different temperatures

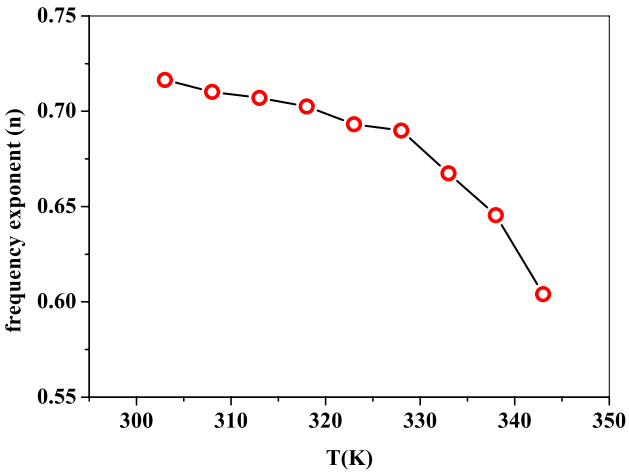

Fig. 8 Variation in frequency exponent (n) with temperature for PVDF–HFP:PMMA–PC:DEC–$LiClO_4$ GPE with 30 wt% PC:DEC

in Table 4, which is calculated from hopping frequencies) evidence of fast ion migration. Similar kind of phenomena have also been observed by Pradhan et al. [24] for $(PEO)_{25}$ − NaI + 5 wt% DMMT + X wt% PEG system where X = 0, 10, 20, 30, 50. To explain ion conduction mechanism involved in the present GPE system based on the variation of frequency exponent (n) with temperature, it is estimated from variation of log σ' as a function of frequency for GPE with 30 wt% PC:DEC at different temperatures (Fig. 7) by fitting it with Eq. 5 The frequency exponent (n) as a function of temperature for the GPE system having 30 wt% of PC:DEC is shown in Fig. 8. Various model have been proposed to explain conductivity mechanism such as correlated barrier hopping (CBH), quantum mechanical tunneling (QMT), the small polaron (SP), and the overlapping large polaron (OLP) given in Table 5 [25].

In our system, the decreasing trend of frequency exponent (n) with temperatures suggests that the CBH model is suitable for interpretation of ionic conduction mechanism.

Table 5 Applicable models with the variation in frequency exponent (n) as a function of temperatures

Variation in frequency exponent (n) with temperatures	Applicable models
Decreases with temperature	Correlated barrier hopping (CBH)
Temperature independent	Quantum mechanical tunneling (QMT)
Increases with temperature	Small polaron (SP)
Decreases with temperature and again increases	Overlapping large polaron (OLP)

3.6 Modulus study

The electric modulus highlights the bulk properties of PE system at higher frequency side and can be used to understand the conductivity relaxation phenomena. The modulus can be expressed by $M^* = j\omega C_0 Z^*$ or $M^* = M' + jM''$, where M' and M'' are the real and imaginary parts of modulus, respectively. Figure 9 shows the frequency dependence imaginary part of modulus (M'') for PVDF–HFP:PMMA–$LiClO_4$–PC:DEC system for different concentration of PC:DEC at 303 K. It shows the high frequency curve (single relaxation peak) may be attributed to bulk effect (ionic conductivity relaxation) [26]. According to Druger S. D. et al., increase in M'' at higher frequency is related to jumping of ion from one site to other site over a long distance [27]. Long tail at lower frequency region is due

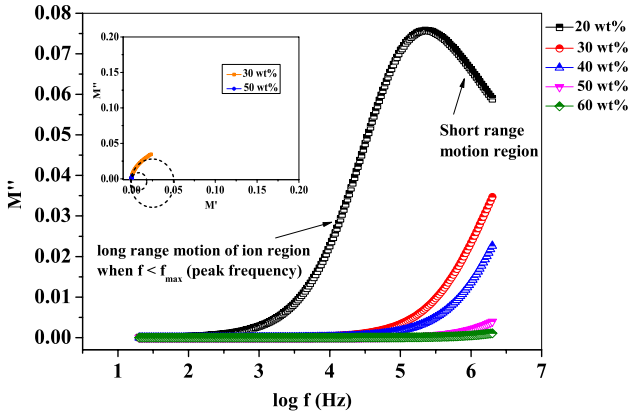

Fig. 9 Imaginary part of modulus (M'') of PVDF:HFP–PMMA–PC:DEC–$LiClO_4$ GPE at different wt% of PC:DEC at 303 K (inset: Argand plot for PVDF:HFP–PMMA–PC:DEC–$LiClO_4$ system with 30 wt% and 50 wt% PC:DEC at 303 K)

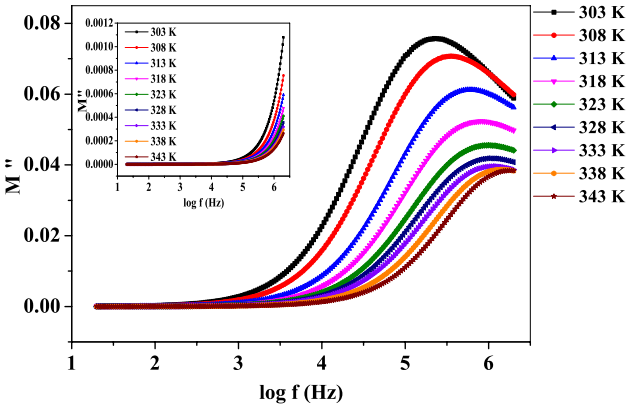

Fig. 10 Imaginary part of modulus (M'') for PVDF:HFP– PMMA–PC:DEC–$LiClO_4$ GPE containing 20 wt% PC:DEC at different temperatures (inset: GPE containing 60 wt% PC:DEC)

to the electrode polarization phenomenon which shows M'' makes a negligible contribution means $M'' \rightarrow 0$ as $\omega \rightarrow 0$ which suggest that the large capacitance values associated with the electrodes. Similar feature is also reported by Saminatha Kumaran et al. [28].

Another conclusion is drawn from the spectra that the position of the peak maximum is shifted to higher frequencies side indicates the occurrence of a relaxation phenomenon with increasing amount of PC:DEC. For higher conducting samples, shorter conductivity relaxation time has been observed. The height of the peak at high frequency changes with plasticizer PC:DEC concentration. This behavior suggests that the charge carrier hopping has taken place due to the addition of plasticizer might be due to the increase in the amorphous nature of GPE. The asymmetric and broad nature of conductivity relaxation can be explained by Kohlrausch–Williams–Watts function [29]

$$\varphi(t) = \varphi_0 exp\left(\frac{-t}{\tau}\right)^{\beta}, \quad 0 < \beta < 1, \tag{7}$$

where τ and β are the conductivity relaxation time and Kohlrausch exponent respectively.

Figure 9 (inset) is the Argand plot for PVDF:HFP–PMMA–$LiClO_4$–PC:DEC system with 30 wt% and 50 wt% PC:DEC concentration shows a deformed semicircle which reveals the broad relaxation processes and non Debye behavior [30]. However complete semicircle is not observed, hence, for better visibility, extrapolation of semicircle is done. Smallest semicircle indicate higher capacitance is associated for GPE system with higher concentration of PC:DEC. M'' versus log f plot for PVDF–HFP: PMMA–PC:DEC–$LiClO_4$ system with 20 wt% and 60 wt% PC:DEC plasticizers at different temperatures from 303 to 343 K is shown in Fig. 10 and inset of Fig. 10 respectively. With the raise of temperature, the peak is shifted towards higher frequency side and height of the peak decreases suggesting that occurrence of relaxation mechanism [31]. The conductivity relaxation is thermally activated.

4 Conclusions

- A GPE comprised of PVDF–HFP and PMMA with lithium perchlorate ($LiClO_4$) salt has been prepared with different concentrations of mixture of PC and DEC (1:1) as plasticizers by using solution casting technique.
- It has been found that the ionic conductivity increases with increasing the PC:DEC plasticizers from 20 to 60 wt% and the maximum room temperature dependent ionic conductivity is found to be 1.03E−03 S cm^{-1} for PVDF–HFP:PMMA–PC: DEC–$LiClO_4$ system with PC:DEC content of 60 wt%.
- The increase in the conductivity is due to increase in the amorphicity of GPE system which is good agreement with the XRD result.
- Temperature dependent conductivity follows the VTF behavior except the system with 20 wt% PC:DEC confirming that ion conduction mechanism is coupled with segmental motion of polymer chain.
- The two and three-dimensional topographic images of the sample having a maximum ionic conductivity show plasticizer rich phase with low rms roughness values which are responsible for easier ionic conduction and high ionic conductivity.
- Frequency dependent AC conductivity has been interpreted by applying Jonscher's power law and from temperature dependent of frequency exponent (n), it can be

concluded that conduction mechanism in our system is attributed to the CBH model.
- The shifting in M'' peak shows that conductivity relaxation occurs due to charge carriers hopping mechanism.
- Broad peak of M'' and deformed semicircle in Argand plot revels the non Debye nature of our GPEs system means wider distribution of relaxation times.

References

1. Z. Dong, Q. Zhang, C. Yu, J. Peng, J. Ma, X. Ju, M. Zhai, Ionics **19**, 1587 (2013)
2. G. Feuillade, P. Perche, J. Appl. Electrochem. **5**, 63 (1975)
3. S. Song, J. Wang, J. Tang, R. Muchakayala, R. Ma, Ionics **23**, 3365 (2017)
4. A.M. Stephan, K. Nahm, Polymer **47**, 5952 (2006)
5. A. Arya, A.L. Sharma, Ionics **23**, 497 (2017)
6. Z. Osman, M.M. Ghazali, L. Othman, K.M. Isa, Results Phys. **2**, 1 (2012)
7. K. Vignarooban, M. Dissanayake, I. Albinsson, B.E. Mellander, Solid State Ion. **266**, 25 (2014)
8. P.C. Sekhar, P.N. Kumar, A.K. Sharma, IOSR J. Appl. Phys. **2**, 01 (2012)
9. R. Baskaran, S. Selvasekarapandian, G. Hirankumar, M. Bhuvaneswari, J. Power Sources **134**, 235 (2004)
10. C.M. Mathew, K. Kesavan, S. Rajendran, Ionics **20**, 439 (2014)
11. R. Subadevi, M. Sivakumar, S. Rajendran, H.C. Wu, N.L. Wu, Ionics **18**, 283 (2012)
12. T. Ren, X. Huang, X. Zhao, X. Tang, J. Mater. Sci. **38**, 3007 (2003)
13. K. Gohel, D.K. Kanchan, J. Adv. Dielectr. **08**, 1850005 (2018)
14. P. Pal, A. Ghosh, J. Appl. Phys. **120**, 045108 (2016)
15. C. Subbu, S. Rajendran, K. Kesavan, R. Premila, Ionics **22**, 229 (2016)
16. O. Mahendran, S. Rajendran, Ionics **9**, 282 (2003)
17. P. Sharma, D.K. Kanchan, N. Gondaliya, Ionics **19**, 777 (2013)
18. M. Ulaganathan, S. Rajendran, Ionics **16**, 667 (2010)
19. M.A. Ratner, P. Johansson, D.F. Shriver, MRS Bull. **25**, 31–37 (2000)
20. S.B. Aziz, T.J. Woo, M. Kadir, H.M. Ahmed, J. Sci. Adv. Mater. Devices **3**, 1 (2018)
21. W. Wang, P. Alexandridis, Polymers **8**, 387 (2016)
22. M.M. Borgohain, T. Joykumar, S. Bhat, Solid State Ion. **181**, 964 (2010)
23. A. Arya, A.L. Sharma, J. Phys. Condens. Matter **30**, 165402 (2018)
24. D.K. Pradhan, R. Choudhary, B. Samantaray, Mater. Chem. Phys. **115**, 557 (2009)
25. S.B. Aziz, OGh Abdullah, S.R. Saeed, H.M. Ahmed, Int. J. Electrochem. Sci. **13**, 3812 (2018)
26. R. Richert, H. Wagner, Solid State Ion. **105**, 167 (1998)
27. S.D. Druger, M.A. Ratner, A. Nitzan, Phys. Rev. B **31**, 3939 (1985)
28. V. Saminatha Kumaran, H.M. Ng, S. Ramesh, K. Ramesh, B. Vengadaesvaran, A. Numan, Ionics **24**, 1947 (2018)
29. G. Williams, D.C. Watts, Trans. Faraday Soc. **66**, 80 (1970)
30. P. Sharma, D.K. Kanchan, N. Gondaliya, M. Pant, M.S. Jayswal, Ionics **19**, 301 (2013)
31. S. Ramesh, O.P. Ling, Polym. Chem. **1**, 702 (2010)

Materials Research Express

PAPER • **OPEN ACCESS**

Gel polymer electrolyte based on PVDF-HFP:PMMA incorporated with propylene carbonate (PC) and diethyl carbonate (DEC) plasticizers : electrical, morphology, structural and electrochemical properties

To cite this article: Khushbu Gohel *et al* 2020 *Mater. Res. Express* **7** 025301

Materials Research Express

PAPER

Gel polymer electrolyte based on PVDF-HFP:PMMA incorporated with propylene carbonate (PC) and diethyl carbonate (DEC) plasticizers : electrical, morphology, structural and electrochemical properties

Khushbu Gohel[1], **D K Kanchan**[1], **Hiren K Machhi**[2], **Saurabh S Soni**[2] **and C Maheshwaran**[1]

[1] Department of Physics, Faculty of Science, The M.S. University of Baroda, Vadodara 390002, Gujarat, India
[2] Department of Chemistry, Sardar Patel University, Vallabh Vidyanagar 388 120, Gujarat, India

E-mail: d_k_kanchan@yahoo.com

Keywords: gel polymer electrolyte, Ionic conductivity, SEM, Dielectric properties, cyclic Voltammetry(CV)

OPEN ACCESS

RECEIVED
30 October 2019

REVISED
21 December 2019

ACCEPTED FOR PUBLICATION
15 January 2020

PUBLISHED
4 February 2020

Abstract

To overcome the drawbacks of organic solvent—based liquid electrolytes and a solid polymer electrolyte as a separator in lithium polymer battery, in the recent study gel polymer electrolyte (GPE) using poly(vinylidene fluoride— hexafluropropylene) (PVDF—HFP) and poly (methyl methacrylate) (PMMA) as host polymers, lithium perchlorate ($LiClO_4$) salt as conducting species and propylene carbonate (PC) and diethyl carbonate (DEC) plasticizers as an organic solvent has been prepared. The solution casting technique has been adopted to fabricate gel polymer electrolyte (GPE). The prepared GPE films were analyzed using different experimental techniques to discover the properties of GPE. The ionic conductivity of GPE films has been carried out using electrochemical impedance spectroscopic technique. The maximum ionic conductivity of 3.97E-4 S cm^{-1} has been obtained for GPE having 60 wt% PC:DEC. As an evidence of change in ionic conductivity, structural characterization has been analyzed using FTIR and SEM where, FTIR spectra reveal complex formation taking place between polymers, salt, and plasticizers and SEM micrograph shows a change in surface morphology with a change in plasticizers amount. Dielectric analysis has been also carried out in terms of dielectric constant (ε') and dielectric loss (ε''). Cyclic voltammetry (CV) has been applied to find electrochemical stability window.

1. Introduction

Nowadays, research has been focused on the development of energy storage and conversion field due to the demand for electrochemical devices in our day to day life. In any electrochemical devices, the electrolyte plays an important role [1]. It is used as a separator to avoid contact between the electrodes and conduction of ions takes place through this electrolyte as shown in figure 1 which depict the basic structure of a battery. As a separator, polymer electrolyte (PE) has been used as a potential candidate in energy storage devices which has taken place of liquid electrolyte (organic solvent + salt) due to certain drawbacks such as leakage of liquid electrolyte, internal shorting of electrodes and explosion etc [2]. These properties of liquid electrolyte make it unsafe during application as separator in electrochemical devices [3]. A number of researches have been attempted to deal with these problems by replacing the liquid electrolyte with polymer electrolyte. As a separator in lithium polymer battery, polymer electrolytes should possess following characteristics :(i) high values of ionic conductivity, (ii) better mechanical integrity, (iii) large electrochemical stability window $\geqslant$ 4 V, (iv) Li^+ transport number $t_{Li^+} \approx 1$, and (v) low electronic conductivity. Polymer electrolytes (PEs) are formed by doping ionic salt/ inorganic acid in polymer doped with ionic salt or inorganic acid which results in the Lewis acid-base complex electrolytes. The ionic conduction in polyether(PEO)— salt complexes to electrochemical devices was first explained by Fenton in 1973 [4]. These polymer electrolytes have been the attraction of many researchers owing to unique properties such as free from leakage, high mechanical strength, more flexible, easy to form in any shape and size [5, 6]. Despite such interesting properties, these solid polymer electrolytes suffer from some

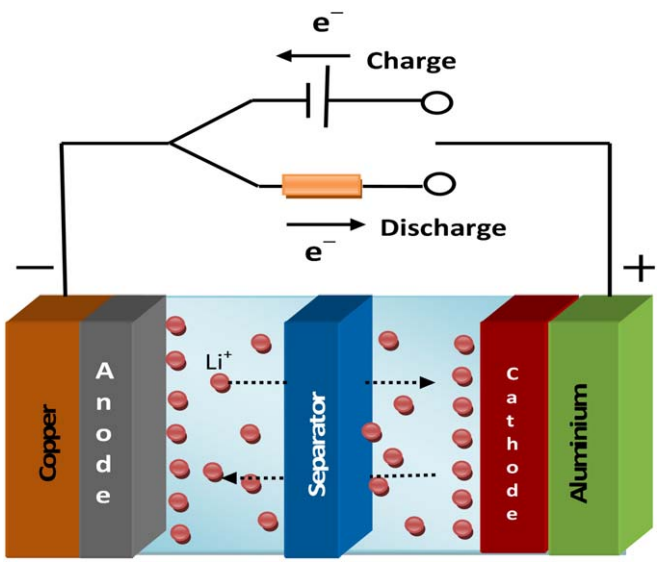

Figure 1. Basic structure of a typical battery.

drawbacks such as low value of ionic conductivity, electrochemical stability window prevent its applications in electrochemical devices [7]. To face the above shortcomings, the research has been carried out on preparing gel polymer electrolyte(GPE) because of its high ionic conductivity very near to the value of liquid electrolyte [8].

In fact, the GPE has the cohesive properties of solid and diffusive properties of the liquid. The GPE can be prepared by trapping the liquid electrolyte (plasticizers/organic solvents + salt) in the host polymer such as such as poly(ethylene oxide)(PEO) [9], poly(methyl methacrylate)(PMMA) [10], poly(vinyl pyrrolidone)(PVP) [11], poly(acrylonitrile)(PAN) [12], poly(vinyl acetate) (PVAc) [13], poly(vinylidene fluoride) (PVDF) [14], and poly (vinylidene fluoride −co− hexafluoropropylene) (PVDF−HFP) [15]. Among all of the above polymers, PVDF −HFP copolymer has been found as a promising polymer host on account of its many excellent properties such as semicrystalline nature, excellent thermal stability, good mechanical, and wider electrochemical stability. Another properties including high dielectric constant ($\varepsilon = 8.4$) as well as low glass transition temperature ($T_g = -62\ ^{\circ}\mathrm{C}$) assist for greater dissociation of lithium ion species which delivers more mobile ions in the system that take part in conduction process [16, 17]. The structure of PVDF−HFP is made up of a crystalline part (VDF unit) and amorphous part (HFP unit) [18]. The crystalline part provides mechanical integrity whereas higher free volume due to the amorphous part assist for a traping liquid electrolyte which results in high ionic mobility hence ionic conductivity [19]. In addition to these, the existence of strong electron withdrawing functional groups (−C−F) in PVDF polymer chains provides better anodic stability [8]. The main component required to prepare GPE is plasticizers which are low molecular weight organic carbonates having slow evaporation.The GPE is comprised of single plasticizer or mixture of two or more includes ethylene carbonate (EC), propylene carbonate (PC), dimethyl carbonate (DMC), diethyl carbonate (DEC), dimethyl formamide (DMF) [1]. Recently, various GPEs system have been reported by a group of researchers by using various plasticizers to boost the structural, electrical and electrochemical properties [20, 21]. Subbu *et al* [22] have designed the GPE system comprised of PEO/PVdC−co−AN /$LiClO_4$/X plasticizers. In their report, they studied the physical and electrochemical properties of GPE with various plasticizers i.e. EC, PC, gBL, DEC, DMP, DBP and reported maximum ionic conductivity of 3×10^{-4} S cm^{-1} at ambient temperature for the film with EC plasticizers by virtue of its high dielectric constant.

When these plasticizers are added to host polymer, it plays following roles (i) reduce ion pairing (dissociation of salt) results in increasing free charge carriers which take part in conduction process and (ii) soften the polymer backbone promotes the higher segmental motion of polymer chains [23]. Thus by introducing plasticizers into polymers, the physical structure can be modified that assist for the easier transportation of ions through polymer and leads to enhancement of ionic conductivity and overall performance of the lithium−ion battery. Hence, the fundamental key to promote greater ion-pair dissociation, high dielectric constant and low viscous properties of plasticizers are essential. In the present study, the combination of PC (dielectric constant, $\varepsilon \approx 64.4$ and viscosity, $\eta \approx 2.53$ mPa S) and DEC (dielectric constant, $\varepsilon \approx 2.82$ and viscosity, $\eta \approx 0.748$ mPa S) have been chosen. A serious drawback of using plasticizers is degrading mechanical strength of polymer electrolytes. To eliminate this issue, blending with poly(methyl methacrylate) (PMMA) has been considered as an effective approach to strengthening mechanical integrity in our present study. In the current study, the investigation on structural,

electrical and electrochemical properties of PVDF−HFP:PMMA−$LiClO_4$ based gel polymer electrolyte system with different amount of PC and DEC plasticizers is reported.

2. Materials and methods

2.1. Materials

As host polymers, Poly(vinylidene fluoride−co−hexafluoropropylene) (PVDF − HFP) ($M_W = 400{,}000$ g mol^{-1}) and poly(methyl methacrylate) (PMMA) ($M_W = 350{,}000$ g mol^{-1}) was purchased from Sigma Aldrich and Alfa Aesar respectively. Lithium perchlorate ($LiClO_4$, 99.99%) from Sigma Aldrich is used as conducting species. The organic solvents propylene carbonate (PC, anhydrous, 99.7%) and diethyl carbonate (DEC, anhydrous, 99.7%) were procured from Sigma Aldrich and it is used as plasticizers to prepare gel polymer electrolyte.

2.2. Methods

The solvent casting technique was used to prepare gel polymer electrolyte system PVDF−HFP:PMMA−$LiClO_4$− PC:DEC with different concentrations of PC:DEC and the compositions of the system are shown in table 1. Fixed amount of polymers, i.e. PVDF−HFP and PMMA in the equal ratio (1:1) were dissolved in acetone. A weighed amount of $LiClO_4$ salt was then dissolved in a different amount of plasticizers PC:DEC which are also taken in the equal ratio (1:1). This electrolyte solution (plasticizers + salt) was then mixed into the polymer blend solution. This mixture was stirred for 8 to 10 hours using a magnetic stirrer to gets a homogeneous solution. Upon continuous stirring, evaporation of acetone was done and viscous solution were obtained. After that, it was poured onto Petri dish and the solution was kept at about 60 °C to form the solution in the form of film. The films were peeled off having thickness of 0.22 mm approximately which was homogeneous and flexible in nature. All films were stored in vacuum desiccators for the further experimental studies. AC impedance spectroscopy method was used to analyze the ionic conductivity of different GPE films in the frequency range 1 Hz to 32 MHz by using a high precision Solartron 1260 Impedance analyzer. The GPE films were sandwiched between two stainless steel electrodes under constant spring pressure to carry out impedance studies. The surface morphology of the films was examined by a JEOL JSM-6010LA scanning electron microscope (SEM). Gel polymer electrolyte films were subjected to Fourier transform infrared (FTIR) study to investigate the complexation behavior. FTIR spectroscopic studies were carried out using FTIR 4100 JASCO model in the wave number range of 400–4000 cm^{-1} with the spectral resolution of 4 cm^{-1}. Cyclic Voltammetry (CV) were performed using Solartron 1287 electrochemical interface and 1260 impedance gain phase analyzer by sandwiched polymeric gel electrolyte between two stainless steel electrode sweeping over a frequency range of 1.2 MHz to 0.1 Hz with 10 mV input of AC amplitude with 50 mV scan rate.

3. Results and discussion

3.1. Ionic Conductivity

Figure 2 represents the complex impedance plots of PVDF−HFP:PMMA −$LiClO_4$− PC:DEC GPE system with various concentrations of PC: DEC plasticizers at 303 K. From the figure, it can be seen that low−frequency spikes is followed by high−frequency semicircle [24]. A high−frequency semicircle represents the parallel combination of a resistor and a capacitor whereas spikes at low− frequency region is indication of charge accumulation due to blocking electrodes [25]. Obviously, the diameter of the semicircle reduces as the amount of PC:DEC plasticizers increases and also the disappearance of semicircle have been observed for GPE with the highest amount of plasticizers i.e. 60 wt%.PC:DEC. The inset of the figure 2 shows an equivalent ac electrical circuit of the impedance information of GPE material consisting of a parallel combination of resistor (R_b) and constant phase element (CPE1) with a constant phase element (CPE2) in series and the importance of the same circuit was addressed previously [26].

The bulk resistance (R_b) of GPE system were extracted by fitting the semicircle using the Z-view software. Generally, R_b is the difference between the real values (Z') of high-frequency and low-frequency values of semicircle.

The ionic conductivity (σ) of electrolyte is given by

$$\sigma = \frac{t}{R_b A} \tag{1}$$

where R_b is the bulk resistance, t represents the film thickness, and A represents the contact area between the film and electrodes. The variation in ionic conductivity with different concentration of PC:DEC plasticizers at 303 K for PVDF−HFP:PMMA−$LiClO_4$− PC:DEC GPE system is shown in figure 3. The values of ionic conductivity

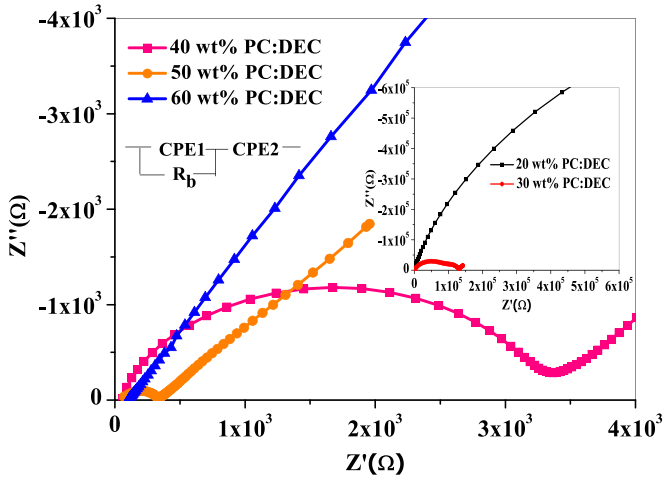

Figure 2. Impedance plot of GPE system with different concentration of PC:DEC plasticizers at 303K.

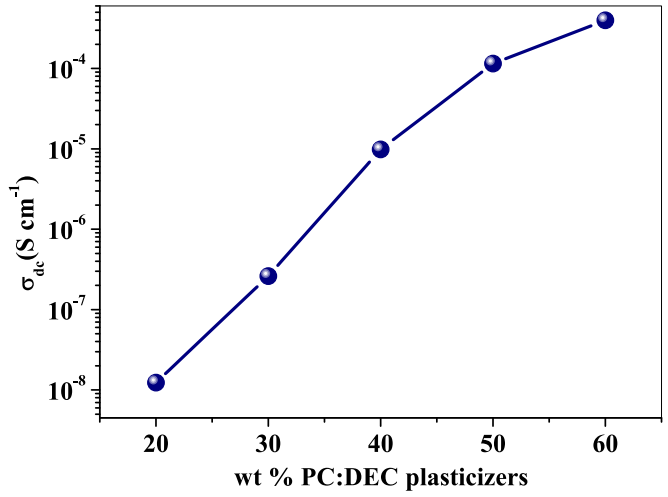

Figure 3. Variation in DC ionic conductivity of GPE films at 303 K.

Table 1. The compositions of GPE system with different concentrations of PC:DEC and DC conductivity values.

Sample Code	PVDF—HFP(gm)	PMMA (gm)	$LiClO_4$ (gm)	PC:DEC (gm)	PVDF—HFP(wt%)	PMMA (wt%)	$LiClO_4$ (wt%)	PC:DEC (wt%)	σ_{DC} S cm^{-1}
S1	0.4	0.4	0.089	0.21	36.0	36.0	8	20	1.24E-8
S2	0.4	0.4	0.089	0.35	31.5	31.5	7	30	2.60E-7
S3	0.4	0.4	0.089	0.55	27.0	27.0	6	40	9.82E-6
S4	0.4	0.4	0.089	0.83	22.5	22.5	5	50	1.15E-4
S5	0.4	0.4	0.089	1.24	18.0	18.0	4	60	3.97E-4

are also listed in table 1. It can be seen that the value of ionic conductivity reaches from 1.24E-8 S cm^{-1} to 3.97E-4 S cm^{-1} with an increasing amount of PC:DEC plasticizers from 20 wt% to 60 wt%. Similar effect has also been observed by Johan *et al* [27] in PEO−$LiCF_3SO_3$− EC complexations with different concentrations of EC plasticizer. According to authors, when plasticizer is added to the system, it can interrupt polymer−polymer interaction due to polymer plasticizer interaction and ion plasticizer coordination. This process will create more free volume and a new path for the conduction of ions. The change in ionic conductivity of the polymer electrolyte (σ) can also be explained by

$$\sigma_{dc} = \sum n_i \mu_i q_i \quad (2)$$

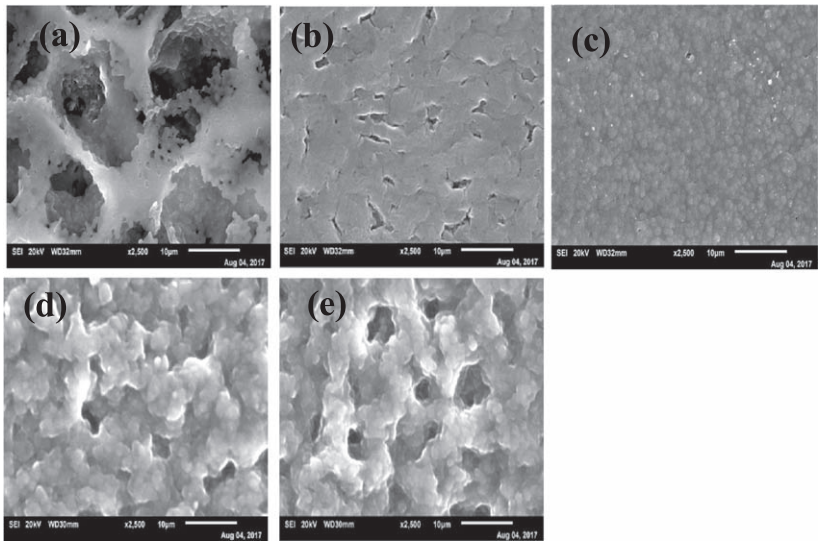

Figure 4. SEM micrographs of GPE with different concentration of PC:DEC (a) 20 wt% (b) 30 wt% (c) 40 wt% (d) 50 wt% (e) 60 wt%.

where n_i is the density of mobile charge carriers, μ_i is the mobility of charge carriers and q_i is the charge of mobile charge carriers [18]. From the above equation, it can be explained that ionic conductivity depends on two-factor n_i and μ_i as q_i is same for all GPE. From equation (2), we can conclude that the addition of plasticizers results in a change in mobility and number of charge carriers. The mobility of charge carriers is associated with the structure. Addition of plasticizers softens the polymer backbone which increases the flexibility of polymer segments through which ion can move easily and interact with the polymer matrix ultimately affect the structure. The second conclusion can be drawn that high dielectric constant of plasticizer can dissociate the charge carriers cause an increase in the n_i. Therefore, the information regarding the micro-structural features could provide some better explanation on the experimental phenomenon mentioned above.

3.2. SEM analysis

To investigate the change in the morphology of the gel polymer electrolyte film with a change in concentrations of PC:DEC plasticizers, films were subjected to SEM analysis. The SEM micrographs are shown in figure 4. Microspores with large size have been observed in GPE film with a lower amount of PC: DEC i.e. 20 wt% PC: DEC. It reveals that these micropores are not filled with the liquid electrolyte due to an insufficient amount of PC: DEC. Addition of more amount of PC: DEC plasticizers to polymer electrolyte leads to increment in more number of embedded small pores with swelled nature of GPE. These micropores filled with liquid electrolytes provide the conducting pathway for a lithium ion [28]. These type of observation have also been reported by Senthil Kumar *et al* [29] in their study on plasticized PVDF−HFP/PEMA blended polymer electrolyte. In our study, surface morphology shows the remarkably increase in swelled nature of the film by incorporating a higher amount of plasticizer.

3.3. FTIR analysis

In the present study, the FTIR assessment was used to define the functional groups in a sample and to evaluate changes in the molecules ' vibrational modes in the polymer electrolyte due to the interaction between polymer, plasticizer and ion [30].

The FTIR spectra of PVDF−HFP:PMMA−$LiClO_4$− PC:DEC GPE with different concentrations of PC: DEC in the wave number range 400–2600 cm^{-1} and 2600–3500 cm^{-1} are presented in figures 5(a) and (b) respectively.

The wave numbers for PVDF−HFP:PMMA−$LiClO_4$− PC: DEC complexation are tabulated in table 2. The FTIR specra of pure polymers and salt have been already reported in our previous study [26].

The assigned bending and wagging vibrations of $-CF_2$ of PVDF-HFP at 509 cm^{-1} and 435 cm^{-1} get shifted to higher wavenumbers 511 cm^{-1} and 440 cm^{-1}, respectively, with increasing amount of PC:DEC. The vibration of amorphous phase at 879 cm^{-1} and 836 cm^{-1} exhibited by PVDF−HFP are observed to be shifted to a higher frequency at 880 cm^{-1} and 838 cm^{-1} respectively. The peak assigned at 1401 cm^{-1} of PVDF−HFP is corresponds to the crystalline phase are getting broadened with reduction in intensity and shifted to 1403 cm^{-1}, specifying that interaction between polymers and plasticizers as well as salt has been taken place. and the intensity of other crystalline peaks at 1072 cm^{-1} and 1182 cm^{-1} of pure PVDF−HFP get reduced and becomes

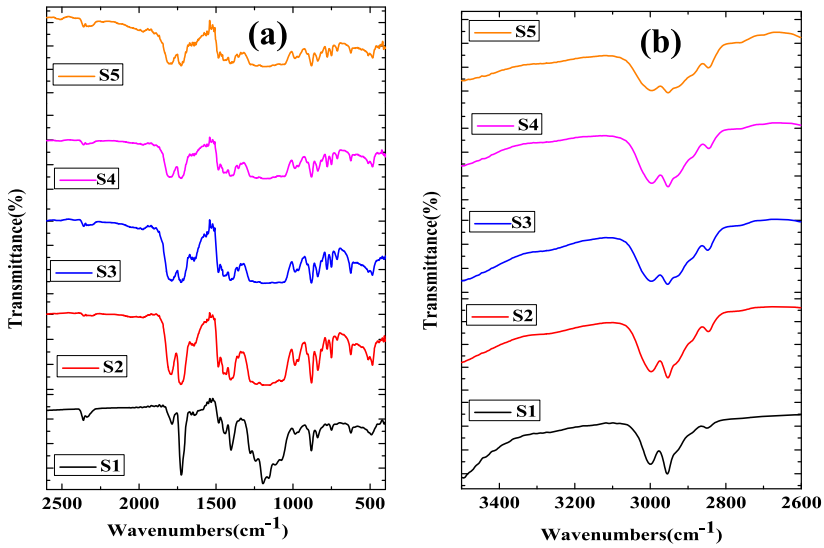

Figure 5. FT−IR spectra of PVDF−HFP:PMMA−$LiClO_4$− PC:DEC (a) spectra range 400–2600 cm^{-1}(b) spectra range 2600-3500 cm^{-1}, with PC:DEC content of (S1) 20 wt%, (S2) 30 wt%, (S3) 40 wt%, (S4) 50 wt% and (S5) 60 wt%.

Table 2. List of wave numbers for PVDF−HFP:PMMA−$LiClO_4$− PC:DEC complexation.

Materials	Assigned characteristics frequency (cm^{-1}))	Wavenumbers (cm^{-1})
PVDF−HFP	3021	3021 shifted to 2996
	2981	2981 shifted to 2952
	1401	1401 shifted to 1403
	879,836	879 shifted to 880 and 836 shifted to 838
	509	509 shifted to 511
	484,435	435 shifted to 440
PMMA	752	752 shifted to 750
	985	985 shifted to 987
	1727	1727 shifted to 1725
	2842	2842 shifted to 2846
$LiClO_4$	628	628 shifted to 624

flatten with addition of more amount of PC:DEC plasticizers. The characteristic peak at 2981 cm^{-1} is ascribed to symmetrical stretching of CH_2 group of pure PVDF−HFP is shifted towards lower frequency side. The CH_3 asymmetric stretching vibration of PMMA at 2842 cm^{-1} gets shifted to 2846 cm^{-1}. The C = O group (carbonyl group) of PMMA at 1727 cm^{-1} shifts towards the lower frequency side at 1725 cm^{-1} and at the same time intensity is reduced significantly upon the addition of PC:DEC plasticizers. This suggest that the occurrence of strong interaction between Li^+ and the carbonyl group of PMMA with the addition of plasticizers because when low molecular plasticizers are added to polymer results in dissociation of salt. Apart from these, intensity of many other peaks has been found to be reduced significantly. This indicates complex formation takes place between polymers, salt, and plasticizers [22].

In addition to this, remarkable changes in the ClO_4^- anion group has been noticed in the range of 600–650 cm^{-1} of FTIR spectra. The intensity and asymmetry of peak change with PC:DEC concentration in this range has been observed. The asymmetry in the perchlorate band arises due to the presence of ion pairs ($Li^+ClO_4^-$) along with free anion (ClO_4^-) in the polymer matrix as reported by Shukla *et al* [31] in their solid polymer electrolyte based on PMMA−$LiClO_4$. In present study to confirm this, the deconvolution of the ClO_4^- mode of $LiClO_4$ salt has been carried out in the wavenumber range 600–650 cm^{-1} for PVDF−HFP:PMMA−$LiClO_4$− PC:DEC complexation using peak fit software. The de−convoluted spectra for GPE with 40 wt% PC:DEC is shown in figure 6. Two degenerate modes have appeared at 624 cm^{-1} of free anions (ClO_4^-) and 633 cm^{-1} of ion pairs ($Li^+ClO_4^-$) in the de-convoluted spectra. The fractional amount of free anions and ion pairs has been calculated by using the following formulas and the variation in fractional amount as a function of PC:DEC is

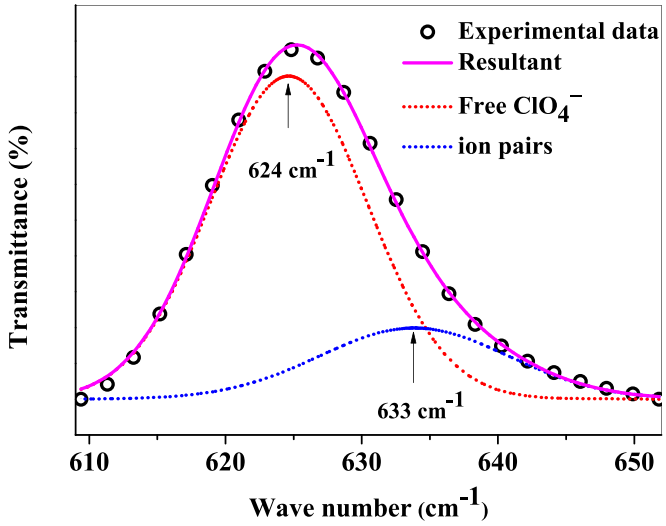

Figure 6. De−convoluted spectra of ClO_4^- mode of $LiClO_4$ for PVDF−HFP:PMMA−$LiClO_4$ − 40 wt% PC:DEC GPE system.

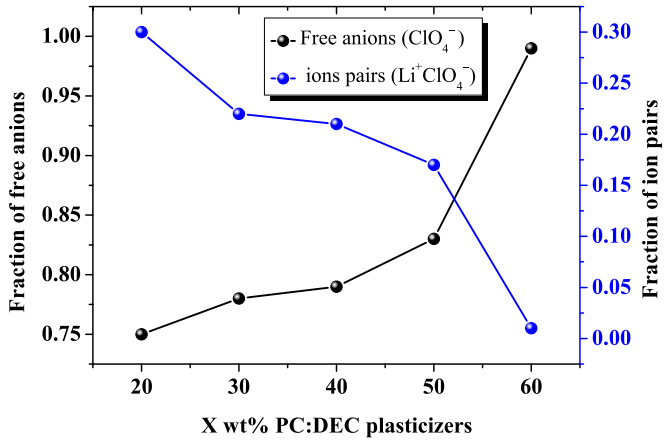

Figure 7. The fractional amount of free anions and ion pairs as a function of plasticizer concentration.

depicted in graphical form in figure 7.

$$Fraction\ of\ free\ anions = \frac{Free\ anion\ peak\ area}{Total\ peak\ area} \tag{3}$$

$$Fraction\ of\ ion\ pairs = \frac{Ion\ pair\ peak\ area}{Total\ peak\ area} \tag{4}$$

The change in the fraction of free anions and ion pairs can be correlated with change in the ionic conductivity. From figure 7, it clearly shows in increase in the fraction of free anions with increasing PC:DEC plasticizers which in turns to increase in ionic conductivity. Highest fraction of anions and the lowest fraction of ion pairs is observed for the highest conducting sample. This is due to dissociation of salt which in turns to enrich of charge carriers when low molecular weight plasticizers are added to the polymer. According to Pal *et al* [32], the cations form a complex with the polar group of polymer while free anions have an affinity to form ion pairs. Hence in the polymer complexes,the fraction of free anions and ion pairs are responsible for the conduction process.

3.4. Dielectric analysis

For ionic transport and relaxation phenomena occurring in polymer electrolyte, dielectric analysis has been carried out [33].

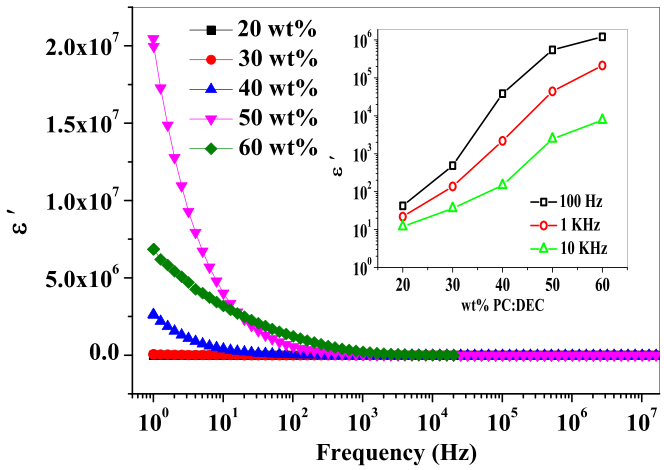

Figure 8. Dielectric constant (ε') versus frequency for PVDF−HFP:PMMA-$LiClO_4$− PC:DEC GPE system at 303 K (inset: Variation in dielectric constant with plasticizers PC:DEC variation at 10 KHz, 1 KHz, 100 Hz).

$$\varepsilon^* = \varepsilon' + j\varepsilon'' = \frac{Z''}{\omega C_0(Z'^2 + Z''^2)} + j\frac{Z'}{\omega C_0(Z'^2 + Z''^2)} \tag{5}$$

Here $C_0 = \frac{\varepsilon_0 A}{t}$, where C_0 is the vacuum capacitance, ε_0 is permittivity of free space, A is the area of electrode-electrolyte contact, and t is the thickness of film. ε' and ε'' are the real part (dielectric constant) and imaginary part(dielectric loss) of the dielectric permittivity [34].

Dielectric constant (ε') versus frequency (in log scale) for PVDF−HFP:PMMA-$LiClO_4$− PC:DEC GPE system at 303 K is shown in figure 8. It clearly shows that dielectric constant (ε') value for all polymer film at low-frequency region is high which is due to accumulation of charges near blocking electrode surface as a result of slow periodic reversal effect of applied AC field. At higher frequency region,charge carriers and dipoles are not able to follow the direction of electric field due to short time period of AC reversal field.As a consequence, the dielectric constant (ε' is found to be decreased. Inset of figure 8 shows the variation in ε' as a function of plasticizer content at 10 KHz, 1 KHz and 100 Hz at 303K. It can be seen that the value of dielectric constant has been increased (i) with increasing the concentrations of PC:DEC plasticizers (ii) change in frequency of applied AC field. The first one may be due to an increase in the charge carriers as a result of dissociation when low molecular weight PC:DEC plasticizers are added to the polymer. The second one is due to the ability of orientation of present dipoles with the time of AC field direction resulting in the increase of the dielectric constant [17]. The value of dielectric constant at 10 KHz (higher frequency) is 7.67E+03 whereas, at 100 Hz (lower frequency), it is 1.21E+06 for GPE system having 60 wt% PC:DEC plasticizers.

The dielectric loss represents represent the dissipation of energy by means of dipole orientation and movement of ion under the effect of the applied field. Figure 9 represent the dielectric loss (ε'') as a function of frequency for PVDF−HFP :PMMA−$LiClO_4$− PC:DEC GPE system at 303 K. The dielectric loss (ε'') is also following the same trend as dielectric constant (ε'). The dielectric loss (ε'') value also became larger at a lower frequency as well as with the increasing amount of plasticizers because of motion of free charge through gel polymer electrolyte. This means that with an increasing amount of PC: DEC, polymer chain segments becomes more flexible and promote mobility of ions, charge carriers and dipoles [35].

3.5. Electrochemical Stability Window

From the point of view of the application of polymer electrolyte in the battery, high conductivity is an essential property, but it is also necessary to measure the electrochemical stability window of an electrolyte [22]. The electrochemical stability window (ESW) is defined as the working voltage(potential) range of a substance [36]. From the cyclic voltammetry(CV) profile, the difference of reduction and oxidation potential gives the stability window of materials. The test of GPE film exhibiting maximum ionic conductivity was done by using Cyclic Voltammetry CV) at a scan rate of 50 mV/s as shown in figure 10 and measurement configuration for the same is SSE/GPE/SSE, where SSE is a stainless steel electrode. The oxidation and reduction peak has not been recorded which might be due to the noninteracting nature of ion species of gel polymer electrolyte with stainless steel electrodes. Cyclability nature of gel polymer electrolyte has also revealed form this CV curve. Electrochemical stability window of ≈4.2 V for the PVDF-HFP-LITFSI-EC:DMC GPE system has been reported by Bose *et al* [37]. Lie *et al* have shown the stability window of ≈4.5 V for the PVDF-HFP-EC:DEC-$LiClO_4$ system [38]. In the inset of figure 10, electrochemical stability window is shown for the system havin 60 wt% PC:DEC. Obviously,

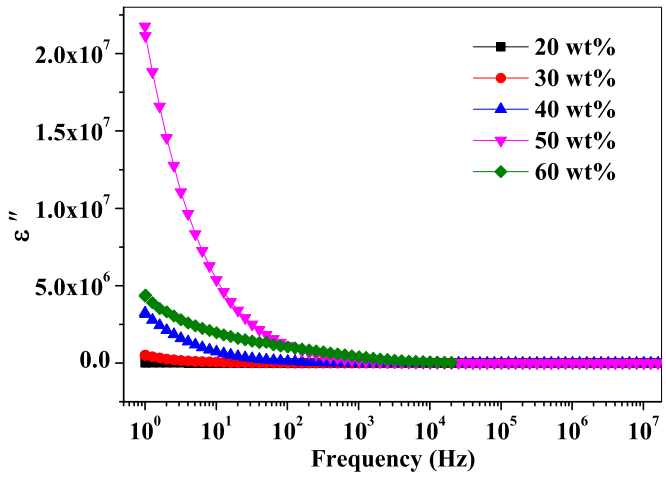

Figure 9. Dielectric loss (ε'') versus frequency for PVDF—HFP:PMMA—$LiClO_4$— PC:DEC GPE system at 303 K.

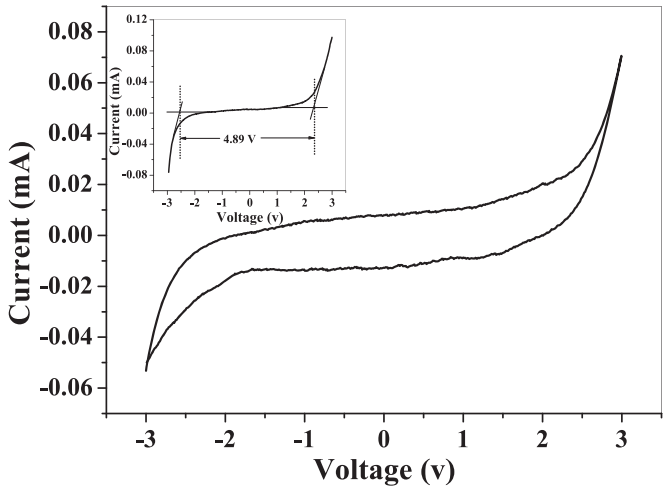

Figure 10. Cyclic Voltammogram of GPE having 60 wt% PC:DEC.

the observed value of ESW is about −2.55 to 2.34 V, i.e. 4.89 V (total) indicates the present gel polymer electrolyte is compatible for implementation in the lithium-ion battery.

4. Conclusions

- In the present study, the gel polymer electrolyte based on PVDF—HFP and PMMA incorporated with different concentrations of mixture of PC: DEC plasticizers have been prepared via solution casting technique.
- Ionic conductivity of present GPE system increases from 1.24E–8 S cm^{-1} to 3.97E—4 S cm^{-1} with addition of PC:DEC plasticizers. This might be due to increase in the free charge carriers as a result of dissociation and decrease in rigidity of polymer chain to avail migration of Li^+ ions. Furthermore, the change in electrical property of GPE is well explained with SEM, FTIR and dielectric studies.
- FTIR study revels that the complex formation is taking place between polymers, salt and plasticizers. The fraction of free anions increases whreas ion—pair decreases with addition of PC:DEC leading to enrichment in the ionic conductivity.
- The cyclic voltammetry curve showed the electrochemical stability window of the electrolytes ≈4.89 V which implies that the present gel polymer electrolyte is applicable as separator in lithium ion batteries.

ORCID iDs

D K Kanchan https://orcid.org/0000-0002-7083-6677

References

[1] Ngai K S, Ramesh S, Ramesh K and Juan J C 2016 *Ionics* **22** 1259–79
[2] Noto V D, Lavina S, Giffin G A, Negro E and Scrosati B 2011 *Electrochim. Acta* **57** 4–13
[3] Dirican M, Yan C, Zhu P and Zhang X 2019 *Materials Science and Engineering: R: Reports* **136** 27–46
[4] Fenton D, Parker J and Wright P 1973 *Polymer* **14** 589
[5] Meyer W H 1998 *Adv. Mater.* **10** 439–48
[6] Scrosati B and Garche J 2010 *J. Power Sources* **195** 2419–30
[7] Wu C G, Lu M I, Tsai C C and Chuang H J 2006 *J. Power Sources* **159** 295–300
[8] Li Z, Su G, Wang X and Gao D 2005 *Solid State Ionics* **176** 1903–8
[9] Shi J, Yang Y and Shao H 2018 *J. Membr. Sci.* **547** 1–10
[10] Kumar D and Hashmi S 2010 *J. Power Sources* **195** 5101–8
[11] Shin I, Lee K, Kim E and Kim T H 2018 *Bull. Korean Chem. Soc.* **39** 1058–65
[12] Dissanayake M, Bandara L, Bokalawala R, Jayathilaka P, Ileperuma O and Somasundaram S 2002 *Mater. Res. Bull.* **37** 867–74
[13] Ulaganathan M and Rajendran S 2010 *Ionics* **16** 667–72
[14] Liu W, Zhang X K, Wu F and Xiang Y 2017 *IOP Conference Series: Materials Science and Engineering* **213** 012036
[15] Vo D T, Do H N, Nguyen T T, Nguyen T T H, Tran V M, Okada S and Le M L P 2019 *Materials Science and Engineering:* B **241** 27–35
[16] Xie H, Tang Z, Li Z, He Y, Liu Y and Wang H 2008 *J. Solid State Electrochem.* **12** 1497–502
[17] Ramesh S and Ling O P 2010 *Polym. Chem.* **1** 702–7
[18] Prabakaran P, Manimuthu R P and Gurusamy S 2017 *J. Solid State Electrochem.* **21** 1273–85
[19] Kim K M, Park N G, Ryu K S and Chang S H 2006 *Electrochim. Acta* **51** 5636–44
[20] Isa K, Osman Z, Arof A, Othman L, Zainol N, Samin S, Chong W and Kamarulzaman N 2014 *Solid State Ionics* **268** 288–93
[21] Flora X, Ulaganathan M and Rajendran S 2013 *Int. J. Polym. Mater.* **62** 737–42
[22] Subbu C, Rajendran S, Kesavan K and Premila R 2016 *Ionics* **22** 229–40
[23] Gohel K and Kanchan D K 2019 *J. Mater. Sci., Mater. Electron.* **30** 12260–8
[24] Cong W, Miao R, Miao F and Tao B 2019 *Mater. Res. Express* **6** 115525
[25] Hari Krishna K, Marino L, Scarpelli F, Petrov A, Marinov Y, Hadjichristov G, Iliev M and Scaramuzza N 2017 *Curr. Appl Phys.* **17** 1518–31
[26] Gohel K and Kanchan D K 2018 *Journal of Advanced Dielectrics* **08** 1850005
[27] Johan M R, Shy O H, Ibrahim S, Yassin S M M and Hui T Y 2011 *Solid State Ionics* **196** 41–7
[28] Bhute M V and Kondawar S B 2019 *Solid State Ionics* **333** 38–44
[29] Kumar P S, Sakunthala A, Reddy M and Prabu M 2018 *Solid State Ionics* **319** 256–65
[30] Sharma P, Kanchan D K and Gondaliya N 2013 *Ionics* **19** 777–85
[31] Shukla N and Thakur A K 2009 *Ionics* **15** 357–67
[32] Pal P and Ghosh A 2016 *J. Appl. Phys.* **120** 045108
[33] Yusof Y M, Illias H A and Kadir M F Z 2014 *Ionics* **20** 1235–45
[34] Dave G, Kanchan D and Singh F 2019 *Radiat. Phys. Chem.* **161** 87–94
[35] Pawlicka A, Tavares F, Dörr D, Cholant C, Ely F, Santos M and Avellaneda C 2019 *Electrochim. Acta* **305** 232–9
[36] Prabakaran P and Manimuthu R P 2016 *Ionics* **22** 827–39
[37] Bose P, Deb D and Bhattacharya S 2019 *Electrochim. Acta* **319** 753–65
[38] Liu W, Zhang X, Wu F and Xiang Y 2017 *IOP Conference Series: Materials Science and Engineering* **213** 012036

Ionic transport studies in PVDF-HFP-PMMA-(PC+DEC)-$LiClO_4$ gel polymer electrolyte

Khushbu Gohel and D. K. Kanchan

Citation: AIP Conference Proceedings **1832**, 140047 (2017); doi: 10.1063/1.4980829
View online: http://dx.doi.org/10.1063/1.4980829
View Table of Contents: http://aip.scitation.org/toc/apc/1832/1
Published by the American Institute of Physics

Ionic transport studies in PVdF-HFP-PMMA-(PC+DEC)-$LiClO_4$ gel polymer electrolyte

Khushbu Gohel and *D.K.Kanchan

Department of Physics, Faculty of Science, The M.S.University of Baroda,Vadodara,Gujarat 390002,India
*dkkanchan.ssi@gmail.com

Abstract. Poly(vinylidene fluoride-hexafluropropylene)(PVdF-HFP) and Polymethylmethacrylate(PMMA) based gel polymer electrolytes comprising Propylene Carbonate and Diethyl Carbonate mixed plasticizers and different concentrations of Lithium Perchlorate ($LiClO_4$) salt have been prepared using a solvent casting technique. Electrical conductivity and transference number measurements have been carried out by Electrochemical Impedance Spectroscopy in the temperature range 303 K to 363 K and Wagner's Polarization method respectively. The maximum room temperature conductivity of 2.83×10^{-4} S cm^{-1} has been observed for the gel polymer electrolytes at 7.5 wt% $LiClO_4$. The variation of ac conductivity with frequency has been discussed.

Keywords: Gel polymer electrolytes, ionic conductivity, transference number
PACS: **72.80. –r, 73.61.-r, 82.35. -x**

INTRODUCTION

The development of ion conducting polymer electrolytes have gained much attention of many researchers as they find application in not only Lithium Ion batteries but also in other electrochemical devices such as fuel cell, electro chromic devices, Super capacitors, Solar cell [1]. Several classes of polymer electrolytes have been developed and characterized by using various host polymer matrix such as Polyethylene oxide(PEO) [2], Polyvinyl chloride(PVC) [3], Poly acrylonitrile (PAN) [4] Polyvinylidene fluoride (PVdF) [5], Polymethyl methacrylate (PMMA) [6]. Gel polymer electrolytes composed of low molecular weight liquid plasticizers along with polymer host offer high ionic conductivity at ambient temperature. In the present study, another polymer Polymethyl methacrylate (PMMA) is used which has an amorphous nature [7] and the addition of PMMA will reduce the crystalline nature of the host polymer since it enhances the ionic conductivity.

The present work has been undertaken to develop novel gel polymer electrolytes consisting PVdF-HFP and PMMA as polymer host, PC+DEC as plasticizers and different concentration of $LiClO_4$ salt.

EXPERIMENTAL

Poly(vinylidene fluoride -co- hexafluoro propylene) P(Vdf-HFP, M_w= 400,000 , Aldrich) and Polymethyl methacrylate(PMMA, Alfa Aesar) as a host polymer, lithium perchlorate ($LiClO_4$, 99.99% from Aldrich) as salt and the organic solvents propylene Carbonate (PC, anhydrous , 99.7% from Sigma Aldrich and diethyl carbonate (DEC, anhydrous , 99.7% from Sigma Aldrich) were used as received. An appropriate weight of P(Vdf-HFP) and PMMA are dissolved in acetone and an appropriate amount of LiClO4 salt were dissolved in equal amount of plasticizers(PC+DEC). The solution was stirred for 24 hours The solution of different compositions was cast on to Teflon Petri dish and acetone was allowed to evaporate slowly at room temperature

The ionic conductivity of the various gel polymer electrolytes films were measured by alternating current(AC) impedance spectroscopy in the frequency range 1 Hz to 32 MHz at different temperatures between ambient and 363 K by using a Solatron 1260 Impedance analyzer. The transference number of the sample was measured by using Wagner's Polarization method. The transference number were calculated by using the following equations

DAE Solid State Physics Symposium 2016
AIP Conf. Proc. 1832, 140047-1–140047-3; doi: 10.1063/1.4980829
Published by AIP Publishing. 978-0-7354-1500-3/$30.00

$$t_{ion} = 1 - \frac{i_e}{i_t}$$

where i_e and i_t are the electronic and total current respectively and t_{ion} is the ionic transport number.

RESULTS AND DISCUSSION

Conductivity Analysis

The complex impedance plot of gel polymer electrolytes containing 4 wt% of $LiClO_4$ at different temperature is shown in Fig. 1. The complex plot shows a high frequency semicircle portion which correspond to the parallel combination of resistor and a capacitor and a low frequency spike due to formation of double layer capacitance at the electrode-electrolyte interface. It has been observed that the bulk resistance R_b decreases as the temperature increases from 303 K to 363 K. The ionic conductivity are calculated and given in Table 1. The highest ionic conductivity is found to be 2.83 × 10^{-4} S cm^{-1} for polymer gel electrolytes system containing 7.5 wt% $LiClO_4$.

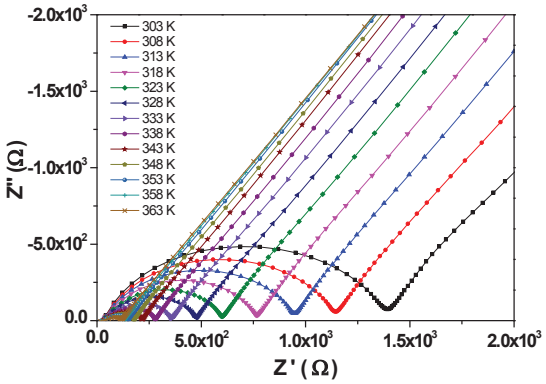

FIGURE 1. Impedance plot of 4 wt% $LiClO_4$ at different temperature

Fig. 2 shows the variation of room temperature ionic conductivity and the activation energy as a function of different concentration of $LiClO_4$ salt. It has been found that the highest conducting polymer electrolyte sample has the lowest activation energy of 0.31 eV.

Fig.3 represents variation of conductivity as a function of frequency at different temperature for the gel polymer electrolytes system containing 4 wt% $LiClO_4$ salt. A mid frequency plateau region represents dc conductivity. An ion successful hop to a neighboring vacant site and contributes to the dc conductivity when the frequency is lower than the hopping frequency (ω_p).

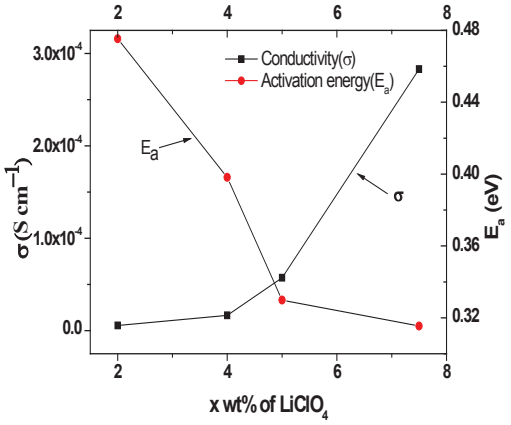

FIGURE 2. conductivity and activation energy versus different concentration of $LiClO_4$

The behavior of the ionic conductivity follows Jonscher's power law $\sigma(\omega)=\sigma_{dc}+ A\omega^n$ where, the σ_{dc} is the frequency independent dc conductivity, A is the pre- exponential constant, ω is the angular frequency and n is the power law exponent. The calculated values of hopping frequency are tabulated in Table 2. It has been observed that as concentration of $LiClO_4$ increases, the transition from frequency independent plateau region to the ac conductivity dispersion region shift towards the higher frequency range [8]. The increase in the hopping frequency leads to a conclusion that the highest conducting sample has the shortest relaxation time [9] .

Transference Number Measurements

The transference number (t_{ion}) for the different gel polymer electrolyte system were estimated using Wagner's Polarization technique [10]. In this technique, the polarization current was monitored as a function of time electrolyte as shown in Fig 4. The calculated data for transport number values are in the range of 0.96-0.99as listed in Table.2. This suggest that the charge transport is mainly due to ions.

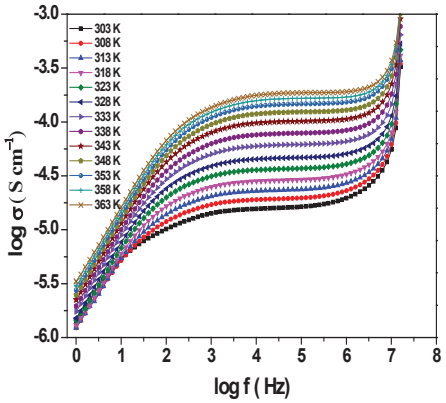

FIGURE 3. Variation of conductivity as a function of frequency of gel polymer electrolytes with 4 wt% $LiClO_4$ at different temperatures

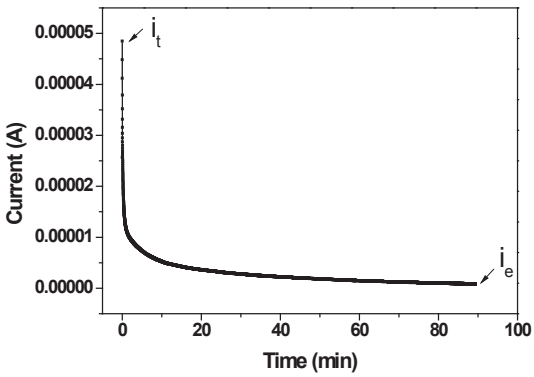

FIGURE 4. Polarization current as a function of time for gel polymer electrolyte with 4 wt% $LiClO_4$

TABLE 1. The compositions of polymers, Plasticizers, Lithium salt and conductivity, activation energy of gel polymer electrolyte system

Sample Code	Polymer PVdF-HFP+PMMA (wt%)	Plasticizers PC+DEC(wt%)	$LiClO_4$ Salt(wt%)	Conductivity(S cm^{-1}) at room temperature	Activation Energy(eV)
S1	49	49	2	5.95×10^{-6}	0.47
S2	48	48	4	1.65×10^{-5}	0.39
S3	47.5	47.5	5	5.73×10^{-5}	0.32
S4	46.25	46.25	7.5	2.83×10^{-4}	0.31

TABLE 2. The transport number and hopping frequency of different gel polymer electrolyte system

Sample Code	Transport Number	ω_p(MHz)
S1	0.97	1.30
S2	0.96	5.25
S3	0.99	6.83
S4	0.99	8.98

CONCLUSIONS

The ionic conductivity has been observed to increase with the salt concentration of gel polymer electrolytes containing PVdF-HFP/PMMA, PC+DEC and $LiClO_4$. The highest conductivity of 2.83 X 10^{-4} S cm^{-1} and low activation energy 0.31 eV is shown by a sample with 7.5 wt% $LiClO_4$. The variation of ac conductivity as a function of frequency obeys the Jonscher Power law. These gel polymer electrolyte samples are mainly ionic conductors as evident from their transport number.

REFERENCES

1. N. Angulakshmi, Sabu Thomas, K. S. Nahm, A Manuel Stephan, R Nimma Elizabeth, *Ionics* **17**, 407-414(2011)
2. R. Chandrasekaran, I. Ruth Managani, R.Vasanthi, S. Selladurai, *Ionics* **7**, 94 – 100(2001)
3. R.H.Y Subban, A.H. Ahmad, N. Kamarulzaman, A.M.M. Ali, *Ionics* **11**,442-444 (2005)
4. A.subramania, N.T. Kalyana Sundaram, G. Vijaya kumar, T. Vasudevan, *Ionics* **12**, 175-178(2006)
5. A.Magistris, E. Qudratone, P. Mustarelli, Y. Saito, H. Kataoka, *Solid State Ionics* **152-153**, 347- 354(2002)
6. Shahzada Ahmad, sharif Ahmad, S.A.Agnihotry,*Ionics* **9**, 439 – 443(2003)
7. Chithra M. Mathew, K. Kesavan, S. Rajendran, *International Journal of Electrochemistry* **2015** 1-6(2015)
8. C.S. Ramya, T. Savitha, S. Selvasekarapandian, G. Hirankumar, *Ionics* **11**,436-441(2005)
9. R.H.Y Subban, A.K. Arol, *Ionics* **9**,375-381(2003)
10. P. Balaji Bhargav, V. Madhu Mohan, A.K. Sharma, V.V.R.N.Rao, *Ionics* **13**, 441-446(2007)

Electrical and dielectric properties of PVdF-HFP – PMMA – (PC + DEC)- $LiClO_4$ based gel polymer electrolyte

Khushbu Gohel, D. K. Kanchan, and C. Maheshwaran

Citation: AIP Conference Proceedings **1942**, 140081 (2018); doi: 10.1063/1.5029212
View online: https://doi.org/10.1063/1.5029212
View Table of Contents: http://aip.scitation.org/toc/apc/1942/1
Published by the American Institute of Physics

Electrical and Dielectric Properties of PVdF-HFP – PMMA – (PC+DEC)- $LiClO_4$ Based Gel Polymer Electrolyte

Khushbu Gohel, D.K. Kanchan[a)] and C. Maheshwaran

Department of Physics, Faculty of Science, The M. S. University of Baroda, Vadodara, Gujarat 390002, India

[a)]*Corresponding author: dkkanchan.ssi@gmail.com*

Abstract. In the present paper, AC impedance studies have been measured to evaluate ion conduction behavior of (PVdF-HFP – PMMA) + (PC-DEC) + $LiClO_4$ gel polymer electrolyte system prepared by solution casting method. Structural characterization and morphology has been carried out using XRD and SEM respectively. The AC conductivity and dielectric permittivity, electric modulus and relaxation mechanism have been studied. The variation of ac conductivity with frequency obeys Jonscher power law. Maximum value of dielectric constant ε′ in the lower frequency region has been observed for the gel polymer electrolyte containing 7.5 wt% $LiClO_4$. The highest conducting sample shows the shortest relaxation time.

INTRODUCTION

Polymer electrolytes have been the subject of increasing interest because of their potential applications in batteries and other electrochemical devices owing to good thermal stability, high electrical conductivity, electrode - electrolyte compatibility etc.[1]. Basically, a polymer electrolyte which is comprised of a host polymer (such as PEO PMMA, PAN,PVA, PVdF, PVdF-HFP) commonly doped with salt in order to achieve high ionic conductivity. The polymer electrolyte based on PEO usually exhibited very low conductivity of the order of 10^{-7} S cm^{-1} mainly because of high crystallinity and poor motion performance of the PEO backbones as reported by Bhargav et al.[2]. As a host polymer, PVdF-HFP has gained much interest due to its excellent properties such as high conductivity and good mechanical strength, co-existence with amorphous phase of HFP and high dielectric constant ($\varepsilon \approx 8.4$). Despite of these favourable features, the fundamental conduction properties of the gel polymer electrolyte are not well known. Understanding of ion transport dynamics and conductivity relaxation mechanism in the gel polymer electrolyte, which is a hybrid material composed of electrolyte solution and polymer is a challenging problem. Therefore, the impedance spectroscopy has been used to understand the relaxation dynamics, ion dynamics and conductivity relaxation with the salt concentration. Furlani et al.[3] carried out the research study on concentration dependence of ionic relaxation in lithium doped polymer electrolytes.

EXPERIMENTAL

Poly(vinylidene fluoride-co-hexafluoropropylene) (PVdF-HFP, M_w= 400,000, Aldrich) and Polymethyl methacrylate (PMMA, M_w = 350,000, Alfa Aesar), lithium perchlorate ($LiClO_4$, 99.99% from Aldrich) as salt and the organic solvents propylene carbonate (PC, anhydrous , 99.7% from Sigma Aldrich) and diethyl carbonate (DEC, anhydrous , 99.7% from Sigma Aldrich) were used to prepare gel polymer electrolyte system (100-X)[$(PVdF\text{-}HFP+PMMA)_{(50wt\%)}$ - $(PC+DEC)_{(50wt\%)}$] - X wt% $LiClO_4$; where X=2,4,5,7.5 and 10. An appropriate amounts of (PVdF-HFP) and PMMA were dissolved in acetone and $LiClO_4$ salt was dissolved in equal amount of (PC+DEC). The solution was stirred for 24 hours until the mixture gets homogeneous in nature. The solution was cast onto Teflon Petri dish and acetone was allowed to evaporate and free standing films of thickness of about 0.12 mm to 0.14 mm were obtained. Structural behavior and surface morphology of samples was examined by using an X-ray diffractometer (BRUKER D2-Phaser) with Cu Kα radiation of wavelength λ=1.540 Å in 2θ range of 5º-70° and a JEOL JSM-6010LA scanning electron microscope (SEM) respectively.

DAE Solid State Physics Symposium 2017
AIP Conf. Proc. 1942, 140081-1–140081-4; https://doi.org/10.1063/1.5029212
Published by AIP Publishing. 978-0-7354-1634-5/$30.00

Electrical measurement were carried out using Solartron 1260 Impedance analyzer in the frequency range 1 Hz to 32 MHz at different temperatures between 303 K and 363 K by sandwiching films between two stainless steel electrodes.

RESULTS AND DISCUSSION

Structural analysis

Surface morphology of the gel polymer electrolyte films with 7.5 wt% of $LiClO_4$ salt is shown in Fig.1 along the XRD pattern given in inset. The morphology change as 7.5 wt% of $LiClO_4$ is doped into the polymer electrolyte to larger pore size. The pores in the polymer complexes help in trapping the large amount of electrolyte. The swelled nature of the gel polymer electrolyte has been observed containing the 7.5 wt% of $LiClO_4$. The observed feature is very similar to those reported by Ramesh et al. [4]. These microstructures lead to the better conducting pathway for Li^+ ions, and consequently leading to higher ionic conductivity. In the inset, XRD pattern shows broad peaks which indicate the amorphous nature of prepared film.

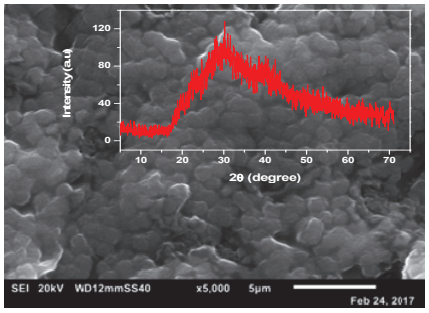

FIGURE 1. SEM micrograph of the gel polymer electrolyte films containing 7.5 wt% of $LiClO_4$

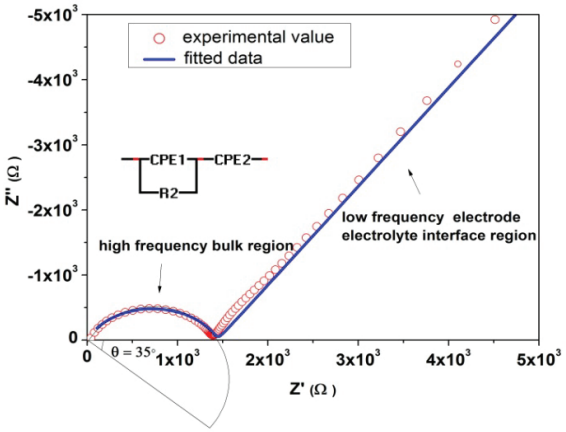

FIGURE 2.Impedance plot of gel polymer electrolyte containing 4 wt% of $LiClO_4$ at 303 K along with equivalent circuit model

Electrical and Dielectric Properties

Figure. 2 shows Impedance plot of gel polymer electrolyte containing 4 wt% of $LiClO_4$ at 303 K fitted with equivalent circuit model comprising of a constant phase element (CPE1) and a resistor connected in parallel that take the shape of a depressed semicircle which exhibit some degree of decentralization at an angle of 35º with real axis along with a tilted spike due to imperfect blocking electrode which is represented by CPE2 connected in series. The depressed semicircle represents typically a phenomenon with a spread of relaxation time. AC conductivity formalism is a powerful tool to have an insight of ion conduction mechanism. The frequency dependent conductivity can be given as

$$\sigma' = \frac{t}{A}\frac{Z'}{Z'^2 + Z''^2} \quad (1),$$

where t and A are thickness and cross sectional area of the sample respectively. Figure 3 shows the variation of conductivity as a function of frequency at different temperatures for 4 wt% $LiClO_4$ salt. At lower frequency region, the conductivity is found to decrease with increasing frequency which is attributed to the electrode polarization due to the accumulation of more charges at the electrode-electrolyte interface. At intermediate frequency, a successful ion hop to a neighboring vacant site contributes to the dc conduction. The high frequency dispersion region is attributed to short range ionic motion [5]. This behavior of the ionic conductivity is given by Jonscher's power law; $\sigma(\omega) = \sigma_{dc} + A\omega^n$, where σ_{dc} is the frequency independent conductivity, A is the pre - exponential constant, ω is the angular frequency and n is the power law exponent. The experimental data has been fitted with Jonscher's power law equation shown in Fig. 3 and parameter σ_{dc}, A and n are

tabulated in Table 1. It is observed that the dc conductivity increases with the temperature and is due to increase in the flexibility of polymer chain resulting into the segmental motion of the polymer which facilitates ion motion [6].

Dielectric study helps to understand the polarization effect at the electrode-electrolyte interface [7].The frequency dependent complex dielectric permittivity is given by $\varepsilon^* = \varepsilon' + j\varepsilon''$, where ε' and ε'' are the real and imaginary parts of the dielectric permittivity, known as dielectric constant and dielectric loss respectively. The equation for dielectric constant is

$$\varepsilon' = \frac{Z''}{\omega C_0 (z'^2 + z''^2)} \tag{2}$$

where Z′ and Z″ are the real and imaginary part of the impedance, ω is angular frequency and C_0 is the vacuum capacitance. The real part ε' of dielectric permittivity for gel polymer electrolyte with different concentration of $LiClO_4$ at 303 K is shown in Fig. 4 as a function of frequency. A dispersive nature at lower frequency is due to electrode polarization effect at the interface because of slow periodic reversal effect of applied field and consequently, the large value of ε′ at lower frequency is observed [8]. While at high frequencies, very low value of dielectric constant is observed because the diffusion of ions is not feasible due to the fast periodic reversal effect of electric field. The higher value of ε' for the gel polymer electrolyte containing 7.5 wt% $LiClO_4$ due to the increase in the charge carrier density and also due to more free volume available for the movement of dipoles because of increased amorphous nature. Hence polarization increases.

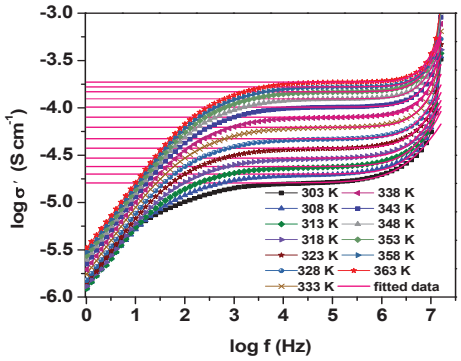

FIGURE 3. AC conductivity as a function of frequency at different temperatures of 4 wt% $LiClO_4$ respectively and solid lines are theoretical fit

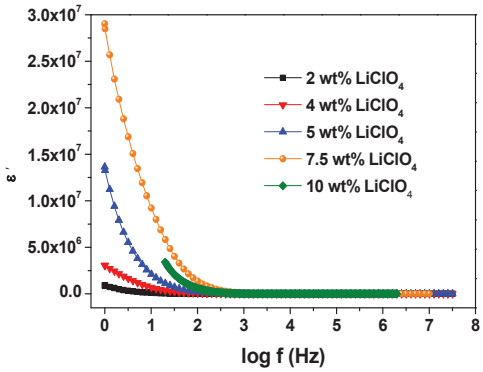

FIGURE 4. Variation in Dielectric constant as a function of frequency at different concentration of $LiClO_4$ at 303 K

Modulus formalism has been used to study their conductivity relaxation behavior which suppresses the effect of the electrode polarization effect at low frequencies and enhances small features at high frequencies. The electric modulus M* is defined as $M^* = M' + jM''$ or $M^* = j\omega C_0 Z^*$, where M' and M'' are the real and imaginary part of modulus respectively. The $\boldsymbol{M''}$ spectra for 5 wt% $LiClO_4$ polymer complex at different temperatures (Fig. 5) shows a long tail at the low frequency region which reveals the large capacitance due to the accumulation of a large amount of charge carries at the electrode- electrolyte interface. It is seen that the peak of M″ spectra shifts to higher frequency side with increase in temperatures which can be ascribed to the temperature dependent hopping mechanism for electrical conduction [9]. It has also been observed that the intensity of the peak maxima reduces gradually with increasing temperature which is attributable to the increase in the mobility of polymer segmental and charge carriers with temperature. It is also observed that the position of the peak maximum (M''_{max}) is shifted to higher frequencies with salt concentration. This indicates the charge carrier hopping which is due to increase in the amorphous nature of gel polymer electrolyte with the addition of the salt. Such a carrier hopping is indicative of a relaxation phenomenon. The conductivity relaxation time $\boldsymbol{\tau}$ is calculated from relaxation frequency f_{max} corresponding to M''_{max}. The calculated relaxation time is listed in Table 2. The electrolyte with the highest conducting sample shows the shortest relaxation time shown in Fig. 6.

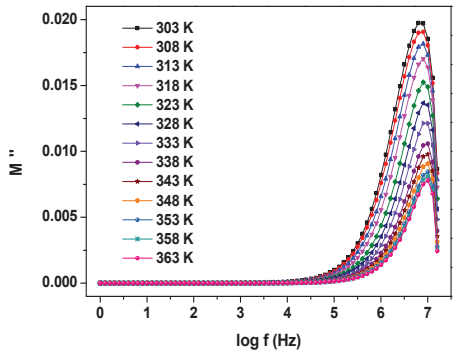

FIGURE 5. Imaginary part (M″) of modulus versus log f at different temperature for Gel polymer electrolyte containing 5 wt% $LiClO_4$

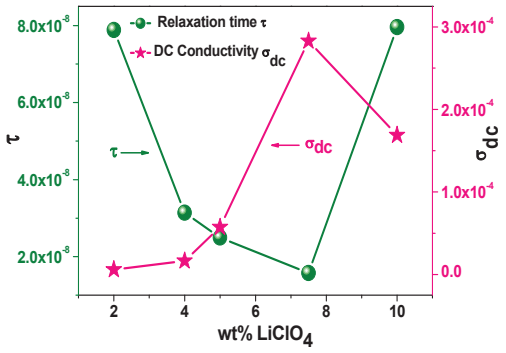

FIGURE 6.Variation of Relaxation time (τ) and conductivity (σ) at different concentration of Lithium salt at 303 K

TABLE 1. Johnscher's power law fitting parameters Conductivity σ_{dc}, A and n from the AC conductivity spectra for gel polymer electrolyte containing 4 wt% of $LiClO_4$

Temperature (K)	Conductivity σ_{dc} (S cm^{-1})	A	n
303 K	1.65E-05	1.04E-13	1.22
313 K	2.39E-05	3.37E-14	1.30
323 K	3.75E-05	5.89E-15	1.42
333 K	6.24E-05	1.16E-15	1.55
343 K	1.02E-04	1.84E-16	1.69
353 K	1.48E-04	3.73E-17	1.80
363 K	1.87E-04	1.02E-17	1.89

TABLE 2. The wt% $LiClO_4$ lithium salt, conductivity and relaxation time of gel polymer electrolyte system

$LiClO_4$ salt (wt%)	Conductivity σ_{dc} (S cm^{-1}) at 303 K	Relaxation time (τ) Sec^{-1}
2	5.94×10^{-6}	7.89E-08
4	1.65×10^{-5}	3.14E-08
5	5.73×10^{-5}	2.49E-08
7.5	2.83×10^{-4}	1.57E-08
10	1.70×10^{-4}	7.96E-08

CONCLUSIONS

SEM and XRD analysis reveal swelled and amorphous nature of gel polymer electrolyte containing 7.5 wt% $LiClO_4$ respectively. The ac conductivity of the prepared gel polymer electrolyte samples follows the Jonscher's power law. At low frequency, the variation of dielectric constant as a function of frequency suggests the electrode–electrolyte interface polarization process. The shifting of peak of the imaginary part of modulus with temperature and salt concentration suggests the conductivity relaxation is taking place in these gel polymer electrolytes. The lowest relaxation time (τ) is found for 7.5 wt% salt.

REFERENCES

1. A.Karmakar, A.Ghosh, Current Applied Physics **12**, 539-543 (2012)
2. P. B. Bhargav a , B. A. Sarada , A. K. Sharma a & V. V. R. Narasimaha Rao, Journal of Macromolecular Science, Part A: Pure and Applied Chemistry, **47:2**, 131-137 (2009)
3. M. Furlani, C. Stappen, B.E Mellander, G. A. Niklasson, Journal of Non-Crystalline Solids **356**, 710–714 (2010)
4. S. Ramesh, Lu SC, Journal of Molecular Liquids **177**:73-77 (2013)
5. T. Dam, S.N.Tripathy, M.Paluch, S.S.Jena, D.K.Pradhan, Electrochimica Acta **202**, 147–156 (2016)
6. P.Tamilselvi, M.Hema, Physica B **437**, 53-57(2014)
7. H.J.Woo, S.R.Majid, A.K.Arof, Materials Chemistry and Physics **134**, 755-761(2012)
8. M. Kumar, T. Tiwari, N. Srivastava, Carbohydrate Polymers **88**, 54-60 (2012)
9. M.Ravi, S.Bhavani, K.K.Kumar,V.V.R.Narasimaha Rao, Solid State Sciences **19**, 85-93(2013)

Conductivity and dielectric behavior of lithium ion conducting gel polymer electrolyte

Khushbu Gohel, and D. K. Kanchan

Citation: AIP Conference Proceedings **2009**, 020034 (2018); doi: 10.1063/1.5052103
View online: https://doi.org/10.1063/1.5052103
View Table of Contents: http://aip.scitation.org/toc/apc/2009/1
Published by the American Institute of Physics

Conductivity and Dielectric Behavior of Lithium Ion Conducting Gel Polymer Electrolyte

Khushbu Gohel and D.K.Kanchan [a)]

Department of Physics, Faculty of Science, The M. S. University of Baroda, Vadodara, Gujarat 390002, India

Email: [a)]dkkanchan.ssi@gmail.com

Abstract. Poly(vinylidene fluoride-hexafluropropylene) (PVdF-HFP) and poly(methyl methacrylate) (PMMA) gel polymer blend electrolyte system complexed with $LiClO_4$ having different concentrations of propylene carbonate (PC) and diethyl carbonate (DEC) (1:1) plasticizers have been prepared using solution cast technique. Structural and surface morphology have been studied by X-ray diffraction and scanning electron microscopy analysis. Electrical conductivity has been carried out by electrochemical impedance spectroscopy in the temperature range 303 K to 343 K. A maximum electrical conductivity of 1.03 X 10^{-3} S cm^{-1} at 303 K has been achieved for the polymer blend gel electrolyte containing 60 wt% of PC:DEC plasticizers. Frequency dependent conductivity follows the Jonscher's power law. The dielectric behavior has been analyzed using dielectric permittivity (ε^*), tangent loss ($tan\delta$) and electric modulus (M^*) of the samples. Dielectric constant has been found to increase with addition of PC:DEC plasticizers.

INTRODUCTION

Since last few decades, the polymer electrolytes are being used extensively due to their properties such as non-leaky in nature, ease of preparation in any shape and size and flexibility with good strength. Such properties of polymer electrolytes make them potential candidate in various electrochemical devices such as Batteries, Fuel cells, Super capacitors, and Solar cells [1]. Many polymers like PEO, PMMA, PVdF-HFP, PAN, PVA etc., have been studied as potential polymer electrolytes [2]. The ionic conductivity of polymer electrolytes prepared from such polymers is very low and its poor electrochemical stability prevents their application in fabrication of batteries [3]. The ionic conductivity is key factor of polymer electrolyte to be used as separator cum electrolyte in lithium ion batteries. It is strongly affected by factors such as (i) simultaneous anion and cations motion (ii) ion- pair formation (iii) amorphous nature of films (iv) less viscous medium for the motion of ions. To meet these entire requirement, gel polymer electrolyte (polymer matrix swollen in a liquid electrolyte) films have attracted much attention as they possess the high ionic conductivity and enhance the interfacial property, electrochemical and structural stabilities [2]. GPE possesses the diffusive property of liquids as well as cohesive property of solids. The (–C–F) group of polymer PVDF-HFP has high dielectric constant and the ability of electron-withdrawing which assist the larger dissolution of salts and enhances the free charge carriers which take part in conduction process [4]. Generally, the plasticizers are organic solvent, such as, propylene carbonate (PC), ethylene carbonate (EC), dimethyl carbonate (DMC) and diethyl carbonate (DEC) are known to behave as plasticizers, prevent ion pairing and enhance the amorphicity as well as flexibility of polymer chains resulting in improvement of the stability of electrode/electrolyte interface and increase in ionic conductivity with battery properties[5]. Song et al.[2] reported the PC+DEC modified PVdF-HFP based gel polymer electrolyte for the lithium ion battery applications. But contrary, it also reduces mechanical strength of polymer electrolyte. Blending of polymer is considered to enhance mechanical stability [5]. Hence, polymethyl methacrylate (PMMA) polymer is used due to the advantages properties such as good compatible nature with other polymers, high chemical resistance, electrical properties etc.[6]. Moreover, the functional group (-CO) of PMMA interacts with cations in the liquid electrolyte [4]. $LiClO_4$ salt is selected as a salt due to its special properties such as smaller radius of ion, low dissociation energy and the high dissolution ability in most of the organic solvents. In the present work, structural, conductivity and dielectric behavior of the Li ion

National Conference on Advanced Materials and Nanotechnology - 2018
AIP Conf. Proc. 2009, 020034-1–020034-4; https://doi.org/10.1063/1.5052103
Published by AIP Publishing. 978-0-7354-1725-0/$30.00

conducting PVdF-HFP and PMMA based gel polymer electrolyte with the variation of PC:DEC plasticizers has been undertaken.

EXPERIMENTAL

Standard solution casting method is used to prepare gel polymer electrolyte (GPE) system [$PVdF\text{-}HFP_{(50wt\%)}$:$PMMA_{(50wt\%)}$]- x wt% (PC:DEC)(1:1) - 10 wt% $LiClO_4$; where x = 20,30,40,50 and 60. Poly (Vinylidene fluoride-co-hexafluoropropylene) (PVdF-HFP Mw=$4x10^5$ from Sigma Aldrich) and poly(methyl methacrylate) (PMMA, M_w = $3.5x10^5$ from Alfa Aesar) as a host polymer. Lithium perchlorate ($LiClO_4$, 99.99% from Sigma Aldrich) and the organic solvents propylene carbonate (PC) and diethyl carbonate (DEC) were purchased from Sigma Aldrich as plasticizers to prepare GPE. Known amount of PVdF-HFP and PMMA were dissolved in acetone and an appropriate amount of $LiClO_4$ salt was dissolved in equal amount of plasticizers (PC:DEC). Electrolyte solution was then transferred to polymer solution. The solution was stirred for 24 hours until the mixture gets homogeneous in nature. The solution with different amount of plasticizers was cast onto Teflon Petri dish and then kept above room temperature at about 60 °C to form the gel in the films and allowed acetone to evaporate slowly. After the evaporation of acetone, free standing and flexible thin films of thickness of about 0.12 mm to 0.14 mm were obtained. Structural behavior and surface morphology of samples was examined by using an X-ray diffractometer (BRUKER D2-Phaser) with Cu Kα radiation of wavelength λ=1.540 Å in 2θ range of 5º-70° and a JEOL JSM-6010LA scanning electron microscope (SEM) respectively. Electrical measurement were carried out using Agilent LCR meter in the frequency range 20 Hz to 2 MHz at different temperatures between 303 K and 343 K by sandwiching films between two stainless steel electrodes.

RESULTS AND DISCUSSION

Structural Analysis

Figure 1 shows SEM micrograph with diffraction pattern in inset. The image shows the swelled nature with small pores in the gel polymer electrolyte. These pores provide more conductive channels for the transportation of lithium ions. Methew *et al.*[5] reported that the presence of a plasticizer rich phase in system leads to ion mobility helps to increase ionic conductivity. The broader peak of XRD pattern indicates amorphous nature of the present system is also increased by increasing the amount of plasticizers. Similar effect has also been reported by Sharma et al. [7]. The addition of low molecular weight plasticizers PC + DEC into the polymer matrix reduces the force of attraction between polymer chains making it more flexible and thus amorphous nature of the polymer enhance resulting into the alteration of physical properties of GPE.

Conductivity and Dielectric Properties

Figure 2 shows the impedance plot of GPE containing 40 wt% of PC:DEC plasticizers. The plot consists low frequency inclined spike (due to the interfaces between electrolyte and electrode) followed by the high frequency semicircle arc (bulk effect). The ionic conductivity σ of the polymer films has been calculated using the given relation

$$\sigma = \frac{t}{R_b A} \tag{1}$$

where t is the thickness of the films, A is the area of the electrolyte film with the electrode in contact and R_b is the bulk resistance. R_b values are determined from the intercepts of spikes with real axis. From the figure, it can be seen the values of the conductivity increase with increasing the amount of PC:DEC plasticizers from 20 wt% to 60 wt%. A maximum electrical conductivity of 1.03 X 10^{-3} S cm^{-1} at 303 K has been achieved for the polymer blend gel electrolyte containing 60 wt% of PC:DEC plasticizers. The enhancement in conductivity due to addition of plasticizers can be attributed to change in both mobility and carrier concentration. Increase in carrier concentration and mobility is expected due to increase the degree of salt dissociation and increased amorphous nature of films respectively. The amorphous nature of the prepared GPE film is revealed from the XRD pattern.

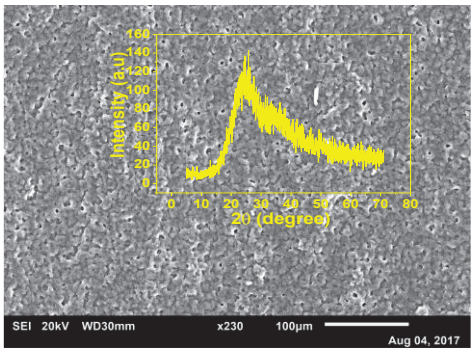

FIGURE 1. SEM micrograph of the GPE film containing 60 wt% PC:DEC plasticizers

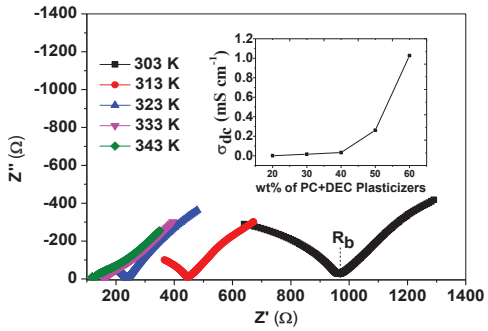

FIGURE 2.Impedance plot of GPE with 40 wt% PC:DEC (inset σ_{dc} at different concentration of PC:DEC at 303 K)

According to Sharma et al.[7] addition of high dielectric constant plasticizers in polymer complexes reduces the inter ion coulomb interaction and more number of ions contributes towards conductivity. In order to explore the ion conduction mechanism, the conductivity is calculated as a function of frequency from the real and imaginary part of impedance data. The frequency dependent AC conductivity at different temperatures for GPE with 40 wt% PC:DEC plasticizers is shown in Fig. 3. The low frequency dispersive region is due to accumulation of charges near electrode-electrolyte interface due to slow periodic reversal effect of electric ac field. The mid frequency plateau region corresponds to the frequency independent conductivity σ_0, known as DC conductivity. The high frequency dispersion region of AC conductivity is analysed and fitted using the universal Jonscher's power law relation $\sigma(\omega) = \sigma_0 + A\omega^n$, where n is the power law exponent $0 < n < 1$. ω is the angular frequency, σ_0 is the DC conductivity, A is a constant at a particular temperature. The values of power law exponent n is found to be decrease from 0.67 to 0.30 with increase in temperature which shows that the correlated barrier–hopping (CBH) model is appropriate to explain frequency and temperature dependence of AC conductivity[8].

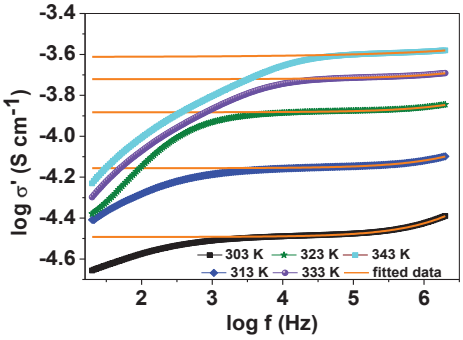

FIGURE 3. AC conductivity as a function of frequency at different temperatures for GPE with 40 wt% PC:DEC

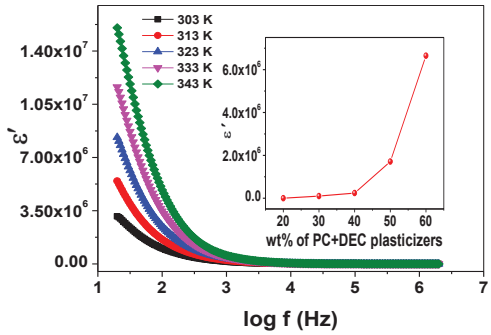

FIGURE 4. Dielectric constant as a function of frequency at different temperatures for GPE with 50 wt% PC:DEC

The study of dielectric property has been carried out in terms of dielectric constant parameter which measures the storage of electrical charges by materials and polarization in a given volume [9]. The dielectric constant (ε') as a function of frequency for GPE with 50 wt% PC:DEC plasticizers at different temperatures is shown in Fig.4. A dispersive nature of ε' towards lower frequency side is attributed space charge polarization due to building up of charge at the interface because of slow periodic reversal effect of applied field, giving the large value of ε' at lower frequency. While at high frequency, diffusion of ions is not feasible because of fast periodic reversal effect of electric field and incapability of dipoles to orient themselves in the direction of the applied alternating field. Hence, the decrease in the value of ε' has been observed with increasing the frequency. From Fig.4 (inset), the variation of dielectric constant (ε') with composition at 50 Hz shows a similar behavior as observed in conductivity. The increase in dielectric constant may be due to increased charge carrier density as result of salt dissociation with increasing the amount of plasticizer [7]. In order to understand conductivity relaxation mechanism in our system, the data has been

analyzed in terms of electric modulus. Figure 5 show the frequency dependent of imaginary (M'') part of modulus at different temperatures for the GPE containing 50 wt% PC:DEC plasticizers. It shows that M'' increase towards high frequency side and gives a long tail at low frequencies due to electrode polarization phenomenon. The long tails indicate that large capacitance values associated with the electrodes. The peak at high frequency shows that the gel polymer electrolyte film is ionic conductor. The presence of peak of the M'' curve at higher frequency side may be due to bulk effect. The ions are spatially confined to their potential wells and make only short-range motion with in the wells at the high frequency side of the modulus spectra and peak suggest the transition from long range to short range motion of ions. The broad nature of the M'' peaks is indicative of distribution of relaxation time in the present GPE system. Figure 6 shows the variation of loss tangent with frequency for different concentration of PC:DEC plasticizers for GPE films at 303 K. The loss spectra consisting of peak at a characteristic frequency is attributed to dipolar relaxation. The shift in peak towards higher frequency side with increase in plasticizer concentration results in faster ionic motion which indicates low relaxation time required to relax the system. The presence of the plasticizer in gel polymer electrolyte reduces the attractive forces between polymer chains consequently the segmental motion enhances [10].

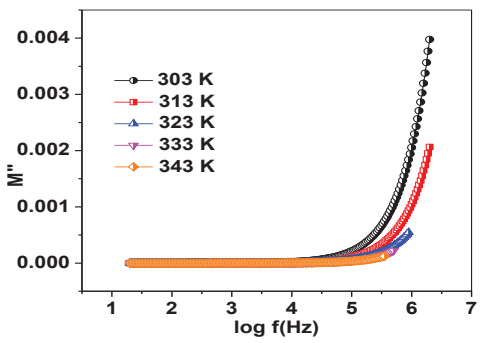

FIGURE 5. M″ versus log f at different temperature for GPE with 50 wt% PC:DEC plasticizers

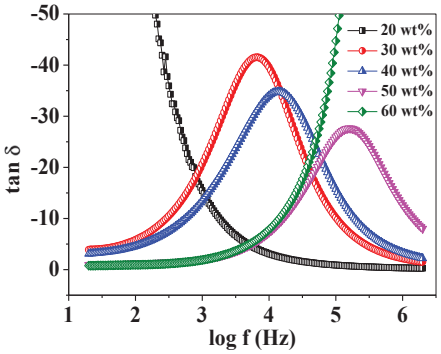

FIGURE 6.Variation of tangent loss at different concentration of PC:DEC plasticizers at 303 K

CONCLUSIONS

The gel polymer electrolyte system comprised of (PVdF-HFP+PMMA)-(PC:DEC) –$LiClO_4$ have been prepared via solution casting method. SEM and XRD analysis reveal swelled and amorphous nature of GPE. The electrical conductivity increases with increasing the plasticizers content from 20 wt% to 60 wt% and highest electrical conductivity of 1.03×10^{-3} S cm^{-1} is observed for the sample containing 60 wt% of PC:DEC plasticizers. These gel polymer electrolyte samples follow the Jonscher's power law. The dielectric constant also increases with increasing plasticizer content attributing its use as a good electrolyte for the battery formation. The electrode–electrolyte interface polarization process is found at lower frequencies. The loss peak of tangent loss suggests that the gel polymer electrolyte system relax much faster with addition of plasticizers.

REFERENCES

1. L. Long, S.Wang, M. Xiao, and Y. Meng, Journal of Materials Chemistry A **4**, 10038-10069 (2016).
2. S. Song, J. Wang, J. Tang, R. Muchakayala, and R. Ma, Ionics **23**, 3365-3375 (2017).
3. S. Ramesh and O. P. Ling, Polym. Chem. **1**, 702–707(2010).
4. Z. He, Q. Cao, B. Jing, X. Wang, and Y. Deng, RSC Adv. **7**, 3240-3248(2017).
5. C. M. Methew, K. Kesavan, and S. Rajendran, Ionics **20**, 439-443 (2014).
6. R. Subadevi, M. Sivakumar, S. Rajendran, H. Wu, and N. Wu, Ionics **18**, 283-289 (2012).
7. P. Sharma, D. K. Kanchan, and N. Gondaliya, Ionics **19**, 777-785 (2013).
8. R. Ondo-Ndong, G. Ferblantier, F. Pascal-Delannoy, A. Boyer, and A. Foucaran, Microelectronics Journal **34**, 1087-1092 (2003).
9. H. J. Woo, S. R. Majid, and A. K. Arof, Material Chemistry and Physics **134**, 755-761(2012).
10. N. Gondaliya, D. K. Kanchan, P. Sharma, and M. S. Jayswal, Polymer Composites **33**, 2195–2200 (2012).

Journal of Solid State Electrochemistry
https://doi.org/10.1007/s10008-020-04507-3

ORIGINAL PAPER

Effect of $Mg(CF_3SO_3)_2$ concentration on structural and electrochemical properties of ionic liquid incorporated polymer electrolyte membranes

C. Maheshwaran[1] · D.K. Kanchan[1] · Khushbu Gohel[1] · Kuldeep Mishra[2] · Deepak Kumar[3]

Received: 4 October 2019 / Revised: 11 December 2019 / Accepted: 17 January 2020

Abstract

In the present study, a magnesium ion conducting polymer electrolyte membrane system based on polyethylene oxide (PEO) containing magnesium triflate $Mg(CF_3SO_3)_2$ salt and 1-ethyl-3-methylimidazolium tetrafluoroborate (EMIM-BF_4) ionic liquid is prepared using standard solution casting technique. X-ray diffraction and differential scanning calorimetry studies reveal change in crystalline character with variation in $Mg(CF_3SO_3)_2$ concentration within PEMs. Fourier transform infrared spectroscopy technique reflects ion-polymer interactions within the prepared polymer electrolyte system. Dielectric and modulus properties of prepared electrolyte membranes show significant changes in dielectric constant and relaxation behavior respectively on varying $Mg(CF_3SO_3)_2$ concentration. The optimized polymer electrolyte membrane with 6 wt% of magnesium triflate salt shows maximum ionic conductivity of $\sim 9.4 \times 10^{-5}$ S cm^{-1} at room temperature. The ionic conductivity variation with temperature shows Arrhenius behavior for PEMs. The Mg^{2+} conduction within the PEMs is established using CV study and electrochemical stability window of ~ 4.0 V is determined using linear sweep voltammetry. The PEMs are dominantly ionic conducting with Mg^{2+} transport number ~ 0.22 for the optimized PEM.

Keywords Polymer electrolyte membranes · Mg ion conductor · Ionic liquid · Ionic conductivity

Introduction

Since the commercialization of first lithium-ion battery in 1991, these batteries, with two Li^+ insertion electrodes and a Li-ion conducting electrolyte, have been established as an ultimate sophisticated energy storage device [1–3]. However, the high cost, less abundance, environmental impacts, and some safety limitations have forced the researchers to look for alternate electrochemical cells based on Na, Mg, Zn, K, Al, etc. [4–9]. Magnesium, with $E°$ of − 1.55 V vs SHE and theoretical capacity of 2205 mA h g^{-1}, appears a good substitute of Li-ion batteries [10]. Further, the cost effectiveness, low toxicity, ease of handling, and lesser reactivity of magnesium make it attractive for fabricating electrochemical devices such as batteries, fuel cells, supercapacitors, solar cells, and electrochemical displays. For realizing commercial Mg-ion batteries, a good ion conducting electrolyte with significant electrochemical and thermal stability is a prerequisite [11].

Polymer electrolyte membranes (PEMs) have recently attracted much attention for applications in energy storage and conversion devices [12, 13]. For fabrication of PEM, various polymers such as poly ethylene oxide (PEO), poly(vinylidene fluoride-co-hexafluoropropylene) (PVDF-HFP), poly(methyl methacrylate) (PMMA), polyvinyl alcohol (PVA), polyvinyl chloride (PVC), polyvinylpyrrolidone (PVP), polyacrylonitrile (PAN), rubber (MG49, ENR50, etc.), polyester, and polycarbonate are utilized. PEO-based PEMs have been extensively reported for various electrochemical devices including the magnesium-ion batteries [14–16]. PEO-based PEMs own low ionic conductivity due to its semi-crystalline nature which seized the segmental motion of polymer chain and restrict the ion mobility. The researchers have attempted to suppress the crystallinity of the

✉ Deepak Kumar
fwtdrdeepak@gmail.com; deepak.kumar06@gov.in

[1] Department of Physics, M.S. University of Baroda, Vadodara, Gujarat 390002, India

[2] Department of Physics, Jaypee University, Anoopshahr, Uttar Pradesh 203390, India

[3] Electronics and Mechanical Engineering School (Affiliated to Gujarat Technological University), Under Corps of EME, Ministry of Defence, Vadodara, Gujarat 390008, India

Published online: 21 January 2020

PEO chain to improve mobility of ions through faster ion hoping, thereby leading to better ionic conduction. The ion hopping is believed to be predominant in amorphous PEO-based PEMs [17].

An alternative method of achieving high conductivity while retaining the useful properties of PEMs is to use ionic liquids (ILs) either as the main conducting species immobilized in a polymer membrane or as a plasticizing agent in the PEMs [18, 19]. The 1-ethyl-3-methylimidazolium tetrafluoroborate (EMIM-BF_4) ionic liquid is a green solvent, which acts as plasticizer and supplier of new charge carriers (bulky and asymmetric organic $EMIM^+$ cations and inorganic BF_4^- anions) for ionic conduction in polymer electrolyte system. This ionic liquid possesses various specific properties such as wide liquid-phase range, non-volatility, non-flammability, eco-friendliness, ability to dissolve in a variety of compounds, negligible vapor pressure at room temperature, wide electrochemical stability window, high ionic conductivity, and excellent thermal/chemical stability [19, 20].

The ion conduction mechanism in polymer electrolytes has been explained by various models [21]. The role of ILs in electrolytic properties of PEO-based Li-ion conducting PEMs has been investigated by Chaurasia et al. [22, 23]. They demonstrated that the IL confined in PEO not only plasticizes the polymer but also coordinates with the electronegative group of PEO and influences free ion concentration within PEM. However, the reports on Mg^{2+}-based PEMs lack in numbers when compared with the existing Li-ion- and Na-ion-based PEMs [6, 24–30]. It is important to note that researchers are trying hard to develop a commercial Mg-ion conducting electrolyte by using ionic liquids as non-flammable molten salts and active/passive nanofillers for better solvent retention within the polymer-based electrolyte systems [31, 32]. The study of ion-dynamics behavior in such PEMs is of fundamental interest to fabricate modern electrolyte systems by tailoring conduction mechanism. However, a systematic study for understanding the role of IL in modifying the structural and electrochemical properties of Mg^{2+} conducting PEM is still lacking. Here, we present a detailed analysis of Mg^{2+} conducting PEMs using PEO and EMIM-BF_4 as ionic liquid with varying concentrations of $Mg(CF_3SO_3)_2$ salt. EMIM-BF_4 is known as moisture-stable form of IL. $EMIM^+$ cation if combined with $CF_3SO_3^-$ anion of $Mg(CF_3SO_3)_2$ also forms EMIM-CF_3SO_3 as moisture-stable forms of IL [33, 34]. Considering the low viscosity (2 cP), high conductivity (15.92 mS cm^{-1}), and high dielectric constant (14.8), we have taken (EMIM-BF_4) IL compared to other imidazole-based ILs. Enhancement of ionic conductivity occurs due to ionic dissociation through Lewis acid–base interaction between IL and polymer/ionic species. In view of this, it would be interesting study to investigate the structural and electrochemical properties of PEMs containing $EMIMBF_4$ as ionic liquid, PEO as polymer host, and $Mg(CF_3SO_3)_2$ as salt.

In this study, we have shown how the salt changes/controls ionic conduction and relaxation parameters in polymer electrolyte for electrochemical performances with these electrolytes.

Experimental section

Materials

The materials used for the preparation of PEMs were PEO of average molecular weight ~ 300,000 from Alfa Aesar, magnesium triflate, $Mg(CF_3SO_3)_2$, salt of 97% purity from Aldrich, and EMIM-BF_4 extrapure for catalysis and nanotechnology grade from SRL. Acetone of purity 99% was obtained from Aldrich and was used as received for dissolving polymer host.

Preparation of PEMs

PEMs were prepared by standard solution casting technique. In this technique, initially stoichiometric amounts of polymer PEO and ionic liquid EMIM-BF_4 (9:1 wt/wt) were dissolved in acetone through continuous stirring for 5–6 h at 40 °C. The homogeneous solution, thus obtained, was poured in Teflon petri dish and left for solvent evaporation at ambient temperature. After complete evaporation of the solvent, free standing membrane containing no magnesium salt was obtained. In order to obtain Mg^{2+} conducting PEM, the various concentrations of $Mg(CF_3SO_3)_2$ salt were added to the PEO + EMIM-BF_4 solution according to compositional formula; (PEO + EMIM-BF_4) + x wt% $Mg(CF_3SO_3)_2$ for $x = 1$ to 7 wt%. After complete evaporation of the solvent, Mg^{2+} conducting free standing PEMs were obtained.

Characterization of PEMs

X-ray diffraction measurements were carried out with XPERT-PRO System using CuKα radiation in the Bragg angle (2θ) ranging from 10° to 70° at scanning rate of 2° min^{-1}. Atomic force microscopy was performed by employing AFM, pico SPM-picoscan 2100, Molecular Imaging, USA. The imaging was performed in tapping mode with a diamond-like carbon coated ultra-sharp silicon tip. Fourier transform infrared spectra of the prepared samples were recorded in the wavenumber range of 650–4000 cm^{-1} using single beam FTIR 4100 JASCO model. The spectra were recorded by averaging 32 scans per sample with an optical resolution of 4 cm^{-1}. The measurements were taken by directly mounting the electrolyte membrane in the sample holder in transmission mode. Thermal properties of these PEMs were studied by differential scanning calorimetry (DSC). For the DSC measurement, samples were hermetically sealed in aluminum pan and DSC thermograms were obtained in the temperature range from RT to 70 °C using

SII EXSTAR-6000 systems at the heating rate of 10 °C min^{-1} under N_2 atmosphere. The electrical characterization of PEMs was performed by impedance spectroscopic technique. Precision Solartron 1260 Impedance analyzer was used in the frequency range from of 1 Hz to 32 MHz with a signal level of 50 mV in temperatures range from 303 and 333 K. The impedance measurements are carried out by sandwiching the PEMs between two stainless steel electrodes under spring pressure. The cyclic voltammetry (CV) and linear sweep voltammetry (LSV) were performed by using electrochemical analyzer (Zive SP1) of WonATech Co., Ltd., Korea at scan rate of 5 mV s^{-1}. The dc polarization measurements were also performed by using electrochemical analyzer (Zive SP1) of WonATech Co., Ltd., Korea.

Results and discussion

X-ray diffraction studies

X-ray diffraction (XRD) patterns have been recorded and shown in Fig. 1 for various $Mg(CF_3SO_3)_2$ salt concentration within the PEMs. The polymer electrolyte consisting of PEO and ionic liquid EMIM-BF_4 shows peaks at 19.6°, 23.4°, and 27.0°, respectively, due to the semi-crystalline nature of PEO polymer. PEMs consisting of PEO + EMIM-BF_4 with varying amount of $Mg(CF_3SO_3)_2$ salt maintain the prominent peaks orientation at 19.6° and 23.4°, respectively [35]. It is important to note that the peak intensity corresponding to 19.6° and 23.4° reduces on increasing the concentration of $Mg(CF_3SO_3)_2$ salt from 0 to 6 wt%. This decrease in peak intensity can be inferred as possible decrease in crystalline character of the PEMs on enhancing the $Mg(CF_3SO_3)_2$ salt concentration. When the $Mg(CF_3SO_3)_2$ salt concentration reaches to 7 wt%, an increase in peak intensity is observed which depicts the rise in crystalline character of the PEMs. Thus, significant structural changes are observed when $Mg(CF_3SO_3)_2$ salt concentration changes within the polymer electrolyte membranes [36].

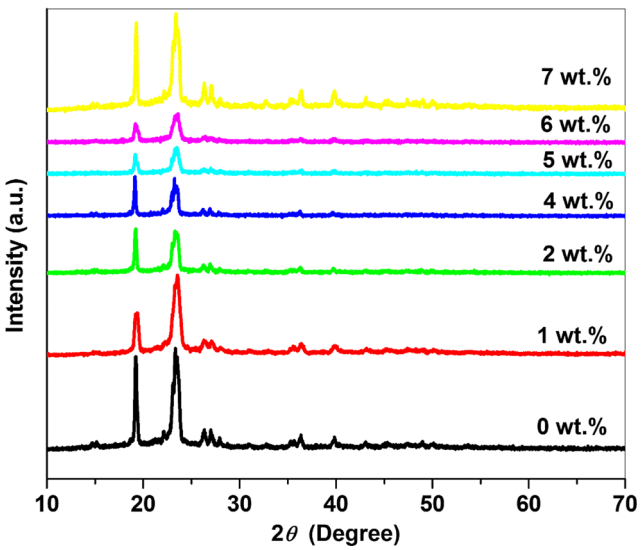

Fig. 1 X-ray diffraction patterns of PEO + EMIMBF_4 with varying amount of $Mg(CF_3SO_3)_2$ salt from 0 to 7 wt%

AFM studies

Figure 2 displays the AFM micrographs of the PEMs consisting of PEO, EMIM-BF_4, and $Mg(CF_3SO_3)_2$ salt. On varying $Mg(CF_3SO_3)_2$ salt concentration within the PEMs, significant morphological changes are observed with respect of roughness events as seen in Fig. 2a–d . On addition of $Mg(CF_3SO_3)_2$ salt concentration from 1 to 6 wt% in PEO + EMIM-BF_4 matrix, the maximum roughness height in AFM graphs changes from 794 to 148 nm while an average roughness height decreases from 340 to 90 nm, respectively. This

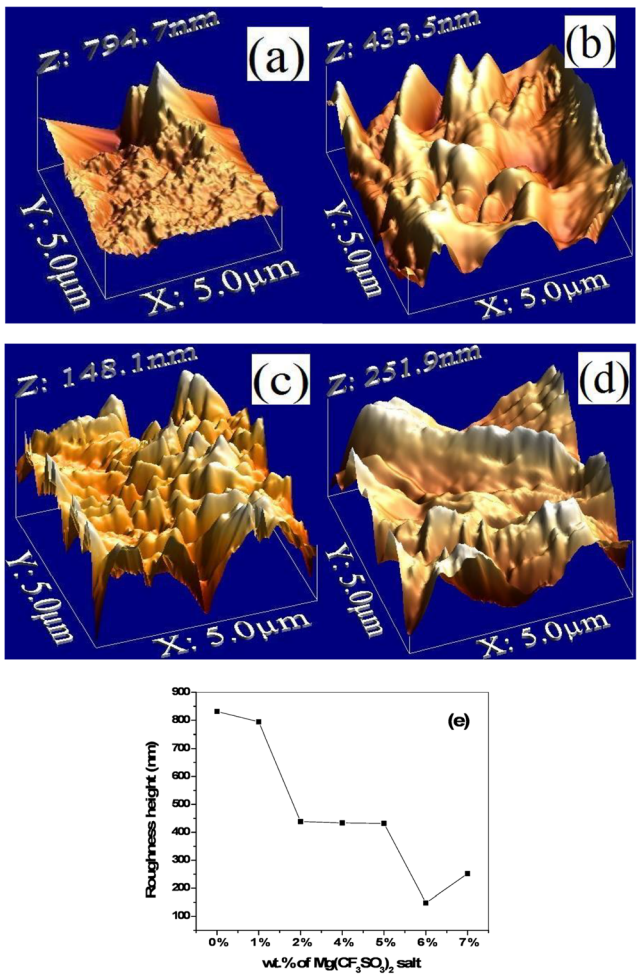

Fig. 2 AFM analysis for PEMs with composition (PEO + EMIM-BF_4) + x wt% $Mg(CF_3SO_3)_2$: **a** $x = 1$, **b** $x = 5$, **c** $x = 6$, **d** $x = 7$, and **e** roughness height verses $Mg(CF_3SO_3)_2$ salt concentration

reduction in roughness peaks is possibly due to initial supportive aggregation of ions from $Mg(CF_3SO_3)_2$ and EMIM-BF_4 occupying the conduction pathways inside the PEO + EMIM-BF_4 matrix [37]. However, at 7 wt% of $Mg(CF_3SO_3)_2$ salt concentration, the maximum roughness height dramatically rises to 251 nm and average roughness height to 125 nm as shown in Fig. 2e . The sudden rise in height of roughness events may be due to blocking effects of salt aggregation as explained by Parthiban et al. [38].

FTIR studies

In order to investigate any change in molecular bond lengths and/or interaction among PEO, EMIM-BF_4, and $Mg(CF_3SO_3)_2$ salt in PEMs, FTIR spectra of pure PEO, (EMIM-BF_4) IL, $Mg(CF_3SO_3)_2$ salt, and (PEO + EMIM-BF_4) + $Mg(CF_3SO_3)_2$ PEMs have been obtained (Fig. 3a). The constituent materials are showing their characteristic bands. The polymer PEO has ethylene group (-CH_2-CH_2-), which shows different twisting, wagging, and rocking type vibrations. The C-O-C group attached to the main chain of PEO possesses symmetric and asymmetric vibration modes with a tendency of forming hydrogen bond with the cation of the ionic liquid EMIM-BF_4 and salt $Mg(CF_3SO_3)_2$ [22]. Thus, the immobilization of EMIM-BF_4 and $Mg(CF_3SO_3)_2$ in PEO may lead significant changes in these IR active modes of PEO. In order to see the effect of addition of IL in PEO with subsequently variation of salt $Mg(CF_3SO_3)_2$ in PEO + EMIM-BF_4, the FTIR spectra of PEO, EMIM-BF_4, $Mg(CF_3SO_3)_2$ salt, PEO with EMIM-BF_4 membrane, and (PEO + EMIM-BF_4) with 6 wt% $Mg(CF_3SO_3)_2$ PEM have been extended because main features are observed in the wavenumber region 700–1700 cm^{-1} (Fig. 3b). The changes in the following features are observed:

(i) The bands at 744 cm^{-1} of C-H bending in pure PEO disappear when IL is added to PEO and (PEO + EMIM-BF_4) + $Mg(CF_3SO_3)_2$ PEMs.

(ii) The band at 840 cm^{-1} of C-O stretching in pure PEO has been shifted to 844 cm^{-1} when $Mg(CF_3SO_3)_2$ salt is increased in the (PEO + EMIM-BF_4) + $Mg(CF_3SO_3)_2$ PEM.

(iii) The bands observed in the region 1000–1200 cm^{-1} corresponding to the C-O-C stretching vibration of PEO are very much sensitive to the cations of both the ionic liquid $EMIM^+$ and Mg^{2+} [36, 39]. The PEO shows characteristic bands at 1009, 1057, 1100, and 1146 cm^{-1} in this region. The band at 1009 cm^{-1} also disappears in (PEO + EMIM-BF_4) + $Mg(CF_3SO_3)_2$ PEM due to addition of IL which is showing a broad flat dip in this region. However, the bands at 1057 and 1146 cm^{-1} of pure PEO have been shifted to 1061 and 1149 cm^{-1}, respectively, when the IL is immobilized in PEO. The band at 1100 cm^{-1} in pure PEO shifts to 1109 cm^{-1} even in (PEO + EMIM-BF_4) membrane as well as in (PEO + EMIM-BF_4) + $Mg(CF_3SO_3)_2$ PEM. These observations suggest the possible interaction of the $EMIM^+$ of IL and Mg^{2+} of salt with ether oxygen of PEO.

(iv) Additionally, the band at 1276 cm^{-1} of pure PEO is observed to shift at 1282 and 1280 cm^{-1} while the band at 1635 cm^{-1} of C=C and C=N stretching of pure IL appears to shift to higher wave number side, i.e., 1656 cm^{-1} in all PEM membranes. It means the bond lengths of C=C and C=N stretching of pure IL slightly decrease due to the interaction with PEO and Mg salt in the PEMs.

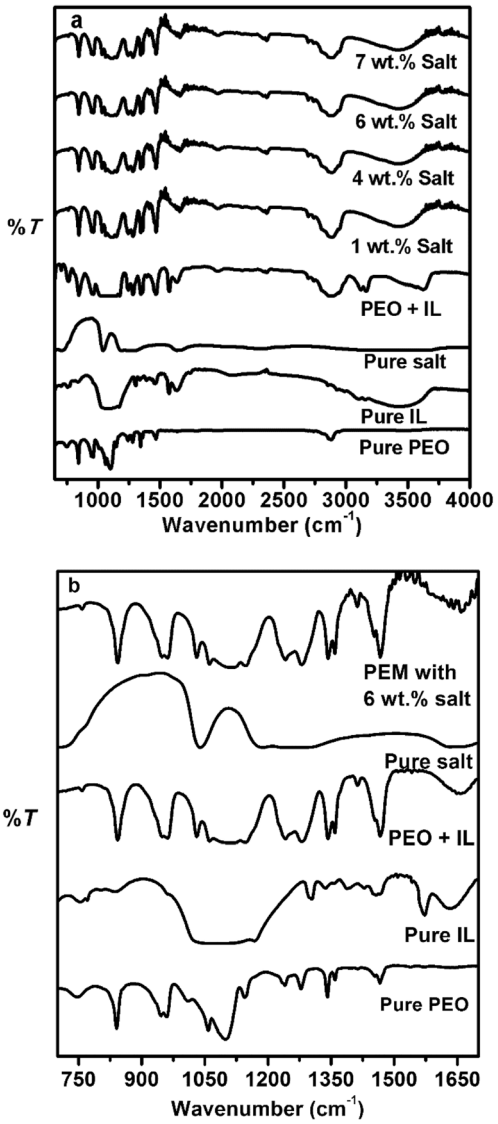

Fig. 3 **a** FTIR spectra of pure PEO, pure EMIM-BF_4 IL, pure $Mg(CF_3SO_3)_2$ salt, PEO + EMIM-BF_4 membrane, and PEO + EMIM-BF_4 containing different $Mg(CF_3SO_3)_2$ concentrations; **b** extended FTIR spectra of pure PEO, pure EMIM-BF_4 IL, PEO + EMIM-BF_4 membrane, pure $Mg(CF_3SO_3)_2$ salt, and PEO + EMIM-BF_4 containing 6 wt% $Mg(CF_3SO_3)_2$ salt in the wavenumber range 700–1700 cm^{-1}

(v) The bands centered at 1298 and 1571 cm^{-1} of pure IL disappear in the IR spectra of (PEO + EMIM-BF_4) + $Mg(CF_3SO_3)_2$ PEMs.

(vi) No separate bands of pure $Mg(CF_3SO_3)_2$ salt have been observed in PEMs, which is indicative of the complete complexation of the salt.

In addition to these observations, the broad band centered at ~ 3440 cm^{-1} in pure EMIM-BF_4 IL is due to the symmetric stretching of the aromatic ring of IL observed in all the PEMs at all salt concentrations [40]. However, this band appears narrower in (PEO + EMIM-BF_4) + $Mg(CF_3SO_3)_2$ PEMs (Fig. 3a). It is well known that the –OH stretching also gives its signature in IR near 3200 cm^{-1} wavenumber which may be due to the hygroscopic nature of $Mg(CF_3SO_3)_2$ salt in the PEMs. But as this peak is centered away from 3400 cm^{-1} and no change in shift is observed with the addition of $Mg(CF_3SO_3)_2$ salt in any of these PEMs, hence presence of –OH stretching vibrations is neglected. These observations suggest the good complexation among PEO, EMIM-BF_4, and $Mg(CF_3SO_3)_2$ in PEMs.

DSC analysis

DSC has been utilized to probe the amorphous or crystalline nature of PEMs membranes. Figure 4 shows the DSC thermograms for the electrolyte system PEO + EMIM-BF_4 with varying amount of $Mg(CF_3SO_3)_2$ salt. The reduction in melting temperature (T_m) is observed with the increasing concentration of $Mg(CF_3SO_3)_2$ till 6 wt%. In addition, the broadening of the peaks with salt concentration enhancement is evident from the thermogram which is indicative of increase in amorphous nature within PEMs.

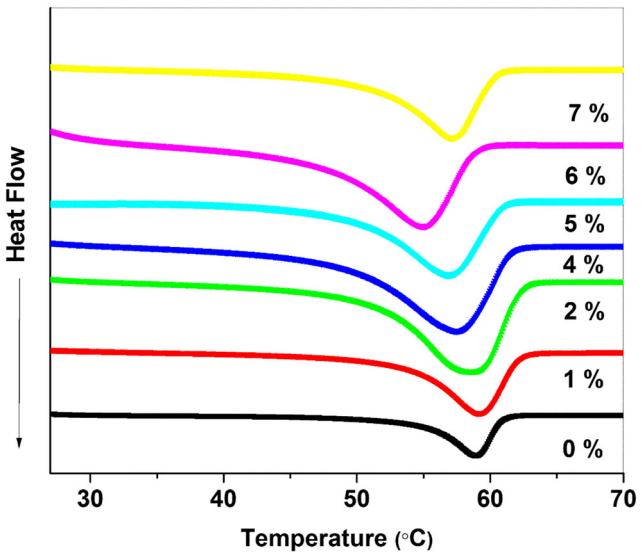

Fig. 4 DSC curves of PEO + EMIM-BF_4 and PEO + EMIM-BF_4 containing different concentrations of $Mg(CF_3SO_3)_2$

The decrease in T_m of polymer with increasing amounts of the $Mg(CF_3SO_3)_2$ leads to the flexible polymer backbone due to the weaker intermolecular interaction between polymer chains. This flexible polymer backbone facilitates higher segmental motion of the polymer backbone and hence high ionic conductivity [25]. Further, the reduction of melting temperature and broadening of melting endothermic peaks with the addition of $Mg(CF_3SO_3)_2$ salt are consistent with increase in the amorphous phase of PEMs which are in consonance with results of XRD pattern. The degree of crystallinity (X_c) is calculated for 100% crystalline PEO phase by the Eq. 1 [41] and results are presented in Table 1.

$$X_c = \left(\frac{\Delta H_m}{\Delta H_m^o}\right) \times 100\% \quad (1)$$

Here ΔH_m^o and ΔH_m are the melting enthalpy of 100% crystalline PEO and prepared PEMs. The endothermic peaks corresponding to melting temperature (T_m) are also indicated in Table 1. It can be noticed that T_m peaks shift towards lower values till 6 wt% concentration of the $Mg(CF_3SO_3)_2$ salt. This change has been attributed to the possible plasticization effect of EMIM-BF_4 ionic liquid [42].

Electrochemical impedance spectroscopy

Nyquist plots and ionic conductivity

The Nyquist plot (Z' vs Z'') for the freshly prepared PEMs with different $Mg(CF_3SO_3)_2$ concentration at temperature 303 K is shown in Fig. 5a . The difference between real part of impedance at high frequency and low frequency end of semicircular portion indicates the bulk resistance (R_b) of the PEMs. From Fig. 5a , we observe that the R_b decreases as the $Mg(CF_3SO_3)_2$ salt concentration increases from 0 to 6 wt%. However, R_b slightly increases for 7 wt% salt concentration. The R_b is inversely proportional to the ionic conductivity and is given by the formula

Table 1 Melting temperature (T_m) and degree of crystallinity (X_c) of PEO + EMIM-BF_4 with increasing $Mg(CF_3SO_3)_2$ concentration

(PEO + EMIM-BF_4) + x wt% $Mg(CF_3SO_3)_2$	T_m (°C)	%X_c
$x = 0$	59.2	52.5
$x = 1$	58.9	46.2
$x = 2$	58.5	35.2
$x = 4$	57.5	33.3
$x = 5$	56.5	28.4
$x = 6$	54.9	16.3
$x = 7$	57.0	35.2

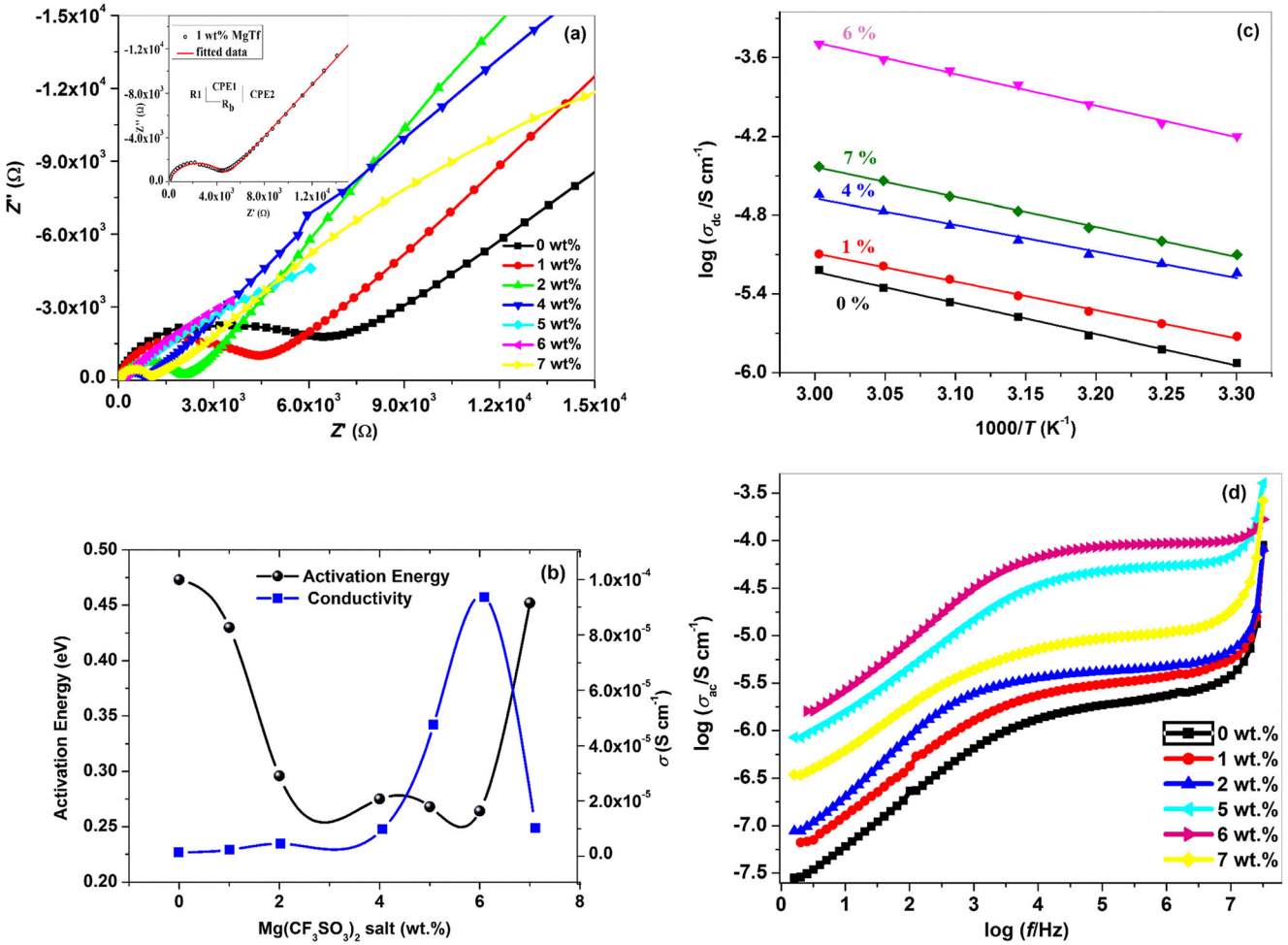

Fig. 5 **a** Nyquist plots of PEO + EMIM-BF_4 PEMs with different concentrations of $Mg(CF_3SO_3)_2$. **b** Variation of ionic conductivity as a function of $Mg(CF_3SO_3)_2$ salt concentration at room temperature. **c** Ionic conductivity as a function of temperature for PEMs containing $Mg(CF_3SO_3)_2$ salt concentration 0, 1, 4, 6, and 7 wt%. **d** Frequency dependent conductivity spectra of PEMs (PEO + EMIM-BF_4) + x wt% $Mg(CF_3SO_3)_2$ where $x = 0$, 1, 2, 5, 6, and 7

$$\sigma = \frac{t}{R_b A} \tag{2}$$

where σ is ionic conductivity of the electrolyte, t is thickness of the electrolyte specimen, R_b is bulk electrolyte resistance, and A is area of cross-section of the electrolyte specimen.

The lowest value of R_b is observed for 6 wt% salt concentration which corresponds to maximum ionic conductivity of 9.4×10^{-5} S cm^{-1} at 303 K. It is important to note that the lowest activation energy has been observed for this PEM with 6 wt% salt concentration. A decrease in ionic conductivity is observed for higher loading of 7 wt% $Mg(CF_3SO_3)_2$ salt concentration as shown in Fig. 5b . Such decreases in ionic conductivity and increase of activation energy values of PEM are attributed to ion-association/aggregation as reported previously [43]. As the salt concentration increases, the value of conductivity is increased monotonically up to 6 wt% at temperature 303 K. The decrease in activation energy and increase in the ionic conductivity with the increases of salt concentration may be related to the increase in the number of mobile charge carriers in the polymer electrolyte [44]. Figure 5c depicts the variation of ionic conductivity (σ) as a function of temperature for prepared PEMs. The straight line feature of σ versus $1000/T$ plots suggests that ion transport in the PEMs follows the typical Arrhenius behavior which can be ascribed by Arrhenius equation

$$\sigma = \sigma_0 \exp\left(\frac{-E_a}{kT}\right) \tag{3}$$

where σ_0 is pre-exponential factor, E_a is the activation energy, k is the Boltzmann constant, and T is absolute temperature [45]. The increase in conductivity with rise in temperature is possibly due to increased thermal movement of polymer chain segments and greater salt dissociation. However at lower temperature, dipole-dipole interaction increases the cohesive energy of polymer matrix thereby giving rising to lesser conductivity values. Such finding has been previously reported by Ramya et al. [46].

Figure 5 d shows the behavior of conductivity as a function of frequency for the six different compositions of the PEM system, (PEO + EMIM-BF_4) + x wt% $Mg(CF_3SO_3)_2$ where x = 0, 1, 2, 5, 6, and 7 wt%, at 303 K. It may be noted that the spectra depicts three distinct region viz., low frequency dispersion region corresponds to the electrode polarization, mid frequency plateau attributed to the dc conductivity, and the high frequency dispersion region which could infer the frequency dependent ion transport [47]. For each PEM, we observe conductivity dispersion in low frequency region arising from space charge polarization at the electrode-electrolyte interface. Mid frequency region indicates a frequency independent plateau corresponding to the dc conductivity of the PEMs. At the high frequency region, a sharp conductivity rise is noticed and such feature may be attributed to displacement of the ionic species under the effect of alternating field.

Dielectric studies

A study of the dielectric behavior of the PEM enables to understand the conductivity behavior of the electrolyte system. The ion conduction and relaxation mechanism of a PEM system can be investigated with the help of dielectric constant and dielectric loss. The complex permittivity ε^*or dielectric constant of a system is defined by:

$$\varepsilon^* = \varepsilon' - j\varepsilon'' = \varepsilon' - j\left(\frac{\sigma}{\omega\varepsilon_o}\right) \tag{4}$$

where ε' is real part of complex permittivity (also known as dielectric constant), ε'' is imaginary part of complex permittivity of material (also known as dielectric loss), σ is conductivity, ω is angular frequency, and $\varepsilon_o$is permittivity of free space. The mathematical expressions for ε' and ε'' are given by the following equations;

$$\varepsilon' = \frac{Z''}{\omega C_o\left(Z'^2 + Z''^2\right)} \tag{5}$$

$$\varepsilon'' = \frac{Z'}{\omega C_o\left(Z'^2 + Z''^2\right)} \tag{6}$$

where ω is angular frequency, C_o is capacitance in vacuum, and Z' and Z'' represent the real and imaginary parts of impedance for electrolyte system.

The value of tan δ has been determined using the following relation

$$\tan(\delta) = \frac{\varepsilon''}{\varepsilon'} = \frac{Z'}{Z''} \tag{7}$$

The variation of dielectric constant (ε') and tangent loss (tan δ) as a function of frequency is shown in Fig. 6a and b for different PEMs. Increase in dielectric constant (ε') at lower frequency region may be ascribed as space charge polarization due to accommodation or build-up of charges near the electrode-electrolyte interface [48–50]. This is because of ion or dipoles are able to orient themselves in the direction of applied reversal AC field at lower frequency region. Whereas, at the higher frequency region, there is occurrence of the fast periodic reversal of the applied field and therefore dipoles have no time to orient themselves. In view of this, ε' and tan (δ) decrease rapidly and approach close to zero at the high frequency portion. Another conclusion can be drawn from Fig. 6a that the value of ε' is increasing with increasing the amount of $Mg(CF_3SO_3)_2$ salt from 0 to 6 wt%, whereas reverse trend has been observed for system with higher $Mg(CF_3SO_3)_2$ concentration. The highest values of ε' for the (PEO + EMIM-BF_4) + 6 wt% $Mg(CF_3SO_3)_2$ PEM is noticed. This may be due to increase in the charge carrier density with increasing the salt concentrations [51].

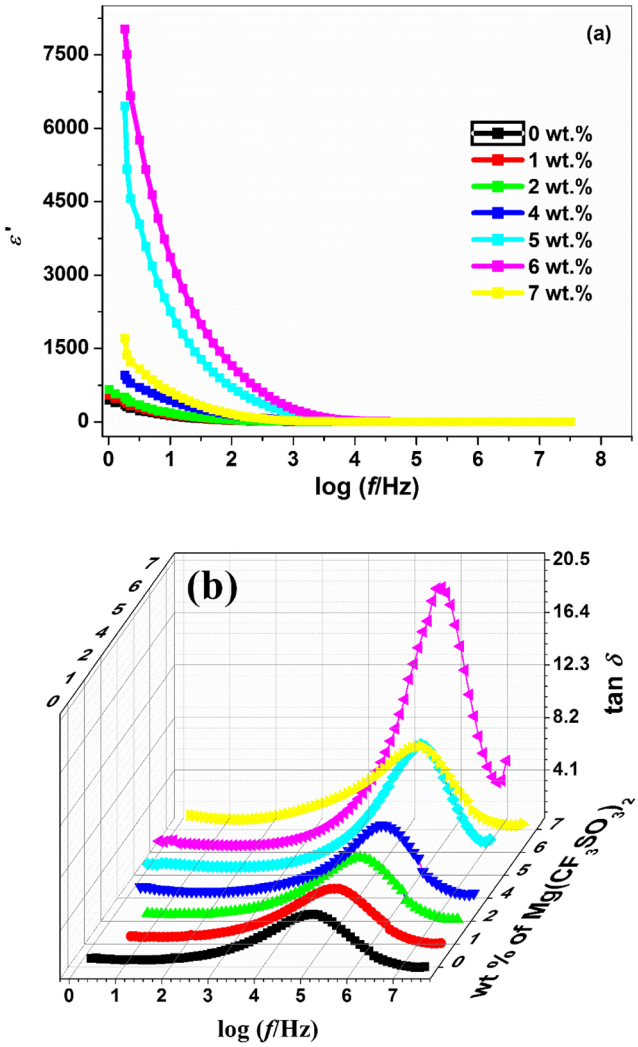

Fig. 6 Frequency-dependent **a** dielectric constant (ε') and **b** tan δ for (PEO + EMIM-BF_4) + x wt% $Mg(CF_3SO_3)_2$ where, x = 0, 1, 2, 4, 5, 6, and 7 at 303 K

Figure 6b shows tan (δ) versus log (f) for (PEO + EMIM-BF_4) + x wt% $Mg(CF_3SO_3)_2$ where $x = 0$, 1, 2, 4, 5, 6, and 7 at 303 K. The plot consists of a peak which shifts towards the higher frequency side with increasing the concentration of $Mg(CF_3SO_3)_2$ salt up to 6 wt%. Beyond this concentration, the maxima of peak shift towards lower frequency side. The shift in the peak indicates the relaxation phenomenon is occurring. The lowest relaxation time is observed for the optimized highest conducting PEM. This might be due to increase in the amorphous nature of the PEM with increasing amount of salt through which polymer chains can easily orient themselves.

Modulus studies

The frequency response of electric modulus representation is an established technique utilized extensively to identify the electrical relaxation and the electrode polarization effect. Mathematically, electric modulus is given by the relation

$$M^* = \left(\frac{1}{\varepsilon^*}\right) = j\omega C_o Z^* = M' + jM'' \quad (8)$$

where the angular frequency $\omega = 2\pi f$ and C_o is the vacuum capacitance of the electrochemical cell, and M' and M'' denote the real and imaginary parts of the modulus M^*, respectively. A true electrical relaxation for the PEMs with various salt concentrations is usually identified by plotting the real M' and imaginary M'' part of electric modulus as a function frequency as presented in Fig. 7a and b . An almost zero value of M' at low frequency indicates the negligible contribution of the electrode polarization. Long tail at lower frequencies stipulates the large capacitance is associated with it [52, 53]. Whereas a considerable raise in M' values as well as a shift in peak maximum towards the higher frequency region in observed as salt concentration increases up to 6 wt% $Mg(CF_3SO_3)_2$. A similar trend has been observed in the imaginary part (M'') of the electrical modulus. The shift in peak maximum with increasing the salt concentrations up to 6 wt%. This behavior indicates the occurrence of charge carriers hopping and relaxation phenomena due to decrease in the crystalline nature of PEM system with addition of more amount of salt concentration up to 6 wt%. Similar kind of behavior has also been reported by the Karmakar et al. [54].

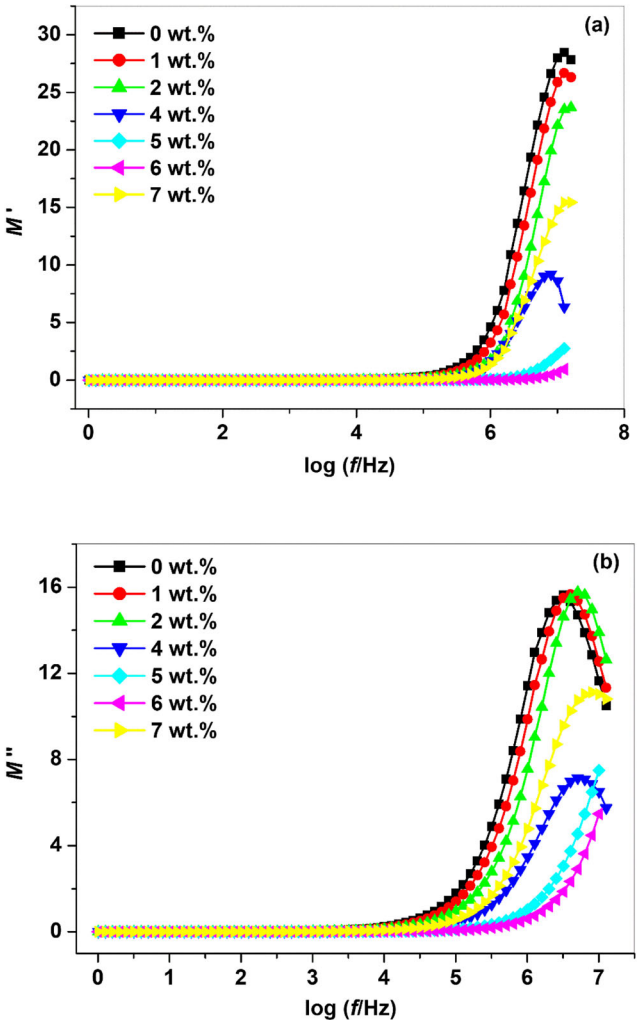

Fig. 7 Frequency-dependent **a** real part of modulus (M') and **b** imaginary part of modulus (M'') for (PEO + EMIM-BF_4) + x wt% $Mg(CF_3SO_3)_2$ where, $x = 0$, 1, 2, 4, 5, 6, and 7 at 303 K

Ion transport studies

Total ion transport number

The total ion transference number (t_{ion}) determines the contribution of ions in the total conductivity of PEM system. The t_{ion} value for optimized PEM, (PEO + EMIM-BF_4) + 6 wt% $Mg(CF_3SO_3)_2$, was estimated using dc polarization technique [55, 56]. As a part of the technique, a dc potential of 0.5 V was applied to the cell configuration SS|PEM|SS (SS, stainless steel) and current was monitored as a function of time. The t_{ion} values were obtained using formula:

$$t_{ion} = \frac{(I_t - I_e)}{I_t} \quad (9)$$

where I_t and I_e are total and saturated currents, respectively.

A typical current vs time plot for cell assemblies, SS|PEM|SS and Mg|PEM|Mg, with optimized PEM is shown in Fig. 8a . In these cell assemblies, SS acts as ion blocking electrode and allows only electronic reversibility at electrolyte/SS interface, while Mg shows reversibility for Mg^{2+} ion at electrolyte/electrode interface. In the polarization curve, initially the current (I_t) is observed as 28.50 μA cm^{-2}, which suddenly drop and saturate at 0.30 μA cm^{-2} (I_e). The t_{ion} value, calculated using Eq. 9 is obtained as ~0.99. This suggests that the conductivity of the prepared PEM system is dominantly due to ions and it is electronically insulating.

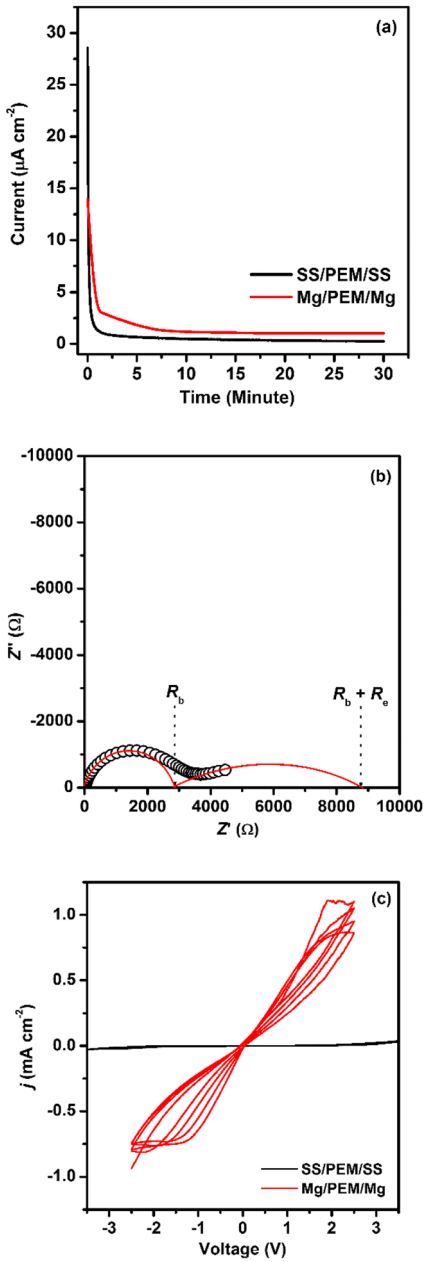

Fig. 8 **a** DC polarization curves for symmetrical cells; SS|PEM|SS and Mg|PEM|Mg. **b** Impedance curve for symmetrical cell; Mg|PEM|Mg. **c** Cyclic voltammograms of symmetrical cells, SS|PEM|SS and Mg|PEM|Mg using optimized PEM with composition (PEO + EMIM-BF_4) + 6 wt% $Mg(CF_3SO_3)_2$

Cation (Mg^{2+}) transport number

The magnesium transport number ($t_{Mg^{2+}}$) of the optimized PEM was estimated by a combination of ac impedance and dc polarization techniques as proposed by Watanabe et al. [57]. The impedance and polarization experiments were performed on the symmetrical Mg|PEM|Mg cell configuration and $t_{Mg^{2+}}$ values were calculated using formula:

$$t_{Mg^{2+}} = \frac{R_b}{\left(\frac{\Delta V}{I_s} - R_e\right)} \quad (10)$$

where R_b is the bulk resistance, R_e is the electrode/electrolyte interfacial resistance, I_s is the saturation current, and ΔV is the small constant voltage (20 mV) applied to the cell assembly.

In the polarization curve of Mg|PEM|Mg cell (Fig. 8a), the current receives saturation at relatively higher value (I_s = 1.03 μA cm^{-2}) as compared to SS|PEM|SS cell, which is an indicative of Mg^{2+} transport at electrolyte/Mg interface. In order to find $t_{Mg^{2+}}$ value for highest conducting composition, impedance plot of Mg|PEM|Mg cell is obtained (Fig. 8b). As illustrated in the figure, the bulk resistance (R_b) and electrode/electrolyte interfacial resistance (R_e) are obtained as 2864 and 5963 Ω, respectively. The $t_{Mg^{2+}}$ value, calculated using Eq. 10, is obtained as 0.22 for the highest conducting optimized composition.

In order to confirm Mg^{2+} conduction in the prepared PEM system and to assess its electrochemical stability, CV was performed on the two symmetrical cells, SS|PEM|SS and Mg|PEM|Mg at a scan rate of 5 mV s^{-1} (Fig. 8c). In the voltammogram of the cell with SS electrode, no anodic or cathodic peak is observed and also the current values are insignificant. This reflects a significantly high electrochemical stability window of the prepared PEM system. However, the voltammogram of Mg|PEM|Mg cell shows several times high current values with a couple of reversible redox peaks corresponding to cathodic deposition and anodic oxidation of Mg^{2+} at electrolyte/Mg interface. This shows the good reversibility of the Mg^{2+}/Mg redox couple in cell. In order to, further, confirm the electrochemical stability window, LSV was

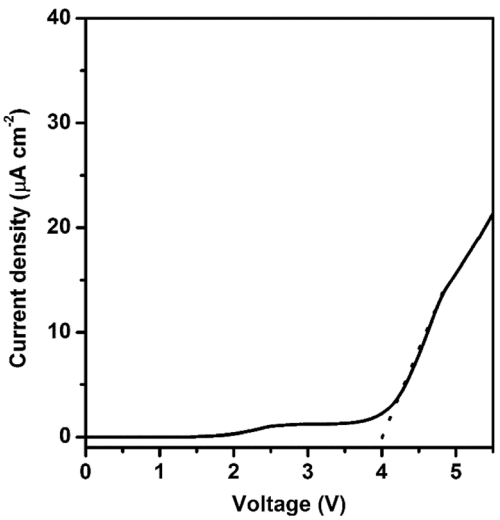

Fig. 9 Linear sweep voltammogram for PEM with composition (PEO + EMIM-BF_4) + 6 wt% $Mg(CF_3SO_3)_2$ in the cell configuration SS|PEM|Mg at a scan rate of 5 mV s^{-1}

performed on the highest conducting composition of the PEM system at a scan rate of 5 mV s^{-1} using SS as a working electrode and magnesium as a combined reference and counter electrode (Fig. 9). The LSV trace confirms the electrochemical stability window the highest conducting composition as ~4.0 V. These observations confirm the Mg^{2+} ion conductivity in the prepared PEM system with significant electrochemical stability. This assessment is an indicative of the potential applicability of the prepared PEMs in electrochemical devices especially the supercapacitors and batteries.

Conclusion

The prepared PEO + EMIM-BF_4 + $Mg(CF_3SO_3)_2$ films have been characterized using XRD, AFM, FTIR, and DSC studies. AFM analysis demonstrates minimum roughness height for optimized PEM with 6 wt% of $Mg(CF_3SO_3)_2$ concentration. FTIR analysis shows coordination of $EMIM^+/Mg^{2+}$ with ether oxygen of PEO and complexation among PEO/EMIM-BF_4/$Mg(CF_3SO_3)_2$. DSC study shows decrease in T_m on increasing $Mg(CF_3SO_3)_2$ concentration suggesting an increase of polymer chain flexibility. From the Nyquist plot, the highest ionic conductivity (~9.4×10^{-5} S cm^{-1}) is observed for optimized PEM with 6 wt% of $Mg(CF_3SO_3)_2$. The dc conductivity variation with temperature shows typical Arrhenius behavior for all PEMs. Dielectric studies depict increased values of dielectric constant (ε') at lower frequencies while the peak of dielectric loss (ε'') shifts towards higher frequency side with the addition of salt up to 6 wt% in the electrolyte films. Modulus studies indicate occurrence of charge carriers hopping and relaxation phenomenon in the PEMs films on adding $Mg(CF_3SO_3)_2$. The peak shift in M'' spectra suggested the decrease in relaxation time with the addition of salt up to 6 wt%. Total ion transport number is close to unity for all electrolytic films which indicates the conductivity is dominantly due to ions and it is electronically insulating. The Mg^{2+} conduction is confirmed using cyclic voltammetry study and Mg^{2+} transport number is determined to be 0.22 for the optimized (6 wt%) PEM. The observed changes in ionic conduction, relaxation parameters, and electrochemical performances with the variation of salt concentration suggest that PEO + EMIM-BF_4 + $Mg(CF_3SO_3)_2$ system may be a good electrolyte for battery applications.

Acknowledgments Deepak Kumar thanks and acknowledges "The M.S. University of Baroda," Vadodara, Gujarat, India. He also acknowledge encouragement and support received from Electronics and Mechanical Engineering School, Affiliated to Gujarat Technological University, Under Corps of EME, Ministry of Defence, Government of India.

Funding information Kuldeep Mishra acknowledges the funding (File No YSS/2015/001234) from Science and Engineering Research Board (SERB) New Delhi, India.

References

1. Deng D (2015) Li-ion batteries: basics, progress, and challenges. Energy Sci & Eng 3:385–418
2. Huang B, Pan Z, Su X, An L (2018) Recycling of lithium-ion batteries: recent advances and perspectives. J Power Sources 399: 274–286
3. Zubi G, López RD, Carvalho M, Pasaoglu G (2018) The lithium-ion battery: state of the art and future perspectives. Renew Sust Energ Rev 89:292–308
4. Vignarooban K, Kushagra R, Elango A, Badani P, Mellander BE, Xu X, Tucker TG, Nam C, Kannan AM (2016) Current trends and future challenges of electrolytes for sodium-ion batteries. Int J Hydrog Energy 41:2829–2846
5. Kumar D, Rajouria SK, Kuhar SB, Kanchan DK (2017) Progress and prospects of sodium-sulfur batteries: a review. Solid State Ionics 312:8–16
6. Deivanayagam R, Ingram BJ, Yassar RS (2019) Progress in development of electrolytes for magnesium batteries. Energy Storage Mater 21:136–153
7. Li H, Ma L, Han C, Wang Z, Liu Z, Tang Z, Zhi C (2019) Advanced rechargeable zinc-based batteries: recent progress and future perspectives. Nano Energy 62:550–587
8. Niu X, Li L, Qiu J, Yang J, Huang J, Wu Z, Zou J, Jiang C, Gao J, Wang L (2019) Salt-concentrated electrolytes for graphite anode in potassium ion battery. Solid State Ionics 341:115050
9. Zafar ZA, Imtiaz S, Li R, Zhang J, Razaq R, Xin Y, Li Q, Zhang Z, Huang Y (2018) A super-long life rechargeable aluminum battery. Solid State Ionics 320:70–75
10. Kong L, Yan C, Huang JQ, Zhao MQ, Titirici MM, Xiang R, Zhang Q (2018) A review of advanced energy materials for magnesium–sulfur batteries. Energy Environ Mater 1:100–112
11. Saha P, Datta MK, Velikokhatnyi OI, Manivannan A, Alman D, Kumta PN (2014) Rechargeable magnesium battery: current status and key challenges for the future. Prog Mater Sci 66:1–86
12. Angell CA (2017) Polymer electrolytes—some principles, cautions, and new practices. Electrochim Acta 250:368–375
13. Wang Y, Sokolov AP (2015) Design of superionic polymer electrolytes. Current Opin Chem Eng 7:113–119
14. Lu D, Liu H, Huang T, Xu Z, Ma L, Yang P, Qiang P, Zhang F, Wu D (2018) Magnesium ion based organic secondary batteries. J Mater Chem A 6:17297–17302
15. Mohanta J, Padhi DK, Si S (2018) Li-ion conductivity in PEO-graphene oxide nanocomposite polymer electrolytes: a study on effect of the counter anion. J Appl Polym Sci 135:46336
16. Ma Z, MacFarlane DR, Kar M (2019) Mg cathode materials and electrolytes for rechargeable Mg batteries: a review. Batteries Supercaps 2:115–127
17. Zardalidis G, Ioannou E, Pispas S, Floudas G (2013) Relating structure, viscoelasticity, and local mobility to conductivity in PEO/LiTf electrolytes. Macromolecules 46:2705–2714
18. Shobukawa H, Tokuda H, Susan MABH, Watanbe M (2005) Ion transport properties of lithium ionic liquids and their ion gels. Electrochim Acta 50:3872–3387
19. Ueki T, Watanabe M (2008) Macromolecules in ionic liquids: progress, challenges, and opportunities. Macromolecules 41:3739–3749
20. Tang J, Muchakayala R, Song S, Wang M, Kumar KN (2016) Effect of $EMIMBF_4$ ionic liquid addition on the structure and ionic conductivity of $LiBF_4$-complexed PVdF-HFP polymer electrolyte films. Polym Test 50:247–254
21. Aziz SB, Woo TJ, Kadir MFZ, Ahmed HM (2018) A conceptual review on polymer electrolytes and ion transport models. J Sci: Adv Mater Devices 3:1–17
22. Chaurasia SK, Singh RK, Chandra S (2011) Dielectric relaxation and conductivity studies on (PEO:LiClO4) polymer electrolyte with

added ionic liquid [BMIM][PF_6]: evidence of ion–ion interaction. J Polym Sci B Polym Phys 49:291–300
23. Chaurasia SK, Singh RK, Chandra S (2011) Ion–polymer and ion–ion interaction in PEO-based polymer electrolytes having complexing salt $LiClO_4$ and/or ionic liquid, [BMIM][PF_6]. J Raman Spectrosc 42:2168–2172
24. Ren C, Liu M, Zhang J, Zhang Q, Zhan X, Chen F (2018) Solid-state single-ion conducting comb-like siloxane copolymer electrolyte with improved conductivity and electrochemical window for lithium batteries. J Appl Polym Sci 135:45848
25. Liebenow C (1998) A novel type of magnesium ion conducting polymer electrolyte. Electrochim Acta 43:1253–1256
26. Pandey GP, Agarwal RC, Hashmi SA (2011) Magnesium ion-conducting gel polymer electrolytes dispersed with fumed silica for rechargeable magnesium battery application. J Solid State Electrochem 15:2253–2264
27. Morita M, Yoshimoto N, Yakushiji S, Ishikawa M (2001) Rechargeable magnesium batteries using a novel polymeric solid electrolyte. Electrochem Solid-State Lett 4:177–179
28. Kumar GG, Munichandraiah N (2000) A gel polymer electrolyte of magnesium triflate. Solid State Ionics 128:203–210
29. Reddy MJ, Chu PP (2002) Ion pair formation and its effect in PEO: Mg solid polymer electrolyte system. J Power Sources 109:340–346
30. Sarangika HNM, Dissanayake MAKL, Senadeera GKR, Rathnayake RRDV, Pitawala HMJC (2016) Polyethylene oxide and ionic liquid-based solid polymer electrolyte for rechargeable magnesium batteries. Ionics 23(10):2829–2835. https://doi.org/10.1007/s11581-016-1870-3
31. Saroj AL, Singh RK, Chandra S (2014) Thermal, vibrational, and dielectric studies on PVP/$LiBF_4$ + ionic liquid [EMIM][BF_4]-based polymer electrolyte films. J Phys Chem Solids 75:849–857
32. Sharma J, Hashmi SA (2019) Magnesium ion-conducting gel polymer electrolyte nanocomposites: effect of active and passive nanofillers. Polym Compos 40:1295–1306
33. Wilkes JS, Zaworotko MJ (1992) Air and water stable I-ethyl-3-methylimidazolium based ionic liquids. J Chem Soc Chem Commun 965-967
34. Cooper EI, O'Sullivan EJM (1992) Proceedings of 8th international symposium on ionic liquids (Eds. R. J. Gale, G. Blomgren, and H. Kojima). The Electrochemical Society, Pennington, NJ, p 386
35. Maurya KK, Srivastava N, Hashmi SA, Chandra S (1992) Proton conducting polymer electrolyte: II poly ethylene oxide + NH_4l system. J Mater Sci 27:6357–6364
36. Chaurasia SK, Saroj AL, Shalu SVK, Tripathi AK, Gupta AK, Verma YL, Singh RK (2015) Studies on structural, thermal and AC conductivity scaling of PEO-$LiPF_6$ polymer electrolyte with added ionic liquid [$BMIMPF_6$]. AIP Adv 5:077178
37. Maruthupandy M, Anand M, Maduraiveran G, Suresh S, Beevi ASH, Priya RJ (2016) Adv Nat Sci Nanosci Nanotechnol 7:045011 (9pp)
38. Parthiban V, Akula S, Peera SG, Islam N, Sahu AK (2016) Proton conducting Nafion-sulfonated graphene hybrid membranes for direct methanol fuel cells with reduced methanol crossover. Energy Fuel 30:725–734
39. Chaurasia SK, Singh RK, Chandra S (2011) Structural and transport studies on polymeric membranes of PEO containing ionic liquid, EMIM-TY: evidence of complexation. Solid State Ionics 183:32–39
40. Pasaribu MH, Arcana IM, Wahyuningrum D (2015) Molecular structure, vibrational spectra, and hydrogen bonding of the ionic liquid 1-ethyl-3-methyl-1H-imidazolium tetrafluoroborate. AIP Conf Proc 1677:070014
41. Skin JH, Kim KW, Ahn HJ, Ahn JH (2002) Electrochemical properties and interfacial stability of $(PEO)_{10}LiCF_3SO_3$–Ti_nO_{2n-1} composite polymer electrolytes for lithium/sulfur battery. J Mater Sci Eng B 95:148–156
42. Mishra K, Hashmi SA, Rai DK (2014) Protic ionic liquid-based gel polymer electrolyte: structural and ion transport studies and its application in proton battery. J Solid State Electrochem 18:2255–2266
43. Kumar D, Hashmi SA (2010) Ion transport and ion–filler-polymer interaction in poly(methyl methacrylate)-based, sodium ion conducting, gel polymer electrolytes dispersed with silica nanoparticles. J Power Sources 195:5101–5108
44. Ramesh S, Lu S (2011) Effect of lithium salt concentration on crystallinity of poly (vinylidene fluoride-co-hexafluoropropylene)-based solid polymer electrolytes. J Mol Struct 994:403–409
45. Pradhan DK, Choudhary RNP, Samantary BK (2008) Studies of dielectric relaxation and AC conductivity behavior of plasticized polymer nanocomposite electrolytes. Int J Electrochem Sci 3:597–608
46. Ramya CS, Pandian SS, Savitha T, Hirankumar G, Angelo PC (2007) Vibrational and impedance spectroscopic study on PVP–NH4SCN based polymer electrolytes. Phys B Condens Matter 393:11–17
47. Osman Z, Ghazali M, Othman L, Isa K (2012) AC ionic conductivity and DC polarization method of lithium ion transport in PMMA–LiBF4 gel polymer electrolytes. Result Phy 2:1–4
48. Kumar D, Kanchan DK (2019) Dielectric and electrochemical studies on carbonate free Na-ion conducting electrolytes for sodium-sulfur batteries. J Energy Storage 22:44–49
49. Gohel K, Kanchan DK (2018) Ionic conductivity and relaxation studies in PVDF-HFP:PMMA-based gel polymer blend electrolyte with LiClO4 salt. J Adv Dielect 8:1850005
50. Al-Gunaid MQA, Saeed AMN (2018) Effects of the electrolyte content on the electrical permittivity, thermal stability, and optical dispersion of poly(vinyl alcohol)–cesium copper oxide–lithium perchlorate nanocomposite solid-polymer electrolytes. J ApplPolym Sci 135:45852
51. Woo HJ, Majid SR, Arof AK (2012) Dielectric properties and morphology of polymer electrolyte based on poly (ε-caprolactone) and ammonium thiocyanate. Mater Chem Phys 134:755–761
52. Gohel K, Kanchan DK (2019) Effect of PC: DEC plasticizers on structural and electrical properties of PVDF–HFP: PMMA based gel polymer electrolyte system. J Mater Sci Mater Electron 30:12260–12268
53. Rathika R, Suthanthiraraj SA (2016) Ionic interactions and dielectric relaxation of PEO/PVDF-Mg[(CF3SO2)2N2] blend electrolytes for magnesium ion rechargeable batteries. Macromol Res 24:422–428
54. Karmakar A, Ghosh A (2012) Dielectric permittivity and electric modulus of polyethylene oxide (PEO)–LiClO4 composite electrolytes. Curr Appl Phys 12:539–543
55. Hashmi SA, Chandra S (1995) Experimental investigations on a sodium-ion-conducting polymer electrolyte based on poly (ethylene oxide) complexed with $NaPF_6$. J Mater Sci Eng B 34:18–26
56. Wagner JB Jr, Wagner C (1957) Electrical conductivity measurements on cuprous halides. J Chem Phys 26:1597
57. Watanabe M, Nagano S, Sanui K, Ogata N (1988) Estimation of Li^+ transport number in polymer electrolytes by the combination of complex impedance and potentiostatic polarization measurements. Solid State Ionics 28-30:911–917

Journal of Materials Science: Materials in Electronics
https://doi.org/10.1007/s10854-020-03877-8

Dielectrics and battery studies on flexible nanocomposite gel polymer electrolyte membranes for sodium batteries

Deepak Kumar[1] · Khushbu Gohel[2] · D. K. Kanchan[2] · Kuldeep Mishra[3]

Received: 29 March 2020 / Accepted: 26 June 2020

Abstract
In the present study, electrochemical impedance analysis in terms of electrical conductivity, dielectric permittivity, and electrical modulus has been carried out of prepared sodium ion-conducting nanocomposite gel polymer electrolyte. To study ion conduction behavior, frequency-dependent AC conductivity has also been analyzed. Dielectric constant (ε') and dielectric loss (ε'') as a function of frequency with different nanofiller SiO_2 concentrations as well as at different temperatures ranging from 303 to 333 K have been discussed. The low-frequency region showed high values of dielectric constant due to polarization at the electrode–electrolyte interface. Frequency-dependent real (M') and imaginary part (M'') of modulus reveal large capacitance associated with it at lower frequency whereas dispersion (conductivity relaxation) at a higher frequency. The tangent loss (tan δ) of the electrolyte systems has been determined for different frequencies and concentrations of fumed silica nanoparticles. The high conducting nanocomposite gel polymer membrane exhibited an electrochemical stability window of ≈ 3.3 V which is sufficient to apply this material as a separator for electrochemical device application. The conductivity, dielectric, modulus, and electrochemical stability studies reveal that sodium ion-conducting nanocomposite gel polymer electrolytes offer good electrochemical properties and are suitable for application in any electrochemical/power conversion device. The optimized flexible nanocomposite gel polymer electrolyte films have been used in a prototype sodium battery, which shows a stable open-circuit potential of ~ 2.1 V and a significant first specific discharge capacity of ~ 500 mAh g^{-1} at a drain current of 14 mA g^{-1}.

1 Introduction

The lithium-based electrolytes and batteries are most successful till date but lithium resources are costly, less abundant, and are concentrated to few countries only [1]. In view of this, research and development on other cell chemistries such as sodium, magnesium, zinc, potassium, aluminum, and so on are growing at a great pace [2–8]. Recently, triboelectric nanogenerators (TENG) and piezoelectric nanogenerators (PENG) are also utilized as energy conversion devices due to their useful properties such as stretchability, self-healability and bio-compatibility [9–13]. The research on sodium batteries is largely motivated by its low cost, high abundance, non-toxicity, and sufficiently high electrochemical reduction potential of ~ 2.7 V vs SHE. The development of the sodium batteries is hampered by the non-availability of suitable and compatible non-aqueous electrolytes. The usage of liquid electrolytes in electrochemical devices poses safety issues and many other drawbacks such as leakage, corrosion, explosion, and so on which results in progressively poor performance of a cell. In view of this, all alkali metal batteries require non-aqueous polymer electrolytes with good electrochemical properties and researchers around the globe are working on the development of these electrolytes since the last many decades [14, 15]. The frequently used polymers to design polymer electrolyte include polyethylene oxide (PEO), poly(vinylidene fluoride-*co*-hexafluoropropylene) (PVDF-HFP), polyvinylpyrrolidone (PVP), poly(methyl methacrylate) (PMMA), polyvinyl alcohol (PVA), polyvinyl chloride (PVC), polyacrylonitrile (PAN), rubber (MG49, ENR50, etc.), polyester and polycarbonate, etc. PMMA is an attractive choice to realize the polymer

✉ Deepak Kumar
fwtdrdeepak@gmail.com

[1] Electronics and Mechanical Engineering School (Affiliated to Gujarat Technological University), Vadodara, Gujarat 390008, India

[2] Department of Physics, M.S. University of Baroda, Baroda, Gujarat 390002, India

[3] Department of Physics, Jaypee University, Anoopshahr, Uttar Pradesh 203390, India

Published online: 06 July 2020

electrolytes due to its amorphous nature, good affinity with organic solvents, and high ionic conductivity it supports after incorporation of liquid electrolytes [16]. The usage of solid polymer electrolytes for designing cell assembly is problematic due to their extremely low ionic conductivity values and poor interfacial contacts with anode and cathode.

Gel polymer electrolytes (GPE) are attractive choices owing to their non-leakage feature and liquid-like high ionic conductivity close to ~ 10^{-3} S cm^{-1}. These electrolytes are prepared by immobilizing the salt solution into the polymer matrix and are mechanical, electrochemical stable with easy mouldability to meet design considerations for any electrochemical device [17]. In this report, we have chosen the ethylene carbonate (EC) and propylene carbonate (PC) as organic solvents due to their high dielectric constant of 89.7 and 66.1 respectively, and their compatibility with the chosen PMMA polymer. In order to enhance the performance characteristics of GPE, the researchers have suggested the usage of micro/nanosized active or passive fillers. The incorporation of these fillers into gel polymer electrolytes results in nanocomposites gel polymer electrolyte (NGPE). The addition of these fillers in a small amount has a tendency to collapse the organization of polymer chain which in turn facilitates higher ionic conduction [18, 19]. In addition, the introduction of these fillers into GPE contributes better dimensional and interfacial stability of the electrolyte during their application in electrochemical devices especially the batteries. In this report, SiO_2 is utilized as a nanofiller to give a porous structure that maximizes the adsorption of liquid electrolyte and reduces the risks of leakage.

Using the Na^+ conducting polymer gel electrolytes, researchers have attempted sodium-based batteries such as sodium ion batteries (SIBs), Na-S cells, ZEBRA cells, etc. [20–23]. Red phosphorus is a commercially promising electrode, which could react with Na to form a Na_3P compound, leading to an extremely high theoretical capacity (2590 mAh g^{-1}). However, inherently low conductivity (10^{-14} S cm^{-1}) and a huge volume variation of red phosphorus during sodiation/desodiation processes can cause severe structural destruction and performance degradation during cycling. To overcome this issue, compositing phosphorus with carbon-based materials (carbon nanotubes, graphene, carbon nanofibers, etc.) is a rational and effective design for P-based electrode materials, because carbon could buffer volume expansion and enhance the conductivity, which is helpful to the rate capability and cycle stability of a battery system [24–27].

There are many reports on PMMA-based nanocomposite gel electrolytes using organic solvents. Sharma et al. presented FTIR spectroscopy, thermal, and conductivity studies on PMMA/PC/NH_4PF_6/SiO_2 nanocomposite electrolyte system [28]. Chew et al. studied the effect of SiO_2 and Al_2O_3 as ceramic fillers on PMMA-based electrolyte system PMMA/PC/$LiCF_3SO_3$ [29]. In an earlier report, we have presented structural, morphological, thermal, and ion transport studies on PMMA/EC-PC/$NaClO_4$/SiO_2 nanocomposite electrolyte system [15]. In this report, we present detailed investigations on the effect of varying the SiO_2 nanoparticles concentration on ionic conductivity, dielectric, and modulus studies. In addition, prototype sodium battery has been assembled using flexible nanocomposite gel polymer electrolyte and composite red phosphorus electrode and tested for open-circuit voltage (OCV), discharge capacity, and impedance characteristics. In this study, we have shown how the SiO_2 nanofiller concentration changes/controls ionic conduction and dielectric/relaxation behavior in the nanocomposite gel polymer electrolyte system.

2 Experimental

Polymer host poly(methyl methacrylate) denoted as PMMA with average molecular weight ~350,000, sodium perchlorate ($NaClO_4$), ethylene carbonate (EC), propylene carbonate (PC), and fumed silica (SiO_2) nanoparticles powder were purchased from Sigma Aldrich and used after vacuum drying for 10 h. Amorphous red phosphorus (P) and activated carbon (C) were procured from Loba Chemie, India, and Fuzhou Carbon Co., China, respectively.

2.1 Preparation of the gel polymer electrolyte nanocomposite membranes

The salt solution has been prepared by taking an equal volume ratio of EC and PC in sodium perchlorate. This sodium salt solution was further entrapped in PMMA polymer host and fumed silica in increasing amounts has been added to form the electrolyte system. The overall composition containing polymer, salt solution, and fumed silica in varying amounts was further magnetically stirred vigorously under the reflux for 10 h at room temperature conditions to obtain flexible gel polymer electrolyte nanocomposite membranes as shown in Fig. 1.

2.2 Preparation of electrodes and fabrication of prototype batteries

The cathode has been prepared by mechanical mixing red phosphorus (P), activated carbon (C), and PVdF-HFP binder in wt. ratio 7:2:1 for 20 h. In order to obtain cathode film, the cathode slurry in acetonitrile is cast on aluminum foil followed by vacuum drying at 60 °C for 12 h. The overall weight of

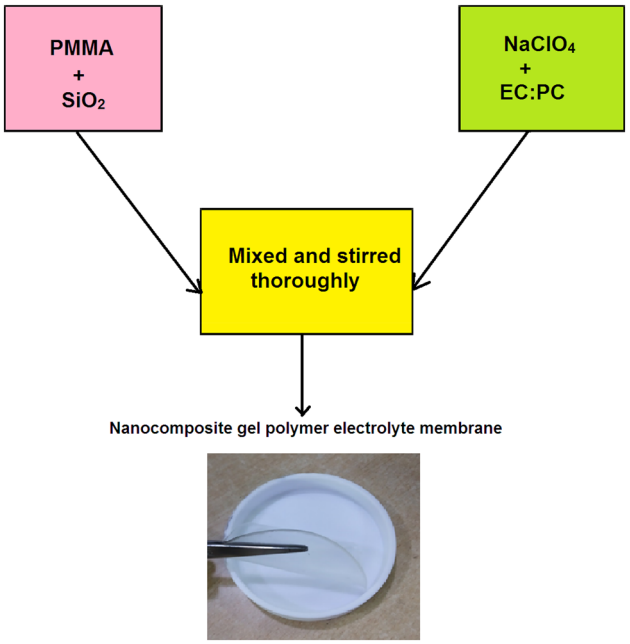

Fig. 1 The pictorial representation of fabricating nanocomposite gel polymer electrolyte membranes

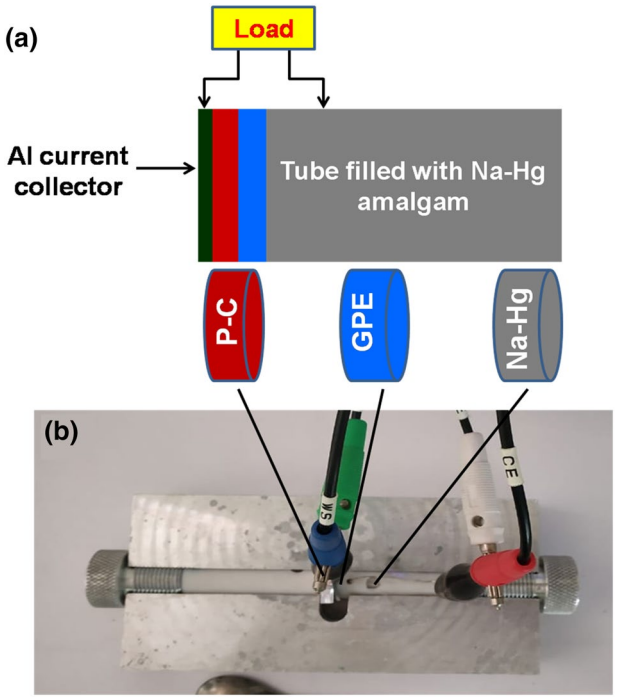

Fig. 2 **a** The schematic and **b** designed prototype assembly for sodium battery at room temperature

the P–C composite cathode was 10 mg and the active mass of the phosphorus was 7 mg. The sodium amalgam (Na–Hg) is used as an anode. A prototype sodium cell is fabricated by sandwiching the optimized polymer gel electrolyte nanocomposite membrane between anode and cathode. The assembly of the designed prototype for sodium battery using phosphorus-carbon composite cathode, Na–Hg anode and optimized nanocomposite gel polymer electrolyte is shown in Fig. 2.

2.3 Instrumentation

The electrochemical impedance spectroscopy measurements were performed using an LCR Hi-Tester (HIOKI-3522-50, Japan) over the frequency range from 1 to 100 kHz with a signal level of 10 mV. The electrochemical impedance spectroscopic measurements are carried out by sandwiching the nanocomposite gel polymer electrolyte membranes between two stainless steel electrodes under spring pressure. Using linear sweep voltammetry (LSV) studies, the 'electrochemical potential window' of optimized gel electrolyte membrane was evaluated at a scan rate of 5 mV s^{-1} using SS as a working electrode and Na–Hg amalgam as a combined reference and counter electrode. The open-circuit voltage (OCV), discharge/charge test, and impedance measurements of the prototype sodium cell were carried out using an electrochemical analyzer (Zive SP1) of WonATech Co., Ltd., Korea.

3 Results and discussion

3.1 DC conductivity analysis

Electrochemical impedance spectroscopy (EIS) is an important technique used to measure the electrochemical properties of chosen system with the application of the AC field. Since, the electrochemical impedance parameters play an important role therefore, it is necessary to validate the data that are experimentally obtained. Kramer–Kronig (KK) relationship is utilized to check the validation of impedance data [30]. After validation of EIS data, the ionic conductivity of the prepared nanocomposite gel polymer electrolyte membranes has been measured by Nyquist plots. The Nyquist plot (Z' versus Z'') for NGPE system PMMA-EC + PC-$NaClO_4$—x wt% SiO_2 where $x = 0$, 2, 4, 7, 9, 15 at 303 K is depicted in Fig. 3a. The features of the Nyquist plot contain high-frequency semicircle which is attributed to bulk property of polymer electrolyte and low-frequency spikes region is due to the electrode–electrolyte interface as reported by Singh et al. [31]. However, the Nyquist plot of our system exhibits only non-vertical spikes at the low-frequency region is attributed to the accumulation of charges due to blocking electrodes and the absence of semicircle at high-frequency region indicates the present gel polymer electrolyte are highly ionic conductor in nature [32]. The intercept of low-frequency

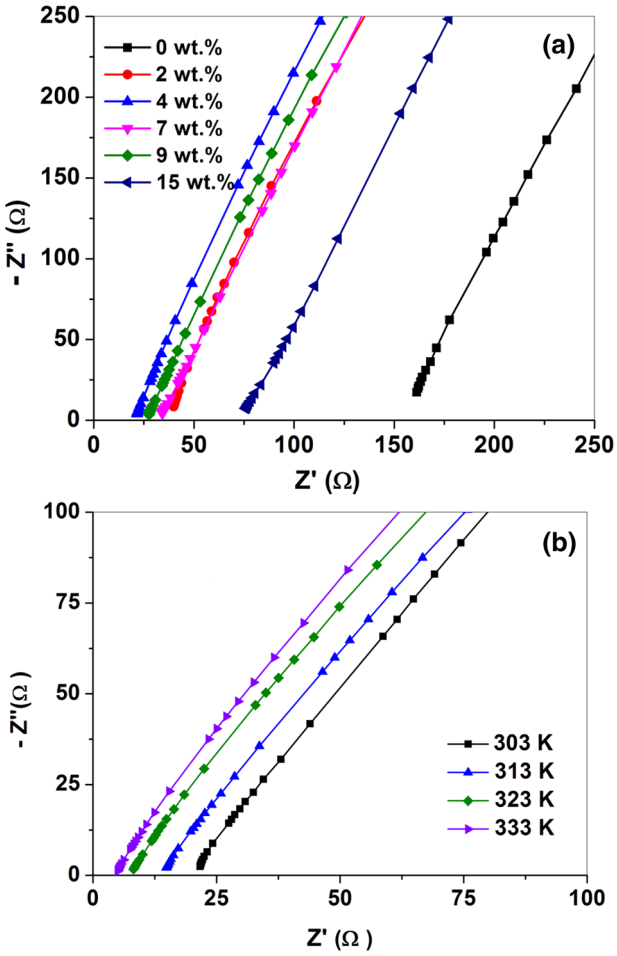

Fig. 3 Nyquist plot (Z'' versus Z') for **a** PMMA-EC + PC-$NaClO_4$—x wt% SiO_2 at different filler concentration of $x = 0$, 2, 4, 7, 9, 15 at 303 K. **b** PMMA-EC + PC-$NaClO_4$—4 wt% SiO_2 at different temperatures from 303 to 338 K

Table 1 DC conductivity values as obtained from bulk resistance (obtained from Nyquist plots) and from AC conductivity spectra

wt% of SiO_2	DC conductivity from bulk resistance (R_b) (S cm^{-1})	DC conductivity (σ_{dc}) from AC conductivity (S cm^{-1})
0	4.55E−04	4.10E−04
2	1.84E−03	1.66E−03
4	3.49E−03	3.14E−03
7	2.11E−03	1.99E−03
9	2.79E−03	2.60E−03
15	9.88E−04	9.14E−04

spikes on the real axis gives the bulk resistance (R_b) of the system. By using the bulk resistance (R_b) value and the known value of the thickness of film and area of electrode–electrolyte contact, the ionic conductivity has been calculated by Eq. 1 and given in Table 1

$$\sigma = \frac{t}{R_b A} \tag{1}$$

To determine the ion transport behavior of the prepared nanocomposite gel polymer electrolyte, the Nyquist plot for PMMA-EC + PC-$NaClO_4$—4 wt% SiO_2 system at different temperatures from 303 to 333 K is shown in Fig. 3b. The observed features of this plot are similar as discussed earlier in this section. With an increase in the temperature, the intercept of low-frequency spike with the real axis is shifting towards origin indicating the decrease in the bulk resistance value (R_b) ultimately enhance the mobility of ion and hence ionic conductivity according to Eq. 1. Enhancement in the mobility of ion due to an increase in the temperature might be due to (1) an increase in the amorphicity (2) increase in the segmental of the polymer chain, where ion conduction (hopping) takes place through the polymer matrix. And it is believed that the principally ion transport occurs through the amorphous phase [33, 34].

3.2 AC conductivity analysis

The frequency dependence of ionic conductivity has been discussed to provide worthwhile information for ionic conduction behavior. The frequency dependence ionic conductivity has been calculated using the following relation

$$\sigma' = \frac{t}{A}\left(\frac{Z'}{Z'^2 + Z^2}\right). \tag{2}$$

The plot of AC ionic conductivity as a function of frequency for nanocomposite gel polymer electrolyte system PMMA-EC + PC-$NaClO_4$—x wt% SiO_2 where $x = 0$, 2, 4, 7, 9, 15 at room temperature is shown in Fig. 4a. Generally, the AC conductance spectra show three distinct regions: (i) low-frequency dispersive region due to the interface of the electrode–electrolyte surface. (ii) The mid-frequency region is attributed to DC ionic conductivity and (iii) a high-frequency dispersive region [35]. However, AC conductance spectra of present nanocomposite gel polymer electrolyte system show only low and mid-frequency region. The absence of a high-frequency conductivity region is due to the frequency limitation of the instrument used in our experimental method. A low-frequency dispersive region is where the accumulation of charges occurs due to the electrode–electrolyte interface. A low-frequency region is followed by the mid-frequency plateau region which is almost independent of frequency. This plateau region is ascribed to the successful hopping of ion from one available site to another and contributes DC conductivity [36]. Here, DC conductivity has been extracted by taking extrapolation of the mid-frequency region (plateau region) to Y-axis. The obtained conductivity values have

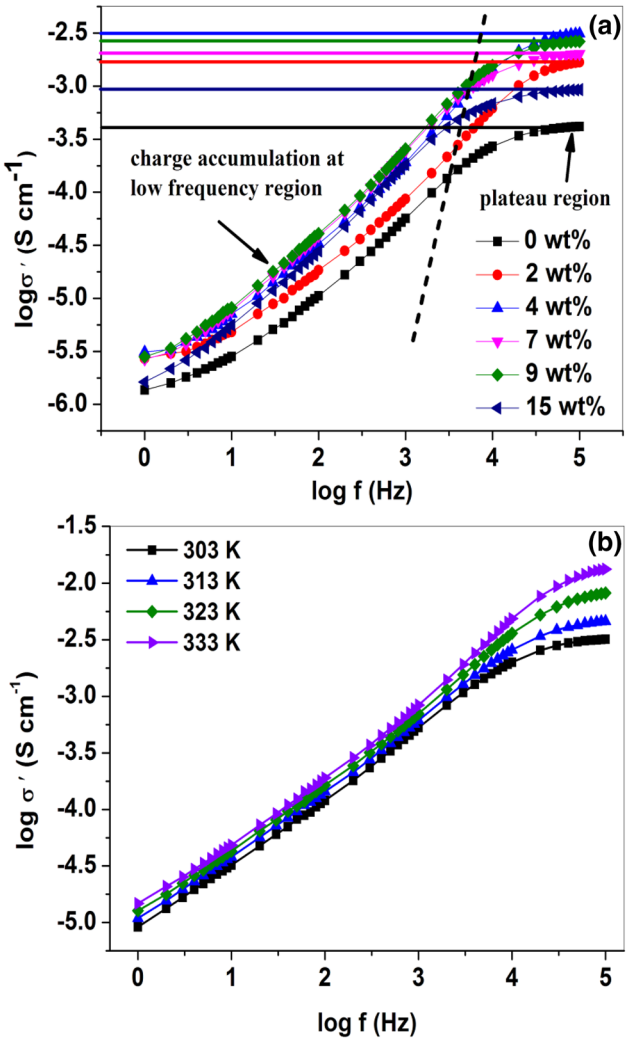

Fig. 4 AC ionic conductivity plots as a function of frequency for **a** PMMA-EC + PC-$NaClO_4$—*x* wt% SiO_2 where *x* = 0, 2, 4, 7, 9, 15 at 303 K. **b** PMMA-EC + PC-$NaClO_4$—4 wt% SiO_2 at different temperatures

been tabulated in Table 1 which is almost comparable to the obtained conductivity data from the Nyquist plot. It has been found that the conductivity of the present electrolyte system increases with increasing the amount of SiO_2 nano particles. The maximum ionic conductivity value of the order of 3.14×10^{-3} S cm^{-1} is achieved for the NGPE sample having 4 wt% SiO_2 nanofiller.

The increase in ionic conductivity may be attributed to an increase in the charge carrier as a result of the dissociation of pair of anion and cation. Apart from this, Lewis acid–base interaction occurs due to the presence of oxygen vacancies at the surface of the SiO_2 nano particles as reported by Wang et al. [37]. The introduction of nanofiller in gel polymer electrolyte increase amorphous phase which avails the conduction pathway for sodium ion due to Lewis acid–base interaction results in an increase in conductivity [38–41]. Furthermore, beyond the amount of 4 wt% SiO_2, the decrease in the conductivity may be due to aggregation of ion-pair or ion cluster. AC ionic conductivity as a function of frequency for optimized NGPE system PMMA-EC + PC-$NaClO_4$—4 wt% SiO_2 at different temperatures is shown in Fig. 4b. The temperature-dependent AC ionic conductivity (σ') increases as temperature increases from 303 to 333 K. This may be attributed to increased ionic mobility due to enhancement in polymer chain segmental motion with an increase in temperature.

3.3 Dielectric analysis

The dielectric behavior of the present NGPE system has been analyzed by using dielectric formalism. The complex permittivity (ε^*) can be given as $\varepsilon^* = \varepsilon' + \varepsilon^{\varepsilon}$, where ε' is dielectric constant and $\varepsilon^{\varepsilon}$ is a dielectric loss. These can be given as

$$\varepsilon' = \frac{z''}{\omega C_0 \left(Z'^2 + Z^2\right)}, \tag{3}$$

$$\varepsilon = \frac{z'}{\omega C_0 \left(Z'^2 + Z^2\right)}, \tag{4}$$

where C_0 is the vacuum capacitance, Z' and Z'' is real and imaginary part of complex impedance.

Figure 5a, b represents the dielectric constant (ε') and dielectric loss (ε'') for PMMA-EC + PC-$NaClO_4$—SiO_2 nanocomposite gel polymer electrolyte membranes with different concentration of SiO_2 nanofiller at room temperature. The figure reveals the high value of the dielectric constant and dielectric loss at lower frequency region may be due to significant contribution of space charge effect (accumulation of charges) near blocking electrodes–electrolyte interface and dipoles alignment with the applied field because of sufficient time. On the other hand, the value of dielectric constant and dielectric loss decreases as the frequency increases. This is because of the rapid changing of applied AC field where dipoles are unable to orient themselves and diffusion of ions cannot take place within available sites with an increase in the frequency of the applied field. Another conclusion can be drawn from the figure that the dielectric constant of present NGPE systems has been varied with changing the content of SiO_2nanofiller. The highest value of dielectric constant has been found for the NGPE system containing 4 wt% SiO_2. It might be due to the incorporation of nanofillers into GPE system that enhances charge carriers as well as mobility of ion through Lewis acid–base interaction. This is indirectly associated with an increase in the amorphous phase of the polymer which creates new conducting pathways for the migration of Na^+ ion via filler surface region. The increase

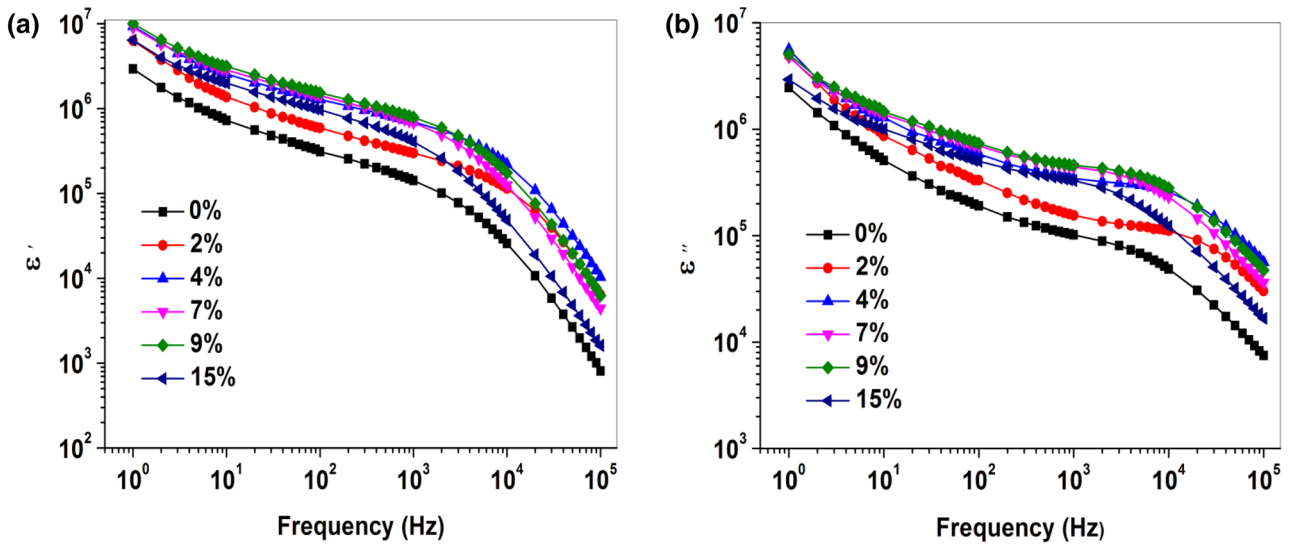

Fig. 5 **a** Dielectric constant (ε') **b** dielectric loss (ε'') versus frequency for PMMA-EC + PC-$NaClO_4$—*x* wt% SiO_2 where *x* = 0, 2, 4, 7, 9, 15

in amorphicity of the present system with the addition of SiO_2 nanoparticles in PMMA-EC + PC-$NaClO_4$ system has been discussed in our previous report [15].

Temperature-dependent dielectric constant (ε') and dielectric loss (ε'') spectra is shown in Fig. 6a, b. Generally, dielectric constant (ε') and dielectric loss (ε'') measure the charge storage and energy dissipation due to the movement of ions and dipoles. Both are found to increase monotonically with an increase in temperature. This might be due to greater freedom for dipoles orientation and motion of charge carrier within the polymer matrix [42]. Similar ion conduction behavior has also been reported by Hemlatha et al. [43].

3.4 Modulus analysis

In the dielectric analysis, the interfacial polarization suppresses conductivity relaxation processes [44]. Hence, further analysis has been carried out using modulus spectroscopy which provides information regarding ion transport and conductivity relaxation phenomenon. An electric modulus (M^*) can be represented as an inverse of the complex dielectric permittivity (ε^*).

$$M^* = \frac{1}{\varepsilon^*} = M' + jM \tag{5}$$

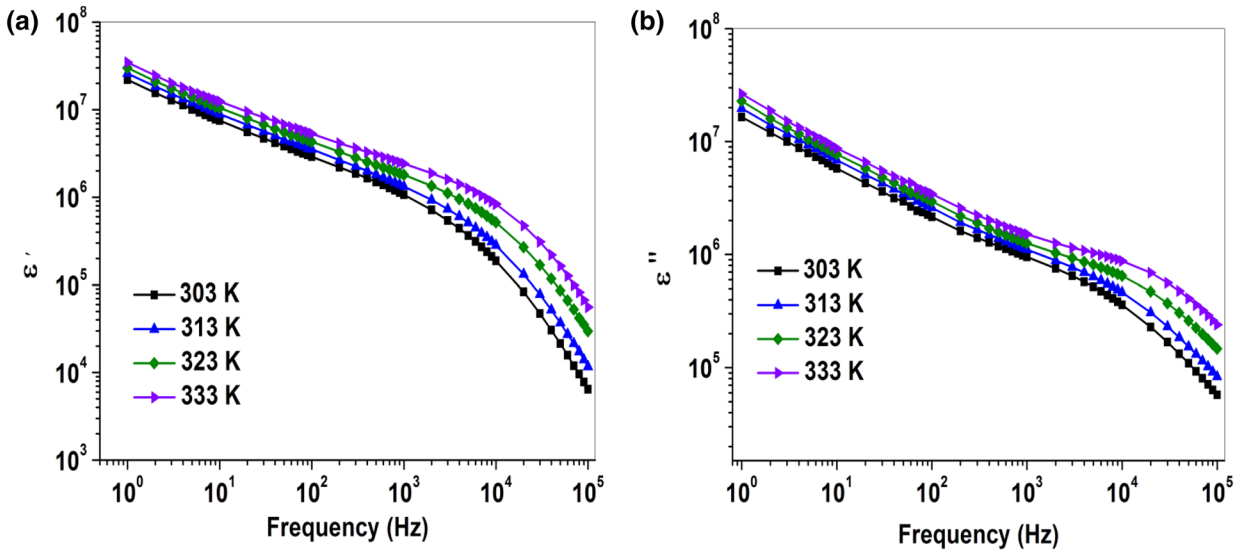

Fig. 6 **a** Dielectric constant (ε') **b** dielectric loss (ε'') versus frequency for PMMA-EC + PC-$NaClO_4$—4 wt% SiO_2 at different temperatures

Figure 7a, b shows the frequency dependence of real (M') and imaginary (M'') part of modulus for PMMA—EC + PC-$NaClO_4$—SiO_2 system with different concentration of SiO_2 nanoparticle at 303 K. The spectra show the $M \rightarrow 0$ at lower frequency region indicates the negligible effect of polarization [45]. The long tail at this frequency region reveals the large capacitance is associated with it [46]. M'' values increase (dispersion) with the increase in frequency due to the bulk effect of the gel polymer electrolyte material. Low-frequency region is due to long-range mobility of ions and migration of Na^+ ions is available here whereas the high-frequency region is due to short-range mobility of ions through the polymer matrix. Another conclusion can be drawn from the spectra that the peak maximum is low for the highest conducting sample. This indicates the hopping of the charge carriers (ions) is predominant.

The temperature-dependent modulus (M' and M'') spectra for the highest conducting sample is shown in Fig. 8a, b. As the temperature increases from 303 to 348 K, the maxima of M' and M'' (peak of M' and M'') shift towards higher frequencies which indicate relaxation phenomenon is occurring [47]. The height of the peak is also found to be decreasing due to decreases in the bulk resistance of the present GPE system. However, the complete peak is not observed due to the upper limit of the frequency of the instrument.

The tangent loss measures the lost electrical energy to stored electrical energy. Mathematically, it can be expressed as

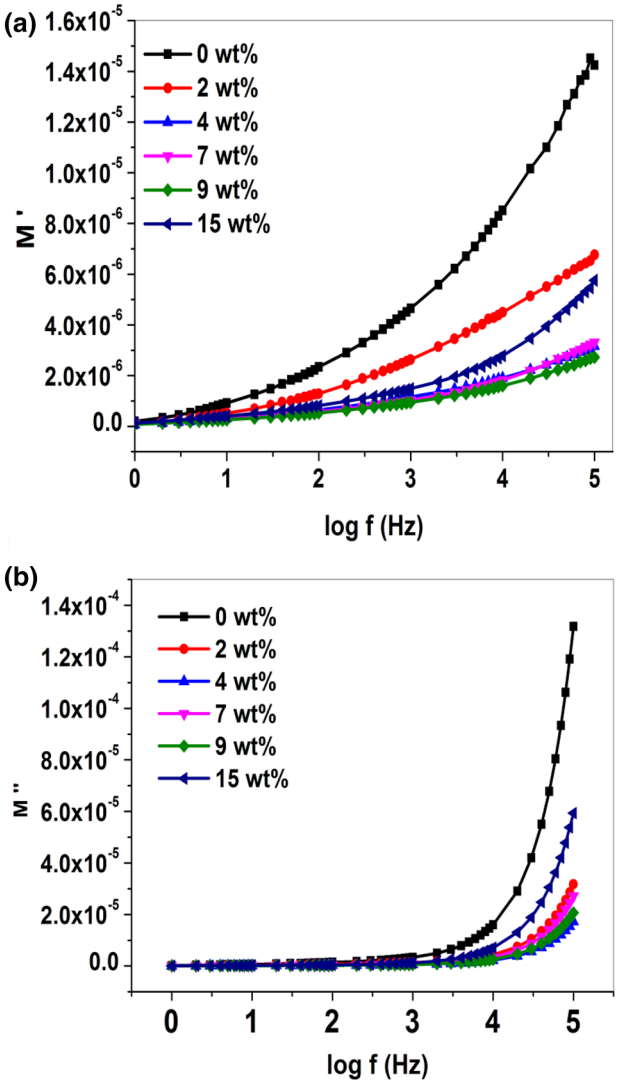

Fig. 7 **a** Real part of modulus (M') **b** imaginary part of modulus (M'') versus log f for PMMA-EC + PC-$NaClO_4$—x wt% SiO_2 where $x = 0, 2, 4, 7, 9, 15$ at 303 K

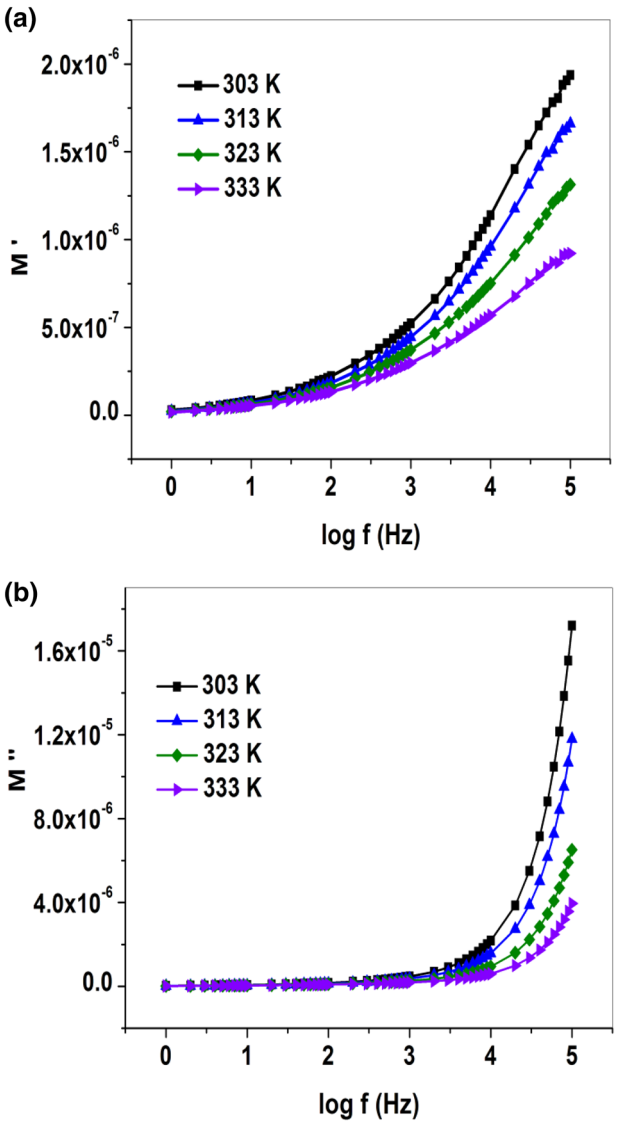

Fig. 8 **a** Real part of modulus (M') **b** imaginary part of modulus (M'') versus log f for PMMA-EC + PC-$NaClO_4$—4 wt% SiO_2 at different temperatures

$$\tan\delta = \frac{\varepsilon''}{\varepsilon'}. \quad (6)$$

In order to enlighten the variation of SiO_2 nanofiller on the relaxation process, a tangent loss study has been carried out.

Figure 9a represents the loss tangent ((tan δ) versus log f at room temperature for different weight percentages of SiO_2 dispersed GPE. It is noted that the increase in the values of tangents loss with increasing frequency and reaches a maximum value. However, complete peak has not been observed due to the frequency limitation of the instrument. The frequency at with maximum loss occurs is characteristic frequency known as relaxation frequency which describes the relaxation time according to relation $\omega\tau = 1$ where $\omega = 2\pi f$. This addresses that the relaxation process occurring in NGPE [5]. The temperature-dependent tangent loss as a function of frequency for the nanocomposite gel polymer electrolyte with a concentration of 4 wt% SiO_2 nanofiller is plotted in Fig. 9b. It is clearly visible that the height of the peak decreases with increasing the temperature as well slight shifting in the peak (maximum value of tangent loss) with a rise in temperature indicates a decrease in relaxation time τ means present NGPE system relax much faster. This behavior might be due to thermally activated ions and dipoles can easily follow the applied field and hopping takes place within available sites. Table 2 highlights the characteristics features of the gel-based polymer electrolyte membrane dispersed with/without SiO_2 nanoparticles. From Table 2, we can observe the optimized nanocomposite gel polymer electrolytes offers superior characteristic features such as low bulk resistance, high conductivity, high dielectric constant, low tangent loss, high liquid retention, better thermal stability and surface morphology as compared to gel polymer electrolytes not dispersed with SiO_2 nanofillers.

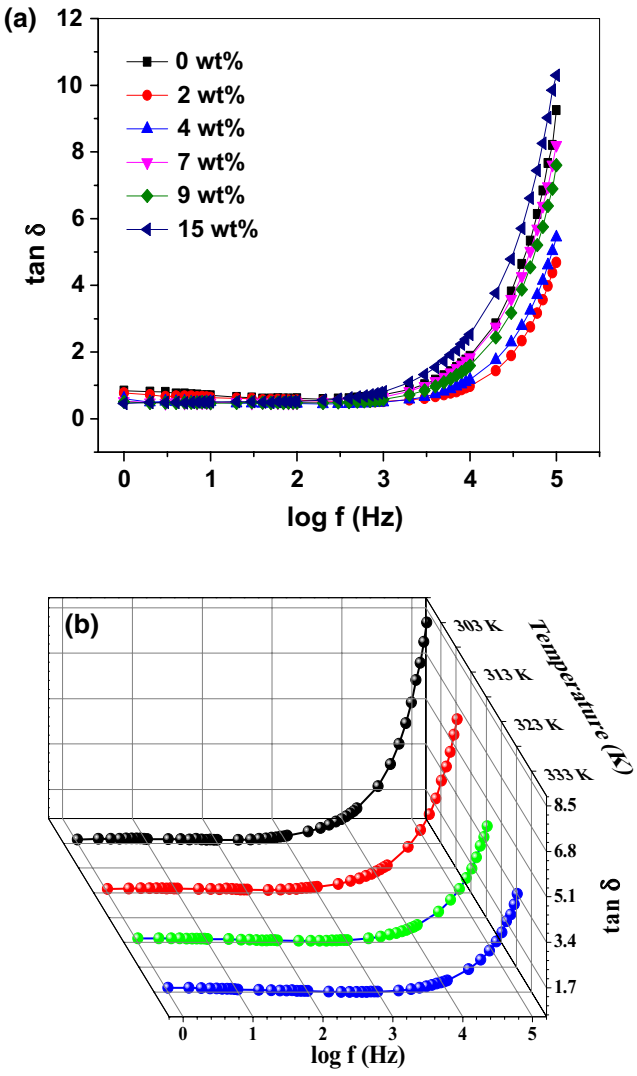

Fig. 9 Loss tangent (tan δ) versus log f for **a** PMMA-EC + PC-$NaClO_4$—x wt% SiO_2 where $x = 0, 2, 4, 7, 9, 15$. **b** PMMA-EC + PC-$NaClO_4$—4 wt% SiO_2 at different temperatures

Table 2 The characteristic features of the gel-based polymer electrolyte membrane dispersed with/without SiO_2 nanoparticles

Characteristic feature	Gel polymer electrolyte membrane without SiO_2 nanofiller	Gel polymer electrolyte membrane with optimized SiO_2 nanofiller concentration (4 wt%)	Remarks
Bulk resistance (Ω)	150	20	From Fig. 1b
Ionic conductivity (S cm^{-1})	4.5×10^{-4}	3.5×10^{-3}	From Fig. 2a
Dielectric constant	783	10,743	From Fig. 3a at 100 kHz
Dielectric loss	7470	54,233	From Fig. 3b at 100 kHz
Loss tangent (tan δ)	9.29	5.54	From Fig. 7a at 100 kHz
Liquid retention	Low	High	Qualitatively
Thermal stability	Low	High	Ref. [15]
SEM morphology	Flat morphology	Highly aligned strands of SiO_2 particles around which polymer gel is wrapped	Ref. [15]

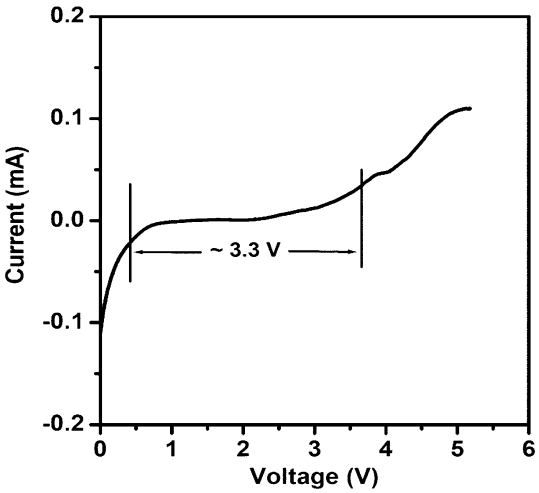

Fig. 10 LSV curve of nanocomposite gel polymer electrolyte with 4 wt% SiO_2 at scan rate of 5 mV s^{-1}

3.5 Linear sweep cyclic voltammetry study

The electrochemical stability window (ESW) of the highest conducting composition of the prepared nanocomposite gel polymer electrolyte is obtained by LSV on the asymmetric cell: SS| nanocomposite gel polymer electrolyte|Na–Hg (Fig. 10). The effective ESW is obtained to be ~ 3.3 V which is a sufficient working voltage range for sodium batteries.

3.6 Prototype sodium cell studies

The highest conducting nanocomposite gel polymer electrolyte with 4 wt% SiO_2 nanofiller has been used in a prototype cell with Na–Hg anode and P–C cathode. The P–C composite is a good electrode material for sodium-based batteries [16, 42]. Figure 11a shows the variation of open-circuit voltage (OCV) of the prototype cell with time. The OCV of the cell is observed stable for the considered experiment time of 10 h. The fabricated cell is discharged through three different specific drain currents, 14, 36, and 57 mA g^{-1} up to 0.5 V. The specific discharge capacities are shown in Fig. 11b. The cell displays the discharge capacity of ~ 500, ~ 250 and ~ 50 mAh g^{-1} at 14, 36, and 57 mA g^{-1}, respectively. The cycling performance of the fabricated cell at 14 mA g^{-1} has been tested between cut-off voltages 2.5 V and 0.5 V.

The variation of specific discharge capacity with cycle number is shown in Fig. 11c. As shown in the figure, the specific capacity fades quickly to ~ 216 mAh g^{-1} during the second discharge and retains only ~ 81 mAh g^{-1} capacity in the 10th discharge. In order to investigate the reason for the capacity fading during the cycling of the cell, complex impedance spectroscopy studies have been done on the prototype cell in full-charged state and after the 10th discharge. The Nyquist plot is shown in Fig. 12. The impedance curve of full-charged cell displays the existence of three typical resistive components as bulk electrolyte resistance (R_b), solid electrolyte interface resistance (R_{SEI}), and faradic charge transfer resistance (R_{CT}) appeared in three different frequency regions of the measurement (Inset Fig. 12).

The total resistance of the cell assembly is considered as the contribution of these three resistances. As can be seen from the figure, the R_{CT} of the cell has been increased to eight times after discharge, from ~ 0.4 kΩ to ~ 3.2 kΩ. This faradic charge transfer observed in the low-frequency region occurs at the electrode/electrolyte interface. The increase in R_{CT} is associated with the volume expansion of cathode and anode during cycling, resulting in poor cycling performance of the fabricated prototype. The volume expansion in the cathode side of the prepared prototype causes the pulverization of the phosphorus particles and the formation of unstable solid electrolyte interphase (SEI). This is reflected in the EIS analysis, as R_{SEI} is observed to be increased in the discharged cell. During the cycling of the prototype, the thickening of the passivation at the electrode/electrolyte interface occurs which is responsible for the capacity deterioration

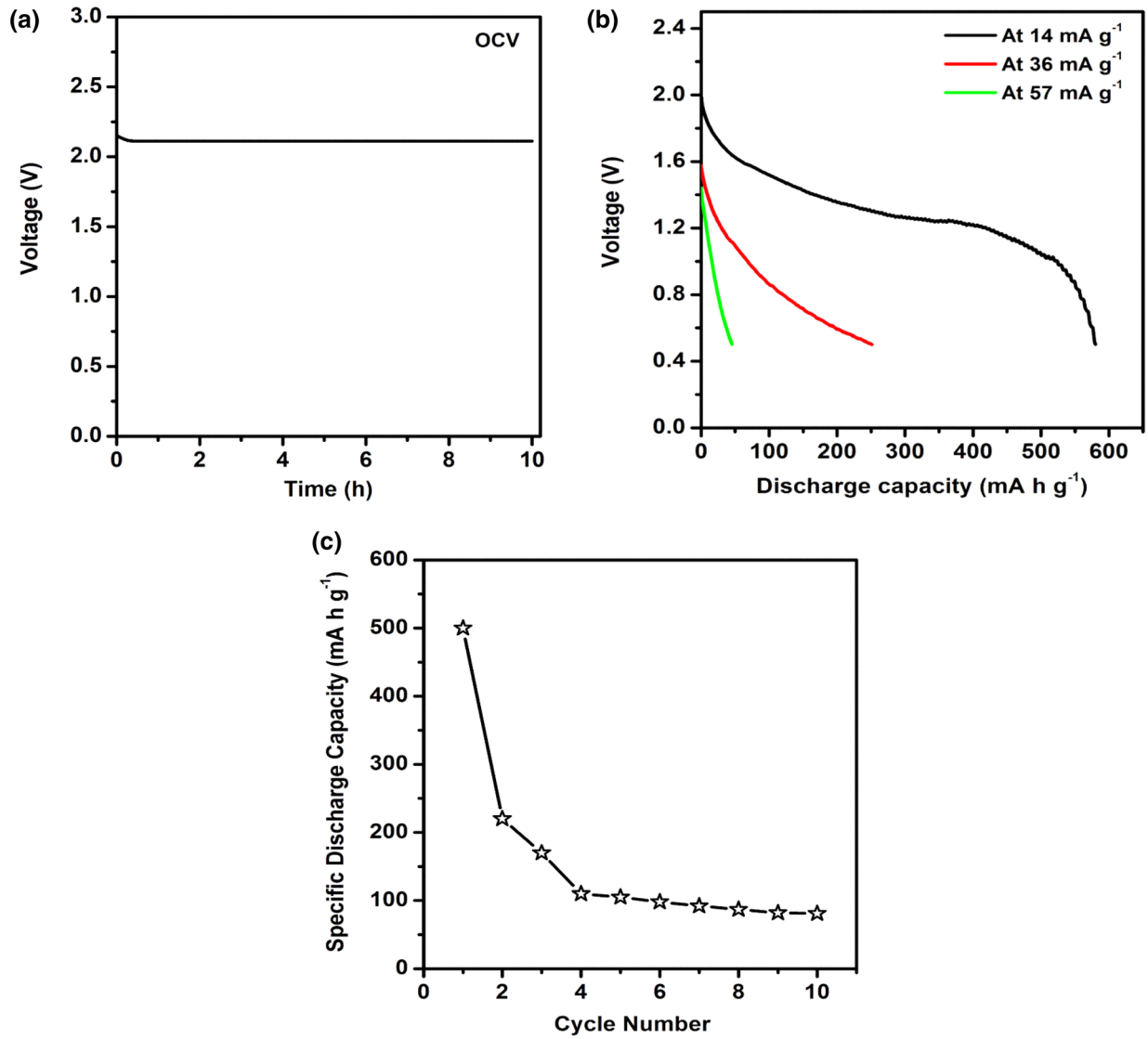

Fig. 11 **a** Variation of open-circuit voltage (OCV) with time, **b** discharge curves at different specific drain currents, **c** variation of specific discharge capacity with cycle numbers

of the prototype. The formation of the passivation layer consumes electrolyte at the electrode/electrolyte interface which causes an increase in the R_b and, in total, a rise in the internal resistance of the battery. The low active material utilization may also be one of the reasons for capacity fading [18, 49]. In order to deal with the volume expansion of the electrode materials, in a sodium ion full-charged cell, the use of composites of phosphorous red (P), at the anode side, and sodiated layered transition metal oxides (TMOs), metal fluorides, metal phosphates, and fluorophosphate, at cathode sides, with high conductivity carbonaceous materials such as carbon nanotubes (CNTs), N-doped micro/nanoporous carbon and carbon nanofibers (CNFs) appears to be an interesting approach [48]. Suitable interfaces, such as artificial mechanical stable biphasic interphase (BPI) and metal–alloy interphase (MAI) can also be employed to check volume expansion of sodium anodes and facilitate reversible deposition of sodium during cell operation [50, 51]. These materials decrease the absolute stress/strain and may hinder large volume change by providing good encapsulation to the active material. Additionally, these materials provide excellent electronic conductivities and promote better charge transfer at the electrode.

4 Conclusions

In the present study, ion conduction behavior has been studied by employing electrochemical investigations on flexible Na^+ conducting nanocomposite gel polymer electrolytes.

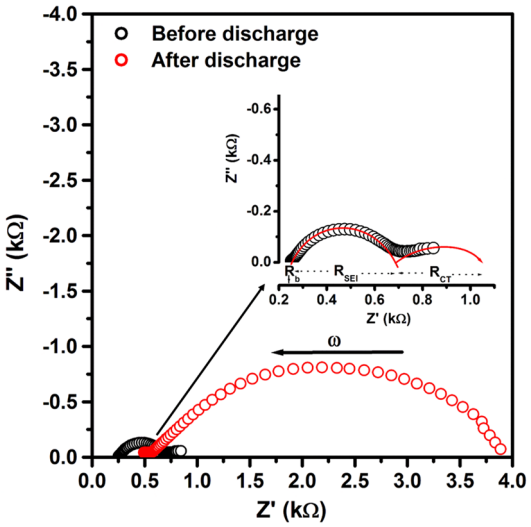

Fig. 12 Nyquist plots of Na–Hg nanocomposite gel polymer electrolyte P–C cell before and after discharge

The AC conductance spectrum of the reported electrolyte system shows the accumulation of charges occurs due to the electrode–electrolyte interface in the low-frequency region. The incorporation of nanofillers into GPE system affects total available charge carriers as well as their mobility through Lewis acid–base interaction and therefore the dielectric constant (ε') tends to vary with SiO_2 concentration. The low-frequency region showed high values of dielectric constant due to polarization at the electrode–electrolyte interface. The real M' and imaginary part M'' of modulus reveal large capacitance associated with it at lower frequency region whereas conductivity relaxation dispersion at higher frequency region. The reported electrolyte membrane exhibited high ionic conducting of the order of 10^{-3} S cm^{-1} with a sufficiently high electrochemical stability window of $\approx$ 3.3 V for electrochemical systems. A prototype sodium battery using the optimized flexible nanocomposite gel polymer electrolyte films showed a stable open-circuit potential of ~ 2.1 V and a significant first specific discharge capacity of ~ 500 mAh g^{-1} at a drain current of 14 mA g^{-1}. From the ionic conductivity, dielectrics, linear sweep voltammetry, open-circuit voltage, and discharge capacities studies revealed that the reported gel-based nanocomposite electrolytes can be utilized as electrolyte/separator by sandwiching it between suitable cathodes for the fabrication of flexible sodium batteries.

Acknowledgements Deepak Kumar thanks and acknowledges "The M.S. University of Baroda," Vadodara, Gujarat, India. He thanks and acknowledges Dr. S.A. Hashmi, University of Delhi, Delhi, India, for constant motivation and support. The encouragement received from Electronics and Mechanical Engineering School (Affiliated to Gujarat Technological University), Corps of Electronics and Mechanical Engineers, Ministry of Defence, Government of India, is highly acknowledged. Part of this research work was performed at University of Delhi, Delhi, India. Kuldeep Mishra acknowledges the funding (File No. YSS/2015/001234) from Science and Engineering Research Board (SERB) New Delhi, India.

Compliance with ethical standards

Conflicts of interest The authors report no conflicting interest in any capacity, competing, or financial.

References

1. J.B. Goodenough, K.-S. Park, The Li-ion rechargeable battery: a perspective. J. Am. Chem. Soc. **135**(4), 1167–1176 (2013)
2. O.V. Lonchakova, O.A. Semenikhin, M.V. Zakharkin, E.A. Karpushkin, V.G. Sergeyev, E.V. Antipov, Efficient gel-polymer electrolyte for sodium-ion batteries based on poly(acrylonitrile-*co*-methyl acrylate). Electrochim. Acta **334**, 135512 (2020)
3. D. Kumar, D.K. Kanchan, S.B. Kuhar, Room temperature sodium-sulfur batteries as emerging energy source. J. Energy Storage **18**, 133–148 (2018)
4. R. Deivanayagam, B.J. Ingram, R.S. Yassar, Progress in development of electrolytes for magnesium batteries. Energy Storage Mater. **21**, 136–153 (2019)
5. C. Maheshwaran, D.K. Kanchan, K. Gohel, K. Mishra, D. Kumar, Effect of $Mg(CF_3SO_3)_2$ concentration on structural and electrochemical properties of ionic liquid incorporated polymer electrolyte membranes. J. Solid State Electrochem. **24**, 655–665 (2020). https://doi.org/10.1007/s10008-020-04507-3
6. X. Zhang, D. Yang, X. Rui, Y. Yu, S. Huang, Advanced cathodes for potassium-ion battery. Curr. Opin. Electrochem. **18**, 24–30 (2019)
7. M. Xu, D.G. Ivey, Z. Xie, W. Qu, Rechargeable Zn-air batteries: progress in electrolyte development and cell configuration advancement. J. Power Sources **283**, 358–371 (2015)
8. A.R. Despić, Design characteristics of an aluminium-air battery with consumable wedge anodes. J. Appl. Electrochem. **15**, 191–200 (1985)
9. A. Chandrasekhar, V. Vivekananthan, S.-J. Kim, A fully packed spheroidal hybrid generator for water wave energy harvesting and self-powered position tracking. Nano Energy **69**, 104439 (2020)
10. A. Sukumaran, V. Vivekananthan, V. Mohan, Z.C. Alex, A. Chandrasekhar, S.-J. Kim, Triboelectric nanogenerators from reused plastic: an approach for vehicle security alarming and tire motion monitoring in rover. Appl. Mater. Today **19**, 100625 (2020)
11. A. Chandrasekhar, V. Vivekananthan, G. Khandelwal, S.-J. Kim, Sustainable human-machine interactive triboelectric nanogenerator toward a smart computer mouse. ACS Sustain. Chem. Eng. **7**(7), 7177–7182 (2019)
12. A. Chandrasekhar, N.R. Alluri, M.S.P. Sudhakaran, Y.S. Mokd, S.-J. Kim, A smart mobile pouch as a biomechanical energy harvester towards self-powered smart wireless power transfer applications. Nanoscale **9**, 9818–9824 (2017)
13. A. Chandrasekhar, N.R. Alluri, V. Vivekananthan, Y. Purusothamana, S.-J. Kim, A sustainable freestanding biomechanical energy harvesting smart backpack as a portable-wearable power source. J. Mater. Chem. C **5**, 1488–1493 (2017)
14. A. Ponrouch, D. Monti, A. Boschin, B. Steen, P. Johansson, M.R. Palacín, Non-aqueous electrolytes for sodium-ion batteries. J. Mater. Chem. A **3**, 22–42 (2015)
15. A. Kumar, S.A. Hashmi, Ion transport and ion–filler-polymer interaction in poly(methyl methacrylate)-based, sodium ion

conducting, gel polymer electrolytes dispersed with silica nanoparticles. J. Power Sources **195**, 5101–5108 (2010)
16. M. Jahn, M. Sedlaříková, J. Vondrák, L. Pařízek, PMMA-based electrolytes for li-ion batteries. ECS Trans. **74**(1), 159–164 (2016)
17. M. Zhu, J. Wu, Y. Wang, M. Song, L. Long, S.H. Siyal, X. Yang, G. Sui, Recent advances in gel polymer electrolyte for high-performance lithium batteries. J. Energy Chem. **37**, 126–142 (2019)
18. K. Mishra, T. Arif, R. Kumar, D. Kumar, Effect of Al_2O_3 nanoparticles on ionic conductivity of PVdF-HFP/PMMA blend-based Na^+-ion conducting nanocomposite gel polymer electrolyte. J. Solid State Electrochem. **23**(8), 2401–2409 (2019)
19. D.J. Kim, M.J. Jo, S.Y. Nam, A review of polymer–nanocomposite electrolyte membranes for fuel cell application. J. Ind. Eng. Chem. **21**, 36–52 (2015)
20. H. Che, S. Chen, Y. Xie, H. Wang, K. Amine, X.-Z. Liao, Z.-F. Ma, Electrolyte design strategies and research progress for room-temperature sodium-ion batteries. Energy Environ. Sci. **10**, 1075–1101 (2017)
21. L.G. Chagas, S. Jeong, I. Hasa, S. Passerini, Ionic liquid-based electrolytes for sodium-ion batteries: tuning properties to enhance the electrochemical performance of manganese-based layered oxide cathode. ACS Appl. Mater. Interfaces **11**(25), 22278–22289 (2019)
22. D. Kumar, Effect of organic solvent addition on electrochemical properties of ionic liquid-based Na^+ conducting gel electrolytes. Solid State Ionics **318**, 65–70 (2018)
23. C.-H. Dustmann, Advances in ZEBRA batteries. J. Power Sources **127**, 85–92 (2004)
24. R. Wang, H. Mo, S. Li, Y. Gong, B. He, H. Wang, Influence of Conductive additives on the stability of red phosphorus carbon anodes for sodium-ion batteries. Sci. Rep. **9**, 946 (2019). https://doi.org/10.1038/s41598-018-36797-z
25. W. Tian, L. Wang, K. Huo, X. He, Red phosphorus filled biomass carbon as high-capacity and long-life anode for sodium-ion batteries. J. Power Sources **430**, 60–66 (2019)
26. Z. Li, H. Zhao, Recent developments of phosphorus-based anodes for sodium ion batteries. J. Mater. Chem. A **6**, 24013 (2018)
27. H. Liu, S. Zhang, Q. Zhu, B. Cao, P. Zhang, N. Sun, B. Xu, F. Wua, R. Chen, Fluffy carbon-coated red phosphorus as a highly stable and high-rate anode for lithium-ion batteries. J. Mater. Chem. **A7**, 11205–11213 (2019)
28. S. Sharma, D. Pathak, N. Dhiman, R. Kumarand, M. Kumar, FTIR, thermal and ionic conductivity studies of nanocomposite polymer electrolytes. Surf. Innov. **7**(1), 51–58 (2019)
29. K.W. Chew, K.W. Tan, The effects of ceramic fillers on PMMA-based polymer electrolyte salted with lithium triflate, $LiCF_3SO_3$. Int. J. Electrochem. Sci. **6**, 5792–5801 (2011)
30. B.A. Boukamp, A Linear Kronig−Kramers transform test for immittance data validation. J. Electrochem. Soc. **142**, 1885–1894 (1995)
31. N.K. Singh, M.L. Verma, M. Minakshi, PEO nanocomposite polymer electrolyte for solid state symmetric capacitors. Bull. Mater. Sci. **38**, 1577–1588 (2015)
32. K. Gohel, D.K. Kanchan, Ionic conductivity and relaxation studies in PVDF-HFP:PMMA-based gel polymer blend electrolyte with $LiClO_4$ salt. J. Adv. Dielectrics **08**(01), 1850005 (2018)
33. F. Croce, B. Scrosati, G. Mariotto, Electrochemical and spectroscopic study of the transport properties of composite polymer electrolytes. J. Chem. Mater. **4**, 1134–1136 (1992)
34. S.B. Aziz, J.W. Thompson, M.F.Z. Kadir, H.M. Ahmed, A conceptual review on polymer electrolytes and ion transport models. J. Sci. **3**, 1–17 (2018)
35. K. Gohel, D.K. Kanchan, Effect of PC: DEC plasticizers on structural and electrical properties of PVDF–HFP:PMMA based gel polymer electrolyte system. J. Mater. Sci. **30**, 12260–12268 (2019)
36. S. Choudhary, R.J. Sengwa, Effects of different inorganic nanoparticles on the structural, dielectric and ion transportation properties of polymers blend based nanocomposite solid polymer electrolytes. Electrochim. Acta **247**, 924–941 (2017)
37. W. Wang, P. Alexandridis, Composite polymer electrolytes: nanoparticles affect structure and properties. Polymers **8**, 1–36 (2016)
38. M. Hema, P. Tamilselvi, Lithium ion conducting PVA:PVdF polymer electrolytes doped with nano SiO_2 and TiO_2 filler. J. Phys. Chem. Solids **97–98**, 42–48 (2016)
39. P. Lun, P. Liu, H. Lin, Z. Dai, Z. Zhang, D. Chen, Ionic conductivity promotion of polymer membranes with oxygen-ion conducting nanowires for rechargeable lithium batteries. J. Membr. Sci. **580**, 92–100 (2019)
40. A. Bhardwaj, A. Kumar, H. Bae, C.-J. Park, S.-J. Song, Surface decorated spinel-oxide electrodes for mixed-potential ammonia sensor: performance and DRT analysis. J. Hazard. Mater. **396**, 122601 (2020)
41. M.S. Munde, D.Z. Gao, A.L. Shluger, Diffusion and aggregation of oxygen vacancies in amorphous silica. J. Phys. **29**, 245701 (2017)
42. A. Karmakar, A. Ghosh, Dielectric permittivity and electric modulus of polyethylene oxide (PEO)-$LiClO_4$ composite electrolytes. Curr. Appl. Phys. **12**, 539–543 (2012)
43. K.S. Hemalatha, G. Sriprakash, M.V.N.A. Prasad, R. Damle, K. Rukmani, Temperature dependent dielectric and conductivity studies of polyvinyl alcohol-ZnO nanocomposite films by impedance spectroscopy. J. Appl. Phys. **118**, 154103–154116 (2015)
44. A. Kyritsis, P. Pissis, J. Grammatikakis, Dielectric relaxation spectroscopy in poly(hydroxyethylene acrylates)/water hydrogels. J. Poly. Sci. Part B Poly. Phys. **33**, 1737–1750 (1995)
45. T. Regu, C. Ambika, K. Karuppasamy, H. Rajan, D. Vikraman, J.-H. Jeon, H.-S. Kim, T.A.B. Raj, Proton transport and dielectric properties of high molecular weight polyvinylpyrrolidone (PVPK90) based solid polymer electrolytes for portable electrochemical devices. J. Mater. Sci. **30**, 11735–11747 (2019)
46. P. Sharma, D.K. Kanchan, A comparison of effect of PEG and EC plasticizers on relaxation dynamics of PEO-PMMA-$AgNO_3$ polymer blend. Ionics **19**, 1285–1290 (2013)
47. D.K. Pradhan, R.N.P. Choudhary, B.K. Samantaray, Studies of dielectric and electrical properties of plasticized polymer nano composite electrolytes. J. Mater. Chem. Phys. **115**, 557–561 (2009)
48. J.Y. Hwang, S.T. Myung, Y.K. Sun, Sodium-ion batteries: present and future. Chem. Soc. Rev. **46**, 3529–3614 (2017)
49. D. Kumar, D.K. Kanchan, S. Kumar, K. Mishra, Recent trends on tailoring cathodes for room-temperature Na-S batteries. Mater. Sci. Energy Technol. **2**, 117–129 (2019)
50. V. Kumar, Y. Wang, A.Y.S. Eng, M.-F. Ng, Z.W. She, A biphasic interphase design enabling high performance in room temperature sodium-sulfur batteries. Cell Rep. Phys. Sci. (2020). https://doi.org/10.1016/j.xcrp.2020.100044
51. V. Kumar, A.Y. Sheng Eng, Y. Wang, D.-T. Nguyen, M.-F. Ng, Z.W. Seh, An artificial metal-alloy interphase for high-rate and long-life sodium–sulfur batteries. Energy Storage Mater. **15**, 20 (2020). https://doi.org/10.1016/j.ensm.2020.03.027

Journal of Materials Science: Materials in Electronics
https://doi.org/10.1007/s10854-020-04065-4

Flexible magnesium-ion conducting polymer electrolyte membranes: mechanical, structural, thermal, and electrochemical impedance spectroscopic properties

C. Maheshwaran[1] · D. K. Kanchan[1] · Kuldeep Mishra[2] · Deepak Kumar[3] · Khushbu Gohel[1]

Received: 20 May 2020 / Accepted: 21 July 2020

Abstract
This paper reports investigations on flexible magnesium-ion-conducting polymer electrolyte membranes using mechanical, structural, and electrochemical impedance spectroscopic analysis. XRD studies reveal significant changes in structural character on varying the concentration of propylene carbonate-diethyl carbonate (PC-DEC) organic solvent within the polymer electrolyte matrix. SEM and AFM studies indicate variation in surface morphology and maximum roughness height by introducing PC-DEC in increasing amount. The plasticized polymer electrolyte membrane with optimum concentration of 15 wt% PC-DEC demonstrates magnesium-ion conductivity of 3×10^{-5} s cm^{-1}at room temperature. This flexible electrolyte has Young's modulus of 100 N mm^{-2}, mechanical strength of 2 Kgf, and ability to withstand stress of 6 N mm^{-2} and strain of 7 N mm^{-2} at a maximum load of 10 Kgf. The electrolyte membranes do not show any degradation after stretching and rolling it for hundred times. The electrolyte membrane offer electrochemical stability window of ~ 3.5 V and Mg^{2+} transport number of 0.32. The reported electrolyte membranes can be employed in fabricating flexible magnesium batteries.

1 Introduction

Fossil fuels have caused global environmental pollution and safe, low cost, and greener energy storage systems are needed to fulfill the global energy demand. Li-ion batteries are well known for their high specific energy density and are widely used in portable electronics and EVs. The concentration of Li resources to limited countries and low natural abundance has contributed to price rise [1, 2]. There are many reports of safety issues with Li-ion batteries which clearly suggest that Li-ion batteries are not ultimate and there is a scope to research on low cost, more abundant resources such as Mg, Na, Zn, K, and Al-based battery system [3–10]. Electrolyte is most important part of any battery system as it ensures proper redox reactions and electrochemistry of cell. The solid electrolytes are widely used to ensure cell safety but they tend to possess low ionic conductivity and poor electrolyte/electrode interfacial contact [11, 12]. Researchers utilize liquid electrolytes primarily, due to their high ionic conductivity but these electrolytes are prone to leakage and are fire hazard [13, 14]. Glyme-based liquid electrolyte are known for the lesser discharge capacity values and therefore carbonate-based electrolytes are preferred due to high ionic conductivity, wide electrochemical stability window, relatively higher discharge capacity, and stable anode passivation layer [15–22].

Plasticized polymer electrolytes are known for liquid-like ionic transport (thereby giving rise to high ionic conductivity, good electrochemical stability window, and high transference number) and solid-like safety and sufficient mechanical strength (as salt solution is immobilized in polymer matrix) [23–25]. Such electrolytes are widely utilized in various electrochemical devices such as batteries, supercapacitor/ultracapacitor, sensors, fuel cells, etc. Incorporation of low molecular weight and high dielectric constant organic solvents in such electrolyte system ensures better salt dissociation and high ionic conduction. The commonly used organic solvents for realizing polymer gel electrolytes are ethylene carbonate (EC), propylene

✉ Deepak Kumar
fwtdrdeepak@gmail.com; deepak.kumar06@gov.in

[1] Department of Physics, M.S. University of Baroda, Vadodara, Gujarat 390002, India

[2] Department of Physics, Jaypee University, Anoopshahr, Uttar Pradesh 203390, India

[3] Electronics and Mechanical Engineering School, Affiliated to Gujarat Technological University, Vadodara, Gujarat 390008, India

Published online: 31 July 2020

carbonate (PC), dimethyl carbonate (DMC), diethylene carbonate (DEC), fluoroethylene carbonate (FEC), and dimethyl formamide (DMF) etc. [26–30]. Magnesium-based batteries have attracted the attention of researchers from last few decades due to low cost, high natural abundance, sufficiently low electrochemical equivalence (12.5 eq^{-1}), and low electrode potential (− 2.3 V versus SHE) [31]. In addition, Mg metal is more stable and can be handled safely in oxygen and humid atmosphere unlike Li, which requires inert atmosphere. The development of rechargeable Mg batteries is largely hampered due to irreversibility of Mg negative electrode and lack of proper Mg^{2+}-conducting non-aqueous, high conducting electrolyte. Muldoon et al. have highlighted the lack of suitable electrolyte as main roadblock for the development of a magnesium rechargeable battery [32].

There are many reports on Mg-ion-conducting polymer electrolytes. Agrawal et al. studied variation in ion-transport properties of $MgTf_2$/PEO system on using different active/passive fillers [33]. In three different reports, Kumar et al. studied electrochemical properties of $MgTf_2$/polymer/EC-PC system by selecting poly(acrylonitrile) (PAN), poly(ethylene oxide) (PEO), and poly(methyl methacrylate) PMMA as polymer matrix [34–36]. Sharma et al. studied the effect of varying succinonitrile on thermal, structural, and conductivity properties of polymer electrolyte system [37]. Das and Ghosh studied the effect of different types of plasticizers on ionic conductivity and dielectric relaxation of $LiClO_4$/PEO polymer electrolytes [38]. Hence, it will be interesting to know the effect of plasticizing $MgTf_2$/PEO polymer electrolyte matrix with PC-DEC as binary organic solvents.

In this report, we study the plasticization effect of PC-DEC binary solvents at different dilution level within $MgTf_2$/PEO matrix using XRD, SEM, and AFM for structural properties, and impedance spectroscopy, cyclic voltammetry, and dc polarization for electrochemical properties. Plasticized flexible Mg^{2+}-conducting polymer electrolyte membranes have been fabricated by standard solution casting technique. Mechanical strength of electrolytes has been evaluated on varying the concentration of PC-DEC organic solvents in it. In order to understand the ion conduction behavior, conductivity and dielectrics studies have been performed for electrolytes with different PC-DEC solvent concentration. Cyclic voltammetry study has been performed to check platting/stripping of Mg^{2+} ions at electrodes. The cation-transport number has been determined for optimized polymer electrolyte membrane with highest conductivity. The investigations revealed significant changes on morphology and ion dynamics within the flexible magnesium-ion-conducting polymer electrolyte membranes.

2 Experimental section

2.1 Material used and preparation of flexible polymer electrolyte membranes

The materials used for the preparation of flexible polymer electrolytes membranes includes poly(ethylene oxide), PEO from Alfa Aesar, $Mg(CF_3SO_3)_2$ salt of 97% purity from Aldrich, propylene carbonate (PC) from Sigma Aldrich with 99.7% purity, and diethyl carbonate (DEC) of 99% purity from Aldrich were used after drying overnight in oven. Acetone of purity 99% was obtained from Sigma Aldrich and was used as received for dissolving PEO polymer host. The flexible Mg^{2+}-conducting polymer electrolyte membranes were fabricated by standard solution casting technique. In this technique, PEO polymer and magnesium triflate salt were separately dissolved in acetone and stirred for 8 h at 40 °C to ensure complete dissociation of polymer and salt. Subsequently, desired weight ratio of PC-DEC plasticizer was added and stirred continuously until a viscous solution was obtained. This viscous solution containing $MgTf_2$/PEO/PC-DEC was poured in glass petri dishes and acetone was allowed to evaporate at ambient condition to obtain free standing plasticized flexible polymer electrolyte membranes of thickness ~ 70 µm (Fig. 1). A total of four electrolyte specimens have been prepared and their codes and constituents are mentioned in Table 1.

2.2 Instrumentation

Mechanical properties were evaluated by recording strain versus stress curves from Instron's mechanical tester (Model 5848, Singapore) at a strain rate of 5 mm min^{-1}, by applying a maximum load of 10 N and a pressure of 1 Bar. X-ray diffraction patterns were recorded by XPERT-PRO system using Cu-Kα radiation in Bragg angle (2θ) range from 10° to 80° at scan rate of 2° min^{-1}. SEM micrographs of polymer electrolyte membrane films were recorded by FEI Quanta 200 microscope equipped with EDAX-EDS analyzer. Atomic force microscopic measurements were carried out by employing AFM, pico SPM-picoscan 2100, Molecular Imaging, USA. The AFM

Table 1 Electrolyte specimens with their codes and chemical composition

Sample code	Electrolyte composition
S-1	$MgTf_2$/PEO
S-2	$MgTf_2$/PEO/PC-DEC (5 wt%)
S-3	$MgTf_2$/PEO/PC-DEC (10 wt%)
S-4	$MgTf_2$/PEO/PC-DEC (15 wt%)

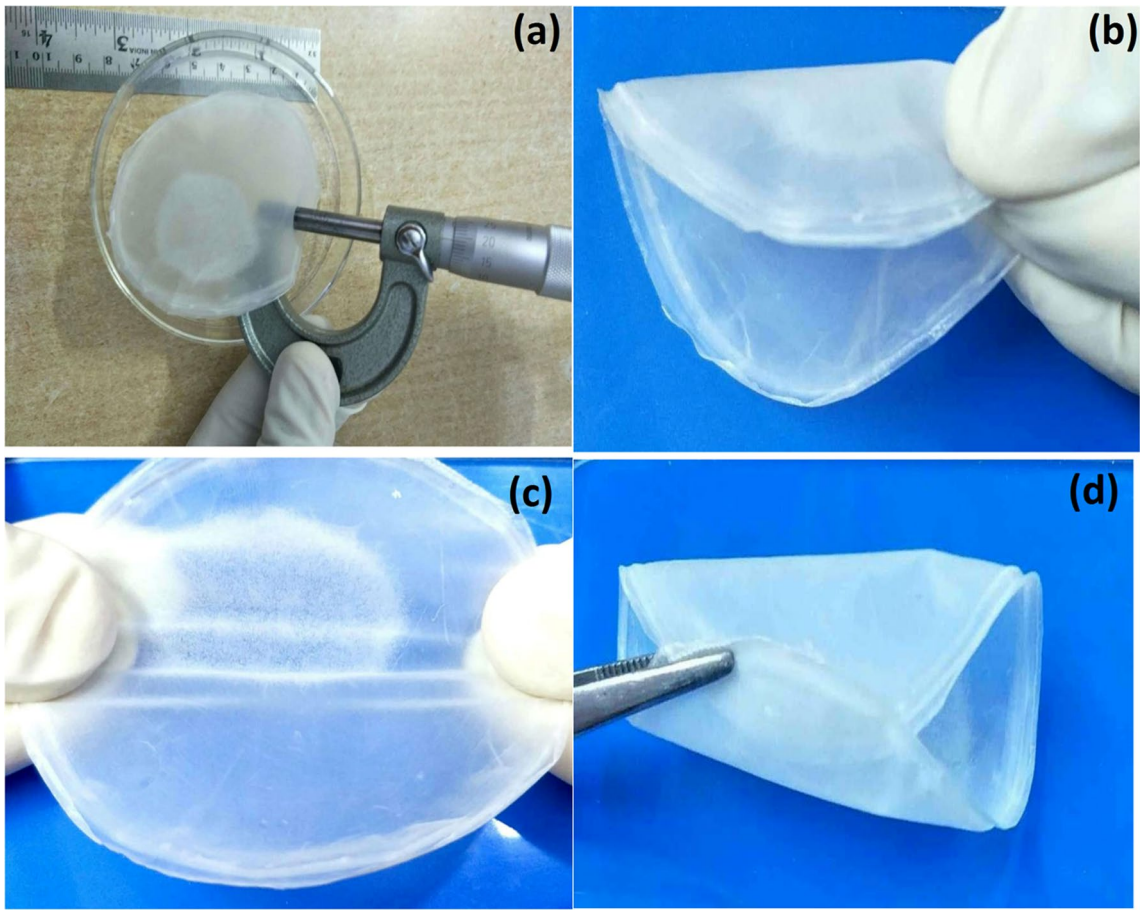

Fig. 1 Magnesium-ion-conducting plasticized polymer electrolyte specimen (S-4) illustrating (**a**) scale and membrane thickness arrangement (**b**) flexibility. Photographs of membranes illustrating (**c**) stretchability (**d**) rollability of the electrolyte film after stretching and rolling it for hundred times

images were recorded in tapping mode with a diamond-like carbon-coated ultra-sharp silicon tip. Thermal properties of these polymer electrolyte membranes were studied by differential scanning calorimetry (DSC). For the DSC measurement, samples were hermetically sealed in an aluminum pan, and DSC thermograms were obtained by SIIEXSTAR − 6000 systems at the heating rate of 10 °C min^{-1} under nitrogen atmosphere. Electrochemical impedance spectroscopy (EIS) measurements were performed at 1260 Solartron Impedance analyzer in frequency range from of 1 Hz to 32 MHz at signal level of 10 mV in temperature range from 303 to 333 K. The EIS measurements were carried out by sandwiching the flexible polymer electrolyte membranes between two stainless steel electrodes under spring pressure. The cyclic voltammetry (CV) was performed by using electrochemical analyzer (Zive SP1) of WonATech Co., Ltd., Korea, at a scan rate of 5 mV s^{-1}. The dc polarization measurements were also performed by using electrochemical analyzer (Zive SP1) of WonATech Co., Ltd., Korea.

3 Results and discussion

3.1 Mechanical and structural studies

The mechanical properties of solid and plasticized polymer electrolyte membranes have been studied with the help of mechanical strength investigations. The Young's modulus and mechanical strength of flexible polymeric electrolyte membranes have been plotted as a function of PC-DEC dilution from 0 to 15 wt% as shown in Fig. 2a. The Young's modulus and mechanical strength of the polymer electrolyte membranes decrease with increase in the plasticizer PC-DEC content within the PEO/$MgTf_2$. However, the S-4 electrolyte membrane with optimum concentration of PC-DEC, i.e., $MgTf_2$/PEO/PC-DEC (15 wt%), shows a Young's modulus of 100 N mm^{-2} and mechanical strength of 2 Kgf. The stress and strain values at maximum load are plotted as a function of PC-DEC dilution and are shown in Fig. 2b. As obvious, with enhancement in PC-DEC content within the PEO/$MgTf_2$ matrix, the stress and stain values tend to

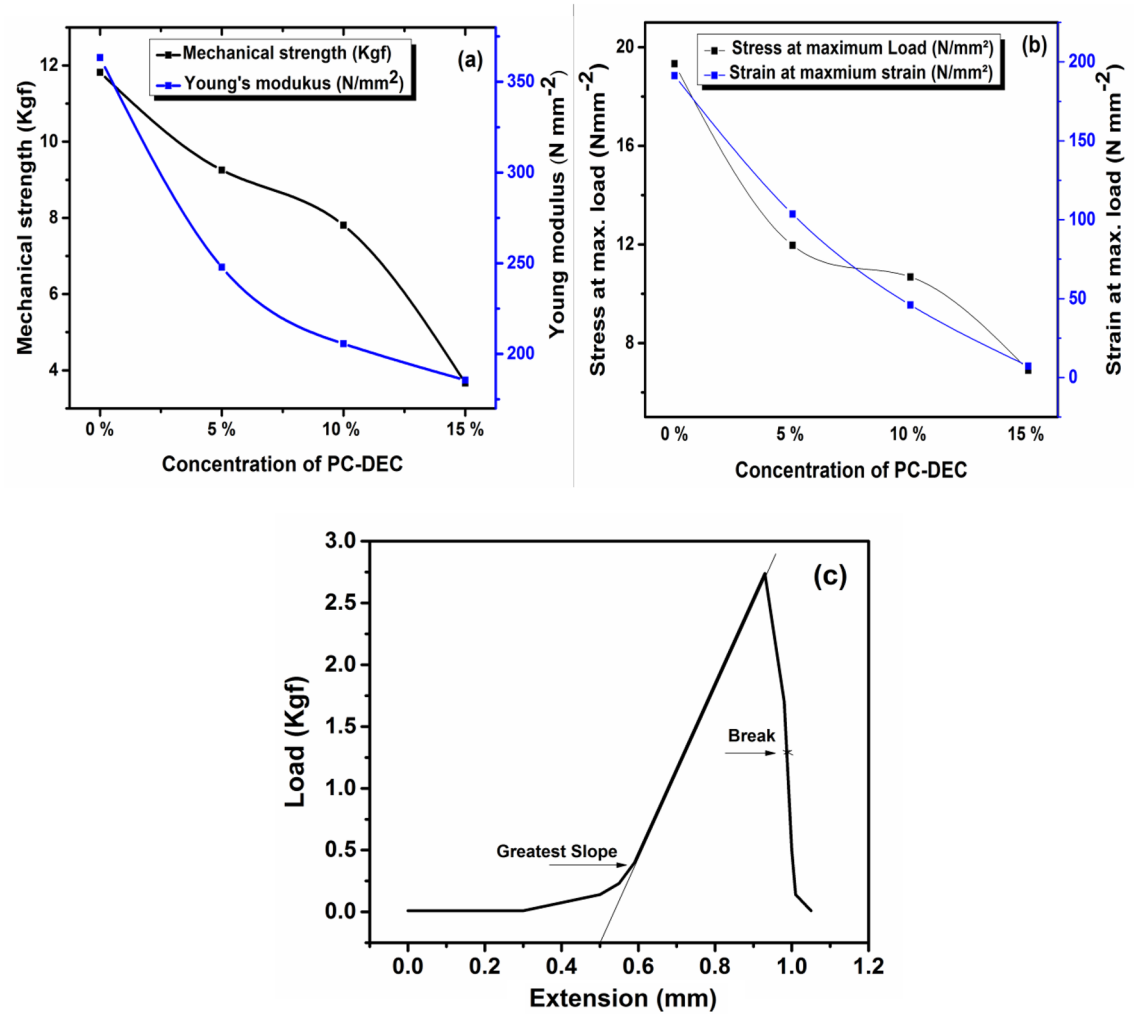

Fig. 2 **a** Young's modulus and mechanical strength and **b** stress and strain at maximum load versus PC-DEC concentration within $MgTf_2$/PEO matrix, and **c** a typical load versus extension plot for plasticized polymer electrolyte membrane $MgTf_2$/PEO/PC-DEC (15 wt%)

continuously decrease. The polymer electrolyte specimen with optimum concentration of PC-DEC, i.e., S-4, could withstand stress of 6 N mm^{-2} and strain of 7 N mm^{-2} at a maximum load of 10 Kgf. The typical response (extension) undergone by electrolyte under the action of applied load for S-4 is shown in Fig. 2c. As observed from the graph, the electrolyte membrane with 15 wt% PC-DEC is able to take a maximum load of 2.6 Kgf and breaking point is observed at extension of 1 mm. It is important to note that solid ceramic electrolyte tends to remain brittle and the optimized flexible polymer electrolyte membrane of this report is expected to ensure better electrolyte/electrodes interfacial contact leading to better electrochemical properties in magnesium-ion-conducting electrochemical devices.

In the present study, the XRD patterns (Fig. 3) of $MgTf_2$/PEO solid polymer electrolyte with no organic solvent content and $MgTf_2$/PEO/PC-DEC with varying concentration of PC-DEC as organic solvent within the $MgTf_2$/PEO matrix are recorded. We observe two prominent blunt crystalline peaks at 19.3° and 23.4° of pure PEO in the diffractogram for all the membranes. This suggests the presence of characteristic semi-crystalline pure PEO dominates in $MgTf_2$/PEO solid polymer electrolyte as well as plasticized polymer electrolytes. Further, on varying the concentration of binary organic solvents up to 15 wt% within the $MgTf_2$/PEO matrix, the characteristic peaks broaden increasingly which indicate decrease of crystalline character. These observations suggest introduction of significant structural disordering in $MgTf_2$/PEO matrix on varying concentration of PC-DEC. These structural changes are likely to affect Mg^{2+} ion conduction behavior within the electrolyte system, as ion conduction is considered to be more prominent in amorphous polymer-based systems.

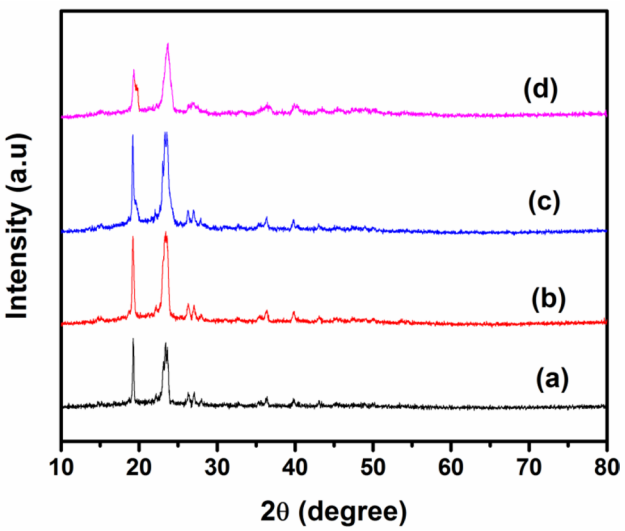

Fig. 3 X-ray diffraction patterns of (a) S-1, (b) S-2, (c) S-3 and (d) S-4

The comparative surface morphologies of $MgTf_2$/PEO solid polymer electrolytes and plasticized polymer electrolyte membranes with different PC-DEC dilution, i.e., $MgTf_2$/PEO/PC-DEC (5 to 15 wt%), respectively, is shown in Fig. 4. The unplasticized $MgTf_2$/PEO membrane possesses tightly integrated spherulites on its surface (Fig. 4a), which is an indicative of high crystallinity of $MgTf_2$/PEO solid polymer electrolyte membrane [39]. On increasing concentration of PC-DEC plasticizer, a significant change in spherulites size and crystalline character is observed. From the micrographs (Fig. 4b–d), we observe that the spherulites are getting more separated with the presence of distributed amorphous lumps in-between. For S-4 composition, i.e., for $MgTf_2$/PEO/PC-DEC (15 wt%), less denser and large sized spherulites are well observed. These observations from SEM are in well corroboration with the XRD results.

Figure 5a-d shows AFM pictures of solid polymer electrolyte and plasticized polymer electrolytes containing PEO as polymer host. A significant variation in the maximum roughness height is observed on changing the PC-DEC carbonate content from 0 to 15 wt% within the MgTf2/PEO

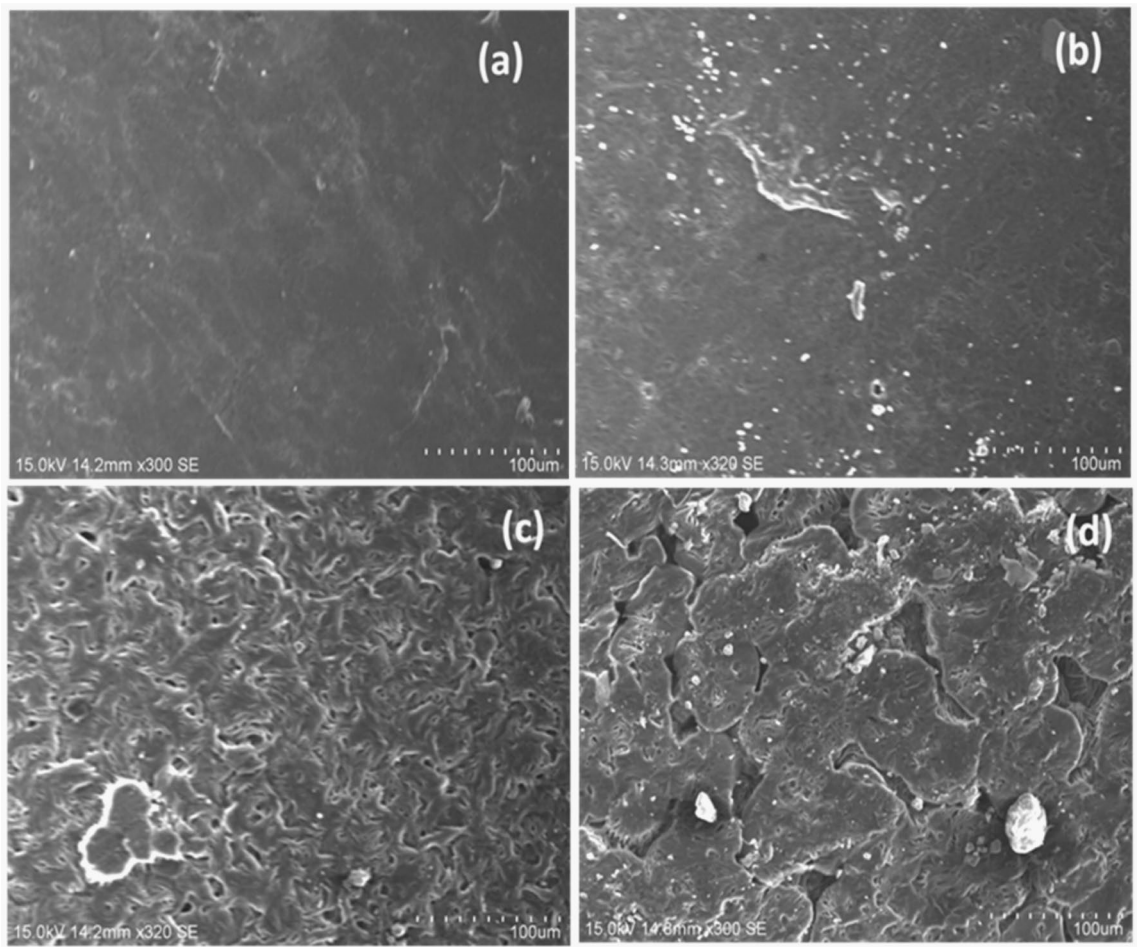

Fig. 4 SEM micrographs of **a** S-1, **b** S-2, **c** S-3 and **d** S-4

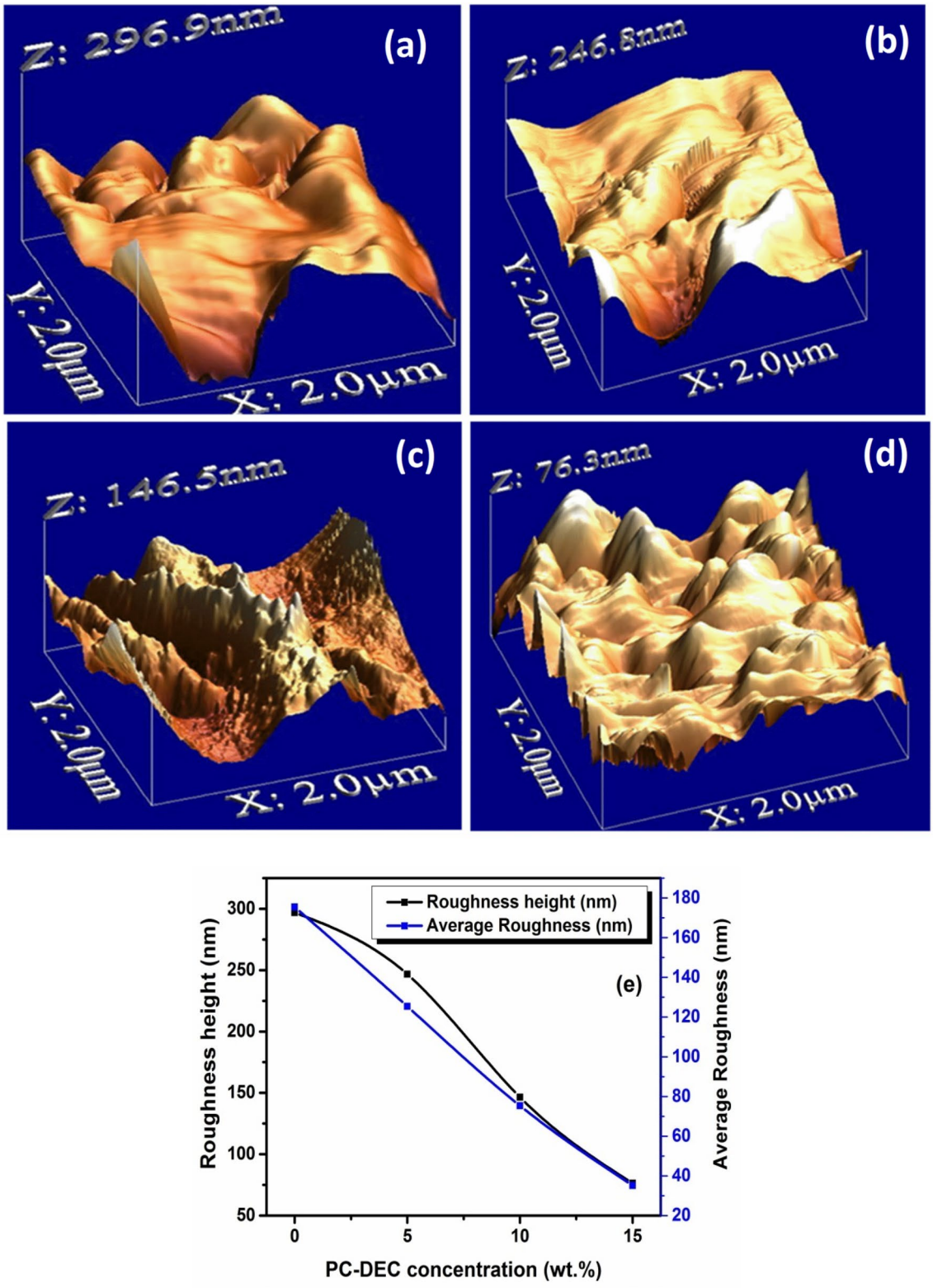

Fig. 5 AFM images of **a** S-1, **b** S-2, **c** S-3 and **d** S-4, and **e** variation of roughness height and average roughness as the PC-DEC concentration changes within $MgTf_2$/PEO matrix

matrix. Figure 5e indicates the maximum roughness height drastically changes from ~300 to 70 nm while PC-DEC concentration changes from 0 to 15 wt%. It is important to note that the S-4 composition carrying 15 wt% PC-DEC content has optimized retention of organic solvents and, therefore, smooth morphology with minimum roughness height

Figure 6a shows the DSC pattern for pure polyethylene oxide film obtained by discussing it in acetone, followed by its slow evaporation. The characteristic melting peak of PEO is obtained at ~60 °C. When magnesium triflate ($MgTf_2$) salt is incorporated in PEO, the DSC profile suddenly changes and the melting temperature of $MgTf_2$/PEO film approaches to 59 °C. Hence, a decrease in melting temperature from 60 to 59 °C is observed when $MgTf_2$ is immobilized in PEO matrix to obtain solid polymer electrolyte. On increasing PC-DEC plasticizer in $MgTf_2$/PEO matrix, the melting temperature further decreases to 57 °C. It is important to note that incorporation of liquid binary organic plasticizer contribute to amorphicity within the PEO polymeric chain and therefore lesser melting temperature is observable for the flexible polymeric electrolyte membranes. The melting points and the percentage crystallinity of the electrolyte compositions obtained from the DSC curves are motioned

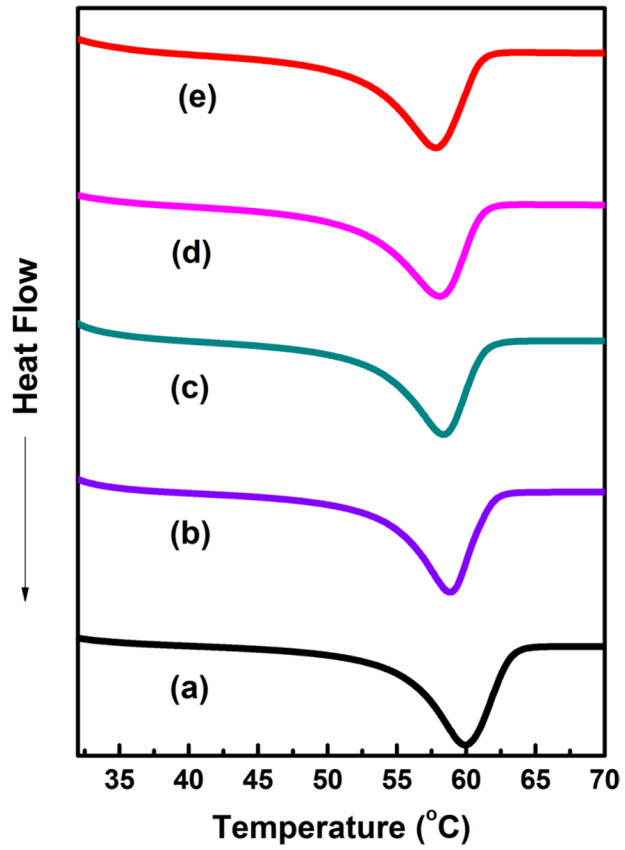

Fig. 6 Differential scanning calorimetry curves (a) pure PEO, (b) S-1, (c) S-2, (d) S-3 and (e) S-4

Table 2 The melting temperature (T_m) and degree of crystallinity (X_c) for various electrolyte membranes with their codes and composition

Sample code	Electrolyte composition	T_m(°C)	X_c(%)
S-1	$MgTf_2$/PEO	60.7	39.2
S-2	$MgTf_2$/PEO/PC-DEC (5 wt%)	59.1	29.4
S-3	$MgTf_2$/PEO/PC-DEC (10 wt%)	58.3	28.7
S-4	$MgTf_2$/PEO/PC-DEC (15 wt%)	57.1	16.2

in Table 2, which clearly indicates a continuous decrease in both the parameters on increasing PC-DEC concentration in $MgTf_2$/PEO solid polymer electrolyte system. Further, it is revealed that the optimized plasticized polymer electrolyte membrane,$MgTf_2$/PEO/PC-DEC (15 wt%),maintains its phase and remains thermally stable up to 57 °C.

3.2 Nyquist plot and ionic conductivity

Electrolyte is very important to maintain facile ionic interface between the electrodes and electrolyte. The plotting of ac data in terms of impedance is extremely important to investigate different electrochemical and ion conduction processes within the polymer electrolyte membranes. In order to understand ion conduction behavior, Nyquist plot and ionic conductivity data have been utilized. From Z'versus Z'' plots (i.e., Nyquist plot), we observe two arcs: first arc is related to the bulk resistance and the second one is due to electrochemical phenomenon at electrode/electrolyte interface [40]. The difference between Z' at high-- and low-frequency end of the first semicircular portion gives the bulk resistance of polymer electrolyte membranes. The highest bulk resistance of 1720 Ω is observed for $MgTf_2$/PEO solid polymer electrolyte (Fig. 7a). However, on enhancing the PC-DEC concentration up to 15 wt%, a systematic decrease in bulk resistance is observed for plasticized polymer electrolyte membranes.

From the literature, we know R_b is inversely proportional to ionic conductivity of electrolyte and is given by the following Eq. (1)

$$\sigma = \frac{t}{R_b \cdot A} \tag{1}$$

where σ is ionic conductivity of the electrolyte, t is the thickness of the electrolyte specimen, R_b is bulk electrolyte resistance, and A is area of cross-section of the electrolyte specimen. The calculated values of ionic conductivity are plotted in Fig. 7b. As can be seen, a continuous enhancement in the ionic conductivity is observed on increasing the concentration of PC-DEC plasticizer. This is associated with the increased mobility of the ions present in the $MgTf_2$/PEO matrix supported well with the amorphicity present in the system, as observed in the XRD, SEM, and DSC

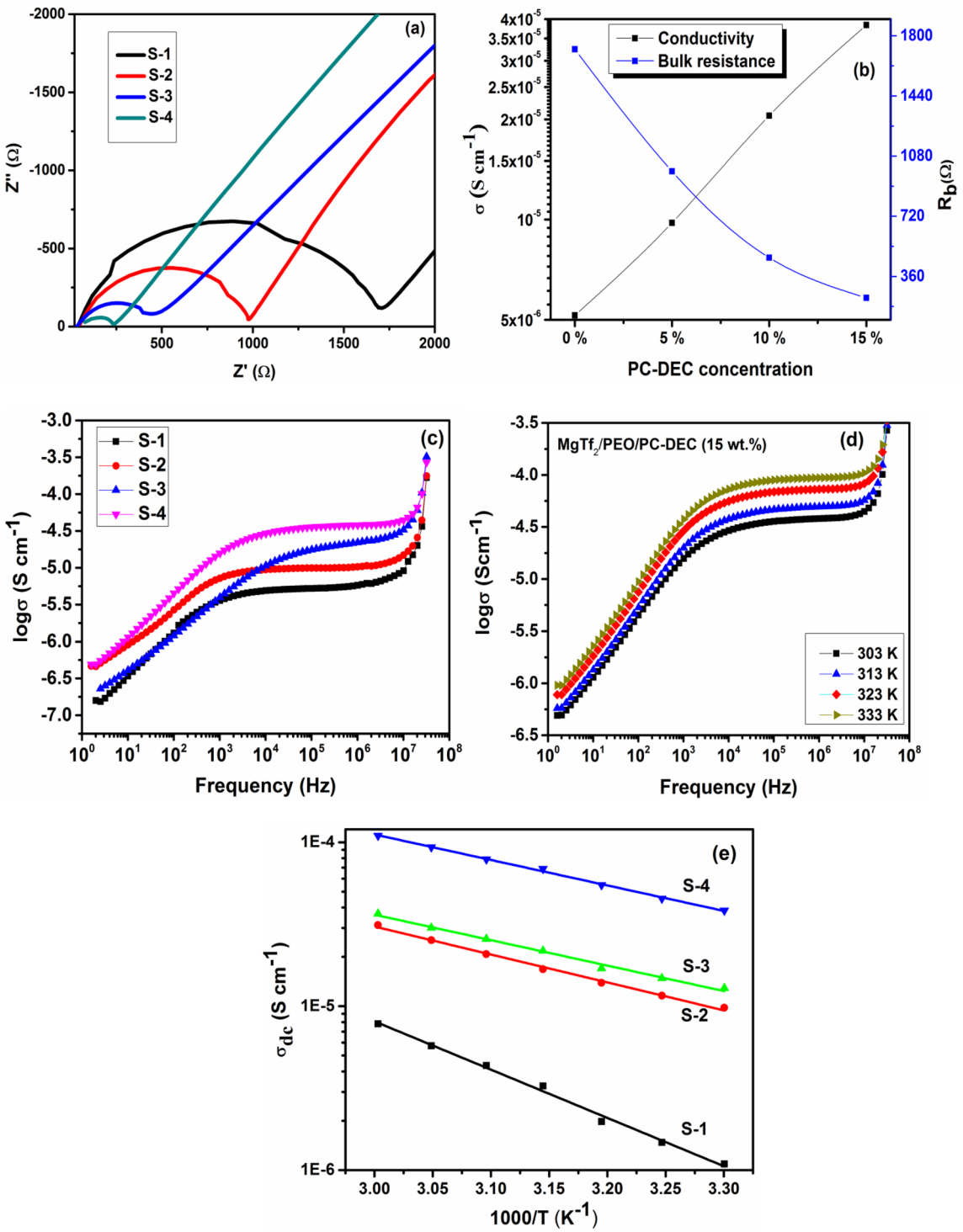

Fig. 7 **a** Complex impedance diagram obtained at 303 K for S-1, S-2, S-3, and S-4, **b** Ionic conductivity and bulk resistance as a function of PC-DEC concentration at 303 K, **c** frequency--dependent conductivity spectra for S-1, S-2, S-3 and S-4, **d** frequency-dependent conductivity spectra at different temperatures for optimized S-4 membrane, and **e** DC conductivity versus temperature plots for S-1, S-2, S-3, and S-4

studies. Hence, we observe maximum ionic conductivity of 3×10^{-5} s cm^{-1} at room temperature for S-4 composition, i.e., $MgTf_2$/PEO/PC-DEC (15 wt%).

The variation of conductivity as a function of frequency for $MgTf_2$/PEO solid polymer electrolyte and $MgTf_2$/PEO/PC-DEC (5 to 15 wt%) plasticized polymer electrolyte membrane at room temperature is shown in Fig. 7c. For all polymeric electrolyte specimens, three different frequency regions, i.e., low-frequency dispersion, plateau-frequency region, and high-frequency dispersion region are observed [41, 42]. The frequency--dependent conductivity feature is typically observed for ion-conducting material having frequency-dependent ion-transport. For mid-frequency region, if plateau is extrapolated, then we obtain ionic conductivity values and these values are quite close with the ionic conductivity values as shown in Fig. 7b. For $MgTf_2$/PEO solid polymer electrolyte and plasticized polymer electrolyte compositions with different amount of PC-DEC content, a dispersion in conductivity is observed at low frequency due to polarization effects at electrode/electrolyte interface. However, observed plateau in mid-frequency region corresponds to dc conductivity (σ_{dc}) of polymeric electrolyte specimen. At high-frequency region, a sharp rise in conductivity is due to the fast displacement of anion/cations under the effect of alternating field. In order to understand ion conduction behavior in more detail, we plot the ionic conductivity as a function of temperature as shown in Fig. 7d and e. For the solid polymer electrolyte (i.e., $MgTf_2$/PEO) and plasticized polymer electrolyte membranes with PC-DEC concentration of 5, 10, and 15 wt%, we observe straight line feature, which corresponds to Arrhenius-type behavior of ions within the electrolyte system. An Arrhenius equation [28, 29] is described by the following expression:

$$\sigma = \sigma_0 \exp\left(-\frac{E_a}{kT}\right) \tag{2}$$

where σ_0 is pre-exponential factor, E_a is the activation energy, k is the Boltzmann constant, and T is temperature in K. This typical Arrhenius ion-transport behavior resembles that of ionic crystal where ion jumps into nearby vacant sites contributing to enhancement in ionic conductivity. The increase in conductivity with temperature is due to possible decreases in PEO viscosity and enhanced flexibility. The activation energy for each electrolyte composition has been calculated using Arrhenius equation and is shown in Table 3. The lowest action energy ~ 0.141 eV has been observed for optimized high conducting electrolyte specimen. Similar io conduction behavior has been reported by many researchers [41–44]. In the temperature range from 303 to 333 K, there is no sign of any irregularity in σ versus 1000/T profile, which indicates no phase change and melting of plasticized polymer electrolyte system.

Table 3 The activation energy as calculated from Arrhenius equation for various electrolytes

Sample code	Electrolyte composition	Activation Energy (eV)
S-1	$MgTf_2$/PEO	1.419
S-2	$MgTf_2$/PEO/PC-DEC (5 wt%)	0.340
S-3	$MgTf_2$/PEO/PC-DEC (10 wt%)	0.310
S-4	$MgTf_2$/PEO/PC-DEC (15 wt%)	0.141

3.3 Dielectric and modulus studies

Dielectric investigations help to understand the conductivity behavior and polarization effects occurring at electrode/electrolyte interface. In general, the complex dielectric permittivity can be written as $\varepsilon^* = \varepsilon' + j\varepsilon''$where ε' and ε'' are dielectric constant (real part of permittivity) and dielectric loss (imaginary part of permittivity) respectively [45–47]. The complex permittivity (ε*) or dielectric constant of a system is defined by:

$$\varepsilon^* = \varepsilon' - j\varepsilon'' = \varepsilon' - j\left(\frac{\sigma}{\omega\varepsilon_0}\right) \tag{3}$$

where ε' is real part of complex permittivity and also known as dielectric constant, ε'' is imaginary part of complex permittivity of electrolyte and also known as dielectric loss, σ is conductivity, ω is angular frequency, and ε_o is permittivity of free space. The mathematical expressions for ε' and ε'' are given by the following expressions;

$$\varepsilon' = \frac{Z''}{\omega C_0(Z'^2 + Z''^2)} \tag{4}$$

$$\varepsilon'' = \frac{Z'}{\omega C_0(Z'^2 + Z''^2)} \tag{5}$$

Figure 8a shows dielectric constant (ε') as a function of frequency as the concentration of PC-DEC varies from 0 to 15 wt% in $MgTf_2$/PEO matrix. In the low-frequency region, the dispersion of permittivity is observed on varying the PC-DEC binary organic solvent concentration in the $MgTf_2$/PEO matrix. For the plasticized polymer electrolyte S-4 carrying optimum concentration (15 wt%) of PC-DEC plasticizer, the dielectric constant is observed to be highest. This high value of dielectric constant contributes in freeing up the ionic charge species within the electrolyte system. As the frequency increases, the values

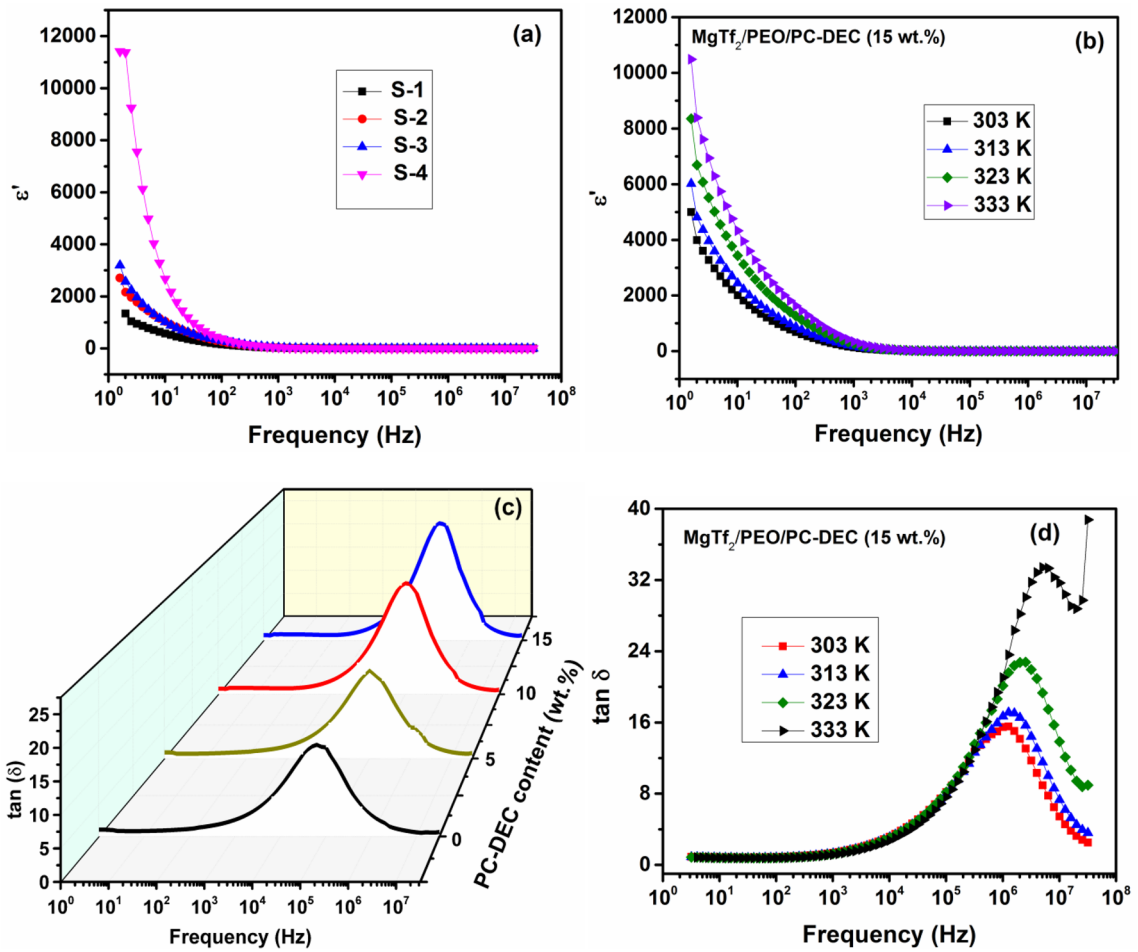

Fig. 8 **a** Frequency-dependent real part of dielectric constant (ε') for S-1, S-2, S-3, and S-4 at room temperature, **b** variation of ε' as a function of frequency for optimized composition S-4 at different temperatures, **c** variation of frequency-dependent dielectric loss for S-1, S-2, S-3 and S-4 at room temperature, and **d** variation of dielectric loss as a function of frequency at different temperatures for optimized composition S-4

of dielectric constant decreases for all polymeric electrolyte specimens due to the electrical relaxation process; however, the electrode polarization impacts cannot be ruled out as the materials are ionic conductors. The strong low-frequency dispersion and high dielectric constant is due to the fact that the presence of plasticizers in increasing amount results in more localization of ionic species within the polymeric electrolyte system. Figure 8b indicates the variation of dielectric constant as the frequency increases for optimized polymer electrolyte $MgTf_2$/PEO/PC-DEC (15 wt%) at different temperatures. The value of the dielectric constant increases as the temperature rises which indicates more ion-dissolving ability of electrolyte as its backbone becomes more flexible. The high value of dielectric constant suggests the presence of different polarization at low-frequency region. However, as the frequency increases, the inability of electric dipole to orient themselves complies with applied a.c. electrical field. Figure 8c indicates variation of loss tangent as the frequency increases for $MgTf_2$/PEO matrix with different dilution of PC-DEC from 0 to 15 wt%. The plots indicate presence of a peak around 10^5 Hz for all polymeric electrolyte compositions. The peak tends to shift towards lower-frequency end as the dilution of PC-DEC binary organic solvent increases from 0 to 15 wt% in $MgTf_2$/PEO matrix. On addition of PC-DEC plasticizers, the polymer backbone becomes flexible and capable of orienting themselves relatively easy and rapidly, thus contributing to shift in relaxation frequency. The ratio of dielectric loss (ε'') and dielectric constant (ε') is called tangent loss and is given by

$$\tan\delta = \frac{\varepsilon''}{\varepsilon'} = \frac{Z'}{Z''} \tag{6}$$

where ω is angular frequency, C_o is capacitance in vacuum, and Z' and Z'' represent the real and imaginary parts of impedance for electrolyte system. Figure 8d shows tangent loss (tan δ) plots with frequency for optimized polymer electrolyte membrane $MgTf_2$/PEO/PC-DEC (15 wt%) as the temperature varies from 303 to 333 K. As the temperature increases, the tangent loss increases and relaxation peak shifts towards higher-frequency side as more number of charge carriers become available for the ionic conduction.

Electrical modulus formulation is very important tool to understand the dispersion behavior of conductivity in specified frequency domain. This tool is widely utilized to study conductivity relaxation behavior of polymer electrolyte membranes. Modulus representation mainly reflects the bulk electrical properties of polymer electrolyte membranes with suppressed electrode polarization effects [48–50]. Mathematically, electric modulus is given by the relation

$$M^* = M' + M'' \tag{7}$$

$$M^* = \left(1/(\varepsilon')\right) = j\omega C0Z^* = M' + jM'' \tag{8}$$

where the angular frequency $\omega = 2\pi f$ and C_o is the vacuum capacitance of the electrochemical cell, and M' and M'' denote the real and imaginary parts of the modulus M^*, respectively.

Figure 9 shows the imaginary part of the modulus for $MgTf_2$/PEO solid polymer electrolyte and $MgTf_2$/PEO/PC-DEC (5 wt% to 15 wt%) plasticized polymer electrolyte membranes. The peak observed in Fig. 9 is related with the translational ion dynamics and mirrors the conductivity

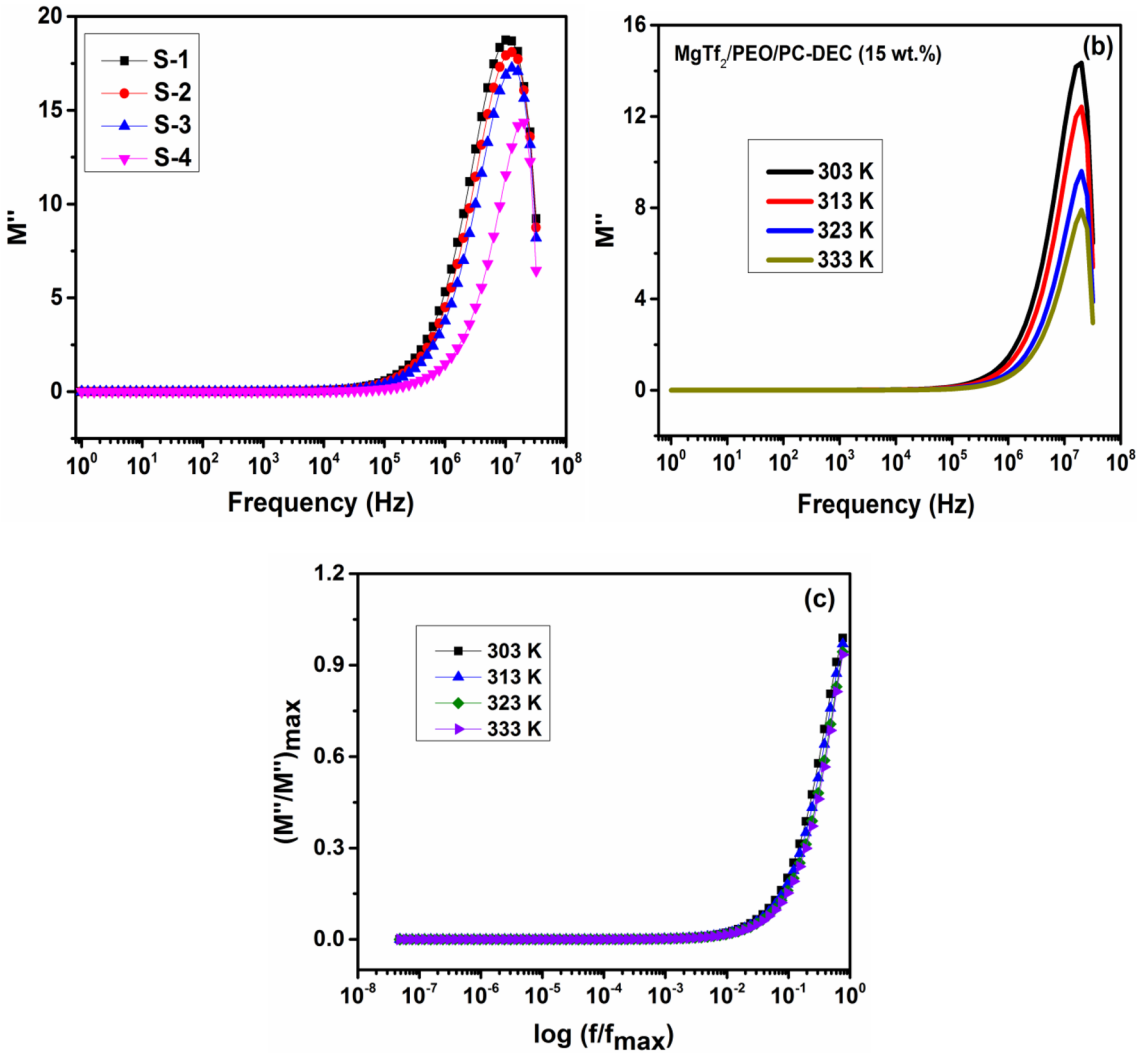

Fig. 9 **a** Variation of imaginary part of electric modulus (M'') with frequency for S-1, S-2, S-3, and S-4, **b** frequency-dependent imaginary part of modulus M'' at various temperatures for optimized composition S-4, and **c** normalized spectra of the imaginary part of modulus using normalized variables M''/M''_{max} and log (f/f_{max}) at various temperatures

relaxation of mobile ions. A prominent peak is observed for the solid polymer electrolyte and optimized polymer electrolyte membranes, which indicate the electrolytes are ionic conductors. As the concentration of binary organic solvents (PC-DEC) is gradually increased from 0 to 15 wt%, the peak maxima of modulus shift towards higher-frequency side. The inconsistency in peak height indicates variation in dielectric constant and conductivity for various concentration of PC-DEC within $MgTf_2$/PEO matrix. The imaginary part of the modulus is also plotted as a function of frequency for the optimized polymer electrolyte membrane S-4, i.e., $MgTf_2$/PEO/PC-DEC (15 wt%) at various temperatures (Fig. 9b). It is observed that the peak maximum of modulus shifts towards higher-frequency side as the temperature increases, this is due to enhanced ionic motion within polymer electrolyte specimen. The scaling of modulus spectra was performed to understand ion dynamics processes at varying temperature for $MgTf_2$/PEO/PC-DEC (15 wt%) as optimized polymer electrolyte specimen. Figure 9c shows normalized spectra of the imaginary part of modulus using normalized variables M''/M''_{max} and log (f/f_{max}) at various temperature for S-4. The approximate overlap of the modulus curve for all temperature indicates the similar dynamical processes occurring at different frequencies and its independence on temperature.

3.4 Cyclic voltammetry and ion-transport studies

In order to calculate the working voltage range, i.e., electrochemical stability window, of the optimized polymer electrolyte composition S-4, cyclic voltammetry (CV) has been performed on symmetrical cell, SS|S-4|SS at scan rate of 5 mV s^{-1} (Fig. 10a). In the cyclic voltammogram, no anodic and cathodic peak is observed from −2.2 to 1.4 V, which suggests a working voltage range of 3.6 V for the optimized S-4 electrolyte membrane. The current values are insignificant in stability region which further suggests the absence of undesirable water contamination and associated reactions in optimized polymer electrolyte membrane. In order to confirm the ion movement (i.e., platting|stripping) of Mg^{2+} ions, cyclic voltammetry study is performed on Mg|S-4|Mg symmetrical cell (Fig. 10b). The occurrence of anodic and cathodic peaks in cyclic voltammogram indicates that platting and stripping of Mg^{2+} ions are prevalent at Mg|electrolyte interface. Many researchers have reported similar ion-conducting behavior using polymer electrolyte membranes and reversible electrode system [51, 52].

In order to confirm the electrochemical stability window of the optimized composition S-4, the membrane is subjected to linear sweep voltammetry (LSV) using SS as working electrode and Mg electrode as combined counter and reference electrode at scan rate of 5 mV s^{-1}. The LSV plot shown in Fig. 10c suggests the electrochemical stability window of ~3.5 V, which is significant for electrochemical applications with maximum voltage of ≤3.5 V. This value of stability window as calculated by linear sweep voltammetry for cell configuration SS|S-4|Mg is almost same as observed in CV study. Therefore, the optimized flexible polymer electrolyte membrane promises sufficiently good electrochemical stability for application in flexible electrochemical devices especially in magnesium batteries.

In order to calculate the total ion-transport number within the optimized polymer electrolyte membrane, dc polarization technique was adopted for the following cell configuration SS|S-4|SS (denoted as cell A) (Fig. 10d). The current density versus time (i.e., the polarization curve) indicates sudden fall in current density which become close to zero value indicating the optimized polymer electrolyte is principally ionic in nature [39, 53]. The total ion-transport number (t_{ion}) can be given by the following formula:

$$t_{ion} = \left(1 - \frac{t_s}{t_T}\right) \ldots\ldots\ldots\ldots (9) \tag{9}$$

where i_T and i_s are total and residual current, respectively. The t_{ion}value is obtained as ~0.99, suggesting the purely ionic nature of the optimized polymer electrolyte system.

In order to estimate the percentage contribution of magnesium ions towards ionic motion within the optimized polymer electrolyte, combined ac and dc technique as suggested by Vincent method is utilized [54, 55]. As a part of the method, the symmetrical cell Mg|S-4|Mg was undergone dc polarization and impedance spectroscopy before and after the polarization. The dc polarization curve for the cell Mg|S-4|Mg is shown in Fig. 10d. The cell delivers an initial current (I_o) of ~13 µA and get saturated at current (I_s) of ~5 µA. The Nyquist plots, obtained from the impedance measurements on the cell Mg|S-4|Mg before and after dc polarization, are given in Fig. 10e. The values of the impedance of the cell before (R_o) and after (R_s) the polarization are obtained as ~600 Ω and ~1118 Ω , respectively. The magnesium-ion-transport number ($t_{mg}{}^{2+}$) can be given by the following formula

$$t_{Mg}^{2+} = \frac{I_s}{I_o} \cdot \left(\frac{\Delta V - R_o I_o}{\Delta V - R_s I_s}\right) \tag{10}$$

where t_{Mg}^{2+} is magnesium transport number within the flexible polymer electrolyte membrane, I_s is saturation current, I_o is the initial current, ΔV is applied small dc voltage, R_0 is impedance before polarization and R_s is impedance after polarization. Using Eq. 10, the magnesium-ion-transport number is determined to be 0.32. This value of Mg^{2+} transport number in this flexible polymer electrolyte membrane suggests significant contribution of other anionic species in the electrolyte system [56, 57].

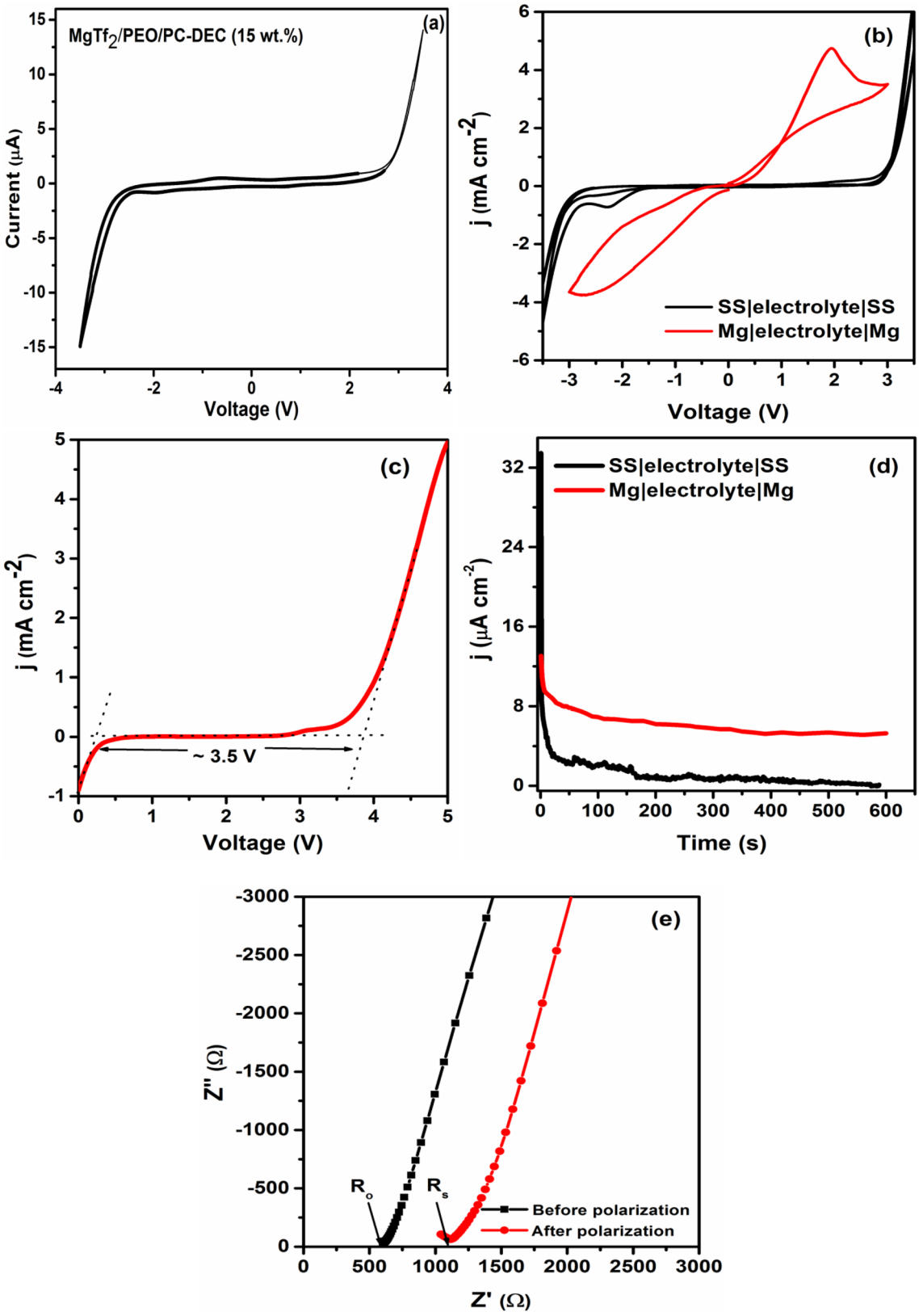

Fig. 10 Cyclic voltammogram and ion-transport studies using optimized flexible polymer electrolyte membrane $MgTf_2$/PEO/PC-DEC (15 wt%), **a** electrochemical stability window, **b** cyclic voltammetry, **c** Linear sweep voltammetry, **d** polarization curves for SS|electrolyte|SS and Mg|electrolyte|Mg cells, **e** Impedance plots before and after polarization

4 Conclusions

In this paper, we report flexible magnesium-ion-conducting solid and plasticized polymer electrolyte membranes. The electrolyte membranes do not exhibit any degradation after rolling and stretching it for hundred times. The optimized flexible electrolyte has Young's modulus of 100 N mm^{-2} and mechanical strength of 2 Kgf and could withstand stress of 6 N mm^{-2} and strain of 7 N mm^{-2} at a maximum load of 10 Kgf without any rupture. The XRD curve confirms the increase in amorphous nature and SEM graphs shows formation of large sized spherulites with the addition of PC-DEC in increasing amounts within the $MgTf_2$/PEO matrix. AFM micrographs of $MgTf_2$/PEO/PC-DEC (15 wt%) electrolyte shows smooth morphology with lowest roughness height and its DSC profile shows this polymer electrolyte membrane maintains its phase and remains thermally stable up to 57 °C. Nyquist plots and conductivity measurement suggest that ion conduction behavior follows Arrhenius pattern and Mg^{2+} conduction becomes favorable with the optimum concentration of PC-DEC binary organic solvent in $MgTf_2$/PEO matrix. The strong low-frequency dispersion and high dielectric constant is observed for electrolytes with increasing amount of plasticizers in $MgTf_2$/PEO matrix due to more localization of ionic species within the polymer electrolyte membrane system. The value of the dielectric constant is found to increase with temperature rise as the backbone become more flexible and ion-dissolving character increases. The modulus curves of optimized electrolyte specimen $MgTf_2$/PEO/PC-DEC (15 wt%) at various temperature shows shift in peak maximum towards higher-frequency side as the temperature increases, this is due to enhanced ionic motion within electrolyte specimen. Electrolyte with optimized concentration of 15 wt% PC-DEC exhibits electrochemical stability window of ~3.5 V, room temperature Mg^{2+} conductivity of 3×10^{-5} s cm^{-1}, and cation-transport number of 0.32. The reported Mg-ion-conducting plasticized polymer electrolyte can be employed in fabricating flexible electrochemical devices especially the magnesium batteries.

Acknowledgements Deepak Kumar thanks and acknowledges "The M.S.University of Baroda" Vadodara, Gujarat, India. The encouragement and support received from Electronics and Mechanical Engineering School (Affiliated to Gujarat Technological University), Government of India, are gratefully acknowledged. Kuldeep Mishra acknowledges the funding (File No YSS/2015/001234) from Science and Engineering Research Board (SERB) New Delhi, India.

Compliance with ethical standards

Conflict of interest The authors report no conflicting interest in any capacity, competing, or financial.

References

1. T. Kim, W. Song, D.-Y. Son, L.K. Ono, Y. Qi, Lithium-ion batteries: outlook on present, future, and hybridized technologies. J. Mater. Chem. A **7**, 2942–2964 (2019)
2. V.H. Pham, J.A. Boscoboinik, D.J. Stacchiola, E.G. Self, P. Manikandan, S. Nagarajan, Y. Wanf, V.G. Pol, J. Nanda, E. Paek, D. Mitlin, Selenium-sulfur (SeS) fast charging cathode for sodium and lithium metal batteries. Energy Storage Mater. **20**, 71–79 (2019)
3. H. Zhang, D. Cao, X. Bai, High rate performance of aqueous magnesium-ion batteries based on the δ-MnO_2@carbon molecular sieves composite as the cathode and nanowire VO_2 as the anode. J. Power Sources **444**, 227299 (2019)
4. R. Deivanayagam, B.J. Ingram, R.S. Yassar, Progress in development of electrolytes for magnesium batteries. Energy Storage Mater. **21**, 136–153 (2019)
5. D. Kumar, S.K. Rajouria, S.B. Kuhar, D.K. Kanchan, Progress and prospects of sodium-sulfur batteries: a review. Solid State Ionics **312**, 8–16 (2017)
6. J. Liu, Y.-G. Xu, L.-B. Kong, Cleverly embedded CoS_2/NiS_2 on two-dimensional graphene nanosheets as high-performance anode material for improved sodium ion batteries and sodium ion capacitors. J. Mater. Sci. **31**, 9946–9959 (2020)
7. H. Li, L. Ma, C. Han, Z. Wang, Z. Liu, Z. Tang, C. Zhi, Advanced rechargeable zinc-based batteries: Recent progress and future perspectives. Nano Energy **62**, 550–587 (2019)
8. Sellam, S.A. Hashmi, Enhanced zinc ion transport in gel polymer electrolyte: effect of nano-sized ZnO dispersion. J. Solid State Electrochem. **16**, 3105–3114 (2012)
9. M. Ravi, S. Bhavani, K.K. Kumar, V.V.R.N. Rao, Investigations on electrical properties of PVP:KIO_4 polymer electrolyte films. Solid State Sci. **19**, 85–93 (2013)
10. Z.A. Zafar, S. Imtiaz, R. Li, J. Zhang, R. Razaq, Y. Xin, Q. Li, Z. Zhang, Y. Huang, A super-long life rechargeable aluminum battery. Solid State Ionics **320**, 70–75 (2018)
11. S. Xia, X. Wu, Z. Zhang, Y. Cui, W. Liu, Practical challenges and future perspectives of all-solid-state lithium-metal batteries. Chemistry **5**, 753–785 (2019)
12. M.Y. Ghotbi, Solid state electrolytes for electrochemical energy devices. J. Mater. Sci. **30**, 13835–13854 (2019)
13. A. Varzi, R. Raccichini, S. Passerini, B. Scrosati, Challenges and prospects of the role of solid electrolytes in the revitalization of lithium metal batteries. J. Mater. Chem. A **4**, 17251–17259 (2016)
14. P.B. Balbuena, Electrolyte Materials – Issues and Challenges, in *AIP Conf. Proc.*, vol. 1597 (2014), pp. 82–97
15. C.-W. Park, J.-H. Ahn, H.-S. Ryu, K.-W. Kim, H.-J. Ahn, Room-temperature solid-state sodium/sulfur battery. Electrochem. Solid-State Lett. **9**(3), A123–A125 (2006)
16. J.-S. Kim, H.-J. Ahn, I.-P. Kim, K.-W. Kim, J.-H. Ahn, C.-W. Park, H.-S. Ryu, The short-term cycling properties of Na/PVdF/S battery at ambient temperature. J. Solid State Electrochem. **12**, 861–865 (2008)
17. S.M.M. Razalli, S.I.Y.S.M. Saaid, T.I.I. Kudin, M.Z.A. Yahya, O.H. Hassan, A.M.M. Ali, Electrochemical properties of glyme based plasticizer on gel polymer electrolytes doped with lithium bis(trifluoromethanesulfonyl) imide. Mater. Res. Forum **846**, 534–538 (2015)
18. I. Bauer, M. Kohl, H. Althues, S. Kaskel, Shuttle suppression in room temperature sodium sulfur batteries using ion selective polymer membranes. Chem. Commun. **50**, 3208–3210 (2014)
19. H. Zhang, T. Diemant, B. Qin, H. Li, R.J. Behm, S. Passerini, Solvent-dictated sodium sulfur redox reactions: investigation of carbonate and ether electrolytes. Energies **13**, 836 (2020)

20. M.J.S. Syali, D. Kumar, K. Mishra, D.K. Kanchan, Recent advances in electrolytes for room-temperature sodium-sulfur batteries: a review. Energy Storage Mater. **31**, 352–372 (2020)
21. H. Wang, M. Matsui, Y. Takeda, O. Yamamoto, D. Im, D. Lee, N. Imanishi, Interface properties between lithium metal and a composite polymer electrolyte of $PEO_{18}Li(CF_3SO_2)_2N$-tetraethylene glycol dimethyl ether. Membranes **3**, 298–310 (2013)
22. S. Komaba, T. Ishikawa, N. Yabuuchi, W. Murata, A. Ito, Y. Ohsawa, Fluorinated ethylene carbonate as electrolyte additive for rechargeable Na batteries. ACS Appl. Mater. Interfaces **3**(11), 4165–4168 (2011)
23. R. Arunkumar, R.S. Babu, M.U. Rani, S. Rajendran, Influence of plasticizer on ionic conductivity of PVC-PBMA polymer electrolytes. Ionics **23**, 3097–3109 (2017)
24. Z. Huang, Q. Pan, D.M. Smith, C.Y. Li, Plasticized Hybrid Network Solid Polymer Electrolytes for Lithium-Metal Batteries. Adv. Mater. Interfaces **6**(2), 1801445 (2019)
25. J.Y. Song, Y.Y. Wang, C.C. Wan, Conductivity study of porous plasticized polymer electrolytes based on poly(vinylidene fluoride) a comparison with polypropylene separators. J. Electrochem. Soc. **147**(9), 3219 (2000)
26. M. Stich, M. Göttlinger, M. Kurniawan, U. Schmidt, A. Bund, Hydrolysis of LiPF6 in carbonate-based electrolytes for lithium-ion batteries and in aqueous media. J. Phys. Chem. C **122**(16), 8836–8842 (2018)
27. O.V. Yarmolenkoz, Y.V. Baskakova, G.Z. Tulibaeva, L.M. Bogdanova, E.A. Dzhavadyan, B.A. Komarov, N.F. Surkov, B.A. Rozenberg, O.N. Efimov, Effect of solvents on properties of polymer gel-electrolyte based on polyester diacrylate. Russ. J. Electrochem. **45**(1), 101–107 (2009)
28. D. Kumar, S.A. Hashmi, Ion transport and ion–filler-polymer interaction in poly(methyl methacrylate)-based, sodium ion conducting, gel polymer electrolytes dispersed with silica nanoparticles. J. Power Sources **195**, 5101–5108 (2010)
29. A.M. Stephan, Review on gel polymer electrolytes for lithium batteries. Eur. Polym. J. **42**, 21–42 (2006)
30. C. Maheshwaran, K. Mishra, D.K. Kanchan, D. Kumar, Mg^{2+} conducting polymer gel electrolytes: physical and electrochemical investigations. Ionics **26**, 2969–2980 (2020)
31. Z. Ma, D.R. MacFarlane, M. Kar, Mg cathode materials and electrolytes for rechargeable Mg batteries: a review. Batter. Supercaps **2**(2), 115–127 (2019)
32. J. Muldoon, C.B. Bucur, A.G. Oliver, T. Sugimoto, M. Matsui, H.S. Kim, G.D. Allred, J. Zajicek, Y. Kotanie, Electrolyte roadblocks to a magnesium rechargeable battery. Energy Environ. Sci. **5**, 5941–5950 (2012)
33. R.C. Agrawal, D.K. Sahu, Y.K. Mahipal, R. Ashrafi, Investigations on ion transport properties of hot-press cast magnesium ion conducting nano-composite polymer electrolyte (NCPE) films: effect of filler particle dispersal on room temperature conductivity. Mater. Chem. Phys. **139**, 410–415 (2013)
34. G.G. Kumar, N. Munichandraiah, Effect of plasticizers on magnesium-poly(ethyleneoxide) polymer electrolyte. J. Electroanal. Chem. **495**, 42–50 (2000)
35. G.G. Kumar, N. Munichandraiah, Solid-state Mg/MnO_2 cell employing a gel polymer electrolyte of magnesium triflate. J. Power Sources **91**, 157–160 (2000)
36. G.G. Kumar, N. Munichandraiah, Poly(methylmethacrylate)-magnesium triflate gel polymer electrolyte for solid state magnesium battery application. Electrochim. Acta **47**, 1013–1022 (2002)
37. J. Sharma, S.A. Hashmi, Plastic crystal-incorporated magnesium ion conducting gel polymer electrolyte for battery application. Bull. Mater. Sci. **41**, 147 (2018)
38. S. Das, A. Ghosh, Effect of plasticizers on ionic conductivity and dielectric relaxation of PEO-$LiClO_4$ polymer electrolyte. Electrochim. Acta **171**, 59–65 (2015)
39. S.A. Hashmi, S.Chandra, Experimental investigations on a sodium-ion-conducting polymer electrolyte based on poly(ethylene oxide) complexed with $NaPF_6$. Mater. Sci. Eng. B **34**(1), 18–26 (1995)
40. J.R. Macdonald, Impedance spectroscopy: models, data fitting, and analysis. Solid State Ionics **176**, 1961–1969 (2005)
41. S.B. Aziz, O.G. Abdullah, S.R. Saeed, H.M. Ahmed, Electrical and dielectric properties of copper ion conducting solid polymer electrolytes based on chitosan: CBH model for ion transport mechanism. Int. J. Electrochem. Sci. **13**, 3812–3826 (2018)
42. K.P. Padmasree, D.K. Kanchan, A.R. Kulkarni, Impedance and modulus studies of the solid electrolyte system $20CdI_2–80[xAg_2O–y(0.7V_2O_5–0.3B_2O_3)]$, where $1 \leq x/y \leq 3$. Solid State Ion. **177**, 475–482 (2006)
43. N. Binesh, S.V. Bhat, VTF to arrhenius crossover in temperature dependence of conductivity in $(PEG)_xNH_4ClO_4$ polymer electrolyte. Polym. Phys. **36**(7), 1201–1209 (1998)
44. M. Petrowsky, R. Frech, Temperature dependence of ion transport: the compensated arrhenius equation. J. Phys. Chem. B **113**(17), 5996–6000 (2009)
45. K. Gohel, D.K. Kanchan, Effect of PC:DEC plasticizers on structural and electrical properties of PVDF–HFP:PMMA based gel polymer electrolyte system. J. Mater. Sci. **30**, 12260–12268 (2019)
46. H.J. Woo, S.R. Majid, A.K. Arof, Dielectric properties and morphology of polymer electrolyte based on poly(ε-caprolactone) and ammonium thiocyanate. Mater. Chem. Phys. **134**, 755–761 (2012)
47. S. Ponmani, M.R. Prabhu, Development and study of solid polymer electrolytes based on PVdF-HFP/PVAc: Mg $(ClO_4)_2$ for Mg ion batteries. J. Mater. Sci. **29**, 15086–15096 (2018)
48. C.H. Chan, H.-W. Kammer, Characterization of polymer electrolytes by dielectric response using electrochemical impedance spectroscopy. Pure Appl. Chem. **90**(6), 939–953 (2018)
49. S. Ramesh, S.-C. Lu, E. Morris, Towards magnesium ion conducting poly(vinylidenefluoride-hexafluoropropylene)-based solid polymer electrolytes with great prospects: Ionic conductivity and dielectric behaviours. J. Taiwan Inst. Chem. Eng. **43**, 806–812 (2012)
50. P. Sharma, D.K. Kanchan, N.Gondaliya,M. Pant, M.S. Jayswal, Conductivity relaxation in Ag^+ ion conducting PEO-PMMA-PEG polymer blends. Ionics **19**, 301–307 (2013)
51. D. Kumar, D.K. Kanchan, Dielectric and electrochemical studies on carbonate free Na-ion conducting electrolytes for sodium-sulfur batteries. J. Energy Storage **22**, 44–49 (2019)
52. G.P. Pandey, R.C. Agarwal, S.A. Hashmi, Magnesium ion-conducting gel polymer electrolytes dispersed with fumed silica for rechargeable magnesium battery application. J. Solid State Electrochem. **15**, 2253–2264 (2011)
53. Z. Osman, M.I.M. Ghazali, L. Othman, K.B.M. Isa, AC ionic conductivity and DC polarization method of lithium ion transport in PMMA-LiBF4 gel polymer electrolytes. Results Phys. **2**, 1–4 (2012)
54. P.G. Bruce, C.A. Vincent, Steady state current flow in solid binary electrolyte cells. J. Electroanal. Chem. **225**, 1–17 (1987)
55. P.G. Bruce, J. Evans, C.A. Vincent, Conductivity and transference number measurements on polymer electrolytes. Solid State Ion. **28–30**, 918–922 (1988)
56. J. Evans, C.A. Vincent, P.G. Bruce, Electrochemical measurement of transference numbers in polymer electrolytes. Polymer **28**, 2324–2328 (1987)
57. D. Kumar, Effect of organic solvent addition on electrochemical properties of ionic liquid based Na^+ conducting gel electrolytes. Solid State Ion. **318**, 65–70 (2018)

Nano-Structures & Nano-Objects 24 (2020) 100587

Contents lists available at ScienceDirect

Nano-Structures & Nano-Objects

journal homepage: www.elsevier.com/locate/nanoso

Effect of active MgO nano-particles dispersion in small amount within magnesium-ion conducting polymer electrolyte matrix

C. Maheshwaran [a], D.K. Kanchan [a], Kuldeep Mishra [b], Deepak Kumar [c,*], Khushbu Gohel [a]

[a] Department of Physics, M.S. University of Baroda, Vadodara, Gujarat 390002, India
[b] Department of Physics, Jaypee University, Anoopshahr, Uttar Pradesh 203390, India
[c] Electronics and Mechanical Engineering School (Affiliated to Gujarat Technological University), Vadodara, Gujarat 390008, India

ARTICLE INFO

Article history:
Received 7 July 2020
Received in revised form 27 August 2020
Accepted 20 September 2020

Keywords:
MgO nano-particles
Nano-composite polymer electrolyte membrane
Ionic conductivity
Electrochemical impedance spectroscopy
Dielectric and modulus analysis
Mechanical stability

ABSTRACT

This paper reports effect of dispersing active MgO nano-particles in small amount within magnesium-ion conducting polymer electrolyte matrix. The electrolyte films are prepared by solution casting techniques and experimental techniques are employed to carry out structural, electrochemical and mechanical analysis. SEM and AFM micrographs demonstrate a variation in surface morphology and maximum roughness height with the incorporation of MgO nano-particles within the polymer electrolyte matrix. The nano-composite polymer electrolyte film with optimized concentration of 1 wt% MgO nano-particles delivered an ionic conductivity of 1.49×10^{-4} S cm^{-1} at 25 °C, though its crystallinity is higher than the pristine. In depth, ion-conduction has been probed with the help of dielectric and modulus behavior of electrolyte system as a function of MgO nano-particles concentration, frequency and temperature. The mechanical studies reveal a Young's modulus of 150 N mm^{-2}, mechanical strength of 2.7 Kgf and stress of 2.6 N mm^{-2} at a maximum load of 10 Kgf for the optimized electrolyte film. The reported electrolyte can be utilized in rechargeable Mg batteries due to its high conductivity, flexibility and mechanically stability.

1. Introduction

The research and development on polymer electrolytes and its variants is largely motivated by their possible application in various electrochemical devices including rechargeable batteries. The existing lithium-ion batteries provide high energy density and recyclability but they suffer from some safety limitations and many other problems [1–3]. Therefore, researchers are working hard to search newer environment friendly and low cost energy storage systems such as magnesium, sodium, zinc, potassium, aluminum etc. [4–14].

Magnesium is attractive cell chemistry due to its high natural abundance in the earth crust, low material cost, reasonably good electrode potential (−2.3 V verses SHE) and low reactivity in comparison to the established lithium cell chemistry [15–21]. Additionally, handling of magnesium is possible in oxygen and humid atmosphere unlike Li, which requires an inert atmosphere. Electrolyte plays a very crucial role in an electrochemical cell as it ensures required redox reactions and associated electrochemistry of cell. The existing organo-Mg complex based electrolytes offers superior electrochemical properties but they have inherent drawback such as corrosiveness and flammability. In addition, these electrolytes are compatible with Chevrel-phase cathodic materials having low discharge capacity (≈130 mAh g^{-1}) values [22–24]. Muldoon et al. has pointed out lack of a commercial high conducting, non-aqueous electrolyte having compatibility with suitable cathode materials as main roadblocks to the development of Mg rechargeable batteries [25].

The polymer based electrolytes appears promising due to their specific features such as non-leakage, flexibility, high ionic conductivity, ease of fabrication as thin films and better electrolyte–electrode interfacial contact [26–28]. The polyethylene oxide (PEO) is most studied polymer host in designing several electrolyte systems owing to its high salvation properties and potential to dissolve a high concentration of various kinds of dopant salts [16,29]. The complexes of PEO with magnesium salt i.e. solid polymer electrolyte offers moderately high ionic conductivity (10^{-5} to 10^{-4} Scm^{-1}) at ∼60 °C and the conductivity values are even lower at room temperature due to retardation of ionic transport imposed by their crystalline phases [30–33]. In order to increase the ionic conductivity, mechanical, thermal and electrochemical properties of PEO based polymer electrolytes, numerous endeavor have been made to improve the structure of PEO polymer by plasticizing them with carbonate solvents and/or by incorporating nano/micro-sized filler particles in it [34–38].

Plasticization of polymer electrolytes with low molecular weight and high dielectric constant organic solvents leads to flexible polymer backbone with enhanced ion-conduction [39–41].

* Corresponding author.
E-mail address: deepak.kumar06@gov.in (D. Kumar).

https://doi.org/10.1016/j.nanoso.2020.100587
2352-507X/

These electrolytes are known to provide liquid like ionic transport and improved electrochemical properties within polymer-salt matrix. The organic solvents such as ethylene carbonate (EC), propylene carbonate (PC), dimethyl carbonate (DMC), diethylene carbonate (DEC), fluoroethylene carbonate (FEC) and dimethyl formamide (DMF) etc. are utilized for fabricating the polymer based electrolytes [42–44]. The incorporation of nano-micro sized active or passive nano-particles in polymer based electrolyte ensures better liquid adsorption, higher ionic conduction and improved electrolyte/electrode interfacial properties [45]. The passive filler particles do not participate in ion-conduction process but supports the more retention of liquid electrolyte, higher mechanical stability and decreases the risk of leakage. On the other hand, the active nano-particles (e.g. $NaAlO_2$ is active particle for Na-ion conducting electrolyte system) take active part in the ion-conduction process and facilitate overall charge transport by enhancing the ionic conductivity, transport number and other electrochemical parameters. The small size of MgO nanoparticles lends them a high specific surface, high adsorption capacity and a high surface charge [46]. In view of this, during the last few years a great enthusiasm has arisen for the study of MgO nanostructure applications as active phase supports, heterogeneous catalysts, adsorbents and as nano-filler in polymer electrolytes [47].

The effect of dispersing magnesium oxide nanoparticles have been studied by various researchers. Ahmed et al. investigated effect of varying MgO in PEO/NaSCN matrix with the help of scanning electron microscopy, conductivity and Fourier transformed infra-red spectroscopic measurements in Na^+ conducting solid polymer electrolyte system [48]. Recently, Nidhi et al. fabricated solid polymer electrolyte by dispersing MgO in $Mg(NO_3)_2$/PVdF matrix and studied conductivity, dielectrics and thermal properties [35]. Pandey et al. performed structural, electrical and electrochemical investigations on $Mg(ClO_4)_2$/EC-PC/PVdF-HFP system dispersed with MgO nano-particles concentration up to 15 wt% [37]. Wu et al. studied conductivity, porosity, structural and voltammetric properties of nanocomposite gel polymer electrolytes consisting of $Mg(ClO_4)_2$ salt, EC-PC binary solvents, MgO nano-filler and blend of PVdF-HFP polymer with thermoplastic polyurethane (TPU) [38]. Sharma et al. studied the effect of dispersing nano-sized passive aluminum oxide (Al_2O_3) and active Mg aluminate ($MgAl_2O_4$) filler in $MgTf_2$/EC-PC/PVdF-HFP system with the help of X-ray diffraction, field emission scanning electron microscopy, electrochemical and tensile strength measurement [45]. A detailed investigation on effect of dispersing MgO nano-particles in small amounts within magnesium-ion conducting polymer electrolyte matrix is lacking. Hence, it will be interesting to investigate the effect of dispersing the MgO active nano-particles in small concentrations on structural, mechanical, dielectric and modulus properties of polymer based electrolyte consisting of PEO as polymer host, $MgTf_2$ as magnesium salt and PC-DEC as binary carbonate solvents.

In this paper, we studied the effect of dispersing MgO nanoparticles in $Mg(CF_3SO_3)_2$/PC-DEC/PEO electrolyte system. The structural properties of the electrolyte films are studied with the help of SEM, AFM and XRD techniques. The electrochemical impedance spectroscopy has been performed to understand the ion-conduction behavior in varying frequency range with the help of conductivity, dielectric and modulus response. To know the suitability of the nanocomposite films under the effect of load, the mechanical study has also been performed for different MgO nano-particles concentration. The studies suggest changes in morphological and ion-conduction behavior on utilizing MgO nano-fillers in varying amounts within the magnesium-ion conducting polymer based electrolyte films.

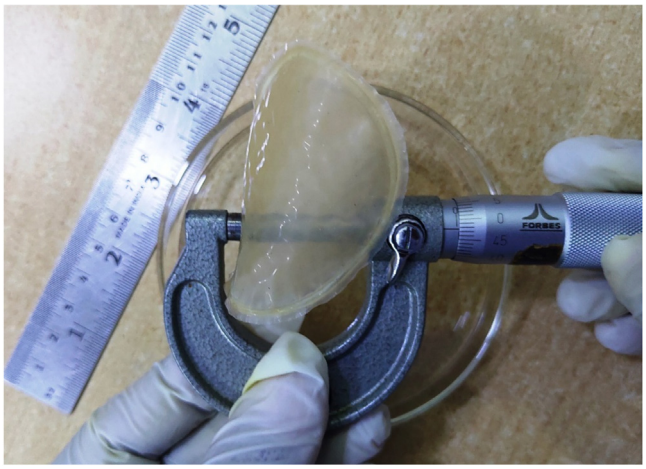

Fig. 1. A plasticized polymer electrolyte specimen $MgTf_2$/PC-DEC/PEO with 1 wt% MgO.

2. Experimental section

2.1. Material

Poly(ethylene oxide), PEO of average molecular weight ~300,000 from Alfa Aesar was utilized as polymer host, magnesium triflate i.e. $Mg(CF_3SO_3)_2$ of 97% purity from Aldrich was used as magnesium salt, propylene carbonate (purity 99.7 %) and diethyl-carbonate (purity 99 % purity) were obtained from Sigma Aldrich and employed as organic carbonate solvents. Magnesium oxide (MgO) nano-particles (purity > 99.9%) of < 50 nm average particle size and was procured from Sigma Aldrich and used after drying overnight in an oven. Acetone (purity 99 %) was purchased from Sigma Aldrich and used as received for dissolving the PEO polymer.

2.2. Preparation of flexible polymer electrolyte membranes

The standard solution cast technique was utilized to prepare nanocomposite Mg^{2+} conducting polymer based electrolyte films dispersed with magnesium oxide (MgO). The polymer host and magnesium salt (i.e. PEO and $Mg(CF_3SO_3)_2$ respectively) were separately dissolved in acetone before mixing them together. Further, optimized weight ratio of PC-DEC plasticizer was added to $Mg(CF_3SO_3)_2$/PEO matrix to obtain plasticized polymer electrolyte solution. The magnesium oxide particles in varying amounts were further dispersed in this electrolyte solution according to the compositional formula; ($MgTf_2$/PEO/PC-DEC) + x wt.% MgO, where x = 0, 0.25, 0.5, 1, 1.5, 2 wt%, and resulting mixture was stirred and ultrasonicated to obtain viscous nanocomposite electrolyte solution. This electrolyte solution containing magnesium oxide in varying concentrations was poured in Teflon petri dishes and acetone was allowed to evaporate at room temperature to obtain the desired free standing nanocomposite polymer electrolyte films. A typical nanocomposite electrolyte membrane is shown in Fig. 1.

2.3. Instrumentation

SEM images of nanocomposite polymer electrolyte films were taken from FEI Quanta 200 microscope fitted with EDAX-EDS analyzer. Atomic force microscopic measurement was performed by utilizing AFM, pico SPM-picoscan 2100, Molecular Imaging, USA. The AFM pictures were obtained in tapping mode with

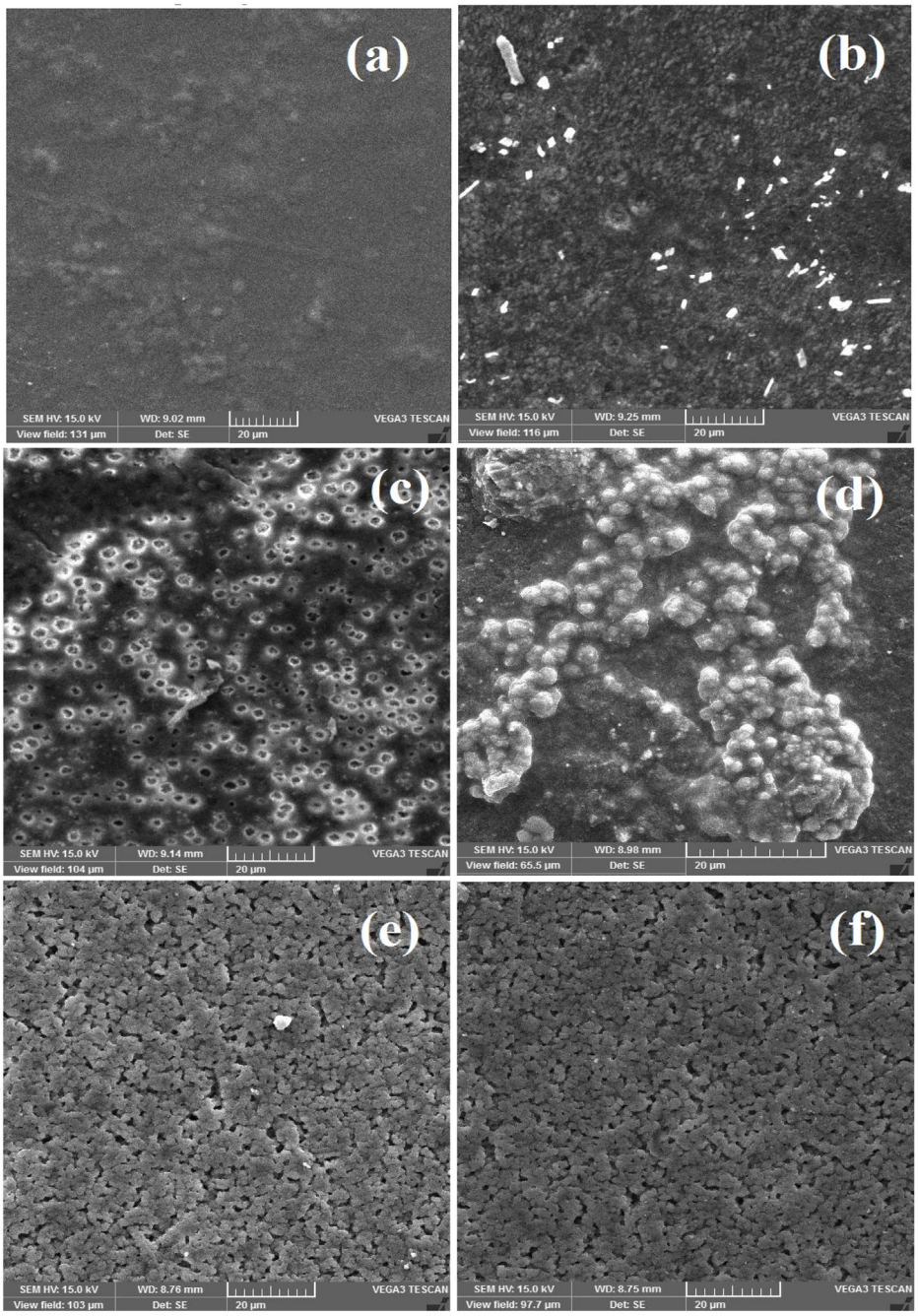

Fig. 2. SEM micrographs of electrolyte specimens ($MgTf_2$/PEO/PC-DEC) + x wt.% MgO (a) x = 0, (b) x = 0.25, (c) x = 0.5, (d) x = 1, (e) x = 1.5 and (f) x = 2.

a diamond-like carbon coated ultra-sharp silicon tip. The X-ray diffraction curves were obtained from XPERT-PRO system using Cu–Kα radiation in Bragg angle (2θ) range from 10° to 80° at scan rate of 2° min^{-1}. Electrochemical Impedance Spectroscopy (EIS) data was recorded using 1260 Solartron Impedance analyzer in the frequency range from of 1 Hz to 32 MHz at signal level of 10 mV in temperature ranging from 303 K to 333 K. In order to perform the EIS measurements, the nano-composite polymer electrolyte films were sandwiched between two stainless steel (SS) electrodes. The mechanical studies were performed by drawing the strain versus stress curves from Instron's mechanical tester (Model 5848, Singapore) at a strain rate of 5 mm min^{-1}, by applying a maximum load of 10 N at a pressure of 1 Bar.

3. Results and discussion

3.1. Structural and morphological studies

Fig. 2 shows the SEM micrographs of polymer electrolyte matrix dispersed with varying concentration of MgO nanoparticles in it. The $MgTf_2$/PEO/PC-DEC film without any MgO content shows a flat surface morphology (Fig. 2a). Fig. 2b indicate the onset of ring type structural formation for 0.25 wt% dispersion of MgO nano-particles. The ring type structures are more prominently observed in electrolyte film dispersed with 0.5 wt% MgO nano-particles (Fig. 2c). From Fig. 2d, we can observe that ring type structures are not observable and instead globular type structure is observed. It is important to note that portion of the micrograph (Fig. 2d) neither contains any ring type nor any globules, possibly

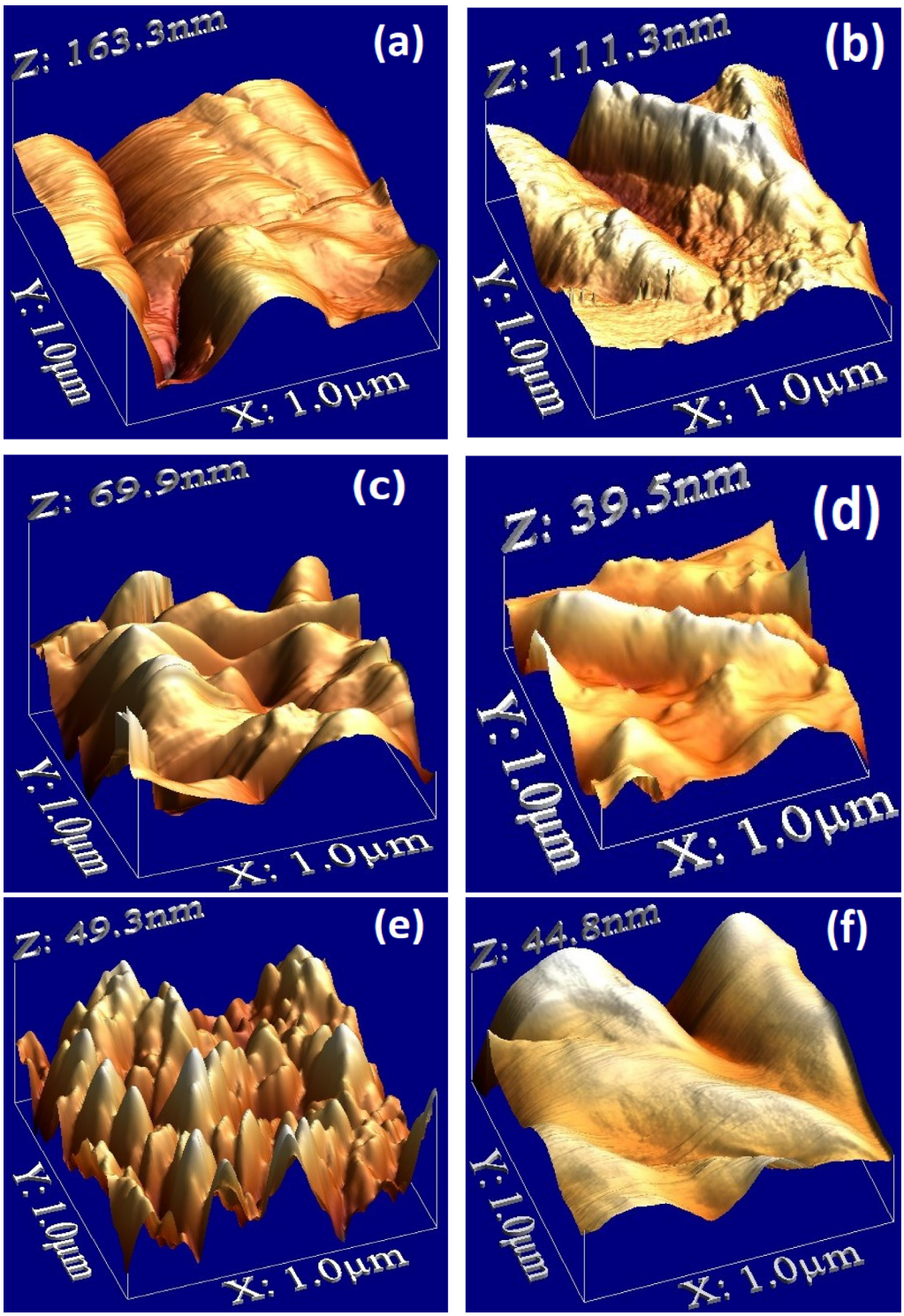

Fig. 3. AFM images of electrolyte specimens ($MgTf_2$/PEO/PC-DEC) + x wt.% MgO (a) x = 0, (b) x = 0.25, (c) x = 0.5, (d) x = 1, (e) x = 1.5 and (f) x = 2.

due to ring type structure being combined in presence of MgO nanoparticles. For 1.5 wt% of MgO nano-particles i.e. Fig. 2e the electrolyte film appears very uniform, however for 2 wt% of MgO nano-particles (Fig. 2f) the surface morphology becomes compact and uniform. Thus, SEM study suggests significant morphological changes on adding MgO nano-particles in small amounts within the $MgTf_2$/PEO/PC-DEC matrix.

Fig. 3a–f depicts the atomic force microscopic measurement for electrolyte films with varying amount of MgO nano-particles in $MgTf_2$/PEO/PC-DEC matrix. The small MgO nano-particles content (from 0 to 2 wt%) was able to significantly alter the morphology, as observed from the change in maximum roughness height for all electrolyte compositions. As the MgO concentration varies from 0 wt% to 1 wt%, the maximum roughness height drastically varies from ∼163.2 nm to 39.5 nm (Fig. 3a–d). This decrease in maximum roughness height may be due to the smaller rings (Fig. 2c) combining together and forming larger sized globules structure (Fig. 2d). However, for the higher MgO content slight increase in maximum roughness height is observed (Fig. 3e–f).

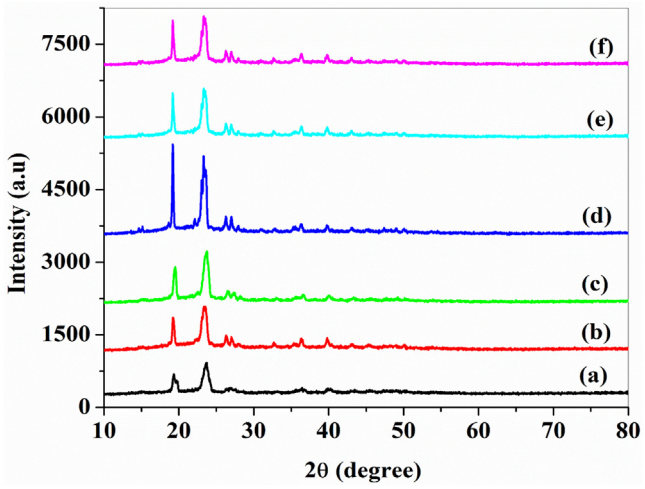

Fig. 4. X-ray diffraction patterns of electrolyte specimens ($MgTf_2$/PEO/PC-DEC) + x wt.% MgO (a) x = 0, (b) x = 0.25, (c) x = 0.5, (d) x = 1, (e) x = 1.5 and (f) x = 2.

Table 1
The values of crystallite size for electrolyte compositions with different MgO nano-particles concentration.

MgO (wt.%)	Crystallite size (D) (Å)
0	3.93
0.25	4.32
0.50	4.97
1.00	6.51
1.50	5.71
2.00	5.71

From the AFM measurement, we can note that electrolyte films undergo significant change in morphology with the addition of MgO nano-particles in it and electrolyte film with 1 wt% MgO content has optimized retention of $MgTf_2$/PC-DEC solution and therefore a relatively smooth morphology.

Fig. 4 depicts the X-ray diffraction (XRD) patterns for $MgTf_2$/PEO/PC-DEC polymer electrolyte films dispersed with varying concentration of MgO nano-particles. All electrolyte films, shows two prominent crystalline peaks at 19.3°, 23.4° due to the predominant semi-crystalline nature of PEO polymer host [49]. Additionally, two smaller peaks appearing at 27° are due to PEO polymer. Form the literature, we observe that MgO is highly crystalline with its principle crystalline peaks located at 37.15° (planes (111)) and 43° (planes (200)) and 62.30° (planes (220)) (JCPDS No-78-0430) respectively [32,50,51]. The XRD pattern of all polymer electrolytes with different amount of nano-particles does not show any significant crystalline peaks relevant to MgO which shows the complete dispersion of nano-particle in the present electrolyte system. However, with the dispersion of MgO nano-particles from 0 wt% to 1 wt% within polymer electrolyte matrix, the XRD spectra show slight increase in the height of peaks at 19.3° and 23.4°. This indicates the crystallinity increases till incorporation of 1 wt%. In support of this, the crystallite size is estimated by calculating change in the peak width at 19.3° and 23.4° according to the Scherrer equation.

$$D = \frac{k\lambda}{\beta \cos\theta} \tag{1}$$

where k is the Scherrer factor ($k = 0.94$), λ is the wavelength of X-rays ($\lambda = 1.54$ Å), θ is the Bragg diffraction angle and β is the full width at half maxima which is calculated using Gaussian fitting.

As it can be seen from Table 1, the crystallite size is increasing with increasing the amount of MgO from 0 wt% to 1 wt%. This may be due to the possible prevention of reorientation of chain of PEO due to increase in the charge carrier as a result of dissociation of $MgTf_2$ salt and MgO active nano-particles which restrict the movement of polymer chain. When MgO nano-particle are added in the polymer matrix, it is expected to have Lewis-acid base interaction at the EO group of PEO polymer chain and Lewis acid sites of MgO nano-filler which result in the increment in the free charge carrier [49]. On further addition of MgO nano filler i.e 1.5 wt% and 2 wt%, the intensity of peaks at 19.3° and 23.4° decreases and the crystallite size has also been found to be decreased. Along with it, the peaks at 43° corresponding to MgO is becoming slight prominent for sample having 1.5 wt% and 2 wt% compare to sample having 1 wt% MgO indication of starting of MgO aggregation cause reduction in the free charge carriers.

3.2. Ionic conductivity

The analysis of frequency dependent impedance not only provides ionic conductivity values but also provides insights on ion-dynamics within the polymer electrolyte membranes. In order to understand ion conduction behavior, the Nyquist plots are drawn for various compositions of MgO dispersed $MgTf_2$/PEO/PC-DEC electrolyte systems are shown in Fig. 5a. All the plots comprise a semi-circle at high frequency range, associated with the ion conduction in the bulk of electrolyte, and a slant corroborating ionic accumulation at electrolyte and ion blocking SS (Stainless Steel) electrode. The common interception of the semi-circle and slant on the real axis (Z') of the Nyquist plot provides bulk resistance (R_b) of the electrolyte membranes, which is used to obtain the ionic conductivity (σ) from the formula:

$$\sigma = \frac{d}{R_b \cdot A} \tag{2}$$

where, d and A are thickness and area of the electrolyte membrane, respectively and R_b is the bulk resistance obtained from Nyquist plots.

The obtained ionic conductivity values are plotted against the concentration of MgO nano-particles in the $MgTf_2$/PEO/PC-DEC polymer electrolyte matrix (Fig. 5b). The ionic conductivity of the electrolyte system is observed to be increasing with MgO concentration and the composition with 1 wt% MgO display maximum ionic conductivity. Thereafter, the conductivity is significantly decreased for MgO nanoparticles concentration up to 2 wt%. This is a typical behavior of composite electrolytes which show highest conductivity at a particular threshold loading of nano-particle fillers. The temperature dependent ionic conductivity of various compositions of the electrolyte systems is shown in Fig. 5c. All the compositions follow straight line Arrhenius behavior, as:

$$\sigma = \sigma_0 exp\left(-\frac{E_a}{kT}\right) \tag{3}$$

where, σ_0 is pre exponential factor, E_a is the activation energy, k is the Boltzmann constant and T is temperature in K. This behavior is a typical of semi-crystalline polymer electrolytes, in which ion-transport take place due to hopping [52,53]. The ionic conductivity increases due to the faster segmental motion of the host polymer supported by the diminution in its viscosity at higher temperatures. The activation energy is another important factor for a feasible electrolyte system, which is a combination of the energy of free-ion creation and their transport via hoping in the present case. The activation energy of the electrolyte system must be as low as possible to facilitate faster ion motion. The activation energy of the different electrolyte compositions has been evaluated using Eq. (3) and plotted with room temperature

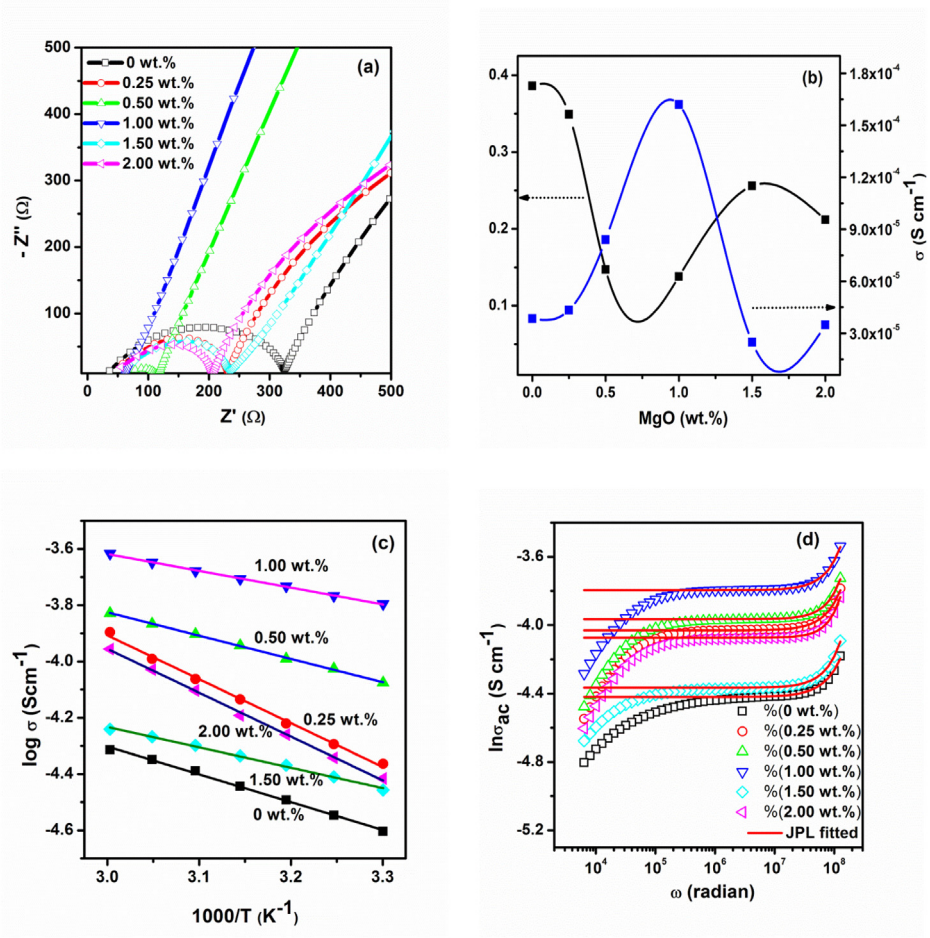

Fig. 5. (a) Nyquist plots (i.e. Z' versus $-Z''$ pattern) (b) activation energy and ionic conductivity values (c) ionic conductivity versus temperature plots (d) ac conductivity versus angular frequency plots for electrolyte films with different MgO nano-particles concentration.

ionic conductivity in Fig. 5b. The activation energy values are well below 0.4 eV for all the composition and the maximum conducting composition, i.e. $MgTf_2$/PEO/PC-DEC with 1 wt% MgO, display minimum activation energy (0.13 eV). The frequency dependent conductivity of all the compositions are also plotted in Fig. 5d. The conductivity pattern is found to obey the well-known Jonscher's Power Law (JPL) [54] in high frequency range, given as:

$$\sigma_{ac} = \sigma_{dc} + A\omega^{\eta} \tag{4}$$

where σ_{dc} is the dc conductivity, A is pre-exponential factor and η is the fractional exponent which reveals the ratio of backward motion of the ions to the site relaxation time in the polymer electrolyte system. A deviation of the conductivity spectra from JPL behavior is observed at low frequency region, where the electrode polarization effect is dominant. In this region, accumulation of ions at SS blocking electrodes results in a decrease in effective numbers of free-ions, which turn out as fast decline in the ionic conductivity. The JPL fitting parameters are listed in Table 2.

The σ_{dc} values are close to those obtained from Nyquist plots (Fig. 5b). The maximum dc conductivity is obtained as 1.60×10^{-4} S cm^{-1} for $MgTf_2$/PEO/PC-DEC with 1 wt% MgO. The η values of all the compositions are greater than unity, this is quite contradictory to the earlier reports on the polymer electrolytes [55,56], in which η remain less than 1 showing the long range translational hopping motion. The obtained values of the η reveal the dominance of localized hopping or reorientational motion of ions in the prepared electrolyte system [57]. The value of $\eta > 1$ has also been observed some other workers also [58,59]. This may be the effect of the enhanced crystalline nature of the polymer electrolyte system on dispersion of MgO fillers, as observed in XRD analysis, which hinders the segmental motion of the electrolyte and hence, the long range ionic translational motion. From the above studies, it is revealed that the translational motion of the ions is seized in the electrolyte system on dispersion of MgO fillers. This is quite strange on the part that the conductivity has been significantly enhanced in dispersed electrolyte compositions up to 1 wt% MgO.

Table 2
Parameters obtained from JPL fitting of the frequency dependent ac conductivity plot.

MgO (wt.%)	σ_{dc} (S cm^{-1})	A	η
0	3.80×10^{-5}	1.37×10^{-13}	1.50
0.25	9.33×10^{-5}	2.06×10^{-14}	1.61
0.50	1.08×10^{-4}	1.27×10^{-15}	1.76
1.00	1.60×10^{-4}	2.44×10^{-14}	1.605
1.50	4.30×10^{-5}	1.28×10^{-14}	1.644
2.00	4.45×10^{-5}	1.65×10^{-16}	1.99

3.3. Dielectric studies

In order to have better understanding of the ion-dynamics in the electrolyte system, dielectric studies have been performed (Fig. 6). The frequency dependence of real (ε') and imaginary (ε'') part of permittivity for various compositions of the polymer electrolyte system are shown in Fig. 6ab. As can be seen from

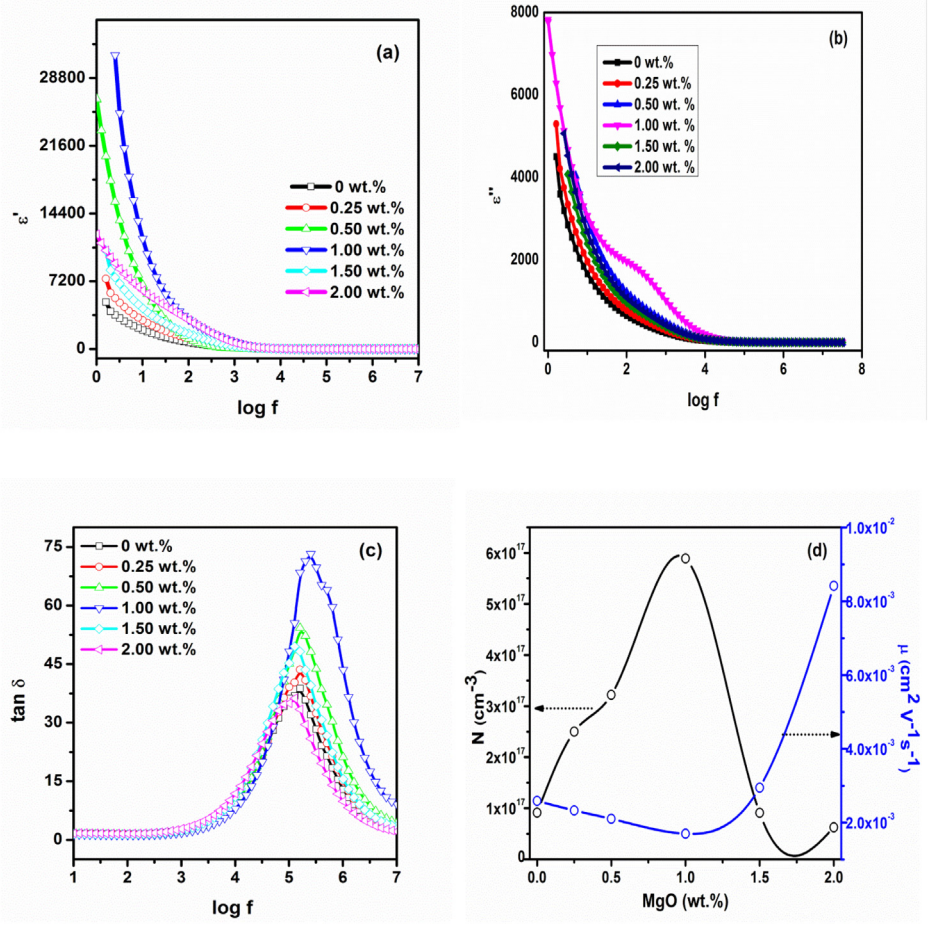

Fig. 6. (a) Dielectric constant (ε') (b) Dielectric loss (ε'') (c) tangent loss versus logarithmic frequency for electrolyte films with different MgO nano-particles concentration (d) Charge carrier concentration (N) and mobility (μ) versus MgO nano-particles concentration.

the figure, dispersion is observed in the both ε'' and ε' traces at low frequency region. It is due to the electrode polarization effect at electrode/electrolyte interface [60]. At higher frequency side, a plateau is observed for all the compositions which is associated with the inability of the ionic dipoles at such frequencies [61,62].

The value of ε' is related to the numbers of dissociated ions present in the electrolyte system, as;

$$n = n_o exp\left(\frac{-U}{\epsilon' KT}\right) \tag{5}$$

where n_o is the pre-exponential factor, U is the dissociation energy and T is the absolute temperature of dielectric measurement, respectively. The values of ε' at 1 kHz, for various electrolyte compositions are listed in Table 3.

As can be seen from Table 3, the ε' values have been significantly enhanced upon dispersion of MgO nano-particles, except for the composition with 0.50 wt% MgO. The highest conducting composition, $MgTf_2$/PEO/PC-DEC with 1 wt% MgO, have the maximum value of ε', which is an indicative of the presence of maximum numbers of dissociated ions present in the electrolyte composition. Additionally, a hump is observed in ε'' vs log f graph (Fig. 6b), between log f = 2 and 3, for the highest conducting composition $MgTf_2$/PEO/PC-DEC with 1 wt% MgO. This may be attributed to the contribution of interfacial polarization, also known as Maxwell-Wagner–Sillars (MWS) polarization, over the dipolar polarization in the above composition of the polymer electrolyte system [56]. In order to access the relaxation time, frequency dependence of the tangent loss (tan δ) is plotted at room temperature (Fig. 6c). A relaxation peak associated with the presence of scaling dipole is observed for all the electrolyte compositions. However, the position and the height of this peak provide important information about the ion dynamics. The portion of the relaxation peak on the frequency-axis reveals the ion relaxation time (τ) in the electrolyte compositions, as;

$$\tau = \frac{1}{2\pi f_{max}} \tag{6}$$

where f_{max} is the frequency of the relaxation peak. The calculated values of τ are listed in Table 2. The highest conducting composition carrying 1 wt% MgO has the minimum relaxation time of 0.61 μs [63]. The compositions with > 1 wt% MgO, display significantly high relaxation time. The conductivity data and the tan δ plots are used to obtain diffusivity (D), free ion number density (N), and ion mobility (μ) in the electrolyte system, using the following formulas [64]:

$$D = \frac{2\pi f_{max} d^2}{32(\text{Tan } \delta_{max})^3} \tag{7}$$

$$N = \frac{\sigma_{dc} K_b T}{Dq^2} \tag{8}$$

$$\mu = \frac{\sigma_{dc}}{qN} \tag{9}$$

where d is the thickness of the electrolyte membrane, q is the elementary charge, Tan δ_{max} is maximum tangent loss and f_{max} is the frequency corresponding to maximum tangent loss. The evaluated parameters are listed in Table 3.

Table 3
Variation of dc conductivity (σ_{dc}), relaxation time (τ), ion diffusivity (D), and number (N) and mobility (μ) of charge carriers (N) for electrolyte compositions with different MgO nano-particles concentration.

MgO (wt.%)	ε' (at 1 kHz)	τ (μs)	D	N (cm^{-3})	μ (cm^2 V^{-1} s^{-1})
0	135	0.98	6.44×10^{-5}	9.15×10^{16}	0.00259
0.25	231	0.97	4.78×10^{-5}	2.50×10^{17}	0.00233
0.50	52	0.97	5.22×10^{-5}	3.22×10^{17}	0.0021
1.00	759	0.61	4.22×10^{-5}	5.89×10^{17}	0.0017
1.50	347	1.23	7.33×10^{-5}	9.11×10^{16}	0.00295
2.00	657	1.28	2.09×10^{-4}	6.27×10^{16}	0.00842

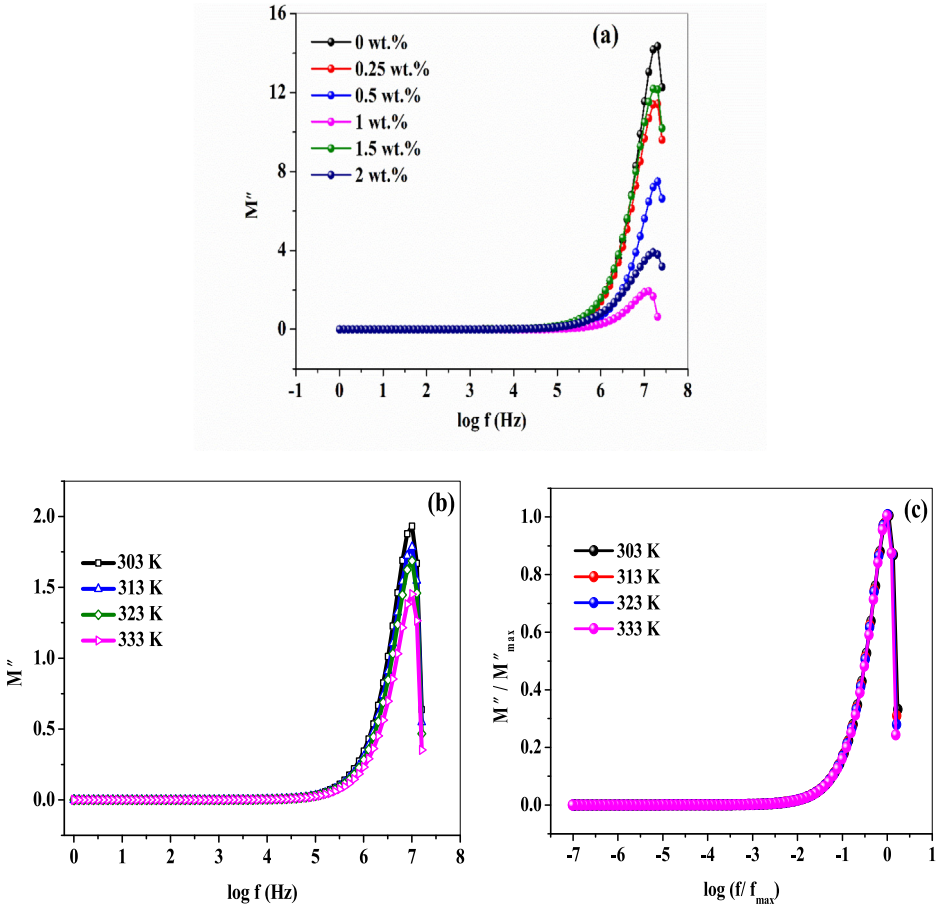

Fig. 7. (a) Imaginary part of modulus (M″) as a function of frequency for $MgTf_2$/PC-DEC/PEO matrix at different concentrations of MgO nano-particles (b) Imaginary part of modulus (M″) as a function of frequency for electrolyte composition with 1 wt% MgO content at different temperatures (c) Scaled spectra of modulus for NGPE with 1 wt% MgO at different temperatures.

The diffusivity and mobility of the ions are found to decrease slightly on increasing the concentration of MgO nano-particles and the composition with 1 wt% MgO possesses the minimum values. Beyond 1 wt% MgO nano-particles concentration, these parameters are increased significantly. On the contrary, the ion number density displays initial increase followed by decline after 1 wt% MgO. Fig. 6d shows the comparative variation of μ and N with MgO filler concentration in polymer electrolyte system. From the figure, it is clear that the number of free ions is dominantly affecting the ionic conductivity of the electrolyte system than the mobility of the ions. The slight reduction in the mobility of the ions is a consequence of the increased crystallinity of the polymer electrolyte membranes on dispersion of MgO fillers, as observed in XRD studies.

3.4. Modulus studies

The bulk behavior of the conductivity is generally suppressed in the dielectric analysis because it highlights lower frequency region i.e. electrode polarization effects. To overcome this problem as well as to investigate the conductivity relaxation process in the present nano-composite polymer electrolyte, modulus analysis has been carried out [65]. The complex electric modulus is inverse of the dielectric permittivity and it can be represented as

$$M^* = \frac{1}{\varepsilon^*} \tag{10}$$

The electric modulus can also be written mathematically in terms of complex impedance

$$M^* = M' + jM' = j\omega C_0 Z^* \tag{11}$$

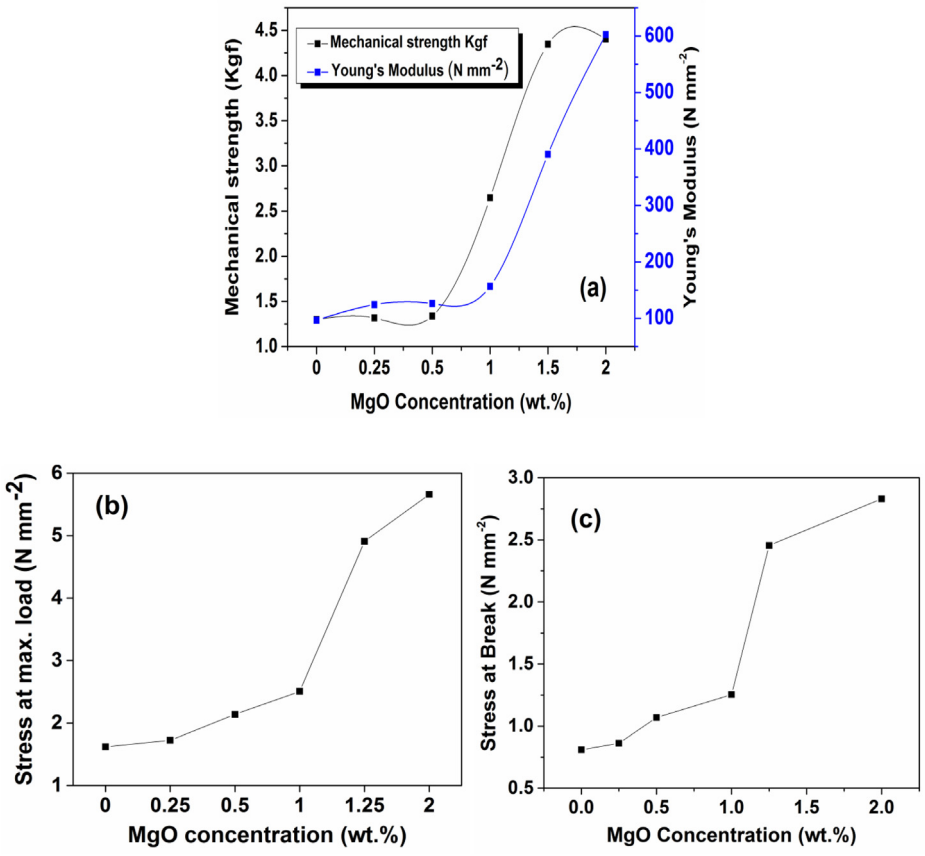

Fig. 8. (a) Young's modulus and mechanical strength (b) stress at maximum load for electrolyte films with different MgO concentration, and (c) stress at break for electrolyte films with different MgO nano-particles concentration.

where, the angular frequency $\omega = 2\pi f$ and C_0 is the vacuum capacitance of the electrochemical cell, and M' and M'' are real and imaginary parts of the complex modulus M^*, respectively.

The M'' (imaginary part of the modulus) as a function of frequency for polymer electrolyte system containing different concentrations of MgO nano-particles at 303 K is shown in Fig. 7a. A prominent peak at a particular frequency is observed in modulus spectra which is the signature of ionic conductivity relaxation. The frequency (f_{max}) corresponding to M''_{max} is called as conductivity relaxation frequency. The region where $f < f_{max}$ is due to the long-range mobility of ion where successful hopping of ion from one available site to another site is feasible and at very low frequency, the plateau region is an indication of large capacitance associated with it [66]. On the other side when $f > f_{max}$, the ions are not able to follow the direction of the applied ac field results in short-range mobility of ion.

Another interesting and notable feature of change in height of the peak is seen with the addition of MgO nano-filler from the 0 wt% to 2 wt%. With increasing the amount of MgO nano-filler from 0 wt% to 1 wt%, the height of the peak is decreasing whereas reverse trend has been seen for the electrolyte system having 1.5 wt% MgO content. The minimum value of the height of the peak is observed for composition $MgTf_2$/PEO/PC-DEC+1 wt% MgO. This suggests occurrence of relaxation phenomena and an increase of ionic conductivity due to increase in number of mobile charge carrier density within the electrolyte system.

Fig. 7b depicts the M'' (imaginary part of the modulus) as a function of frequency for polymer electrolyte composition containing 1 wt% MgO nan-particles content in temperature range from 303 K to 333 K. The peak maximum is found to be shifted towards a higher frequency side with a rise in temperature. Aziz et al. [67] have also observed the similar behavior in sodium ion-conducting Chitosan-based solid polymer electrolyte with different concentrations of Al_2O_3 nano-filler. This indicates thermally activated conductivity relaxation process within electrolyte system with a decrease in relaxation time as per the relation $\omega\tau = 1$, where angular frequency $\omega = 2\pi f$ and τ is relaxation time. A decrease in relaxation time clearly supports the increasing mobility of free charge carriers as well as polymer segments which results in an enhancement of ionic conductivity values.

In order to get more insight into temperature dependents ion dynamics, the scaling tool is adopted. The scaling is also known as the "Time–temperature superposition principle". The main aim of the scaling is to probe whether the conduction mechanism is temperature-dependent or independent in the present system. Sharma et al. [68] reported the merging of M'' at different temperatures (single normalized peak) in their PEO/PMMA based system confirming that relaxation behavior is temperature independent.

In the present study, the Ghosh scaling is approached given as below

$$\frac{M''}{M''_{max}} = F\left(\frac{f}{f_{max}}\right) \tag{12}$$

where M''_{max} is peak maxima and f_{max} is frequency corresponds to the peak.

The scaled spectra of the imaginary part of modulus for $MgTf_2$/PEO/PC-DEC with 1 wt% MgO content is shown in Fig. 7c. The scaling of M'' spectra result in superimposed curves which suggests the ion-dynamics is temperature independent. Similar kind of scaling behavior has also been reported by Karmakar et al. in their study for PEO-$LiClO_4$ based polymer electrolyte system where the spectra scaled to common master curve suggesting

that the charge carriers follow similar ion-transport behavior throughout the temperature range [69].

3.5. Mechanical studies

The mechanical properties of polymer based electrolytes dispersed with MgO nano-particles have been evaluated using mechanical studies. The mechanical strength and Young's modulus of the films have been plotted for varying concentration of MgO nano-particles in it (Fig. 8a). The values of Young's modulus and mechanical strength are found to be improved with the dispersion of MgO nano-particles within PEO/$MgTf_2$/PC-DEC matrix. The undispersed electrolyte $MgTf_2$/PEO/PC-DEC i.e. PE offers a Young's modulus of 100 N mm^{-2} and mechanical strength of 1.2 Kgf. The optimized electrolyte $MgTf_2$/PEO/PC-DEC/1 wt% MgO offers a Young's modulus of 150 N mm^{-2} and mechanical strength of 2.7 Kgf.

The stress at maximum load and stress at break is demonstrated (Fig. 8b and c) with variation in MgO nano-particles concentration. The undispersed electrolyte films could withstand stress of ~1.6 N mm^{-2} at maximum load and stress at break is observed to be 0.6 N mm^{-2}. However, the optimized electrolyte could withstand stress of 2.5 N mm^{-2} at maximum load and stress at break is found to be 1.25 N mm^{-2}. The mechanical studies reveal a significant enhancement in mechanical strength, Young's modulus and stress bearing capacity of the electrolyte films with the addition of MgO nano-particles in it.

4. Conclusion

In this paper, the effect of dispersing active MgO nano-particles in small amount within magnesium-ion conducting polymer electrolyte matrix have been studied by structural, conductivity, dielectrics and mechanical investigations. AFM micrographs of $MgTf_2$/PEO/PC-DEC electrolyte matrix with 1 wt% MgO dispersion shows smooth morphology with lowest roughness height. The XRD curves indicate an increase in crystalline character with PEO prominent peak increasing in height with the dispersion of MgO nano-particles up to 1 wt%. However, on contrary the ionic conductivity is found to increase with MgO dispersion up to 1 wt%. The ion dynamics studies reveal the dominance of enhanced numbers of free charge carriers prompted by MgO nano-particles over the seized ion mobility due to increased crystallinity of the electrolyte system. The nano-composite polymer electrolyte film with optimized concentration of 1 wt% MgO nano-particles delivered an ionic conductivity of 1.49×10^{-4} S cm^{-1} at 25 °C. The mechanical studies on optimized nano-composite polymer electrolyte membrane reveal a Young's modulus of 150 N mm^{-2}, mechanical strength of 2.7 Kgf and stress of 2.6 N mm^{-2} at a maximum load of 10 Kgf. The reported Mg-ion conducting plasticized polymer electrolyte can be employed in fabricating flexible electrochemical devices especially the magnesium batteries.

CRediT authorship contribution statement

C. Maheshwaran: Conceptualization, Methodology, Investigation, Writing - original draft preparation. **D.K. Kanchan:** Supervision, Funding acquisition. **Kuldeep Mishra:** Visualization, Validation, Writing- Reviewing, Funding acquisition. **Deepak Kumar:** Investigation, Resources, Writing - review & editing. **Khushbu Gohel:** Visualization, Validation, Writing- Reviewing.

Declaration of competing interest

The authors declare that they have no known competing financial interests or personal relationships that could have appeared to influence the work reported in this paper.

Acknowledgments

Deepak Kumar thanks and acknowledges "The M.S. University of Baroda" Vadodara, Gujarat, India. The encouragement and support received from Electronics and Mechanical Engineering School (Affiliated to Gujarat Technological University), Government of India, are gratefully acknowledged. Kuldeep Mishra acknowledges the funding (File No YSS/2015/001234) from Science and Engineering Research Board (SERB) New Delhi, India.

References

[1] S. Passerini, B. Scrosati, Lithium and lithium-ion batteries: Challenges and prospects, Electrochem. Soc. Interface 25 (2016) 85, http://dx.doi.org/10.1149/2.F09163if.
[2] A. Manthiram, Materials challenges and opportunities of lithium ion batteries, J. Phys. Chem. Lett. 2 (3) (2011) 176–184, http://dx.doi.org/10.1021/jz1015422.
[3] X. Han, L. Lu, Y. Zheng, X. Feng, Z. Li, J. Li, M. Ouyang, A review on the key issues of the lithium ion battery degradation among the whole life cycle, eTransportation 1 (2019) 100005, http://dx.doi.org/10.1016/j.etran.2019.100005.
[4] Y. Wu, P. Nie, H. Dou, J. Jiang, Y. Zhu, X. Zhang, Graphene scrolls coated Sb_2S_3 nanowires as anodes for sodium and lithium ion batteries, Nano-Struct. Nano-Objects 15 (2018) 197–204, http://dx.doi.org/10.1016/j.nanoso.2017.09.015.
[5] Y. Orikasa, T. Masese, Y. Koyama, T. Mori, M. Hattori, K. Yamamoto, T. Okado, Z.-D. Huang, T. Minato, C. Tassel, J. Kim, Y. Kobayashi, T. Abe, H. Kageyama, Y. Uchimoto, High energy density rechargeable magnesium battery using earth-abundant and non-toxic elements, Sci. Rep. 4 (2015) 5622, http://dx.doi.org/10.1038/srep05622.
[6] P. Saha, M.K. Datta, O.I. Velikokhatnyi, A. Manivannan, D. Alman, P.N. Kumta, Rechargeable magnesium battery: Current status and key challenges for the future, Prog. Mater. Sci. 66 (2014) 1–86, http://dx.doi.org/10.1016/j.pmatsci.2014.04.001.
[7] D. Kumar, K. Gohel, D.K. Kanchan, K. Mishra, Dielectrics and battery studies on flexible nanocomposite gel polymer electrolyte membranes for sodium batteries, J. Mater. Sci., Mater. Electron. (2020) http://dx.doi.org/10.1007/s10854-020-03877-8.
[8] M.J.S. Syali, D. Kumar, K. Mishra, D.K. Kanchan, Recent advances in electrolytes for room-temperature sodium-sulfur batteries: A review, Energy Storage Mater. 31 (2020) 352–372.
[9] D. Kumar, D.K. Kanchan, Dielectric and electrochemical studies on carbonate free Na-ion conducting electrolytes for sodium-sulfur batteries, J. Energy Storage 22 (2019) 44–49, http://dx.doi.org/10.1016/j.est.2019.01.020.
[10] M. Xu, D.G. Ivey, Z. Xie, W. Qu, Rechargeable Zn-air batteries: Progress in electrolyte development and cell configuration advancement, J. Power Sources 283 (2015) 358–371, http://dx.doi.org/10.1016/j.jpowsour.2015.02.114.
[11] W. Xu, Y. Wang, Recent progress on zinc-ion rechargeable batteries, Nano-Micro Lett. 11 (2019) 90, http://dx.doi.org/10.1007/s40820-019-0322-9.
[12] A.R. Despić, Design characteristics of an aluminium-air battery with consumable wedge anodes, J. Appl. Electrochem. 15 (1985) 191–200, http://dx.doi.org/10.1007/BF00620933.
[13] R. Ranu, Y. Chauhan, A. Ratan, P.K. Singh, B. Bhattacharya, The biogenic synthesis and thermo-magnetic study of highly porous carbon nanotubes, IET Nanobiotechnology 13 (2019) 363–367, http://dx.doi.org/10.1049/iet-nbt.2018.5105.
[14] V. Singh, M.S. Pathak, N. Singh, P.K. Singh, H.D. Jirimali, Sol-gel derived Green emitting Tb^{3+} doped $Sr_2La_8(SiO_4)_6O_2$ phosphors, Optik 168 (2018) 475–480, http://dx.doi.org/10.1016/j.ijleo.2018.04.072.
[15] S. Ramesh, S.-C. Lu, E. Morris, Towards magnesium ion conducting poly(vinylidene fluoride-hexafluoropropylene) based solid polymer electrolytes with great prospects: ionic conductivity and dielectric behaviours, J. Taiwan Inst. Chem. Eng. 43 (2012) 806–812, http://dx.doi.org/10.1016/j.jtice.2012.04.004.
[16] T. Kimura, K. Fujii, Y. Sato, M. Morita, N. Yoshimoto, Solvation of magnesium ion in triglyme-based electrolyte solutions, J. Phys. Chem. C 119 (2015) 18911–18917, http://dx.doi.org/10.1021/acs.jpcc.5b04626.
[17] G.P. Pandey, S.A. Hashmi, Y. Kumar, Performance studies of activated charcoal based electrical double layer capacitors with ionic liquid gel polymer electrolytes, Energy Fuel 24 (2010) 6644–6652, http://dx.doi.org/10.1021/ef1010447.
[18] C. Liebenow, A novel type of magnesium ion conducting polymer electrolyte, Electrochim. Acta 43 (1998) 1253–1256, http://dx.doi.org/10.1016/S0013-4686(97)10026-3.

[19] G.G. Kumar, N. Munichandraiah, Effect of plasticizers on magnesium-poly (ethyleneoxide) polymer electrolyte, J. Electron Chem. 495 (2000) 42–50, http://dx.doi.org/10.1016/S0022-0728(00)00404-6.

[20] N. Yoshimoto, S. Yakushiji, M. Ishikawa, M. Morita, Rechargeable magnesium batteries with polymeric gel electrolytes containing magnesium salts, Electrochim. Acta 48 (14) (2003) 2317–2322, http://dx.doi.org/10.1016/S0013-4686(03)00221-4.

[21] C. Maheshwaran, D.K. Kanchan, K. Gohel, K. Mishra, D. Kumar, Effect of $Mg(CF_3SO_3)_2$ concentration on structural and electrochemical properties of ionic liquid incorporated polymer electrolyte membranes, J. Solid State Electr. 24 (3) (2020) 655–665, http://dx.doi.org/10.1007/s10008-020-04507-3.

[22] P. Saha, M.K. Datta, O.I. Velikokhatnyi, A. Manivannan, D. Alman, P.N. Kumta, Rechargeable magnesium battery: current status and key challenges for the future, Prog. Mater. Sci. 66 (2014) 1–86, http://dx.doi.org/10.1016/j.pmatsci.2014.04.001.

[23] D. Aurbach, G.S. Suresh, E. Levi, A. Mitelman, O. Mizrahi, O. Chusid, M. Brunelli, Progress in rechargeable magnesium battery technology, Adv. Mater. 19 (2007) 4260–4267, http://dx.doi.org/10.1002/adma.200701495.

[24] F. Bertasi, F. Sepehr, G. Pagot, S.J. Paddison, V.D. Noto, Toward a magnesium-iodine battery, Adv. Funct. Mater. 26 (2016) 4860–4865, http://dx.doi.org/10.1002/adfm.201601448.

[25] J. Muldoon, C.B. Bucur, A.G. Oliver, T. Sugimoto, M. Matsui, H.S. Kim, G.D. Allred, J. Zajicek, Y. Kotanie, Electrolyte roadblocks to a magnesium rechargeable battery, Energy Environ. Sci. 5 (2012) 5941–5950, http://dx.doi.org/10.1039/C2EE03029B.

[26] M. Grünebaum, M.M. Hiller, S. Jankowsky, S. Jeschke, B. Pohl, T. Schürmann, P. Vettikuzha, A.-C. Gentschev, R. Stolina, R. Müller, H.-D. Wiemhöfer, Synthesis and electrochemistry of polymer based electrolytes for lithium batteries, Prog. Solid State Chem. 42 (2014) 85–105, http://dx.doi.org/10.1016/j.progsolidstchem.2014.04.004.

[27] S.-J. Tan, X.-X. Zeng, Q. Ma, X.-W. Wu, Y.-G. Guo, Recent advancements in polymer-based composite electrolytes for rechargeable lithium batteries, Electrochem. Energy Rev. 1 (2018) 113–138, http://dx.doi.org/10.1007/s41918-018-0011-2.

[28] N. Boaretto, L. Meabe, M.M. Ibañez, M. Armand, H. Zhang, Review—polymer electrolytes for rechargeable batteries: From nanocomposite to nanohybrid, J. Electrochem. Soc. 167 (2020) 070524, http://dx.doi.org/10.1149/1945-7111/ab7221.

[29] Z. Stoeva, I.M. Litas, E. Staunton, Y.G. Andreev, P.G. Bruce, Ionic conductivity in the crystalline polymer electrolytes PEO_6:$LiXF_6$, X = P, As, Sb, J. Am. Chem. Soc. 125 (2003) 4619–4626, http://dx.doi.org/10.1021/ja029326t.

[30] M.J. Reddy, P.P.-J. Chu, Ion pair formation and its effect in PEO:Mg solid polymer electrolyte system, J. Power Sources 109 (2) (2002) 340–346, http://dx.doi.org/10.1016/S0378-7753(02)00084-8.

[31] Y. Yang, H. Huo, Investigation of structures of PEO-$MgCl_2$ based solid polymer electrolytes, Polym. Sci. 51 (15) (2013) 1162–1174, http://dx.doi.org/10.1002/polb.23315.

[32] R. Rathika, S.A. Suthanthiraraj, Ionic interactions and dielectric relaxation of PEO/PVDF-Mg[$(CF_3SO_2)_2N_2$)] blend electrolytes for magnesium ion rechargeable batteries, Macromol. Res. 24 (2016) 422–428, http://dx.doi.org/10.1007/s13233-016-4053-1.

[33] E. Roedern, R. Kühnel, A. Remhof, Magnesium ethylenediamine borohydride as solid-state electrolyte for magnesium batteries, Sci. Rep. 7 (2017) 46189, http://dx.doi.org/10.1038/srep46189.

[34] C. Maheshwaran, K. Mishra, D.K. Kanchan, D. Kumar, Mg^{2+} conducting polymer gel electrolytes: physical and electrochemical investigations, Ionics 26 (2020) 2969–2980, http://dx.doi.org/10.1007/s11581-020-03459-y.

[35] Nidhi S. Patel, R. Kumar, Synthesis and characterization of magnesium ion conductivity in PVDF based nanocomposite polymer electrolytes disperse with MgO, J. Alloys Compd. 789 (2019) 6–14, http://dx.doi.org/10.1016/j.jallcom.2019.03.089.

[36] M.M. Zaky, H.M. Eyssa, R.F. Sadek, Improvement of the magnesium battery electrolyte properties through gamma irradiation of nano polymer electrolytes doped with magnesium oxide nanoparticles, J. Vinyl Addit. Technol. 25 (3) (2019) 243–254, http://dx.doi.org/10.1002/vnl.21683.

[37] G.P. Pandey, R.C. Agrawal, S.A. Hashmi, Magnesium ion-conducting gel polymer electrolytes dispersed with nanosized magnesium oxide, J. Power Sources 190 (2009) 563–572, http://dx.doi.org/10.1016/j.jpowsour.2009.01.057.

[38] N. Wu, W. Wang, Y. Wei, T. Li, Studies on the effect of nano-sized MgO in magnesium-ion conducting gel polymer electrolyte for rechargeable magnesium batteries, Energies 10 (2017) 1215, http://dx.doi.org/10.3390/en10081215.

[39] R. Arunkumar, R.S. Babu, M.U. Rani, S. Rajendran, Influence of plasticizer on ionic conductivity of PVC-PBMA polymer electrolytes, Ionics 23 (2017) 3097–3109, http://dx.doi.org/10.1007/s11581-017-2101-2.

[40] Z. Huang, Q. Pan, D.M. Smith, C.Y. Li, Plasticized hybrid network solid polymer electrolytes for lithium-metal batteries, Adv. Mater. Interfaces 6 (2) (2019) 1801445, http://dx.doi.org/10.1002/admi.201801445.

[41] J.Y. Song, Y.Y. Wang, C.C. Wan, Conductivity study of porous plasticized polymer electrolytes based on poly(vinylidene fluoride) a comparison with polypropylene separators, J. Electrochem. Soc. 147 (9) (2000) 3219, http://dx.doi.org/10.1149/1.1393886.

[42] A.M. Stephan, Review on gel polymer electrolytes for lithium batteries, Eur. Polym. J. 42 (2006) 21–42, http://dx.doi.org/10.1016/j.eurpolymj.2005.09.017.

[43] K. Mishra, T. Arif, R. Kumar, D. Kumar, Effect of Al_2O_3 nanoparticles on ionic conductivity of PVdF-HFP/PMMA blend-based Na^+-ion conducting nanocomposite gel polymer electrolyte, J. Solid State Electr. 23 (8) (2019) 2401–2409, http://dx.doi.org/10.1007/s10008-019-04348-9.

[44] C. Maheshwaran, D.K. Kanchan, K. Mishra, D. Kumar, K. Gohel, Flexible magnesium-ion conducting polymer electrolyte membranes: Mechanical, structural, thermal and electrochemical impedance spectroscopic properties, J. Mater. Sci., Mater. Electron. 31 (2020) 15013–15027, http://dx.doi.org/10.1007/s10854-020-04065-4.

[45] J. Sharma, S.A. Hashmi, Magnesium ion-conducting gel polymer electrolyte nanocomposites: Effect of active and passive nanofillers, Polym. Compos. 40 (4) (2019) 1295–1306, http://dx.doi.org/10.1002/pc.24853.

[46] D.C. Prado, I. Fernández, J.E.R. Páez, Mgo nanostructures: Synthesis, characterization and tentative mechanisms of nanoparticles formation, Nano-Struct. Nano-Objects 23 (2020) 100482, http://dx.doi.org/10.1016/j.nanoso.2020.100482.

[47] X.D. Peng, M.A. Barteau, Characterization of oxide layers on M_g(0001) and comparison of H_2O adsorption on surface and bulk oxides, Surf. Sci. 233 (1990) 283–292, http://dx.doi.org/10.1016/0039-6028(90)90641-K.

[48] T.O. Ahmed, P.O. Akusu, A. Ismaila, A. Maryam, Morphology and transport properties of polyethylene oxide (PEO)-based nanocomposite polymer electrolytes, Int. Res. J. Pure Appl. Chem. 4 (2) (2014) 170–180, http://dx.doi.org/10.9734/IRJPAC/2014/5358.

[49] A.C. Nancy, S.A. Suthanthiraraj, Effect of Al_2O_3 nanofiller on the electrical, thermal and structural properties of PEO:PPG based nanocomposite polymer electrolyte, Ionics 23 (2017) 1439–1449, http://dx.doi.org/10.1007/s11581-017-1976-2.

[50] J.P. Singh, W.C. Lim, S.O. Won, J. Song, K.H. Chae, Synthesis and characterization of some alkaline-Earth-oxide nanoparticles, J. Korean Phys. Soc. 72 (2018) 890–899.

[51] K.R. Nemade, S.A. Waghuley, Synthesis of MgO nanoparticles by solvent mixed spray pyrolysis technique for optical investigation, Int. J. Met. (2014) http://dx.doi.org/10.1155/2014/389416, Article ID 389416.

[52] R.C. Agrawal, G.P. Pandey, Solid polymer electrolytes: materials designing and all-solid-state battery applications: an overview, J. Phys. D 41 (2008) 223001, http://dx.doi.org/10.1088/0022-3727/41/22/223001.

[53] Z. Xue, D. He, X.Xie, Poly (ethylene oxide)-based electrolytes for lithium-ion batteries, J. Mater. Chem. A 3 (38) (2015) 19218–19253, http://dx.doi.org/10.1039/C5TA03471J.

[54] A.K. Jonscher, The 'universal' dielectric response, Nature 167 (1977) 673–679, http://dx.doi.org/10.1038/267673a0.

[55] S. Choudhury, S. Stalin, D. Vu, A. Warren, Y. Deng, P. Biswal, L.A. Archer, Solid-state polymer electrolytes for high-performance lithium metal batteries, Nature Commun. 10 (2019) 1–8, http://dx.doi.org/10.1038/s41467-019-12423-y.

[56] R.J. Sengwa, P. Dhatarwal, Predominantly chain segmental relaxation dependent ionic conductivity of multiphase semicrystalline PVDF/PEO/LiClO4 solid polymer electrolytes, Electrochim. Acta 338 (2020) 135890, http://dx.doi.org/10.1016/j.electacta.2020.135890.

[57] K. Funke, Jump relaxation in solid electrolytes, Prog. Solid State Chem. 22 (1993) 111–195, http://dx.doi.org/10.1016/S0167-2738(88)80015-8.

[58] S.K. Chaurasia, A.L. Saroj, Shalu, V.K. Singh, A.K. Tripathi, A.K. Gupta, Y.L. Verma, R.K. Singh, Studies on structural thermal and AC conductivity scaling of PEO-$LiPF_6$ polymer electrolyte with added ionic liquid [BMIM-PF6], AIP Adv. 5 (2015) 077178, http://dx.doi.org/10.1063/1.4927768.

[59] A. Karmakar, A. Ghosh, Charge carrier dynamics and relaxation in (polyethylene oxide-lithium-salt)-based polymer electrolyte containing 1-butyl-1-methylpyrrolidinium bis(trifluoromethylsulfonyl)imide as ionic liquid, Phys. Rev. E 84 (2011) 051802, http://dx.doi.org/10.1103/PhysRevE.84.051802.

[60] K.S. Ngai, S. Ramesh, K. Ramesh, J.C. Juan, Electrical, Dielectric and electrochemical characterization of novel poly(acrylic acid)-based polymer electrolytes complexed with lithium tetrafluoroborate, Chem. Phys. Lett. 692 (2018) 19–27, http://dx.doi.org/10.1016/j.cplett.2017.11.042.

[61] Pritam A. Arya, A.L. Sharma, Dielectric relaxations and transport properties parameter analysis of novel blended solid polymer electrolyte for sodium-ion rechargeable batteries, J. Mater Sci. 54 (2019) 7131–7155.

[62] I.I. Perepechko, An Introduction to Polymer Physics, Central Books Ltd., London, United Kingdom, 1983.

[63] S. Choudhary, Dielectric dispersion and relaxations in (PVA-PEO)-ZnO polymer nanocomposites, Physica B 522 (2017) 48–56, http://dx.doi.org/10.1016/j.physb.2017.07.066.

[64] P. Singh, P.N. Gupta, A.L. Saroj, Ion dynamics and dielectric relaxation behavior of PVA-PVP-NaI-SiO_2 based nano-composites polymer blend electrolytes, Physica B 578 (2020) 411850, http://dx.doi.org/10.1016/j.physb.2019.411850.

[65] A. Pawlicka, F.C. Tavares, D.S. Dörr, C.M. Cholant, F. Ely, M.J.L. Santos, C.O. Avellaneda, Dielectric behavior and FTIR studies of xanthan gum-based solid polymer electrolytes, Electrochim. Acta 305 (2019) 232–239, http://dx.doi.org/10.1016/j.electacta.2019.03.055.

[66] A. Arya, M. Sadiq, A.L. Sharma, Effect of variation of different nanofillers on structural, electrical, dielectric, and transport properties of blend polymer nanocomposites, Ionics 24 (2018) 2295–2319, http://dx.doi.org/10.1007/s11581-017-2364-7.

[67] S.B. Aziz, Z.H.Z. Abidin, Ion-transport study in nanocomposite solid polymer electrolytes based on chitosan: Electrical and dielectric analysis, J. Appl. Polym. Sci. 132 (2015) 41774, http://dx.doi.org/10.1002/APP.41774.

[68] P. Sharma, D.K. Kanchan, N. Gondaliya, M. Pant, M.S. Jayswal, Conductivity relaxation in Ag^+ ion-conducting PEO–PMMA–PEG polymer blends, Ionics 19 (2013) 301–307, http://dx.doi.org/10.1007/s11581-012-0738-4.

[69] A. Karmkar, A. Ghosh, Dielectric permittivity and electric modulus of polyethylene oxide (PEO)-$LiClO_4$ composite electrolytes, Curr. Appl. Phys. 12 (2012) http://dx.doi.org/10.1016/j.cap.2011.08.017, 539-534.